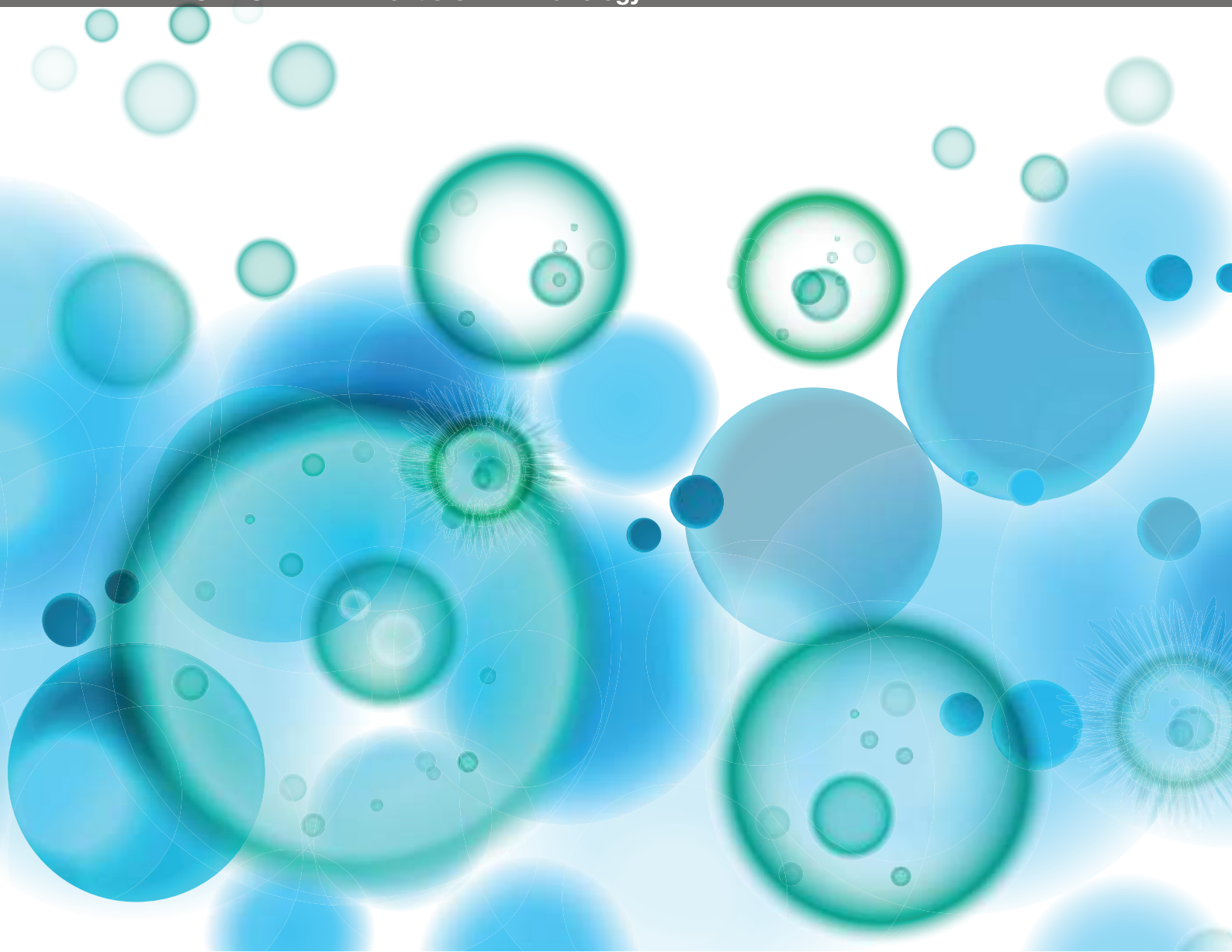
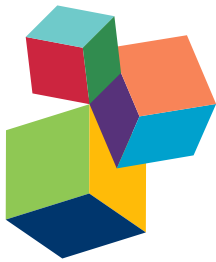


TRANSPLANT REJECTION AND TOLERANCE: ADVANCING THE FIELD THROUGH INTEGRATION OF COMPUTATIONAL AND EXPERIMENTAL INVESTIGATIONS

EDITED BY: Giorgio Raimondi, Kathryn J. Wood, Alan S. Perelson and
Julia C. Arciero
PUBLISHED IN: Frontiers in Immunology





frontiers

Frontiers Copyright Statement

© Copyright 2007-2017 Frontiers Media SA. All rights reserved.

All content included on this site, such as text, graphics, logos, button icons, images, video/audio clips, downloads, data compilations and software, is the property of or is licensed to Frontiers Media SA ("Frontiers") or its licensees and/or subcontractors. The copyright in the text of individual articles is the property of their respective authors, subject to a license granted to Frontiers.

The compilation of articles constituting this e-book, wherever published, as well as the compilation of all other content on this site, is the exclusive property of Frontiers. For the conditions for downloading and copying of e-books from Frontiers' website, please see the Terms for Website Use. If purchasing Frontiers e-books from other websites or sources, the conditions of the website concerned apply.

Images and graphics not forming part of user-contributed materials may not be downloaded or copied without permission.

Individual articles may be downloaded and reproduced in accordance with the principles of the CC-BY licence subject to any copyright or other notices. They may not be re-sold as an e-book.

As author or other contributor you grant a CC-BY licence to others to reproduce your articles, including any graphics and third-party materials supplied by you, in accordance with the Conditions for Website Use and subject to any copyright notices which you include in connection with your articles and materials.

All copyright, and all rights therein, are protected by national and international copyright laws.

The above represents a summary only. For the full conditions see the Conditions for Authors and the Conditions for Website Use.

ISSN 1664-8714

ISBN 978-2-88945-292-7

DOI 10.3389/978-2-88945-292-7

About Frontiers

Frontiers is more than just an open-access publisher of scholarly articles: it is a pioneering approach to the world of academia, radically improving the way scholarly research is managed. The grand vision of Frontiers is a world where all people have an equal opportunity to seek, share and generate knowledge. Frontiers provides immediate and permanent online open access to all its publications, but this alone is not enough to realize our grand goals.

Frontiers Journal Series

The Frontiers Journal Series is a multi-tier and interdisciplinary set of open-access, online journals, promising a paradigm shift from the current review, selection and dissemination processes in academic publishing. All Frontiers journals are driven by researchers for researchers; therefore, they constitute a service to the scholarly community. At the same time, the Frontiers Journal Series operates on a revolutionary invention, the tiered publishing system, initially addressing specific communities of scholars, and gradually climbing up to broader public understanding, thus serving the interests of the lay society, too.

Dedication to quality

Each Frontiers article is a landmark of the highest quality, thanks to genuinely collaborative interactions between authors and review editors, who include some of the world's best academicians. Research must be certified by peers before entering a stream of knowledge that may eventually reach the public - and shape society; therefore, Frontiers only applies the most rigorous and unbiased reviews.

Frontiers revolutionizes research publishing by freely delivering the most outstanding research, evaluated with no bias from both the academic and social point of view.

By applying the most advanced information technologies, Frontiers is catapulting scholarly publishing into a new generation.

What are Frontiers Research Topics?

Frontiers Research Topics are very popular trademarks of the Frontiers Journals Series: they are collections of at least ten articles, all centered on a particular subject. With their unique mix of varied contributions from Original Research to Review Articles, Frontiers Research Topics unify the most influential researchers, the latest key findings and historical advances in a hot research area! Find out more on how to host your own Frontiers Research Topic or contribute to one as an author by contacting the Frontiers Editorial Office: researchtopics@frontiersin.org

TRANSPLANT REJECTION AND TOLERANCE: ADVANCING THE FIELD THROUGH INTEGRATION OF COMPUTATIONAL AND EXPERIMENTAL INVESTIGATIONS

Topic Editors:

Giorgio Raimondi, Johns Hopkins University, United States

Kathryn J. Wood, Oxford University, United Kingdom

Alan S. Perelson, Los Alamos National Laboratory, United States

Julia C. Arciero, Indiana University – Purdue University Indianapolis, United States

Organ transplantation is a life-saving surgical procedure through which the functionality of a failing organ system can be restored. However, without the life-long administration of immunosuppressive drugs, the recipient's immune system will launch a massive immune attack that will ultimately destroy the graft. Although successful at protecting the graft from an immune attack, long-term use of immunosuppressive drugs leads to serious complications (e.g., increased risk of infection, diabetes, hypertension, cardiovascular disease, and cancer). Moreover, recipients suffer from limited long-term graft survival rates due to the inability of current treatments to establish tolerance to the transplanted tissues. Thus, there is a great medical need to understand the complex network of immune system interactions that lead to transplant rejection so that new strategies of intervention can be determined that will redirect the system toward transplant acceptance while preserving immune competence against offending agents.

In the past 20 years, the discovery and growing understanding of the positive and negative regulators of the activation of the immune system have fostered new interventional procedures targeting one or the other. While pre-clinical results proved the validity of these strategies, their clinical implementation has been troublesome. These results underscore the need for additional methods to determine the most effective interventions to prevent long-term transplant rejection. New tools of genomics, proteomics and metabolomics are being implemented in powerful analyses that promise the development of better, safer personalized treatments. In parallel, theoretical modeling has emerged as a tool that transcends investigations of individual mechanistic processes and instead unravels the relevant mechanisms of complex systems such as the immune response triggered by a transplant. In this way, theoretical models can be used to identify important behavior that arises from complex systems and thereby

delineate emergent properties of biological systems that could not be identified studying single components. Employing this approach, interdisciplinary collaborations among immunologists, mathematicians, and system biologists will yield novel perspectives in the development of more effective strategies of intervention.

The aim of this Research Topic is to demonstrate how new insight and methods from theoretical and experimental studies of the immune response can aid in identifying new research directions in transplant immunology. First, techniques from various theoretical and experimental studies with applications to the immune response will be reviewed to determine how they can be adapted to explore the complexity of transplant rejection. Second, recent advances in the acquisition and mining of large data sets related to transplant genomics, proteomics, and metabolomics will be discussed in the context of their predictive power and potential for optimizing and personalizing patient treatment. Last, new perspectives will be offered on the integration of computational immune modeling with transplant and omics data to establish more effective strategies of intervention that promote transplant tolerance.

Citation: Raimondi, G., Wood, K. J., Perelson, A. S., Arciero, J. C., eds. (2017). *Transplant Rejection and Tolerance: Advancing the Field through Integration of Computational and Experimental Investigations*. Lausanne: Frontiers Media. doi: 10.3389/978-2-88945-292-7

Table of Contents

- 06 Editorial: Transplant Rejection and Tolerance—Advancing the Field through Integration of Computational and Experimental Investigation**
Giorgio Raimondi, Kathryn J. Wood, Alan S. Perelson and Julia C. Arciero
- Section 1. Review of Current Approaches**
- 08 Computational Models for Transplant Biomarker Discovery**
Anyou Wang and Minnie M. Sarwal
- 17 Emergent Transcriptomic Technologies and their Role in the Discovery of Biomarkers of Liver Transplant Tolerance**
Sotiris Mastoridis, Marc Martínez-Llordella and Alberto Sanchez-Fueyo
- 25 Computational Biology: Modeling Chronic Renal Allograft Injury**
Mark D. Stegall and Richard Borrows
- Section 2. Big Data and Bioinformatics**
- 29 PD1-Expressing T Cell Subsets Modify the Rejection Risk in Renal Transplant Patients**
Rebecca Pike, Niclas Thomas, Sarita Workman, Lyn Ambrose, David Guzman, Shivajanani Sivakumaran, Margaret Johnson, Douglas Thorburn, Mark Harber, Benny Chain and Hans J. Stauss
- 41 Precision Subtypes of T Cell-Mediated Rejection Identified by Molecular Profiles**
Paul Ostrom Kadota, Zahraa Hajjiri, Patricia W. Finn and David L. Perkins
- 51 Cardiac Arrest Disrupts Caspase-1 and Patterns of Inflammatory Mediators Differently in Skin and Muscle Following Localized Tissue Injury in Rats: Insights from Data-Driven Modeling**
Ravi Starzl, Dolores Wolfram, Ruben Zamora, Bahiyyah Jefferson, Derek Barclay, Chien Ho, Vijay Gorantla, Gerald Brandacher, Stefan Schneeberger, W. P. Andrew Lee, Jaime Carbonell and Yoram Vodovotz
- Section 3. Mechanistic and Equation-Based Models of Rejection**
- 64 Introduction of a Framework for Dynamic Knowledge Representation of the Control Structure of Transplant Immunology: Employing the Power of Abstraction with a Solid Organ Transplant Agent-Based Model**
Gary An
- 79 Combining Theoretical and Experimental Techniques to Study Murine Heart Transplant Rejection**
Julia C. Arciero, Andrew Maturo, Anirudh Arun, Byoung Chol Oh, Gerald Brandacher and Giorgio Raimondi

- 94 Mathematical Modeling of Early Cellular Innate and Adaptive Immune Responses to Ischemia/Reperfusion Injury and Solid Organ Allograft Transplantation**
Judy D. Day, Diana M. Metes and Yoram Vodovotz
- 113 Immune Tolerance Maintained by Cooperative Interactions between T Cells and Antigen Presenting Cells Shapes a Diverse TCR Repertoire**
Katharine Best, Benny Chain and Chris Watkins
- 127 The Limits of Linked Suppression for Regulatory T Cells**
Toshiro Ito, Akira Yamada, Ibrahim Batal, Melissa Y. Yeung, Martina M. McGrath, Mohamed H. Sayegh, Anil Chandraker and Takuya Ueno



Editorial: Transplant Rejection and Tolerance—Advancing the Field through Integration of Computational and Experimental Investigation

Giorgio Raimondi^{1*}, Kathryn J. Wood², Alan S. Perelson³ and Julia C. Arciero^{4*}

¹Vascularized and Composite Allograft Laboratory, Department of Plastic and Reconstructive Surgery, Johns Hopkins School of Medicine, Baltimore, MD, USA, ²Nuffield Department of Surgical Sciences, Oxford University, John Radcliffe Hospital, Oxford, UK, ³Theoretical Biology and Biophysics Group, Los Alamos National Laboratory, Los Alamos, NM, USA, ⁴Department of Mathematical Sciences, Indiana University – Purdue University Indianapolis, Indianapolis, IN, USA

Keywords: transplant rejection, transplant tolerance, theoretical modeling, big data and bioinformatics, mechanistic models, transplant immunology, biomarkers, systems biology

The Editorial on the Research Topic

Transplant Rejection and Tolerance—Advancing the Field through Integration of Computational and Experimental Investigation

Seventy years after the first proof of concept that the immune system can be trained to accept transplanted tissues *via* induction of immune tolerance, we are still waiting for a clinical approach that could be used routinely in transplant patients. Transplantation is a life-saving surgical procedure that is still only successful when paired with life-long administration of immunosuppressive drugs. However, the debilitating side effects of the long-term use of these drugs, together with their incomplete control of the immune system, compromise the quality of life and survival of transplant recipients. Thus, there is a strong push to find new therapeutic strategies that promote indefinite acceptance of a transplanted tissue without compromising the effectiveness of the patient's immune system. Although many exciting ideas have been explored, none of the resulting strategies have been successfully converted into a widely applicable therapeutic approach.

Our knowledge of the complex immunological processes leading to transplant rejection continues to grow, and our understanding of the limitations associated with experimental models deepens. There is a great opportunity to foster a different approach to identify novel interventions. New tools of genomics, proteomics, and metabolomics are being implemented in powerful analyses that promise the development of better and safer personalized treatments. In parallel, theoretical modeling is slowly but progressively being welcomed among experimentalists due to its ability to unravel relevant mechanisms of complex systems and generate new hypotheses (1). The successful employment of these promising tools requires effective communication and collaboration among immunologists, data-driven modelers, and system biologists.

This Research Topic provides a venue for stimulating these interdisciplinary conversations in the context of transplantation. The articles collected under this Research Topic introduce new theoretical and experimental studies that describe novel techniques and methods for understanding the interactions between the immune response and transplants and for establishing more effective strategies of diagnosis and intervention that will promote transplant tolerance. The contributions of this Research Topic can be divided into two main groups according to the approaches they implement: (i) big data and bioinformatics and (ii) mechanistic and equation-based models of rejection.

To identify correlations and sensitivities from large data sets, various statistical methods and bioinformatics approaches are needed. Wang and Sarwal offer a concise review of the current uses and advances in statistical approaches and high-dimensional data applications for identifying possible transplant biomarkers. Identifying markers of injury, causative markers, and predictive markers is key for monitoring, managing patients, and identifying the re-purposing potential of existing drugs.

OPEN ACCESS

Edited and Reviewed by:

Antoine Toubert,
Paris Diderot University, France

*Correspondence:

Giorgio Raimondi
g.raimondi@jhmi.edu;
Julia C. Arciero
jarciero@iupui.edu

Specialty section:

This article was submitted to
Alloimmunity and Transplantation,
a section of the journal
Frontiers in Immunology

Received: 19 April 2017

Accepted: 10 May 2017

Published: 30 May 2017

Citation:

Raimondi G, Wood KJ, Perelson AS
and Arciero JC (2017) Editorial:
Transplant Rejection and Tolerance—
Advancing the Field through
Integration of Computational and
Experimental Investigation.
Front. Immunol. 8:616.
doi: 10.3389/fimmu.2017.00616

Mastoridis et al. review current techniques (transcriptomic technologies) and propose future ideas for identifying biomarkers predictive of tolerance in the context of liver transplantation. They also explore how this knowledge could offer great insight into studying tolerance to other organs. In their perspective article, Stegall and Borrows argue that more accurate and mechanistic mathematical models can be designed to predict (renal) allograft loss or chronic injury, but they note that this will require access to more detailed molecular, histologic, and serologic data. Mechanistic studies conducted in parallel to focused clinical trials also would be tremendously useful for understanding why grafts fail and for designing tailored intervention.

Several statistical methods are applied to transplant data in articles of this collection to identify key biomarkers. Pike et al. used principle component analysis and other tools to analyze a large set of T cell immunophenotyping data before and after renal transplantation. They discovered that pretransplant frequency of programmed death 1 (PD-1) expressing T cell subsets stratifies patients at risk of developing rejection episodes. In a study of kidney transplants, Kadota et al. used various statistical algorithms to analyze the transcriptome of allograft biopsies and showed that histological classification of T cell mediated rejection contains multiple subtypes of rejection amenable to more personalized treatments. When studying the inflammatory response associated with ischemic injury, Starzl et al. combined principal component analysis and a regression approach to discover a cytokine-based signature to define the type and severity of the inflammatory response.

In transplant modeling, identifying the key players and interactions between transplants and the immune system is critical to understanding the pathway to rejection or tolerance. An agent-based model presented by An provides a dynamic and mechanistic understanding of transplant immunology so that control strategies to induce tolerance can be built. Arciero et al. provide one of the first comprehensive mathematical models of mouse heart transplant rejection. This ordinary differential equation-based model tracks innate and adaptive immunity and provides important suggestions of new investigations to improve the understanding of rejection. Day et al. present an ordinary differential equation model focused on the inflammatory response to surgical and ischemia/reperfusion injury. The model predicts specific conditions that lead to tolerance and others that lead to an exaggerated rejection response. Best et al. use a computational model of T cell repertoire development to examine self/non-self discrimination when incorporating features of cross-reactivity and T cell cooperativity. The resulting dynamic state of tolerance suggests specific opportunities for therapeutic intervention to achieve long-term tolerance.

Overall, all of the contributions to this Research Topic highlight the still largely untapped potential of integrating data-driven

and mechanistic modeling into the “ordinary” experimental scientific approach to address key questions of transplant immunology in academic settings. As noted at a recent workshop of computational and experimental immunologists convened by the NIAID (2), there is still a broad divergence among researchers on how to approach fundamental immunological questions. This separation between modelers and experimentalists is even deeper in transplant immunology. However, all researchers share the common goal of improving the life of transplanted patients by understanding how to predict the behavior of immunological responses underlying graft rejection and failure. Despite the continuous growth of technological advances, it is still difficult to predict how a certain molecular or cellular intervention will affect the behavior of the entire system over time. This could be achieved, however, by properly integrating experimentation, data-driven modeling, and mechanistic modeling to test non-intuitive conditions impractical to explore using experimentation alone. The close collaboration between experimentalists and modelers necessary to reach this result requires a novel component of formal training of each part that will lead to productive communication and work integration. This Research Topic encourages the research community to embrace and implement this approach and witness exciting new discoveries that will ultimately benefit the patient population.

AUTHOR CONTRIBUTIONS

GR and JA prepared the first draft. KW and AP made critical revisions and provided valuable feedback.

ACKNOWLEDGMENTS

We are grateful to all the authors who contributed to this Research Topic. We also thank the editors and reviewers of the articles for their invaluable help.

FUNDING

This work was supported by a National Institutes of Health grant number UL1TR000005 in the form of a CTSI-PEIR and grant number R21HL127355 (to GR), Burroughs Wellcome Fund BWF Collaborative Research Travel Grant and the IUPUI School of Science Institute for Mathematical Modeling and Computational Science Grant to Enhance Interdisciplinary Research and Education (iM2CS-GEIRE) award (to JA), NIH grants R01-OD011095 and R01-AI028433 (to AP), and grant from the European Commission for the ONE Study and BioDRIM FP7 Consortia (to KW).

Copyright © 2017 Raimondi, Wood, Perelson and Arciero. This is an open-access article distributed under the terms of the Creative Commons Attribution License (CC BY). The use, distribution or reproduction in other forums is permitted, provided the original author(s) or licensor are credited and that the original publication in this journal is cited, in accordance with accepted academic practice. No use, distribution or reproduction is permitted which does not comply with these terms.

REFERENCES

1. Germain RN, Meier-Schellersheim M, Nita-Lazar A, Fraser ID. Systems biology in immunology: a computational modeling perspective. *Annu Rev Immunol* (2010) 29:527–85. doi:10.1146/annurev-immunol-030409-101317
2. Vodovotz Y, Xia A, Read EL, Bassaganya-Riera J, Hafler DA, Sontag E, et al. Solving immunology? *Trends Immunol* (2017) 38(2):116–27. doi:10.1016/j.it.2016.11.006

Conflict of Interest Statement: The authors declare that the research was conducted in the absence of any commercial or financial relationships that could be construed as a potential conflict of interest.

Computational models for transplant biomarker discovery

Anyou Wang and Minnie M. Sarwal *

Department of Surgery, Division of MultiOrgan Transplantation, University of California San Francisco, San Francisco, CA, USA

Translational medicine offers a rich promise for improved diagnostics and drug discovery for biomedical research in the field of transplantation, where continued unmet diagnostic and therapeutic needs persist. Current advent of genomics and proteomics profiling called “omics” provides new resources to develop novel biomarkers for clinical routine. Establishing such a marker system heavily depends on appropriate applications of computational algorithms and software, which are basically based on mathematical theories and models. Understanding these theories would help to apply appropriate algorithms to ensure biomarker systems successful. Here, we review the key advances in theories and mathematical models relevant to transplant biomarker developments. Advantages and limitations inherent inside these models are discussed. The principles of key computational approaches for selecting efficiently the best subset of biomarkers from high-dimensional omics data are highlighted. Prediction models are also introduced, and the integration of multi-microarray data is also discussed. Appreciating these key advances would help to accelerate the development of clinically reliable biomarker systems.

OPEN ACCESS

Edited by:

Giorgio Raimondi,
Johns Hopkins School of Medicine,
USA

Reviewed by:

Mark D. Stegall,
Mayo Clinic, USA

Li Li,

Icahn School of Medicine at Mount
Sinai, USA

***Correspondence:**

Minnie M. Sarwal,

Department of Surgery, Division of
MultiOrgan Transplantation, University
of California San Francisco,
505 Parnassus, San Francisco,
CA 94107, USA
minnie.sarwal@ucsf.edu

Specialty section:

This article was submitted to
Alloimmunity and Transplantation,
a section of the journal
Frontiers in Immunology

Received: 30 June 2015

Accepted: 24 August 2015

Published: 08 September 2015

Citation:

Wang A and Sarwal MM (2015)
Computational models for transplant
biomarker discovery.
Front. Immunol. 6:458.
doi: 10.3389/fimmu.2015.00458

Introduction

In the new era of biomedical research, it is being increasingly recognized by funding agencies and journals that traditional hypothesis-driven research alone cannot provide the rapid and incremental advances needed to change the current clinical practice management for transplant patients, so as to positively impact long-term graft outcomes. In addition, given that organ transplantation is an orphan disease, there are few if any focused efforts for discovery of new immunosuppressive drugs for transplant recipients. In fact, the number of Food and Drug Administration (FDA) approved drugs has been relatively constant to about 20 drugs per year, yet the cost of drug discovery has ramped up (\$138 million in 1975 to \$1.3 billion in 2006), and the rate of new drug production by a pharmaceutical company generally follows a Poisson distribution and is constant (about 2–3 drugs per year at most) (1). This constant rate of output is often blamed on the traditional hypothesis-driven research model, primarily because hypotheses derived from complex experimental models often do not translate to human pathology. Hence, there is a growing need to harness “big data” at the RNA/protein/metabolite/antibody/DNA level to get novel insights into interlinked global processes that have been hitherto poorly understood. With this direction, comes the companion need to develop and apply the right computational tools to harness this data and interlink it to the entire electronic medical record (EMR) in an identified, regulated process.

Although short-term survival rates of grafts have increased, long-term graft survival rates have shown little improvement (2, 3). Five-year graft survival for transplanted organs varies from 43% for lung to 78% for kidney, highlighting the need for improved analysis of post-transplant injury

pathways. There is a desperate urgency to advance the field of organ transplantation through improved monitoring by (a) the discovery of informative biomarkers, specific and sensitive to phenotypes of injury and acceptance, and (b) through improved algorithms and/or drugs for treatment with targeted efficacy and reduced toxicity (4, 5). Many single gene/protein pathway studies have shown associative and mechanistic insights into animal and restricted human sample studies, but the field has stalled with regard to the additional exponential insights needed at a genome-wide level to develop significant improvements in biomarker discovery for diagnosis/prediction and to evaluate the role of novel pathways for improved rational drug design as it applies to organ transplantation. In this review, we focus on the application of different computational approaches to mine high-dimensional human data in transplantation with a view to changing current clinical practice and patient management. Some of the critical requirements that the transplantation process needs to fulfill with this meta-data approach are highlighted in **Figure 1**.

Biological experimental tools that explore genome-wide profiling referred as “omics” provide promising pathways to investigate transplant biology, and they have been increasingly applied in transplantation, with the number of generated data tripling over last decade (**Figure 2**). These omics technologies (e.g., functional genomics for RNA analysis, proteomics for protein and peptide analysis, metabolomics for metabolite analysis, and antibiomics for HLA- and non-HLA-antibody analysis) also provide “big data” that contains high-dimensional variables. Harnessing the “big data” to low dimensional variables could generate small sets of biomarkers for diagnostic tools, which detect and predict

transplant injury as well as discriminate different causes of injuries. However, these omics data are generally complex, due to its inherent high-dimensional complexity, platform differences, hybridization variations, and different data scales. These complexities challenge scientists to directly extract biologically valid and clinically useful information by selecting, generating, and using the appropriate computational tools to meet the demands of the composition of the input data.

Decomposing the complex omics datasets to derive biomarkers often requires customization of computer algorithms and software. Limitations and pitfalls inherent inside these software tools, such as biased *p*-value estimation, over-estimated prediction accuracy, could derail the successful selection of biomarkers due to enhanced false positives and negatives. Thus, applying appropriate algorithms to decompose the complexity requires an understanding of the theories and principles behind these algorithms. Here, we review key advances of theory and computational models relevant to transplant biomarker development. Understanding these key advances would help to master the wave of biomarker development and to develop novel reliable biomarker systems (4, 7–9).

High-Dimensional Data Applications in Transplantation

Gene expression microarrays have been the most commonly used high-throughput technology in transplantation (10, 11). Microarrays were applied to biomedical science in 1995, and the first landmark study of kidney biopsy microarrays was

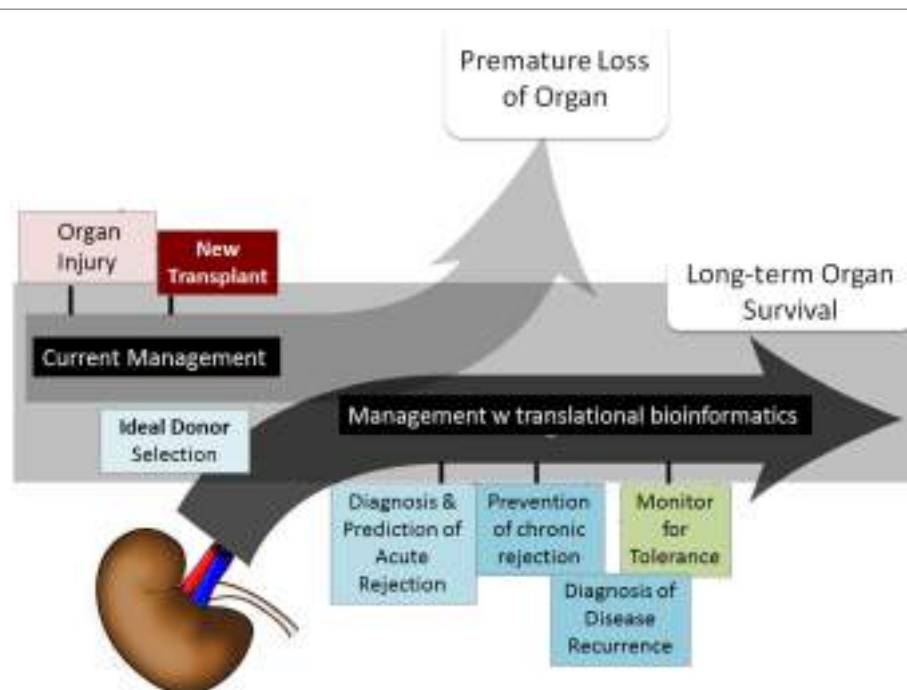


FIGURE 1 | Transplant fields require computations. The boxes show the areas of investigation needed by translational computational methods to advance organ transplant management. Figure adapted from Ref. (6).

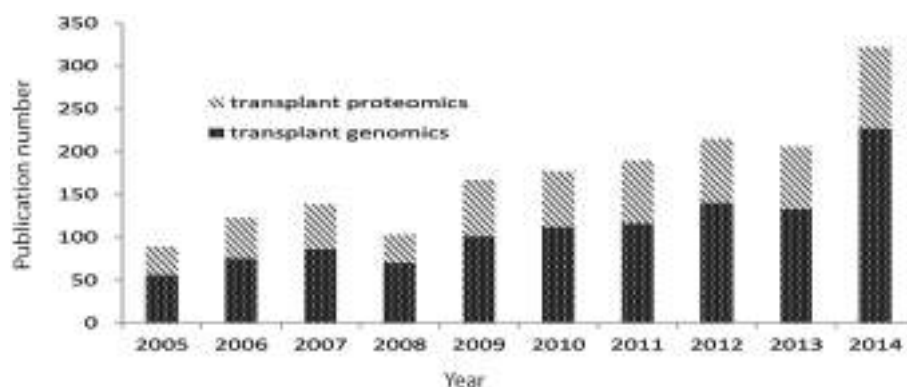


FIGURE 2 | Pubmed publications on transplant genomics and proteomics paper over last 10 years. Data were extracted from Pubmed by searching transplant and genomics or transplant and proteomics.

published in 2003 [Sarwal et al. (12), *NEJM*], uncovering for the first time molecular heterogeneity in acute rejection that was far greater than previously understood by histology alone and a pivotal role for B cells in steroid-resistant late post-transplant rejections occurring secondary to treatment non-adherence. There are an increasing number of human studies in the public domain profiling biopsy, bronchoalveolar lavage, and blood and urine samples from different organ transplant recipients, with phenotypes defined by matching graft biopsies as acute rejection, chronic injury, recurrent glomerulonephritis, viral nephritis, operational and induced tolerance, and drug toxicity. Transcriptional profiling of peripheral blood as a correlate of intragraft events has been successfully applied in the IMAGE Study in heart transplantation (13) and in the SNSO1 (14) and AART (15) studies in kidney transplantation and for the detection of chronic graft vs. host disease in bone marrow transplantation (16). Pathogenesis-based transcripts (PBT) expression panels have been inferred from mouse experiments and applied to human transplant expression patterns in an effort to develop correlates of histopathological lesions in renal transplant biopsies (17).

A major challenge in transplantation is the life-long administration of immunosuppressive drugs with multiple side effects. Calcineurin inhibitors are associated with nephrotoxicity, which in turn can contribute to long-term graft failure, along with opportunistic infections. To better understand the mediators of calcineurin inhibitor toxicity, selected patients from the BENEFIT trial (Vincenti, *NEJM*), had their 1-year protocol biopsies profiled against gene-sets selected after loading cyclosporine and tacrolimus on renal proximal tubular cells, as the *in vitro* model of calcineurin inhibitor toxicity. Patients receiving Belatacept and no calcineurin inhibitor agents demonstrated more immune reactivity, but reduced expression of profibrotic genes and increased expression of solute transporter genes, correlating with the preserved renal architecture seen in these patients (18). To better understand how to optimally dose patients with immunosuppressive drugs, operationally tolerant patients were profiled (19), and informative genes were used to identify patients on full dose immunosuppression that may benefit from safe

immunosuppression wean (19), after controlling for multiple clinical variables and confounders.

High-throughput technologies have also been expanded to study the role of microRNAs (miRNAs) in graft rejection in peripheral blood (20) and the allograft (18), and suggests that intragraft changes in miRNA levels are explained by the burden and composition of infiltrating cells in the course of injury.

The introduction of high-density protein arrays as allowed for the evaluation of serological responses to ~9,000 human full-length proteins on a single slide. This technology was used to understand the differential immunogenicity of different tissue compartments of the transplanted kidney (21), and identified that the renal outer cortex, glomerulus, and the deep pelvis antigens mount new autoantibody responses after organ engraftment, most of which may not be pathogenic. In addition, this technology was also used to evaluate the identity of novel non-HLA antibodies in patients with HLA-antibody-negative acute renal transplant rejection, and identified a novel target, Kinase C- ζ (PKC ζ), as a dysregulated epitope in severe allograft injury (22). Additionally, using protein microarrays, Angiotensinogen and PRKRP1 were identified as biomarkers of chronic kidney injury, with correlative results with hypertension in patients with high-antibody titers. These results suggested for the first time that autoantibodies are raised against previously unknown antigenic targets in the transplanted organ, which are likely exposed to the immune system of the recipient in the process of cellular damage in the organ (23).

Recent advances in small molecule identification technologies (e.g., mass spectrometry, surface enhanced laser desorption/ionization, liquid chromatography/mass spectrometry, nuclear magnetic resonance) have given rise to the application of proteomics, peptidomics, and metabolomics to transplantation. Urine is a rich biofluid source for biomarker discovery in organ transplantation. Shotgun proteomics provides us with a map the entire urinary proteome (24) in health and transplant injury states. Smaller fragments of the urinary peptidome, consisting of degraded byproducts of intact proteins by enzymatic cleavage, also provide insights into the perturbations in chemical balance during kidney injury (25, 26). Metabolomics has been used for identifying graft injury as well as for monitoring drug toxicity (27–29).

Computational Challenges and Approaches for Selecting Biomarkers from High-Dimensional Data

The integration of hypothesis generation by high-dimensional data analysis is poised to fulfill the current unmet needs in organ transplantation, which relates to poor long-term survival despite improvement in short-term outcomes, the need for life-long immunosuppressive medications and their associated morbidities, and the lack of non-invasive markers for monitoring and predicting graft injury, superior to current standards of monitoring. Computational biology expands from the traditional molecular biological method of studying pair-wise interactions into a network-based approach by integrating individual components to model a complex system, thus beginning to understand disease at the level of regulatory pathways in tissues and organs, even in whole organisms, while also accounting for dynamics within regulatory networks. A large number of computational approaches have been developed to generate co-expression networks from protein binding data (30), functional annotations (31), and drug activity (32). Using these approaches, it has been shown that such networks have properties that are not otherwise discernable from the relations themselves, and have preferential connectivity that results in "hub" nodes, which are molecules that connect to a larger number of other molecules (33).

To date, a large number of biomarkers have been identified for various post-transplant conditions as markers of an ongoing injury (effect markers) or related to the actual causes of the injury (causal markers). Development of new drugs that reduce drug toxicity and chronic rejection requires identification of causal markers that can be targeted for novel therapeutics. The use of systems and computational biology is the critical next step for deeper understanding and the identification of causal markers of graft injury in transplantation.

One of the reasons for the limited impact of the high-throughput studies in transplantation relates to low number of individuals and samples used resulting in lack of sufficient independent validation. As described in our previous review (6), searching the NCBI GEO for microarray studies in humans described with the term "transplant" yields 69 experiments, of which only 16 have more than 50 samples and only 6 have more than 100 samples. These numbers are even more disappointing when put into the context that these experiments are divided among four different organs (lung, kidney, liver, heart) studying at least three different conditions (acute rejection, chronic rejection, tolerance). The sample limitations relate to sample availability and assay cost, both of which truncate greater enrollment. We addressed the sample availability shortcoming by performing meta-analysis by integrating smaller independent experiments, and customized algorithms were generated to deal with experiment-specific technical biases, such as microarray platform or hybridization protocol (6, 34). This approach allowed for the identification of a core of 12 genes (BASP1, CD6, CD7, CXCL9, CXCL10, INPPD5, LCK, NKG7, PSMB9, RUNX3, TAP1, ISG20), called the common immune response module, which was a similarly dysregulated set of genes in acute rejection across tissue source; these genes were all upregulated in kidney, heart, liver, and lung rejection

across 236 microarrays downloaded from GEO. Their biological relevance in graft rejection was further tested by repositioning two drugs against LCK (Dasatinib) and CXCL10 (Atorvastatin) in a murine heart transplant model of rejection; thus suggesting that FDA-approved drugs for indications other than transplant immunosuppression may be repositioned across the remainder of the gene-set to identify new drug targets for organ transplant recipients. In another example of an integrative analysis, Chen et al. performed a meta-analysis using three transplant RNA microarray data sets from biopsies with kidney and heart acute rejection (35), and then the corresponding significant proteins (inferring gene/protein 1:1 mapping) coded for by these RNA were then screened as potential blood markers for acute rejection. This approach confirmed that three proteins (PECAM1, CD44, and CXCL9) were significantly over-expressed in blood samples in both kidney and heart transplant patients. These integrative approaches demonstrate that integration of data sets can reduce biological bias across experiments, experimenters, platforms, and tissue source, while allowing for the generation of novel hypotheses and drug repositioning.

Data integration can also be performed across different types of molecular measurements. Li et al. integrated antibody-level measurements from a protein array with renal compartment-specific gene expression data (21) and demonstrated that post-transplant serological responses observed using protein microarrays were specific to the transplanted organ and to specific organ compartments.

The efficient selection of biomarkers to limit *false negatives* and *false positives* is another challenge for high-dimensional data analysis. A typical microarray experiment produces approximately 50,000 data points per sample. An experiment with 50 samples will produce more than 2.5 million data points. Millions of data points are generated by SNP genotyping platforms for thousands of samples in a typical genome-wide association study. The amount of data generated increases again exponentially for next-generation sequencing population studies. Incorporation of computational skills into the curricula of transplantation training program needs to be a high priority, to arm the next-generation clinician scientist.

Various methods are used to limit false-positive/negative signals and reduce variables. These mainly use stepwise regression models (36, 37), principal component analysis (PCA) (38, 39), T-statistic, and correlation to clinical variables (7, 8, 40–43).

Stepwise-Based Models

Traditional Stepwise Methods

Many regression models are available to select a particular set of independent variables and the commonly used methods are stepwise techniques (36, 37). Traditional stepwise selection alternates between forward and backward regression selection, in which variables are added or removed that meet a selection criteria setting for entry or removal, until a final subset of variables make the model saturated. However, this stepwise method has essential problems. It applies methods intended for one single hypothesis test to many tests, leading to results biased to a certain degree, such as higher in R^2 (explained variation/total variation), lower in standard errors and p -values than the actual values, and as models they can be complex to develop.

Vorlat et al. used stepwise multiple regression and identified B-type natriuretic peptide (BNP) and age as the most important factors in evaluating outcomes after heart transplantation, after evaluating many variables, such as body mass index, age, BNP, norepinephrine dose, gender, and total ischemic time (37).

Lasso (Least Absolute Shrinkage and Selection Operator)

Lasso (least absolute shrinkage and selection operator) (44) is a penalized regression method for shrinkage and variable selection, and uses the equation:

$$\sum_{i=1}^n \left(y_i - \sum_j x_{ij} \beta_j \right)^2 + \lambda \sum_{j=1}^p |\beta_j|$$

$i = 1, 2, \dots, n$ (n equivalent to sample size);

$j = 1, 2, \dots, p$ (p equivalent to omics gene number);

y_i = response variable of sample i , β_j = coefficient for gene j , $j = 1, 2, \dots, p$, and x_{ij} = observation value of sample i and gene j .

Lasso estimation actually introduces a penalized constraint to minimize the usual sum of squared errors to get solution. This penalization is estimated by $\sum |\beta_j| \leq s$, sum of the absolute coefficients.

If s is set to a large number, it does not affect Lasso estimation that actually acts as a usual multiple linear least squares estimates. Then, a large number of genes might be selected as biomarkers. However, if s is small ($s \geq 0$), Lasso works as shrunken least squares regression and then only a few genes would be selected as biomarkers. Lasso has several limitations. For example, the gene number (p) is usually large and sample size (n) is small. In this case, at most n genes are selected by Lasso before the model saturates. In addition, Lasso tends to select the biomarker with greater variance (44) and it might likely ignore some important genes in a correlated group.

Elastic-Net

To overcome the limitations existing in Lasso, elastic-net adds an additional quadratic part $\sum_j \beta_j^2 \leq t$ to the penalization to make it work for both variable selection and shrinkage (45). Many modifications have been made to improve its prediction performance. Elastic-net and lasso are arguably the best methods so far for shrinkage and biomarker selection. Lasso and elastic-net were to select a best subset of 17 genes as biomarkers to predict the most informative acute rejection blood-based biomarkers (15).

Modified t -Statistic Methods

Prediction Analysis of Microarrays

Prediction analysis of microarrays (PAM) has been commonly applied in transplant (40, 46, 47). PAM uses the following equation to determine if a gene is significant for classification:

$$d_{ik} = \frac{\bar{x}_{ik} - \bar{x}_i}{w_k (s_i + s_0)}$$

where $w_k = (1/n_k - 1/n)^{1/2}$

It actually looks like t -statistic formula, where $w_k \times s_i$ is the standard error of the numerator. The only modification is to add s_0 as a fudge factor to avoid very large statistics for very small standard errors. Thus, PAM is a modified t -statistic to measure the difference between the mean of gene i in class k with the overall mean of gene i . A gene with a statistic of large absolute value discriminates one class from the rest. PAM then selects significant genes by then shrinking the d_{ik} toward zero.

This measurement in PAM actually shrinks each gene toward its overall mean cross classes. After this shrinkage, all class centroids become more similar to each other than before. This might not help to improve the overall discriminant accuracy in omics data.

Reeve et al. used PAM to select the most significant genes from 186 microarrays to build a classifier system to predict acute rejection. These genes are mostly associated with interferon-gamma-inducible or cytotoxic T-cell associated, such as CXCL9, CXCL11, GBP1, and INDO (47).

ClaNC

To circumvent the PAM limitations, an alternative classifier called ClaNC (42) has been developed. ClaNC uses standard statistics to select genes and does not shrink centroids, and it also selects class-specific gene and allows a gene to be active only in one class. Kurian et al. used this algorithm to select 200 biomarkers from genome-wide gene expression profiling and created a discriminant system for classifying three phenotypes in kidney transplantation (48).

Principal Component Analysis

Principal component analysis method selects biomarkers based on an eigengene score (38), $\text{score} = |\text{cor}(x_i, E)|$, $|\text{cor}(x_i, E)|$ is the absolute value of Pearson correlation coefficient, where x_i is a vector of gene i , and E is a eigenvalue.

Genes Selected by Correlating with Clinical Variables

A subset of genes can also be selected by correlating gene expression level and clinical variables, such as patient survival or graft loss. This correlation can be measured by univariate Cox proportional hazards scores that derived from Cox regression model. Genes that pass the interquartile range (IQR) filter are considered as significant (40, 41).

Evaluation of Models and Biomarkers Requires Robust Validation

Many biomarker systems published to date for transplant fail in the real world, partially due to lack of robust model validation. Models usually should be subject to cross-validation, a technique for evaluating the performance of predictive models, like linear models for discriminating acute rejection against stable samples, with the use of independent samples in the different subsets. Different types of cross-validations are available. *Repeated random sub-sampling validation* randomly splits all samples into subsets of samples, a training set, and validating set. The training subset is used to fit a model and the validating set is for examining predictive accuracy. A large iteration of splits (e.g., 10,000) is usually run to avoid splitting sample bias. The accuracy is calculated by the average of all iterations. *k-fold cross-validation* randomly splits total

samples into k subgroups with equal size. One out of k subgroups is treated as testing validation and the remaining $k - 1$ subgroups are used as training data to train models. The whole process is run k times (k folds). Each time, each of the k subgroups is used as validation but each group is used only once. The sensitivity and specificity can be calculated by combined result from each run. We have extensively used these systems of study (15, 19), and the process of robust cross-validation has also been extensively reviewed in a recent publication by Roedder et al. (49).

The binary classified performance of an entire biomarker system should typically be evaluated by *receiver operating characteristic curve*, ROC curve. ROC is a graphical plot of the true positive rate (sensitivity) against specificity or false positive rate (1-specificity) at various threshold settings. The sensitivity is equal to the proportion of correctly classified positive observations, and the specificity is calculated as the proportion of correctly classified negative observations. Area under the curve (AUC) serves as estimated index of overall accuracy and serves a useful practice to compare different ROCs, and it is usually plotted within ROC curve. The biomarker panels developed for graft rejection and tolerance in recent studies provide ROC curves of >85% (15, 19).

Prediction Models for Biomarker Risk Analysis

One of the most interesting goals in developing biomarker systems is to predict and monitor the phenotype outcome of transplantation. For example, selecting biomarkers from short-term data (e.g., 3 months biopsy profiling) may be associated with a phenotype of long-term (e.g., 1-year graft chronic injury) outcomes. Predictive models have been applied to reach this purpose. Although all machine learning models have predictive functions, such as Support Vector Machine (38, 39) and LASSO described above, two out of them, linear discriminant analysis (LDA) and logistic regression, have been widely applied in transplant biomarker systems to classify the discrete classes of variables (40, 48, 50, 51).

Linear Discriminant Analysis

Linear discriminant analysis has been widely applied to transplant biomarker development (40, 48). LDA is a classifier (52) that classifies samples to their nearest given centroid. Assuming that we have k classes with prior probabilities π_k , then LDA can be defined below:

$$\check{y} = \arg \min_k \left\{ (x - \mu_k)^T \Sigma^{-1} (x - \mu_k) - 2 \log(\pi_k) \right\}$$

where $\|x - u\|^2$ is the square of the Mahalanobis distance between sample value (x) and centroid or mean (u).

Logistic Regression

Logit link function can be understood as follows:

$$\text{log odds} = \log \frac{p}{1-p} = \beta_0 + \beta_1 x_1 + \beta_2 x_2 + \dots + \beta_k x_k$$

$$p = \text{probability of one phenotype; odds} = \frac{p}{1-p}$$

$x_i = i^{\text{th}}$ biomarker value, $i = 1, 2, \dots, k$

The left side of logit link function above can be signed as Y , and then this function can be simply written as $Y = \beta_0 + \beta X$, so it can actually be understood as a linear regression. The phenotype variable in logit could be binary value (e.g., AR vs. non-AR) or multinomial.

Correlation

Besides machine learning, other mathematical methods have also been employed to establish quantitative biomarker system. Here, we introduce one, kSORT (15), based on Pearson correlation coefficients of multiple genes (12 genes). Genes for kSORT were selected by Lasso and elastic-net. Binary classification of AR vs. non-AR was based on accumulated scores. These scores were accumulated from running correlation for 13 times with 12 gene panels. The score was assigned as 1 (if greater correlation to AR) or -1 (if greater correlation to non-AR). After 13 runs, the final score of a sample would be in the range from -13 to 13. This rank is then used as an index of a risk factor for acute rejection.

Data Integration Strategies

Many omic experiments have been performed with different platforms by different laboratories. These omics data cannot be treated as a single experiment and a meta-analysis strategy should be applied to integrate these data to get a panel of prioritized genes. Several techniques and theories have been proposed (34, 53, 54). Here, we only briefly described four methods employed in transplant biomarker development.

Normalization and Batch Effect Removal

For combining small set of microarray data with a big data set, normalization can be performed using Lowess (locally weighted scatterplot smoothing) or Loess (55) (later generalization of Lowess), and then batch effect should be removed. Lowess is a non-parametric regression method for fitting a smoothing curve to a dataset by combining regression models and weights of local neighbors. It splits the microarray intensity curve into a series of windows by a given window size and then performs regression locally with nearest weight to smooth the curve. A larger window size produces a smoother curve, and a smaller window size generates more local variation. After normalized, batch effect can be removed by using empirical Bayes methods (56) before combining the data (57).

Frozen Robust Multiarray Analysis

Robust multiarray analysis (RMA) is a pre-processing algorithm that pre-processes microarray data by background correction, quantile normalization, and summarization in a modular way by fitting the normalized data with models. It is widely used, but RMA cannot be used in clinical data directly because these data are normally in small batches, and clinical samples are normally processed individually and separately and they are comparable. Therefore, a modified RMA, frozen robust multiarray analysis (fRMA), has been proposed. fRMA computes and freezes probe-specific effects and variances of a dataset, and with new data sets coming, these precomputed and frozen info are used in concert with those from the new coming microarrays to normalize and

TABLE 1 | Primary computational algorithms for transplant biomarker discovery.

Name	Environment	Features and functions	Limitations	Availability	Web resources
Biomarker selection					
Traditional stepwise methods	R/SAS	Stepwise regression	High R ² , low SE	Free/commercial	www.r-project.org , www.sas.com
LASSO and Elastic-net	R/SAS	Shrinkage and biomarker selection	Model could be saturated for Lasso when sample size is small	Free/commercial	www.r-project.org , www.sas.com
Prediction analysis of microarrays (PAM)	Excel/R	Shrinkage and biomarker selection	Might not improve the overall discriminant accuracy	Free	http://statweb.stanford.edu/~tibs/PAM/
ClaNC	R	Classification and biomarker selection	Limited improvement in discriminant accuracy	Free	http://www.stat.tamu.edu/~adabney/clanc/
Principal component analysis	R/SAS	Classification and biomarker selection	Sometimes it is hard to interpret data	Free/commercial	www.r-project.org , www.sas.com
Prediction models					
Linear discriminant analysis (LDA)	R/SAS	Classification and prediction	Linear	Free/commercial	www.r-project.org , www.sas.com
logistic regression	R/SAS	Classification and prediction	Requires large sample size	Free/commercial	www.r-project.org , www.sas.com
Data integration strategies					
Normalization and batch effect removal	R	Pre-processing	Might not fit clinical data directly	Free	https://www.r-project.org/
Frozen robust multiarray analysis (fRMA)	R	Pre-processing	Requires large data set and platform limitation	Free	https://www.r-project.org/
P-value meta-analysis	Any/R	Gene prioritization	Significance test only	Free	https://www.r-project.org/
Fold-change meta-analysis	Any/R	Gene prioritization	Fold-change-based effect size only	Free	https://www.r-project.org/

summarize the data. Thus, it provides a way to combine data analyzed individually or in small batches (53).

When merging multiple datasets, the raw data (e.g., CEL file for Affymetrix array) are usually used in order to pre-processing all data (e.g., outlier deletion and normalization) with the same algorithm and the similar criteria. If multiple probes exist for a transcript, the mean of probes is used to represent the expression level of this transcript. The genome annotation IDs (e.g., refGene IDs) universal for all platforms are usually employed to combine the data.

p-Value Meta-Analysis

p-value meta-analysis uses Fisher's method to combine the squares of the p-values as defined below (34):

$$\chi^2_{2k} = -2 \sum_{i=1}^k \log(p_i)$$

where k = experiment number, p_i is devised from each experiment. This p-value combination would generate a list of genes with meta p-value for each gene. Genes with up- and down-regulation is separated into two groups during combining p-value but only one with minimum p-value is selected. The meta p-value can then further be corrected by multiple hypothesis testing to obtain adjusted p-value. The final adjusted p-value is used to prioritize genes. Lower in adjusted p-value ranked in the top.

Fold-Change Meta-Analysis

Another prioritized gene method is based on fold-change meta-analysis as defined below (34):

$$f_{\text{meta}} = \frac{(f_1 w_1 + f_2 w_2 + f_3 w_3 + \dots)}{(w_1 + w_2 + w_3 + \dots)}, w_i = \frac{1}{\text{var}(f_i)}$$

where,

f_i = fold-changes in sample i ;

w_i = reverse variance of the f_i .

It should be noted that meta-analyses might produce different rank prioritizations of genes differentially expressed across studies, and the final biological relevance of the selected genes also becomes important in the final gene selection.

Conclusion and Future Directions

In order to take our understanding of injury mechanisms in organ transplantations to the next level, integration of molecular measurement data from different experiments and different technologies is required. Furthermore, these integrated data need to be analyzed at a global, systems biology level to identify better diagnostic and therapeutic markers. Predictive biomarkers should cover diverse genetic and epigenetic backgrounds. Clinical and pathology-based variables should be considered as confounding variables during biomarker development. Next-gen sequencing will provide much higher resolution than microarrays to get insights into the diversity of injury and patient-specific responses. With new advances in mathematical theories, a new biomarker system may include many variables from different biology aspects, such as genetics, epigenetics, clinical variables, and pathology.

Biomarker discovery suffers from difficulties in selecting "noise" from "true biology" as this discovery relies on human studies and human samples, which are inherently associated with sample and tissue variation, and often result from the use of multiple measurement platforms, with experimental methodology variations, all of which challenge the process of robust biomarkers

discovery. Hence, publications suggest that a set of biomarker that works well for one center or one set of patients based on well-conducted statistical methods may not work as well for another center or a different set of patients with variable demographics or other previously unrecognized clinical confounders. It is also important to recognize that most of the biomarkers in transplantation are still in development, as they do not have the support of robust prospective clinical trials. The biomarkers also face the challenge of their correlation being based on histology as the “gold standard,” a standard that we know is not perfect, as it underdiagnoses alloimmune injury and is not really a predictive measure. Thus, most of the biomarkers in research are really just “associated” with histologic findings. It is still unclear if using these biomarkers will ever actually improve graft survival as this requires the conduct of large clinical trials with long-term follow-up, making this research very expensive and often untenable in clinical practice; thus, most omic studies are underpowered with

it comes to predicting graft loss. Biomarkers often do not dictate the type of therapy, but accurate prediction of immune risk may allow for their use as companion diagnostics for specific drugs or for safe immunosuppression minimization. Biomarkers may also not always obviate the need for a biopsy, as often they do not differentiate between infections such as polyoma and rejection as both are associated with graft inflammation. Thus, there may still be the need for confirmatory biopsies for the cause or type of organ injury.

The fragmented and incomplete nature of the existing knowledge bases poses a challenge to achieving these goals, and wider adoption of a policy to submit raw data into public repository should be required by the transplant-related journals. It is also imperative that the next generation of clinician scientists is armed with computational skills that will ensure novel questions continued to be posed and answered, enabled by the proper integration of diverse sources of data.

References

- Dudley JT, Schadt E, Sirota M, Butte AJ, Ashley E. Drug discovery in a multi-dimensional world: systems, patterns, and networks. *J Cardiovasc Transl Res* (2010) **3**(5):438–47. doi:10.1007/s12265-010-9214-6
- Matas AJ, Smith JM, Skeans MA, Lamb KE, Gustafson SK, Samana CJ, et al. OPTN/SRTR 2011 annual data report: kidney. *Am J Transplant* (2013) **13**(Suppl 1):11–46. doi:10.1111/ajt.12019
- Mas VR, Mueller TF, Archer KJ, Maluf DG. Identifying biomarkers as diagnostic tools in kidney transplantation. *Expert Rev Mol Diagn* (2011) **11**(2):183–96. doi:10.1586/erm.10.119
- Lo DJ, Kaplan B, Kirk AD. Biomarkers for kidney transplant rejection. *Nat Rev Nephrol* (2014) **10**(4):215–25. doi:10.1038/nrneph.2013.281
- Lee JR, Muthukumar T, Dadhania D, Ding R, Sharma VK, Schwartz JE, et al. Urinary cell mRNA profiles predictive of human kidney allograft status. *Immunol Rev* (2014) **258**(1):218–40. doi:10.1111/imr.12159
- Khatri P, Sarwal MM, Butte AJ. Applications of translational bioinformatics in transplantation. *Clin Pharmacol Ther* (2011) **90**(2):323–7. doi:10.1038/clpt.2011.120
- Gong W, Whitcher GH, Townamchai N, Xiao X, Ge F. Biomarkers for monitoring therapeutic side effects or various supratherapeutic confounders after kidney transplantation. *Transplant Proc* (2012) **44**(5):1265–9. doi:10.1016/j.transproceed.2011.11.069
- Halawa A. The early diagnosis of acute renal graft dysfunction: a challenge we face. The role of novel biomarkers. *Ann Transplant* (2011) **16**(1):90–8.
- Mannon RB. Immune monitoring and biomarkers to predict chronic allograft dysfunction. *Kidney Int Suppl* (2010) **119**:S59–65. doi:10.1038/ki.2010.425
- Khatri P, Sarwal MM. Using gene arrays in diagnosis of rejection. *Curr Opin Organ Transplant* (2009) **14**(1):34–9. doi:10.1097/MOT.0b013e32831e13d0
- Khatri P, Sarwal MM. Functional pathway analysis for understanding immunologic signature of rejection: current approaches and outstanding challenges. *Immunol Signatures of Rejection*. (Vol. **2011**) (2010). p. 239–56.
- Sarwal M, Chua M-S, Kambham N, Hsieh S-C, Satterwhite T, Masek M, et al. Molecular heterogeneity in acute renal allograft rejection identified by DNA microarray profiling. *N Engl J Med* (2003) **349**:125–38. doi:10.1056/NEJMoa035588
- Pham MX, Teuteberg JJ, Kfouri AG, Starling RC, Deng MC, Cappola TP, et al. Gene-expression profiling for rejection surveillance after cardiac transplantation. *N Engl J Med* (2010) **362**(20):1890–900. doi:10.1056/NEJMoa0912965
- Chaudhuri A, Ozawa M, Everly MJ, Ettenger R, Dharnidharka V, Benfield M, et al. The clinical impact of humoral immunity in pediatric renal transplantation. *J Am Soc Nephrol* (2013) **24**(4):655–64. doi:10.1681/asn.2012070663
- Roedder S, Sigdel T, Salomonis N, Hsieh S, Dai H, Bestard O, et al. The kSORT assay to detect renal transplant patients at high risk for acute rejection: results of the multicenter AART study. *PLoS Med* (2014) **11**(11):e1001759. doi:10.1371/journal.pmed.1001759
- Kohrt HE, Tian L, Li L, Alizadeh AA, Hsieh S, Tibshirani RJ, et al. Identification of gene microarray expression profiles in patients with chronic graft-versus-host disease following allogeneic hematopoietic cell transplantation. *Clin Immunol* (2013) **148**(1):124–35. doi:10.1016/j.clim.2013.04.013
- Mueller TF, Einecke G, Reeve J, Sis B, Mengel M, Jhangri GS, et al. Microarray analysis of rejection in human kidney transplants using pathogenesis-based transcript sets. *Am J Transplant* (2007) **7**(12):2712–22. doi:10.1111/j.1600-6143.2007.02005.x
- Vitalone MJ, Ganguly B, Hsieh S, Latek R, Kulbokas EJ, Townsend R, et al. Transcriptional profiling of belatacept and calcineurin inhibitor therapy in renal allograft recipients. *Am J Transplant* (2014) **14**(8):1912–21. doi:10.1111/ajt.12746
- Roedder S, Li L, Alonso MN, Hsieh SC, Vu MT, Dai H, et al. A three-gene assay for monitoring immune quiescence in kidney transplantation. *J Am Soc Nephrol* (2014) **26**(8):2042–53. doi:10.1681/asn.2013111239
- Anglicheau D, Sharma VK, Ding R, Hummel A, Snopkowski C, Dadhania D, et al. MicroRNA expression profiles predictive of human renal allograft status. *Proc Natl Acad Sci U S A* (2009) **106**(13):5330–5. doi:10.1073/pnas.0813121106
- Li L, Wadia P, Chen R, Kambham N, Naesens M, Sigdel TK, et al. Identifying compartment-specific non-HLA targets after renal transplantation by integrating transcriptome and “antibodyome” measures. *Proc Natl Acad Sci U S A* (2009) **106**(11):4148–53. doi:10.1073/pnas.0900563106
- Sutherland SM, Li L, Sigdel TK, Wadia PP, Miklos DB, Butte AJ, et al. Protein microarrays identify antibodies to protein kinase Czeta that are associated with a greater risk of allograft loss in pediatric renal transplant recipients. *Kidney Int* (2009) **76**(12):1277–83. doi:10.1038/ki.2009.384
- Butte AJ, Sigdel TK, Wadia PP, Miklos DB, Sarwal MM. Protein microarrays discover angiotensinogen and PRKRP1 as novel targets for autoantibodies in chronic renal disease. *Mol Cell Proteomics* (2011) **10**(3):M110.000497. doi:10.1074/mcp.M110.000497
- Sigdel TK, Kaushal A, Gritsenko M, Norbeck AD, Qian WJ, Xiao W, et al. Shotgun proteomics identifies proteins specific for acute renal transplant rejection. *Proteomics Clin Appl* (2010) **4**(1):32–47. doi:10.1002/prca.200900124
- Ling XB, Sigdel TK, Lau K, Ying L, Lau I, Schilling J, et al. Integrative urinary peptidomics in renal transplantation identifies biomarkers for acute rejection. *J Am Soc Nephrol* (2010) **21**(4):646–53. doi:10.1681/asn.2009080876
- Sigdel TK, Sarwal MM. The proteogenomic path towards biomarker discovery. *Pediatr Transplant* (2008) **12**(7):737–47. doi:10.1111/j.1399-3046.2008.01018.x
- Annesley TM, Clayton LT. Quantification of mycophenolic acid and glucuronide metabolite in human serum by HPLC-tandem mass spectrometry. *Clin Chem* (2005) **51**(5):872–7. doi:10.1373/clinchem.2004.047357
- Wishart DS. Metabolomics: a complementary tool in renal transplantation. *Contrib Nephrol* (2008) **160**:76–87. doi:10.1159/000125935

29. Wishart DS. Metabolomics in monitoring kidney transplants. *Curr Opin Nephrol Hypertens* (2006) **15**(6):637–42. doi:10.1097/01.mnh.0000247499.64291.52
30. Suthram S, Dudley JT, Chiang AP, Chen R, Hastie TJ, Butte AJ. Network-based elucidation of human disease similarities reveals common functional modules enriched for pluripotent drug targets. *PLoS Comput Biol* (2010) **6**(2):e1000662. doi:10.1371/journal.pcbi.1000662
31. Yang X, Deignan JL, Qi H, Zhu J, Qian S, Zhong J, et al. Validation of candidate causal genes for obesity that affect shared metabolic pathways and networks. *Nat Genet* (2009) **41**(4):415–23. doi:10.1038/ng.325
32. Butte AJ, Tamayo P, Slonim D, Golub TR, Kohane IS. Discovering functional relationships between RNA expression and chemotherapeutic susceptibility using relevance networks. *Proc Natl Acad Sci U S A* (2000) **97**(22):12182–6. doi:10.1073/pnas.220392197
33. Taylor IW, Linding R, Warde-Farley D, Liu Y, Pesquita C, Faria D, et al. Dynamic modularity in protein interaction networks predicts breast cancer outcome. *Nat Biotechnol* (2009) **27**(2):199–204. doi:10.1038/nbt.1522
34. Morgan AA, Khatri P, Jones RH, Sarwal MM, Butte AJ. Comparison of multiplex meta analysis techniques for understanding the acute rejection of solid organ transplants. *BMC Bioinformatics* (2010) **11**(Suppl 9):S6. doi:10.1186/1471-2105-11-S9-S6
35. Chen R, Sigdel TK, Li L, Kambham N, Dudley JT, Hsieh SC, et al. Differentially expressed RNA from public microarray data identifies serum protein biomarkers for cross-organ transplant rejection and other conditions. *PLoS Comput Biol* (2010) **6**(9):e1000940. doi:10.1371/journal.pcbi.1000940
36. Schots R, Van Riet I, Othman TB, Trullemans F, De Waele M, Van Camp B, et al. An early increase in serum levels of C-reactive protein is an independent risk factor for the occurrence of major complications and 100-day transplant-related mortality after allogeneic bone marrow transplantation. *Bone Marrow Transplant* (2002) **30**(7):441–6. doi:10.1038/sj.bmt.1703672
37. Vorlat A, Conraads VM, Jorens PG, Aerts S, Van Gorp S, Vermeulen T, et al. Donor B-type natriuretic peptide predicts early cardiac performance after heart transplantation. *J Heart Lung Transplant* (2012) **31**(6):579–84. doi:10.1016/j.healun.2012.02.009
38. Wang A, Du Y, He Q, Zhou C. A quantitative system for discriminating induced pluripotent stem cells, embryonic stem cells and somatic cells. *PLoS One* (2013) **8**(2):e56095. doi:10.1371/journal.pone.0056095
39. Wang A, Zhong Y, Wang Y, He Q. A web-server of cell type discrimination system. *ScientificWorldJournal* (2014) **2014**:459064. doi:10.1155/2014/459064
40. Einecke G, Reeve J, Sis B, Mengel M, Hidalgo L, Famulski KS, et al. A molecular classifier for predicting future graft loss in late kidney transplant biopsies. *J Clin Invest* (2010) **120**(6):1862–72. doi:10.1172/JCI41789
41. Bair E, Tibshirani R. Semi-supervised methods to predict patient survival from gene expression data. *PLoS Biol* (2004) **2**(4):E108. doi:10.1371/journal.pbio.0020108
42. Dabney AR. Classification of microarrays to nearest centroids. *Bioinformatics* (2005) **21**(22):4148–54. doi:10.1093/bioinformatics/bti681
43. Dudoit S, Fridlyand J, Speed TP. Comparison of discrimination methods for the classification of tumors using gene expression data. *J Am Stat Assoc* (2002) **97**:77–87. doi:10.1198/016214502753479248
44. Tibshirani R. Regression selection and shrinkage via the lasso. *J R Stat Soc Series B* (1994) **58**:267–88.
45. Zou H, Hastie T. Regularization and variable selection via the elastic net. *J R Stat Soc Ser B Stat Methodol* (2005) **67**:301–20. doi:10.1093/brain/awv075
46. Tibshirani R, Hastie T, Narasimhan B, Chu G. Diagnosis of multiple cancer types by shrunken centroids of gene expression. *Proc Natl Acad Sci U S A* (2002) **99**(10):6567–72. doi:10.1073/pnas.082099299
47. Reeve J, Einecke G, Mengel M, Sis B, Kayser N, Kaplan B, et al. Diagnosing rejection in renal transplants: a comparison of molecular- and histopathology-based approaches. *Am J Transplant* (2009) **9**(8):1802–10. doi:10.1111/j.1600-6143.2009.02694.x
48. Kurian SM, Williams AN, Gelbart T, Campbell D, Mondala TS, Head SR, et al. Molecular classifiers for acute kidney transplant rejection in peripheral blood by whole genome gene expression profiling. *Am J Transplant* (2014) **14**(5):1164–72. doi:10.1111/ajt.12671
49. Roedder S, Vitalone M, Khatri P, Sarwal MM. Biomarkers in solid organ transplantation: establishing personalized transplantation medicine. *Genome Med* (2011) **3**(6):37. doi:10.1186/gm253
50. San Segundo D, Millan O, Munoz-Cacho P, Boix F, Paz-Artal E, Talayero P, et al. High proportion of pretransplantation activated regulatory T cells (CD4+CD25highCD62L+CD45RO+) predicts acute rejection in kidney transplantation: results of a multicenter study. *Transplantation* (2014) **98**(11):1213–8. doi:10.1097/TP.0000000000000202
51. Lin D, Hollander Z, Ng RT, Imai C, Ignaszewski A, Balshaw R, et al. Whole blood genomic biomarkers of acute cardiac allograft rejection. *J Heart Lung Transplant* (2009) **28**(9):927–35. doi:10.1016/j.healun.2009.04.025
52. Mardia K, Kent J, Bibby JM. Multivariate analysis. *Analysis* (1979) **97**:1–4.
53. McCall MN, Bolstad BM, Irizarry RA. Frozen robust multiarray analysis (fRMA). *Biostatistics* (2010) **11**(2):242–53. doi:10.1093/biostatistics/kxp059
54. Hedges LV, Cooper H, Bushman BJ. Testing the null hypothesis in meta-analysis: a comparison of combined probability and confidence interval procedures. *Psychol Bull* (1992) **111**:188–94. doi:10.1037/0033-2909.111.1.188
55. Cleveland WS. Robust locally weighted regression and smoothing scatterplots. *J Am Stat Assoc* (1979) **74**:829–36. doi:10.1080/01621459.1979.10481038
56. Johnson WE, Li C, Rabinovic A. Adjusting batch effects in microarray expression data using empirical Bayes methods. *Biostatistics* (2007) **8**(1):118–27. doi:10.1093/biostatistics/kxj037
57. Wang A, Huang K, Shen Y, Xue Z, Cai C, Horvath S, et al. Functional modules distinguish human induced pluripotent stem cells from embryonic stem cells. *Stem Cells Dev* (2011) **20**(11):1937–50. doi:10.1089/scd.2010.0574

Conflict of Interest Statement: The authors declare that the research was conducted in the absence of any commercial or financial relationships that could be construed as a potential conflict of interest.

Copyright © 2015 Wang and Sarwal. This is an open-access article distributed under the terms of the Creative Commons Attribution License (CC BY). The use, distribution or reproduction in other forums is permitted, provided the original author(s) or licensor are credited and that the original publication in this journal is cited, in accordance with accepted academic practice. No use, distribution or reproduction is permitted which does not comply with these terms.

Emergent transcriptomic technologies and their role in the discovery of biomarkers of liver transplant tolerance

Sotiris Mastoridis, Marc Martínez-Llordella and Alberto Sanchez-Fueyo*

Institute of Liver Studies, King's College Hospital, London, UK

OPEN ACCESS

Edited by:

Giorgio Raimondi,
Johns Hopkins School of Medicine,
USA

Reviewed by:

Minnie M. Sarwal,
University of California San Francisco,
USA

Olivia M. Martinez,
Stanford University School of
Medicine, USA

Leonardo V. Riella,
Brigham and Women's Hospital,
USA

*Correspondence:

Alberto Sanchez-Fueyo,
Institute of Liver Studies, King's
College Hospital, Denmark Hill,
London SE59RS, UK
sanchez_fueyo@kcl.ac.uk

Specialty section:

This article was submitted to
Alloimmunity and Transplantation, a
section of the journal
Frontiers in Immunology

Received: 30 March 2015

Accepted: 27 May 2015

Published: 22 June 2015

Citation:

Mastoridis S, Martínez-Llordella M
and Sanchez-Fueyo A (2015)

Emergent transcriptomic
technologies and their role in the
discovery of biomarkers of liver
transplant tolerance.

Front. Immunol. 6:304.

doi: 10.3389/fimmu.2015.00304

Liver transplantation offers a unique window into transplant immunology due, in part, to the considerable proportion of recipients who develop immunological tolerance to their allograft. Biomarkers are able to identify and predict such a state of tolerance, and thereby able to establish suitable candidates for the minimization of hazardous immunosuppressive therapies, are not only of great potential clinical benefit but might also shed light on the immunological mechanisms underlying tolerance and rejection. Here, we review the emergent transcriptomic technologies serving as drivers of biomarker discovery, we appraise efforts to identify a molecular signature of liver allograft tolerance, and we consider the implications of this work on the mechanistic understanding of immunological tolerance.

Keywords: liver, transplant, tolerance, biomarkers, transcriptome, gene, transplantomics

Introduction

The liver represents a unique window to the immune system. Unlike other transplanted organs, it exhibits immunoregulatory, tolerogenic properties, enabling an allograft to be more readily spontaneously accepted. The phenomenon of operational tolerance, i.e., stable allograft function in spite of complete discontinuation of immunosuppressive therapy, while rarely achieved in cases of renal transplantation, for instance, is relatively commonplace in liver transplant recipients. Indeed, the prevalence of operational tolerance following liver transplantation appears to be far greater than previously appreciated. Until recent clinical trial evidence to the contrary, an average estimate was that approximately 20% of liver allograft recipients were able to successfully be weaned off immunosuppression, and thereby to achieve a state of induced operational tolerance (1, 2). Benítez and colleagues, however, showed that a remarkable 42% of 98 liver allograft recipients undergoing weaning of immunosuppression achieved operational tolerance. Furthermore, the propensity to tolerance was noted to develop over time, with those who had had their graft for 10.6 years or more achieving tolerance in 79.2% of cases (3). While these results should be taken with some caution, the inescapable implication is that a significant proportion of liver transplant recipients, particularly if in the second decade of graft survival, are unnecessarily subjected to immunosuppressive therapy and the significant risks associated with it. The incentive, therefore, to search for a biomarker by which to identify patients amenable to drug minimization, becomes clear. Furthermore, the pursuit of such biomarkers might aid in the fuller characterization of the immunological phenotype associated with tolerance, and so offer a mechanistic understanding of the processes by which tolerance is achieved and might be induced.

Major advances have been made in recent years in the fields of genetic and molecular biology. Large international collaborations such as the human genome and proteome projects enabled further

technological developments of high-throughput technologies. Broadly, with new technologies, arise new investigative paradigms. Reductionist scientific approaches have been overtaken, to an extent, by the generation of vast biological datasets enabling the study of complete sets of molecules. The umbrella neologism “omics” has appeared in order to describe these changes and to classify emerging fields – metabolomics, proteomics, transcriptomics, and so on. The systems biology approach has developed to offer a computational and mathematical framework enabling the integration and analysis of data from these seemingly disparate fields. The application of these developing fields to the arena of transplantation, with a view to the personalized treatment of patients, has recently been dubbed as “transplantomics” (4, 5).

Regarding the identification of biomarkers of tolerance, of all the emerging work in transplantomics, the high-throughput measurement of the transcriptome has shown the greatest promise and formed a focus of research. Here, we review the application of transcriptomic technologies to the unique window proffered by liver transplantation tolerance. We set out an overview of the technologies and of the associated analytical tools. We review recent progress in developing novel biomarkers of tolerance, and look at their application in trials of immunosuppression withdrawal. We discuss the limitations and pitfalls associated with high-throughput transcriptomic research. Finally, we consider the implications of these tools on our mechanistic understanding of operational tolerance and how this might guide future therapeutic developments.

Principles of Transcriptome Analysis

The “transcriptome” describes the complete set of messenger RNA (mRNA) and non-coding RNA (ncRNA) transcripts, which include micro RNA (miRNA), small nuclear RNA (snRNA), and small nucleolar RNA (snoRNA) among others. Comprehensive understanding of the transcriptome must also take into consideration further complexities – splicing isoforms, gene-fusion transcripts, post-translational modifications, and epigenetic controls for example. Thus, “Transcriptomics,” can be understood as the large-scale study of transcriptional products as well as their regulation and modification (5, 6).

Transcriptome Profiling

Transcriptome profiling can be subdivided into two general approaches for simplicity – the candidate gene strategy focuses on single gene transcripts, while high-throughput approaches allow for the simultaneous measurements of thousands of transcripts. The first candidate gene-based studies utilized the Northern Blot (7). This method fixed RNA on a solid support, following its separation by electrophoresis, and then the presence and abundance of the fixed RNA species of interest were deduced by hybridization with complementary labeled radioactive nucleic acid probes. The low throughput and requirement of large quantities of input RNA made this technique cumbersome. Reverse transcriptase polymerase chain reaction (RT-PCR) is now the method most commonly used for candidate gene transcript measurement and has broad applications in the clinical setting (8). In this approach, mRNA is reverse transcribed to complementary DNA (cDNA) and

amplified with primers specific for the gene of interest using PCR. Quantitative measures of mRNA abundance are made possible by monitoring the accumulation of PCR product (9). While the method requires only small quantities of input RNA, is robust, cost-effective, and rapid, the throughput remains in the order of hundreds of known transcripts at a time and so is not amenable to transcriptome-wide investigations (10).

Microarray technology, on the other hand, has enabled the rapid, simultaneous measurement of the whole transcriptome. mRNA is hybridized to an array of oligonucleotide or cDNA probes that are robotically spotted onto a solid support chip, thereby allowing the identity of each probe to be defined by its location. Hybridization intensity to a particular probe is related to the abundance of corresponding transcript (11, 12). Microarray technology has been applied to the gamut of transplantation biology over the last decade, including studies of acute and chronic rejection, and more relevant herein, the understanding of immune tolerance and identification of biomarkers. Microarrays have become the best standardized, most affordable, and widely accessible of the high-throughput omics technologies (13).

Microarray Experimental Design and Analysis

A typical microarray generates expression levels for thousands of genes, thereby producing vast quantities of data. The major challenge is to analyze and understand these data, to distinguish true from misleading signals on the one hand, and to uncover clinically relevant findings on the other. The steps typically involved in a microarray experiment are (i) experimental design, (ii) sample preparation and processing, and (iii) data analysis and interpretation. Careful experimental design is crucial. It depends heavily on the array technology used and, of course, on the research objectives (14, 15). Objectives are often characterized as either “class comparison” or “class prediction” (16). In this setting, the former describes attempts to identify genes differentially expressed between operationally tolerant recipients and another comparison group. The latter involves the development of multi-gene formulae able to predict which patients might exhibit tolerance based on their expression profiles. The high-dimensional datasets generated cannot be adequately analyzed with conventional comparative statistics. The complexity of analysis and the potential pitfalls require a team approach and a good understanding of the relevant software required for the steps of quality control, normalization, clustering, classification, and pathway analyses (8, 17).

More Data Herald More Challenges...

Rigorous quality control criteria help to ensure high quality data collection from arrays that are reproducible and comparable. The MicroArray Quality Control project (MAQC), an unprecedented, community-wide effort to appraise microarray reliability and quality control metrics, reported that, with careful experimental design and appropriate data transformation and analysis, data can be reproducible and comparable across laboratories, institutions, and researchers (18). A number of commercial software packages have been developed to aid the quality control process (19–22). Specialist software is also available to aid with data normalization, a crucial step in the conversion of raw data into scaled relative expression levels

(8, 23, 24). Statistical packages are also utilized for calculating differential expression, controlling for false positives, selecting significance cut-offs, the clustering of genes thought to be similar or co-regulated, and final pathway analyses, enabling the identification of gene sets associated with specific biological functions (25–27).

Much of the complexity involved in the statistical analyses stems not only from the high numbers of genes measured per sample (“curse of dimensionality”) but also the disproportion between this and the limited numbers of samples available for testing (“curse of scarcity”) – a difficulty often faced in biomarker research. This is overcome, in part, through adjusted *p*-values (*q*-value) such as false discovery rates (5). Tools for analysis are often free to download and now widely used. They include significance analysis of microarrays (SAM), GenePattern, and GenMAPP (5). Despite robust analytical tools, an undiscerning researcher can erroneously use data to “discover” sets of genes that are able to differentiate the samples on which the gene algorithm modeling was based even when the data are completely random. This problem should be circumvented by ensuring that a gene model is tested on a validation group that is independent from the training set used to create the model in the first place. This approach is more desirable than cross-validation techniques sometimes employed (28–30). Further, technical validation of microarray results on a different transcriptional platform, usually RT-PCR, is also recommended to minimize inter- or intra-platform variability in hybridization noise that may arise between batches or laboratories.

In order to verify the reproducibility of analyses and to corroborate clinical validity, public microarray databases serve as essential repositories. In the transplant setting, where studies often include only small numbers of recipients, these resources are especially important. The Functional Genomics Data (FGED) Society (formerly the MGED Society), a non-profit, volunteer run organization promoting the sharing of high-throughput research data, helped to define the Minimum Information About a Microarray Experiment (MIAME) guidelines for data content standards. The Society also set the standard data exchange format, known as the Microarray Genetic Expression Markup Language (MAGE-ML). Thorough reviews of the numerous databases in existence have been set out in the literature (31).

Microarray data output is necessarily dependent on the quality of the original biological samples. RNA is considerably more susceptible to rapid enzymatic degradation than DNA, thereby making efficient processing and appropriate storage using robust protocols essential. Microarrays offer snapshots of gene expression. The kinetics of transcripts and the variability of changing levels of expression in relation to their baseline remain little understood and so are not amenable to statistical interpretation (32, 33). Matters are further complicated by tissue heterogeneity, as is the case in blood samples for instance. This heterogeneity makes anatomical detail in the microarray approach difficult, in that it is difficult to know which cells’ gene expression profiles are being analyzed. Cell sorting and microdissection are ways to tackle this difficulty, as is the application of statistical deconvolution methods such as the cell-specific significance analysis of microarrays (csSAM) (34). While peripheral blood has been at the forefront of efforts to identify biomarkers, the possibility of interrogating RNA extracted

from paraffin embedded biopsies is a useful addition to investigative efforts.

It becomes clear then, that to discern biological fact from mere noise, it is essential that due attention is paid to the analytical complexities involved in microarray interpretation. Although, as we will see, microarray profiling has yielded important data in the pursuit of biomarkers of tolerance, and the technology is becoming more commonplace in transplantation research, the promise of emerging next-generation sequencing (NGS) technologies is likely to eclipse many microarray applications. In essence, NGS involves the sequential identification of the bases of small fragments of DNA from signals, which are emitted when each fragment is re-synthesized from a DNA template strand. By extending this process across millions of reactions in parallel, the technology enables rapid sequencing of large stretches of DNA base-pairs spanning entire genomes (35).

In part, the promise of NGS stems from sidestepping some of the aforementioned problems inherent in microarray technology. NGS is highly reliable, and has greater dynamic range as it directly quantifies discrete digital sequencing readouts as opposed to relying on hybridization steps. Loss of specificity due to cross-hybridization is controlled; the detection of rare and low abundance transcripts is made more achievable; the unbiased detection of novel transcripts is made possible since the need for transcript-specific probes utilized by microarray become redundant; and errors in probe design, which are relatively common in microarray chips, are avoided. In addition to these technical considerations, NGS technology is advancing at such a pace that the prospect of “sequencing everything” (genome, epigenome, transcriptome) in a timely and cost-effective manner is well within reach. In the 4 years between 2007 and 2011, a single sequencing run’s output increased 1000×, far outstripping Moore’s law, while the cost of sequencing the entire genome has fallen from over 150,000 USD in 2009, to less than 5000 USD in 2014 (36). Of course, NGS presents its own technological and bioinformatics challenges – which have been comprehensively reviewed elsewhere (37, 38).

Identification of Tolerance Biomarkers

Much hope has been placed upon transcriptomic technologies as the drivers of a “new era of individualized therapy” (4). The application of these technologies in the discovery of novel diagnostic and predictive markers has spanned diverse transplantation research fields, including the development of predictors of allograft risk, the identification of biomarkers of acute and chronic allograft injury, the assessment of organ suitability and viability during the preservation period, and forming the focus here, the discovery of biomarkers of tolerance.

Much of this work is in its infancy; transcriptomic investigation of biomarkers of liver allograft tolerance began less than a decade ago (39). Already though, biomarker-based diagnostic tests have gained regulatory approval and have reached the market (40–42). A diagnostic kit based on an 11-transcript set identified with microarray technology is used to non-invasively identify rejection in heart transplant recipients (41). As we will see, biomarkers of liver transplant tolerance have also yielded extremely promising results showing good potential for clinical translation in the near future.

Martínez-Llordella and colleagues were the first to use microarray technology for the gene expression profiling of blood samples from operationally tolerant liver transplant patients (39). This retrospective, cross-sectional study compared 16 operationally tolerant recipients to 16 recipients failing to undergo immunosuppression withdrawal, and found 462 positively and 166 negatively regulated genes. Functional analysis revealed that tolerance expression profiles were enriched in gamma-delta T ($\gamma\delta$ T) cells and natural killer (NK) cells (see Table 1). Genes involved in mRNA processing, protein biosynthesis, DNA repair, cell cycle control, Interleukin 2 receptor signaling, and transcription regulation were also noted to be differentially expressed. While this was a first step toward proof of principle, there were considerable methodological limitations. One difficulty common to all studies of tolerant patients is the selection of an appropriate control group. Stable transplant patients are sometimes used as a control, but the immunosuppressive medications they receive may skew any comparative interpretations. Another approach is to use healthy controls to circumvent the concerns with immunosuppressive therapy, but in this case the absence of transplantation becomes a

significant limitation in itself. Without a perfect control population, one reasonable approach is to use multiple control groups. In an attempt to address other methodological limitations with their first study, Martínez-Llordella's group followed up with a more robust analysis of a larger cohort of patients and incorporated both training and validation sets, as well as the necessary cross-validation checkpoint procedures (43). Of 1932 differentially expressed genes identified in this follow-up study, RT-PCR validation of 68 promising candidate genes was performed with good correlation shown between platforms. Utilizing a novel modeling approach based on the misclassified penalized posterior (MiPP) algorithm, three optimally parsimonious gene signatures were identified, containing 2, 6, and 7 genes, respectively, and altogether comprising 12 different genes (see Table 1). These signatures were shown to be capable of accurately predicting the clinical status not only of the group of recipients from whom they were derived but also of an independent validation cohort of 23 patients. When these gene signatures were evaluated against a cohort of stable recipients on maintenance immunosuppression, they predicted that 26% of these patients would be tolerant; a prediction that is

TABLE 1 | Studies using microarray transcriptomic profiling to identify biomarkers of liver transplant tolerance.

Study	Study population	Tissues analyzed	Microarray platform	Summary/significance	Reference
Martínez-Llordella (2007)	16 OLTT; 16 nOLTT	Blood	Affimetrix	Retrospective, cross-sectional study 462 up-regulated, 166 down-regulated genes identified OLTT expression profiles enriched in gamma-delta T cells and natural killer cells (CD94, NKG2D, NKG7, TRD@, KLRC1, KLRC2, KLRB1, CD160)	(39)
Kawasaki (2007)	11 OLTT; 11 HV	Blood	Agilent	Retrospective, cross-sectional study 627 up-regulated and 90 down-regulated genes identified No independent data validation steps performed	(46)
Martínez-Llordella (2008)	28 OLTT; 33 nOLTT	Blood	Affimetrix	Retrospective, cross-sectional study Identification of three gene signatures, containing 2, 6, and 7 genes, respectively, and altogether comprising 12 different genes (KLRF1, SLAMF7, NKG7, IL2RB, KLRB1, FANCG, GNPTAB, CLIC3, PSMD14, ALG8, CX3CR1, RGS3)	(43)
Lozano (2011)	12 OLTT; 12 nOLTT; 12 OKTT; 12 nOKTT; 12 HV	Blood	Affimetrix	Retrospective, cross-sectional study, multicenter study Enrichment of B cell-related transcript in OKTT, stable over time and across cohorts. Enrichment in natural killer cells in OLTT. Liver and kidney tolerant recipients exhibited distinct transcriptional and cell phenotypic patterns with little overlap	(47)
Bohne (2012)	33 OLTT; 42 AR	Blood and biopsy	Affimetrix	Prospective, multicenter trial of immunosuppressive withdrawal in liver transplant recipients Enrichment of natural killer and gamma-delta cell transcripts corroborated Accurate prognostic model developed using intragraft expression profiles, mainly enriched with genes involved in iron homeostasis	(48)
Li (2012)	Pediatric: 16 OLTT; 19 nOLTT; 6HV; 22 STA; 20 MIS Adult: 17 OLTT; 21 nOLTT; 19 STA	Blood	Affimetrix and Agilent	Amalgamation of publicly available gene-expression data, and data generated in two US centers of pediatric liver transplant recipients Identification of 13-gene signature, of high predictive accuracy, and independent of recipient age, donor type, and concomitant viral infection Enriched in natural killer cell transcripts (SENP6, FEM1C, ERBB2, AKR1C3, MAN1A1, UBAC2, GPR68, NFKB1, MAFG, BT3G, ASPH, PTBP2, PDE4DIP)	(49)

OLTT, patients exhibiting operational liver transplant tolerance; nOLTT, patients not achieving a state of operational liver transplant tolerance; OKTT, patients exhibiting operational kidney transplant tolerance; nOKTT, patients not achieving a state of operational kidney transplant tolerance; HV, healthy volunteer; STA, stable under standard immunosuppressive therapy; MIS, minimally immunosuppressed; AR, acute rejection.

roughly equivalent to the prevalence of tolerance indicated by the literature (1, 44, 45).

Mechanistic interpretations of these findings were hampered by the retrospective study design and the lack of simultaneous molecular analyses of allograft tissue. These issues were addressed in a prospective, multi-center immunosuppression withdrawal trial in liver transplant recipients, as reported by Bohne and colleagues (48). Of 75 recipients completing the trial, 42 underwent rejection, while 33 were successfully weaned off immunosuppression, thereby achieving a tolerant state. Microarray and RT-PCR analyses of both peripheral blood and the grafts themselves were conducted. While previous conclusions regarding peripheral blood mononuclear cell (PBMC) enrichment in NK and $\gamma\delta$ cells were corroborated, of special interest is the fact that, in side-by-side comparisons, liver tissue-derived transcriptional signatures proved more robust, accurate, and reproducible than PBMC derived signatures. The intragraft expression profile was mainly enriched with genes involved in iron homeostasis, and showed no overlap with genes identified from PBMC. The role of iron redistribution is a well-established antimicrobial strategy and has been shown to play a significant part in pathogenic infection of the liver, where iron overload is associated with poorer outcomes (50–52). Whether this is a property mediated through effects on pathogen growth, or on the host immune response itself is unclear. What this study is first to highlight, though, is the possibility that the dampening of alloreactive immune responses required for the establishment of tolerance may be dependent on the iron-store status of the allograft.

Liver biopsy tissue was also analyzed in a more recent study by Zhao and colleagues looking at a cohort of pediatric patients (53). While previous work had already identified the enrichment of $\gamma\delta$ T cell subpopulations and the genes associated with their expression in the peripheral blood of tolerant recipients, Zhao's group examined these cells at the transcriptional level within the graft itself. Two prominent subsets of $\gamma\delta$ T cells have been defined based on their δ chain – V δ 1 and V δ 2 T cells. V δ 2 cells are normally the predominant subset in blood and are involved in the inflammatory response. V δ 1 cells normally reside and are predominant in mucosal surfaces, possess potent immunoregulatory and suppressive capacities, and have been shown to emerge into the peripheral blood to a degree, which gives them predominance over V δ 2 cells in tolerant liver transplant recipients (39, 54). Zhao et al. showed that V δ 1 cells also accumulated within the grafts of operationally tolerant recipients in an antigen driven process, and that the complementarity-determining region 3 (CDR3) sequence of the δ chain of these V δ 1 cells specifically undergoes oligoclonal expansion, thereby suggesting that tolerance might be identified through sequencing analysis of these intragraft cells.

In the largest analysis of transcriptomic data pertaining to transplant tolerance, Li and colleagues extended previous work by developing a tolerance signature independent of recipient age and donor source, cause of end-stage liver disease, or concomitant viral infection (49). This was achieved through the amalgamation of living and deceased donor and pediatric, as well as adult data from across different clinical centers. The 13-gene tolerance signature identified (**Table 1**) was highly associated with NK cells, corroborating earlier work, and proved to have striking predictive

accuracy, exhibiting 100% sensitivity and 83% specificity. This degree of predictive capacity would appear to obviate the need for the biopsy derived gene signatures, thought to be of superior utility as biomarkers of tolerance in earlier studies (43).

The benefits of identifying robust non-invasive biomarkers over those derived from biopsy tissue are self-evident. Non-coding transcripts such as miRNAs have been shown to be more stable in peripheral blood than mRNA, have been shown to be implicated in the control of genes relevant to alloreactive immune responses, and with the advent of NGS techniques offer the promise of novel PBMC-derived tolerance signatures (55, 56). Using miRNA Taqman low-density arrays targeting 381 human miRNAs, Danger et al. reported on the modulation of expression of eight miRNAs in peripheral blood samples, nine tolerant kidney transplant recipients as compared to 10 patients with stable renal function under immunosuppression (57). They noted that B cells from the operationally tolerant group overexpressed miR-142-3p, and that this expression was not modulated by immunosuppression. The stability of miRNA in biofluids allowed Lorenzen et al. to investigate miRNA levels in the urine of a small retrospective cohort of kidney transplant recipients, and to identify miR-210 as a reliable marker of acute rejection and predictor of long-term graft function (58). In a multicentre cohort of renal allograft recipients, Suthanthiran and colleagues prospectively validated a three-gene urinary mRNA signature [interferon inducible protein 10 (IP-10) mRNA, 18S rRNA, and CD3e mRNA] (59). Their results represent a major step toward achieving non-invasive diagnosis and prediction of acute allograft rejection, and highlight the utility of pursuing biomarkers across varied tissue and biofluid samples. The success of miRNA biomarkers in studies of renal allograft tolerance and rejection has helped to instigate some early work in rodent models of liver transplant tolerance, while human studies are still awaited (60, 61).

As highlighted by miRNA biomarkers, it would be remiss to conclude this review of transcriptomic research into biomarkers of liver transplant tolerance without reference to the important cross-fertilization of ideas, of methodological approaches, and of data and sample sharing with research groups investigating kidney transplantation tolerance. Transcriptomic research into kidney transplantation faces some unique challenges, the scarcity of patients able to achieve operational tolerance being one important example. Fewer than 200 cases of kidney operational tolerance have been described over the last 40 years (62). Nevertheless, with the successful development of research consortia in this field, a number of transcriptional studies have been successfully undertaken (47, 63–69). Very broadly, these reports presented gene lists converging toward a B cell signature of tolerance, and in so doing corroborated other data showing that both the percentage and the absolute number of B cells are increased in operationally tolerant kidney allograft recipients (64, 65, 70, 71). Despite efforts to coordinate these studies, reports on kidney transplant tolerance have been extremely heterogeneous in terms of the techniques used, the controls groups drawn upon, and the various clinical profiles of the patients studied. Unsurprisingly then, overlap between the gene-markers identified between research groups has been poor, raising questions about their reliability and about their eventual applicability in clinical contexts (72).

Similarly, while identifying shared features of tolerance between kidney and liver transplant recipients would be helpful in finding common mechanistic processes underpinning tolerance induction, in developing therapeutic strategies, and in identifying novel biomarkers, it is the case that comparisons of data from disparate studies can be problematic. Array platforms often vary significantly in the probes they have in common; lymphochip and affymetrix chips, for instance, have only a few probes in common (43). Furthermore, in their direct comparison, employing the same transcriptional technology, Lozano et al. revealed an absence of significant overlap in blood phenotypic and transcriptional patterns between operationally tolerant liver and kidney recipients (47). Nevertheless, in recent work, the power of transplantomic technologies coupled with novel statistical techniques have helped to overcome many of these difficulties. This was exemplified by the recent identification of a common rejection molecule (CRM) across multiple transplanted organs (liver, kidney, heart, and lung) by Khatri and colleagues, who were able to compare and integrate data from several transcriptional studies by meta-analysis (73). The CRM consists of an 11-gene signature able to diagnose acute rejection with high sensitivity and specificity and could accurately predict future injury to a graft across all four organs. In recent months, a similar methodological approach was applied to integrate five of the disparate kidney transcriptional datasets aforementioned, in order to define a robust gene signature of operational tolerance (72). The meta-analytical methodology was able to reconcile the lack of overlap between the five studies, and to identify a gene-signature involving proliferation of B and CD4 T cells, and inhibition of CD14 monocytes. This gene signature, narrowed down to 20 biomarkers, underwent full cross validation, and was shown to be highly predictive in new samples and new patients, independent of the array technology used. It is critical that similar meta-analyses are performed on the liver tolerance datasets discussed here. The proof of the clinical utility of all these

predictive biomarker sets rests on their successful application in prospective studies of biomarker-targeted immunosuppression weaning within a randomized, controlled setting. This precisely, is the purpose of a large, European trial currently underway called “BIOmarker-Driven personalized IMunosuppression,” or BIO-DrIM (www.biodrim.eu).

Conclusion

The unique characteristics of the liver transplant setting, alongside the technological advances in transplantomic disciplines, which have enabled the discrimination of operational tolerance at a molecular level, present researchers with the opportunities to decipher the immunological mechanisms underlying drug-free allograft survival and to develop therapeutic targets aimed toward tolerance induction strategies.

The understanding that a large proportion of liver transplant recipients, particularly those living with their graft for a number of years, are over-immunosuppressed, must act to incentivize the translation of biomarker discovery into everyday clinical practice.

Emergent technologies, including next generation sequencing, must be capitalized upon to provide insights into normal, pathological, and pharmacological processes. As the diverse omics fields become more elaborate and produce ever more data, the collaboration between researchers, laboratories, hospitals and other institutions, and the integration of clinical and molecular data become essential to the pursuit of advancing the field of transplantation and developing personalized therapy.

Author Contributions

SM, MM-L, and AS-F all contributed to the conception, drafting, critical revision, and final approval of this work. All are accountable for its content.

References

- Heidt S, Wood KJ. Biomarkers of operational tolerance in solid organ transplantation. *Expert Opin Med Diagn* (2012) **6**:281–93. doi:10.1517/17530059.2012.680019
- Sawitzki B, Pascher A, Babel N, Reinke P, Volk H-D. Can we use biomarkers and functional assays to implement personalized therapies in transplantation? *Transplantation* (2009) **87**:1595–601. doi:10.1097/TP.0b013e3181a6b2cf
- Benítez C, Londoño M-C, Miquel R, Manzia T-M, Abraldes JG, Lozano J-J, et al. Prospective multicenter clinical trial of immunosuppressive drug withdrawal in stable adult liver transplant recipients. *Hepatology* (2013) **58**:1824–35. doi:10.1002/hep.26426
- Sarwal MM, Benjamin J, Butte AJ, Davis MM, Wood K, Chapman J. Transplantomics and biomarkers in organ transplantation: a report from the first international conference. *Transplantation* (2011) **91**:379–82. doi:10.1097/TP.0b013e3182105fb8
- Naesens M, Sarwal MM. Molecular diagnostics in transplantation. *Nat Rev Nephrol* (2010) **6**:614–28. doi:10.1038/nrneph.2010.113
- Martin JA, Wang Z. Next-generation transcriptome assembly. *Nat Rev Genet* (2011) **12**:671–82. doi:10.1038/nrg3068
- Alwine JC, Kemp DJ, Stark GR. Method for detection of specific RNAs in agarose gels by transfer to diazobenzyloxymethyl-paper and hybridization with DNA probes. *Proc Natl Acad Sci U S A* (1977) **74**:5350–4. doi:10.1073/pnas.74.12.5350
- Mueller TF, Mas VR. Microarray applications in nephrology with special focus on transplantation. *J Nephrol* (2012) **25**:589–602. doi:10.5301/jn.5000205
- Becker-André M, Hahlbrock K. Absolute mRNA quantification using the polymerase chain reaction (PCR). A novel approach by a PCR aided transcript titration assay (PATTY). *Nucleic Acids Res* (1989) **17**:9437–46. doi:10.1093/nar/17.22.9437
- Van Guilder HD, Vrana KE, Freeman WM. Twenty-five years of quantitative PCR for gene expression analysis. *Biotechniques* (2008) **44**:619–26. doi:10.2144/000112776
- Pozhitkov AE, Tautz D, Noble PA. Oligonucleotide microarrays: widely applied poorly understood. *Brief Funct Genomic Proteomic* (2007) **6**:141–8. doi:10.1093/bfgp/elm014
- Schena M, Shalon D, Davis RW, Brown PO. Quantitative monitoring of gene expression patterns with a complementary DNA microarray. *Science* (1995) **270**:467–70. doi:10.1126/science.270.5235.467
- Londoño MC, Danger R, Giral M, Souillou JP, Sánchez-Fueyo A, Brouard S. A need for biomarkers of operational tolerance in liver and kidney transplantation. *Am J Transplant* (2012) **12**:1370–7. doi:10.1111/j.1600-6143.2012.04035.x
- Olson NE. The microarray data analysis process: from raw data to biological significance. *NeuroRx* (2006) **3**:373–83. doi:10.1016/j.nurx.2006.05.005
- Slonim DK, Yanai I. Getting started in gene expression microarray analysis. *PLoS Comput Biol* (2009) **5**:e1000543. doi:10.1371/journal.pcbi.1000543
- Simon RM, Dobbin K. Experimental design of DNA microarray experiments. *Biotechniques* (2003) (Suppl):16–21.
- Naidu CN, Suneetha Y. Review article: current knowledge on microarray technology – an overview. *Trop J Pharm Res* (2012) **11**:1–12. doi:10.4314/tjpr.v11i1.20
- Editorial. Making the most of microarrays. *Nat Biotech* (2006) **24**:1039–1039.

19. Kauffmann A, Gentleman R, Huber W. arrayQualityMetrics – a bioconductor package for quality assessment of microarray data. *Bioinformatics* (2009) **25**:415–6. doi:10.1093/bioinformatics/btn647
20. Du P, Kibbe WA, Lin SM. lumi: a pipeline for processing Illumina microarray. *Bioinformatics* (2008) **24**:1547–8. doi:10.1093/bioinformatics/btn224
21. Luo W, Gudipati M, Jung K, Chen M, Marschke KB. Goober: a fully integrated and user-friendly microarray data management and analysis solution for core labs and bench biologists. *J Integr Bioinform* (2009) **6**:108. doi:10.2390/biecoll-jib-2009-108
22. Chatzioannou A, Moulos P, Kolisis FN. Gene ARMADA: an integrated multi-analysis platform for microarray data implemented in MATLAB. *BMC Bioinformatics* (2009) **10**:354. doi:10.1186/1471-2105-10-354
23. Quackenbush J. Computational analysis of microarray data. *Nat Rev Genet* (2001) **2**:418–27. doi:10.1038/35076576
24. Tárraga J, Medina I, Carbonell J, Huerta-Cepas J, Minguez P, Alloza E, et al. GEPAS, a web-based tool for microarray data analysis and interpretation. *Nucleic Acids Res* (2008) **36**:W308–14. doi:10.1093/nar/gkn303
25. Dinu I, Potter JD, Mueller T, Liu Q, Adewale AJ, Jhangri GS, et al. Improving gene set analysis of microarray data by SAM-GS. *BMC Bioinformatics* (2007) **8**:242. doi:10.1186/1471-2105-8-242
26. Bittner M, Meltzer P, Trent J. Data analysis and integration: of steps and arrows. *Nat Genet* (1999) **22**:213–5. doi:10.1038/10265
27. Vingron M. Bioinformatics needs to adopt statistical thinking. *Bioinformatics* (2001) **17**:389–90. doi:10.1093/bioinformatics/17.5.389
28. Simon R. Roadmap for developing and validating therapeutically relevant genomic classifiers. *J Clin Oncol* (2005) **23**:7332–41. doi:10.1200/JCO.2005.02.8712
29. Simon R, Radmacher MD, Dobbin K, McShane LM. Pitfalls in the use of DNA microarray data for diagnostic and prognostic classification. *J Natl Cancer Inst* (2003) **95**:14–8. doi:10.1093/jnci/95.1.14
30. Ioannidis JPA, Khouri MJ. Improving validation practices in “omics” research. *Science* (2011) **334**:1230–2. doi:10.1126/science.1211811
31. Penkett CJ, Bähler J. Navigating public microarray databases. *Comp Funct Genomics* (2004) **5**:471–9. doi:10.1002/cfg.427
32. Suter DM, Molina N, Gatfield D, Schneider K, Schibler U, Naef F. Mammalian genes are transcribed with widely different bursting kinetics. *Science* (2011) **332**:472–4. doi:10.1126/science.1198817
33. Raghavan A, Ogilvie RL, Reilly C, Abelson ML, Raghavan S, Vasdevani J, et al. Genome-wide analysis of mRNA decay in resting and activated primary human T lymphocytes. *Nucleic Acids Res* (2002) **30**:5529–38. doi:10.1093/nar/gkf682
34. Shen-Orr SS, Tibshirani R, Khatri P, Bodian DL, Staedtler F, Perry NM, et al. Cell type-specific gene expression differences in complex tissues. *Nat Meth* (2010) **7**:287–9. doi:10.1038/nmeth.1439
35. Hall N. Advanced sequencing technologies and their wider impact in microbiology. *J Exp Biol* (2007) **210**:1518–25. doi:10.1242/jeb.001370
36. Wetterstrand KA. *DNA Sequencing Costs: Data from The NHGRI Genome Sequencing Program (Gsp)*. Available from: www.genome.gov/sequencingcosts
37. Wolf JBW. Principles of transcriptome analysis and gene expression quantification: an RNA-seq tutorial. *Mol Ecol Resour* (2013) **13**:559–72. doi:10.1111/1755-0998.12109
38. Scherer A. Clinical and ethical considerations of massively parallel sequencing in transplantation science. *World J Transplant* (2013) **3**:62–7. doi:10.5500/wjt.v3.i4.62
39. Martínez-Llordella M, Puig-Pey I, Orlando G, Ramoni M, Tisone G, Rimola A, et al. Multiparameter immune profiling of operational tolerance in liver transplantation. *Am J Transplant* (2007) **7**:309–19. doi:10.1111/j.1600-6143.2006.01621.x
40. Ashton-Chess J, Giral M, Brouard S, Soulillou J-P. Spontaneous operational tolerance after immunosuppressive drug withdrawal in clinical renal allotransplantation. *Transplantation* (2007) **84**:1215–9. doi:10.1097/01.tp.0000290683.54937.1b
41. Pham MX, Teuteberg JJ, Kfouri AG, Starling RC, Deng MC, Cappola TP, et al. Gene-expression profiling for rejection surveillance after cardiac transplantation. *N Engl J Med* (2010) **362**:1890–900. doi:10.1056/NEJMoa0912965
42. Ashton-Chess J, Giral M, Mengel M, Renaudin K, Foucher Y, Gwinner W, et al. Tribbles-1 as a novel biomarker of chronic antibody-mediated rejection. *J Am Soc Nephrol* (2008) **19**:1116–27. doi:10.1681/ASN.2007101056
43. Martínez-Llordella M, Lozano J-J, Puig-Pey I, Orlando G, Tisone G, Lerut J, et al. Using transcriptional profiling to develop a diagnostic test of operational tolerance in liver transplant recipients. *J Clin Invest* (2008) **118**:2845–57. doi:10.1172/JCI35342
44. Pons JA, Yélamos J, Ramírez P, Oliver-Bonet M, Sánchez A, Rodríguez-Gago M, et al. Endothelial cell chimerism does not influence allograft tolerance in liver transplant patients after withdrawal of immunosuppression. *Transplantation* (2003) **75**:1045–7. doi:10.1097/01.TP.000058472.71775.7D
45. Tisone G, Orlando G, Cardillo A, Palmieri G, Manzia T-M, Baiocchi L, et al. Complete weaning off immunosuppression in HCV liver transplant recipients is feasible and favourably impacts on the progression of disease recurrence. *J Hepatol* (2006) **44**:702–9. doi:10.1016/j.jhep.2005.11.047
46. Kawasaki M, Iwasaki M, Koshiba T, Fujino M, Hara Y, Kitazawa Y, et al. Gene expression profile analysis of the peripheral blood mononuclear cells from tolerant living-donor liver transplant recipients. *Int Surg* (2007) **92**:276–86.
47. Lozano JJ, Pallier A, Martínez-Llordella M, Danger R, López M, Giral M, et al. Comparison of transcriptional and blood cell-phenotypic markers between operationally tolerant liver and kidney recipients. *Am J Transplant* (2011) **11**:1916–26. doi:10.1111/j.1600-6143.2011.03638.x
48. Bohne F, Martínez-Llordella M, Lozano J-J, Miquel R, Benítez C, Londoño M-C, et al. Intra-graft expression of genes involved in iron homeostasis predicts the development of operational tolerance in human liver transplantation. *J Clin Invest* (2012) **122**:368–82. doi:10.1172/JCI59411
49. Li L, Wozniak LJ, Rodder S, Heish S, Talisetti A, Wang Q, et al. A common peripheral blood gene set for diagnosis of operational tolerance in pediatric and adult liver transplantation. *Am J Transplant* (2012) **12**:1218–28. doi:10.1111/j.1600-6143.2011.03928.x
50. Weiss G. Iron and immunity: a double-edged sword. *Eur J Clin Invest* (2002) **32**(Suppl 1):70–8. doi:10.1046/j.1365-2362.2002.0320s1070.x
51. Wang L, Cherayil BJ. Ironing out the wrinkles in host defense: interactions between iron homeostasis and innate immunity. *J Innate Immun* (2009) **1**:455–64. doi:10.1159/000210016
52. Girelli D, Pasino M, Goodnough JB, Nemeth E, Guido M, Castagna A, et al. Reduced serum hepcidin levels in patients with chronic hepatitis C. *C. J Hepatol* (2009) **51**:845–52. doi:10.1016/j.jhep.2009.06.027
53. Zhao X, Li Y, Ohe H, Nafady-Hego H, Uemoto S, Bishop GA, et al. Intragraft V81 γδ T cells with a unique T-cell receptor are closely associated with pediatric semiallogeneic liver transplant tolerance. *Transplantation* (2013) **95**:192–202. doi:10.1097/TP.0b013e3182782f9f
54. Li Y, Koshiba T, Yoshizawa A, Yonekawa Y, Masuda K, Ito A, et al. Analyses of peripheral blood mononuclear cells in operational tolerance after pediatric living donor liver transplantation. *Am J Transplant* (2004) **4**:2118–25. doi:10.1111/j.1600-6143.2004.00611.x
55. Wei L, Gong X, Martinez OM, Krams SM. Differential expression and functions of microRNAs in liver transplantation and potential use as non-invasive biomarkers. *Transpl Immunol* (2013) **29**:123–9. doi:10.1016/j.trim.2013.08.005
56. Mas VR, Dumur CI, Scian MJ, Gehrau RC, Maluf DG. MicroRNAs as biomarkers in solid organ transplantation. *Am J Transplant* (2012) **13**:11–9. doi:10.1111/j.1600-6143.2012.04313.x
57. Danger R, Pallier A, Giral M, Martínez-Llordella M, Lozano J-J, Degauque N, et al. Upregulation of miR-142-3p in peripheral blood mononuclear cells of operationally tolerant patients with a renal transplant. *J Am Soc Nephrol* (2012) **23**:597–606. doi:10.1681/ASN.2011060543
58. Lorenzen JM, Volkmann I, Fiedler J, Schmidt M, Scheffner I, Haller H, et al. Urinary miR-210 as a mediator of acute t-cell mediated rejection in renal allograft recipients. *Am J Transplant* (2011) **11**:2221–7. doi:10.1111/j.1600-6143.2011.03679.x
59. Suthanthiran M, Schwartz JE, Ding R, Abecassis M, Dadhania D, Samstein B, et al. Urinary-cell mRNA profile and acute cellular rejection in kidney allografts. *N Engl J Med* (2013) **369**:20–31. doi:10.1056/NEJMoa1215555
60. Morita M, Chen J, Fujino M, Kitazawa Y, Sugioka A, Zhong L, et al. Identification of microRNAs involved in acute rejection and spontaneous tolerance in murine hepatic allografts. *Sci Rep* (2014) **4**:6649. doi:10.1038/srep06649
61. Wang Y, Tian Y, Ding Y, Wang J, Yan S, Zhou L, et al. MiR-152 may silence translation of CaMK II and induce spontaneous immune tolerance in mouse liver transplantation. *PLoS One* (2014) **9**:e105096. doi:10.1371/journal.pone.0105096
62. Dugast E, Chesneau M, Soulillou J-P, Brouard S. Biomarkers and possible mechanisms of operational tolerance in kidney transplant patients. *Immunol Rev* (2014) **258**:208–17. doi:10.1111/imr.12156
63. Brouard S, Mansfield E, Braud C, Li L, Giral M, Hsieh S-C, et al. Identification of a peripheral blood transcriptional biomarker panel associated with operational renal allograft tolerance. *Proc Natl Acad Sci U S A* (2007) **104**:15448–53. doi:10.1073/pnas.0705834104

64. Newell KA, Asare A, Kirk AD, Gisler TD, Bourcier K, Suthanthiran M, et al. Identification of a B cell signature associated with renal transplant tolerance in humans. *J Clin Invest* (2010) **120**:1836–47. doi:10.1172/JCI39933
65. Pallier A, Hillion S, Danger R, Giral M, Racapé M, Degauque N, et al. Patients with drug-free long-term graft function display increased numbers of peripheral B cells with a memory and inhibitory phenotype. *Kidney Int* (2010) **78**:503–13. doi:10.1038/ki.2010.162
66. Sagoo P, Perucha E, Sawitzki B, Tomiuk S, Stephens DA, Miqueu P, et al. Development of a cross-platform biomarker signature to detect renal transplant tolerance in humans. *J Clin Invest* (2010) **120**:1848–61. doi:10.1172/JCI39922
67. Braud C, Baeten D, Giral M, Pallier A, Ashton-Chess J, Braudeau C, et al. Immunosuppressive drug-free operational immune tolerance in human kidney transplant recipients: part I. Blood gene expression statistical analysis. *J Cell Biochem* (2008) **103**:1681–92. doi:10.1002/jcb.21574
68. Braudeau C, Ashton-Chess J, Giral M, Dugast E, Louis S, Pallier A, et al. Contrasted blood and intragraft toll-like receptor 4 mRNA profiles in operational tolerance versus chronic rejection in kidney transplant recipients. *Transplantation* (2008) **86**:130–6. doi:10.1097/TP.0b013e31817b8dc5
69. Danger R, Thervet E, Grisoni ML, Puig PL, Pallier A, Tregouet D, et al. PARVG gene polymorphism and operational renal allograft tolerance. *Transplant Proc* (2012) **44**:2845–8. doi:10.1016/j.transproceed.2012.09.034
70. Bluestone JA, Matthews JB. The immune tolerance network – an NIH/JDF-supported initiative to bring tolerance research into the clinic: a major new resource for clinical immunologists. *Clin Immunol* (2000) **96**:171–3. doi:10.1006/clim.2000.4892
71. Louis SP, Braudeau CC, Giral M, Dupont A, Moizant FDR, Robillard N, et al. Contrasting CD25hiCD4+T cells/FOXP3 patterns in chronic rejection and operational drug-free tolerance. *Transplantation* (2006) **81**:398–407. doi:10.1097/01.tp.0000203166.44968.86
72. Baron D, Ramstein GER, Chesneau MEL, Echasserau Y, Pallier A, Paul CE, et al. A common gene signature across multiple studies relate biomarkers and functional regulation in tolerance to renal allograft. *Kidney Int* (2015) **87**:1–12. doi:10.1038/ki.2014.395
73. Khatri P, Roedder S, Kimura N, De Vusser K, Morgan AA, Gong Y, et al. A common rejection module (CRM) for acute rejection across multiple organs identifies novel therapeutics for organ transplantation. *J Exp Med* (2013) **210**:2205–21. doi:10.1084/jem.20122709

Conflict of Interest Statement: The authors declare that the research was conducted in the absence of any commercial or financial relationships that could be construed as a potential conflict of interest.

Copyright © 2015 Mastoridis, Martínez-Llordella and Sanchez-Fueyo. This is an open-access article distributed under the terms of the Creative Commons Attribution License (CC BY). The use, distribution or reproduction in other forums is permitted, provided the original author(s) or licensor are credited and that the original publication in this journal is cited, in accordance with accepted academic practice. No use, distribution or reproduction is permitted which does not comply with these terms.

Computational biology: modeling chronic renal allograft injury

Mark D. Stegall^{1*} and Richard Borrows²

¹ Department of Surgery, von Liebig Transplant Center, Mayo Clinic, Rochester, MN, USA, ² Queen Elizabeth Hospital Centre, Nephrology, Birmingham, UK

New approaches are needed to develop more effective interventions to prevent long-term rejection of organ allografts. Computational biology provides a powerful tool to assess the large amount of complex data that is generated in longitudinal studies in this area. This manuscript outlines how our two groups are using mathematical modeling to analyze predictors of graft loss using both clinical and experimental data and how we plan to expand this approach to investigate specific mechanisms of chronic renal allograft injury.

OPEN ACCESS

Edited by:

Giorgio Raimondi,
Johns Hopkins School of Medicine,
USA

Reviewed by:

Maarten Naesens,
KU Leuven – University of Leuven,
Belgium

Paolo Cravedi,
Mount Sinai Hospital, USA

*Correspondence:

Mark D. Stegall,
Departments of Surgery and
Immunology, von Liebig Transplant
Center, Mayo Clinic, 200 First Street
SW, Rochester, MN 55905, USA
stegall.mark@mayo.edu

Specialty section:

This article was submitted to
Alloimmunity and Transplantation,
a section of the
journal Frontiers in Immunology

Received: 16 May 2015

Accepted: 13 July 2015

Published: 03 August 2015

Citation:

Stegall MD and Borrows R (2015)
Computational biology: modeling
chronic renal allograft injury.
Front. Immunol. 6:385.
doi: 10.3389/fimmu.2015.00385

Keywords: renal transplantation, computational biology, chronic renal allograft dysfunction, immunology, mathematical modeling

Introduction

Improving long-term renal allograft survival is one of the major unmet needs in organ transplantation. It is a sad fact that the rate of late graft loss (2–3%/year beyond the first year) appears to have changed little over the past two decades (1). While some progress has been made in understanding the multiple causes of late renal allograft loss, our picture is still incomplete (2, 3).

The goal of this manuscript is to outline how our two groups have already started to use mathematical modeling to analyze predictors of graft loss using both conventional clinical data and more detailed histologic and genomic data. We also outline how we plan to expand this approach going forward to investigate specific mechanisms of progressive injury.

Complexity of Transplant Outcomes

Post-transplant events are maddeningly complex. All renal allografts are exposed to at least one type of injury-causing process and most are exposed to several. Yet, the vast majority of grafts function quite well for many years. Serial surveillance biopsies suggest that several pathologic processes may lead to chronic injury ultimately resulting in graft loss (3). Importantly, these studies suggest that the process may be present for years before a clinically significant endpoint is reached and patients who seem to have similar pathologic processes may have very different outcomes. Some progress to graft loss, some develop chronic injury yet maintain function, and still others appear to have no injury. Subclinical inflammation and chronic antibody-mediated rejection due to donor-specific alloantibody (DSA) are two good examples. A remarkable calculus exists in which multiple different pathologic influences, occurring with varying frequency and severity at different time points, result in an almost linear rate of graft loss over many years in the entire population.

It is important to identify grafts that will fail at an early time point when the graft function is good and thus salvageable. Since not all grafts with DSA or subclinical inflammation will fail, it is also important to determine which features of the chronic immunologic injury process predispose to graft failure and thus develop specific therapy for progressors.

Our understanding of the mechanisms by which a biological process takes years to reach a clinically significant endpoint is lacking. However, mathematical modeling of increasingly comprehensive and complex data appears to be a promising path forward.

Modeling Renal Allograft Loss Using Clinical Factors

Mathematical models that aim to predict renal allograft outcomes based on clinical factors have been around for years. In the United States, the Federal Government through the Scientific Registry of Transplant Recipients issues “center-specific” expected outcomes for patient and graft survival based on a combination of donor and recipient factors present pretransplant (4). Combined, the C-statistic for this model is estimated to be only 0.6 (5). Two of the most important recipient factors affecting outcomes that are present pretransplant are age and diabetes.

However, renal transplantation is a dynamic process, and post-transplant events clearly affect outcomes. Several groups have tried to develop outcomes models based on post-transplant factors. One such model from Birmingham, UK, uses factors present at 1-year post-transplantation to predict graft survival at 5 years (6). The factors that go into the predictive formula are both demographic data and clinical data points present at 1 year including estimated glomerular filtration rate at 1 year, age at 1 year, recipient race, sex, presence of absence of rejection at 1 year, urinary albumin to creatinine ratio at 1 year, and serum albumin at 1 year. Risk scores were generated based on calculations of weighted coefficients from the regression analyses.

This “Birmingham Model” was validated in four independent cohorts from three other centers (Tours, France; Leeds, United Kingdom; and Halifax, Canada). It showed good discrimination for both overall graft failure (C statistics 0.75–0.81) and for death-censored graft failure (C statistics 0.78–0.90). Discrimination alone is insufficient to determine the utility of a risk model. Therefore, other measures were evaluated in the cohorts described above, specifically calibration (a comparison of rates of expected and observed outcomes across risk strata) and risk reclassification [evaluation of incremental accuracy of the model above and beyond accepted and existing measures, in this case renal function (eGFR)]. The “Birmingham Risk Score” similarly performed well across these domains.

However, other potentially important biological data were lacking from these studied datasets. Notably, histological data (specifically protocol biopsy findings at the 1-year time point post-transplantation) were not analyzed and anti-HLA antibodies (“alloantibody”) tested simultaneously were not evaluated. These potential “predictors” have much in common: they are both emerging risk factors for outcome, but are not yet universally incorporated into clinical practice; they require specialist analysis, which is time-consuming, labor-intensive, and expensive; the results require careful evaluation alongside clinical data; the results may be bewilderingly complex with a single “analysis” yielding multiple outputs, which may or may not be interdependent. It is for the former reasons that many centers do not collect these data, and it is for the latter reasons that detailed

mathematical and computational modeling is vital to understand their relevance.

Adding Histology and Alloantibody Data to Predictive Models

Histologic findings at 1 year have been shown to correlate with outcomes (7). In a recent collaborative study between the Birmingham group and the Mayo Clinic, Rochester, MN, USA, the Birmingham model was again validated in a Mayo Clinic population consisting primarily of living donor kidney transplants (8). In the Mayo cohort, the presence of glomerulitis (g) and chronic interstitial fibrosis (ci) found on 1 year protocol biopsy independently predicted 5-year graft failure. The presence of anti-class II donor-specific antibody (DSA) in the serum 1 year post-transplantation was also associated with adverse outcome. When a new prognostic model was developed by incorporating these standard histological qualifiers (by conventional light microscopy) alongside other clinical variables, discrimination (compared with the original Birmingham risk Score) was improved, with the C-statistic increasing from 0.84 to 0.90 (Figure 1). The stepwise addition of DSA data did not further improve discrimination, presumably because the presence of alloantibody-associated histological injury already “captured” the antibody effect. Furthermore, the new risk model improved calibration and (again, in comparison with the original model) resulted in statistically significant and clinically relevant risk reclassification with a net reclassification improvement (“NRI”) of 29% for the endpoint of death-censored graft survival ($p = 0.01$). The inclusion of both histology and antibody also resulted in improved reclassification of outcome, although with borderline statistical significance ($p = 0.11$).

Mathematical Modeling: A Method to Identify Mechanisms of Chronic Injury?

In reality, clinical factors such as age and race are simply surrogates for biological processes that cause graft loss. Similarly, non-specific laboratory findings, such as renal function and proteinuria, although good readouts for damage, do not provide

5-year Death Censored Graft Loss: Adding Histology to the Birmingham Model

	Model - 1	C-statistic
1. Histology only (g and ci)		
• H-L Test $p = 0.01$	Existing risk score	0.84 (0.78, 0.90)
• NRI 29% ($p < 0.001$)*	New model (g and ci)	0.90 (0.85, 0.95)
	Model - 2	C-statistic
2. Antibody only (Class II DSA MFI>800)		
• H-L Test $p = 0.32$	Existing risk score	0.82 (0.72, 0.92)
• NRI 1.2% ($p = 0.9$)*	New model (class II DSA)	0.83 (0.72, 0.94)
	Model - 3	C-statistic
3. Histology and Antibody		
• H-L Test $p = 0.53$	Existing risk score	0.76 (0.64, 0.89)
• NRI 14.4% ($p = 0.11$)*	New model (g, ci and class II DSA)	0.83 (0.69, 0.96)

*Compared Birmingham Model

FIGURE 1 | Data showing that the risk score C-statistic is improved by adding histology and calibration improves by adding antibody.

detailed insight into the actual mechanisms of renal allograft injury. As we move further down the pathway from non-specific data to more detailed data, we likely will not only reach higher levels of prediction but also begin to understand the underlying mechanisms of progressive injury. Using the approach outlined above, any type of molecular, histologic, or serologic data can be examined in mathematical models to determine its effect on outcome.

Molecular Signatures and Other Biomarkers

The past several years have seen the development of novel biomarkers and it is possible that the inclusion of some of these variables might further improve our ability to predict graft outcome. They might also improve our ability to diagnose specific pathologic processes and design intervention studies. These other approaches include gene expression and proteomic profiles in the graft, peripheral blood, or urine; more detailed DSA characterization, such as C1q binding; and/or more detailed histologic studies including immunohistochemistry for specific cell types of the infiltrates. Of these, “omics” studies deserve special mention here (9–19).

Gene expression signatures correlating with acute cellular rejection have been identified in peripheral blood and they are on their way to becoming clinically-available tests (13, 17). A signature has been identified in renal allograft biopsies that correlates with antibody-mediated rejection (9, 15). Other signatures have been identified that correlate with patients who are “operationally tolerant” (i.e., off immunosuppression and have stable kidney or liver allograft function). In addition, microRNA signatures have been correlated with rejection (18) and diabetic nephropathy (19).

It is likely that some of these molecular signatures also might be shown to correlate with late graft outcomes, but how well they actually predict graft loss is unclear. Currently, these primary value of these tests is that they appear to correlate well with known histologic findings and thus in some cases they may obviate the need for surveillance biopsies. Currently, none of these novel signatures is being used to identify progression of injury or is used in a model of chronic injury similar to the Birmingham model.

Another possible use of these omics data is that of a biomarker that would serve as a surrogate endpoint for clinical trials aimed at improving long-term graft survival. Under “accelerated approval,” the FDA might approve a drug based on its improving surrogate makers at an early time point (20). Longer-follow up would then be continued in Phase 3 studies to confirm improvement in the true clinical endpoint, such as graft survival. Thus, modeling the mechanisms of long-term graft survival will be important in the development of new therapeutics. Unfortunately, the development of effective biomarkers has been difficult in almost all fields of medicine and we must proceed down this pathway with some caution (21).

Other Mathematical Model Issues

There are several causes of late graft loss and each may require a different therapeutic approach. Thus, identifying specific subtypes of patients with a specific known injury process and then

modeling what aspects of that process are involved in progression will be an important path toward new therapy. One of the most important issues to consider when we begin to concentrate on subtypes of chronic injury is the issue of patient classification. Clearly identifying the phenotype categories will be important. We are unlikely to find the cause of progression in patients with alloantibody at 1 year if they are lumped together with all patients with low renal function at 1 year. Indeed, computational methods might be able to identify the phenotypes.

Another issue is dealing with several factors that are all part of the same process. For example, in the histologic study mentioned above, the inclusion of glomerulitis (a process associated with alloantibody) probably obviated the need to include DSA in order to improve the discrimination of the model. However, this does not mean that DSA is unimportant in chronic injury, and in fact is likely to be a major mechanistic driver. Underpowered studies also can lead to false-negative assessment in modeling and must be considered. There are far more “null” studies in transplantation than truly “negative” ones, and although the latter may inform practice, the former require recognition and refinement.

Mathematical modeling may identify the presence of processes for which we have no data. In the case of DSA, there is experimental data suggesting that an allograft may develop resistance of DSA, termed accommodation (22–24). Mathematically, this might be viewed as a “vector” that would favor graft survival even when erstwhile injury-causing stimuli are present. We then would be charged with searching for processes that might explain the observed outcomes. Sir Arthur Eddington might understand this (25).

Finally, when considering a process that occurs over many years, it is likely that other injury-causing events might also occur. For example, in the renal allograft setting, chronic hypertension, diabetes, nephrotoxicity from calcineurin inhibitors, and recurrent disease are just a few of the many possible injury stimuli that might also be occurring in addition to immunologic injury. Mathematical modeling also will likely able to control for all of the different injury processes present in the graft. It is likely that there will be common features and, hopefully, specific features. Separating other causes of injury from the primary process being studied adds yet another complicating factor in this type of research.

How to Optimize Mathematical Modeling in Transplantation?

We contend that a major impact of computational biology will be to enhance our ability to study chronic renal allograft injury in humans (**Table 1**). The critical component for these studies will be data –lots and lots of detailed, accurate data. Data regarding the recipient’s immune response and biomarkers that are related to the pathologic process under study would be helpful. Mechanistic studies done in parallel to focused clinical trials also would be tremendously useful. For example, combining gene expression studies with a trial of an agent that specifically blocks one pathway (e.g., eculizumab or IL-6 receptor) might provide new insight into why grafts fail.

We also need detailed long-term data beyond what is currently available. Graft survival at 5 years is just the beginning.

TABLE 1 | Possible approaches to using computational biology to studying chronic renal allograft injury.

- Comprehensive assessment of subjects
 - Immune system assays
 - Target tissue assessment
- Long-term studies with serial assessments
- Biomarkers related to the biology/targeted interventions
 - Omics studies of peripheral blood lymphocytes, serum, plasma, urine, or tissue
 - Detailed alloantibody studies

What happens between 5 and 10 years? We need to model these later time points and this will require data that are rarely captured.

In most disease groups, there are many phenotypes and small numbers of patients in each phenotype. Thus, in order to study sufficient numbers of patients, these studies will need to be

References

1. Lamb KE, Lodhi S, Meier-Kriesche H-U. Long-term renal allograft survival in the United States: a critical reappraisal. *Am J Transplant* (2011) **11**:450–62. doi:10.1111/j.1600-6143.2010.03283.x
2. El-Zoghby ZM, Stegall MD, Lager DJ, Kremers WK, Amer H, Gloor JM, et al. Identifying specific causes of kidney allograft loss. *Am J Transplant* (2009) **9**:527–35. doi:10.1111/j.1600-6143.2008.02519.x
3. Stegall MD, Gaston RS, Cosio FG, Matas A. Through a glass darkly: seeking clarity in preventing late kidney transplant failure. *J Am Soc Nephrol* (2015) **26**:20–9. doi:10.1681/ASN.2014040378
4. Available from: http://www.srtr.org/csr/current/Centers/201412/all_csr_documentation.pdf
5. Wolfe RA, McCullough KP, Schaubel DE, Kalbfleisch JD, Murray S, Stegall MD, et al. Calculating life years from transplant (LYFT): methods for kidney and kidney-pancreas candidates. *Am J Transplant* (2008) **8**:997–1011. doi:10.1111/j.1600-6143.2008.02177.x
6. Shabir S, Halimi JM, Cherukuri A, Ball S, Ferro C, Lipkin G, et al. Predicting 5-year risk of kidney transplant failure: a prediction instrument using data available at 1 year posttransplantation. *Am J Kidney Dis* (2014) **4**:643–51. doi:10.1053/j.ajkd.2013.10.059
7. Cosio FG, Grande JP, Wadei H, Larson TS, Griffin MD, Stegall MD. Predicting subsequent decline in kidney allograft function from early surveillance biopsies. *Am J Transplant* (2005) **5**:2464–72. doi:10.1111/j.1600-6143.2005.01050.x
8. Moreno-Gonzalez M, Bentall A, Borrows R, Stegall MD. Predicting 5-year risk of kidney transplant failure: does histology add to clinical parameters available at 1 year post-transplantation? *Am J Transplant* (2015) **15**:1. doi:10.1111/ajt.13359
9. Sis B, Jhangri GS, Bunnag S, Allanach K, Kaplan B, Halloran PF. Endothelial gene expression in kidney transplants with alloantibody indicates antibody-mediated damage despite lack of C4d staining. *Am J Transplant* (2009) **9**:2312–23. doi:10.1111/j.1600-6143.2009.02761.x
10. Park WD, Griffin MD, Cornell LD, Cosio FG, Stegall MD. Fibrosis with inflammation at one year predicts transplant functional decline. *J Am Soc Nephrol* (2010) **21**:1987–97. doi:10.1681/ASN.2010010049
11. Newell KA, Asare A, Kirk AD, Gisler TD, Courcier K, Suthanthiran M, et al. Identification of a B cell signature associated with renal transplant tolerance in humans. *J Clin Invest* (2010) **120**:1836–47. doi:10.1172/JCI39933
12. Baron D, Ramstein G, Chesneau M, Echasserau Y, Pallier A, Paul C, et al. A common gene signature across multiple studies relate to biomarkers and functional regulation in tolerant to renal allograft. *Kidney Int* (2015) **87**:984–95. doi:10.1038/ki.2014.395
13. Kurian SM, Williams AN, Gelbart T, Campbell D, Mondala TS, Head SR, et al. Molecular classifiers for acute kidney transplant rejection in peripheral blood by whole genome gene expression profiling. *Am J Transplant* (2014) **14**:1164–72. doi:10.1111/ajt.12671
14. Kurian SM, Fournaschen SM, Langfelder P, Horvath S, Shaked A, Salomon DR, et al. Genomic profiles and predictors of early allograft dysfunction after human liver transplantation. *Am J Transplant* (2015) **15**:1605–14. doi:10.1111/ajt.13145
15. Loupy A, Lefaucheur C, Vernerey D, Chang J, Hidalgo LG, Beuscart T, et al. Molecular microscope strategy to improve risk stratification in early antibody-mediated kidney allograft rejection. *J Am Soc Nephrol* (2014) **25**:2267–77. doi:10.1681/ASN.2013111149
16. Roedder S, Li L, Alonso MN, Hsieh SC, Vu MT, Dai H, et al. A three-gene assay for monitoring immune quiescence in kidney transplantation. *J Am Soc Nephrol* (2014). doi:10.1681/ASN.2013111239
17. Roedder S, Sigdal T, Salamonis N, Hsieh S, Dai H, Bestard O, et al. The kSORT assay to detect renal transplant patients at high risk for acute rejection: results of the multicenter AART study. *PLoS Med* (2014) **11**:e1001759. doi:10.1371/journal.pmed.1001759
18. Anglicheau D, Sharma VK, Ding R, Hummel A, Snopkowski C, Dadhania D, et al. MicroRNA expression profiles predictive of human renal allograft status. *Proc Nat Acad Sci U S A* (2009) **106**:5330–5. doi:10.1073/pnas.0813121106
19. Bijkerk R, Duijs JM, Khairoun M, Ter Horst CJ, van der Pol P, Mallat MJ, et al. Circulating microRNAs associate with diabetic nephropathy and systemic microvascular damage and normalize after simultaneous pancreas-kidney transplantation. *Am J Transplant* (2015) **15**:1081–90. doi:10.1111/ajt.13072
20. Subpart H. *Accelerate Approval for New Drugs for Serious or Life-Threatening Illnesses* 20xx. Available from: <http://www.accessdata.fda.gov/scripts/cdrh/cfdocs/cfcfr/CFRSearch.cfm?CFRPart=314&showFR=1&subpartNode=21:5.0.1.1.4.8>
21. Ioannidis JPA. Biomarkers failures. *Clin Chem* (2013) **59**:202–4. doi:10.1373/clinchem.2012.185801
22. Koch CA, Khalpey ZI, Platt JL. Accommodation: preventing injury in transplantation and disease. *J Immunol* (2004) **172**:5143–8. doi:10.4049/jimmunol.172.9.5143
23. Chen Song S, Zhong S, Xiang Y, Li JH, Guo H, Wang WY, et al. Complement inhibition enables renal allograft accommodation and long-term engraftment in presensitized nonhuman primates. *Am J Transplant* (2011) **11**:2057–66. doi:10.1111/j.1600-6143.2011.03646.x
24. Dorling A. Transplant accommodation – are the lessons learned from xenotransplantation pertinent for clinical allotransplantation? *Am J Transplant* (2012) **12**:545–53. doi:10.1111/j.1600-6143.2011.03821.x
25. Available from: http://www.wired.com/2009/05/dayintech_0529/

multicenter and very collaborative and we may need to combine data from many different databases.

Finally, studying a complex biologic process, such as chronic injury, probably will require a change in mindset among researchers. We tend to strive to make model systems as simple as possible with as few variables. While this makes for good science, it may be an inadequate approach to studying chronic injury.

Summary

The application of computational biology to transplantation seems to be a natural progression of both fields. The interaction between mathematicians and transplant biologists will likely lead to novel new interpretations of phenomena and new understanding of the mechanisms of chronic injury.

Conflict of Interest Statement: Mark D. Stegall has research contracts or consulting with Alexion, Astellas, Millennium, True North, Immunocor, and Genentech. Richard Borrows declares no conflict of interest.

Copyright © 2015 Stegall and Borrows. This is an open-access article distributed under the terms of the Creative Commons Attribution License (CC BY). The use, distribution or reproduction in other forums is permitted, provided the original author(s) or licensor are credited and that the original publication in this journal is cited, in accordance with accepted academic practice. No use, distribution or reproduction is permitted which does not comply with these terms.



PD1-Expressing T Cell Subsets Modify the Rejection Risk in Renal Transplant Patients

Rebecca Pike^{1†}, Niclas Thomas^{1†}, Sarita Workman¹, Lyn Ambrose¹, David Guzman¹, Shivajanani Sivakumaran¹, Margaret Johnson², Douglas Thorburn³, Mark Harber⁴, Benny Chain^{1‡} and Hans J. Stauss^{1*}

¹Institute of Immunity and Transplantation, University College London, London, UK, ²Department of HIV Medicine, Royal Free London NHS Foundation Trust, London, UK, ³Sheila Sherlock Liver Centre, Royal Free London NHS Foundation Trust, London, UK, ⁴Department of Renal Medicine, Royal Free London NHS Foundation Trust, London, UK

OPEN ACCESS

Edited by:

Kathryn Wood,
University of Oxford, UK

Reviewed by:

Nuala Mooney,
Centre National pour la Recherche
Scientifique, France

Philippe Saas,

Etablissement Français du Sang
BFC, France

*Correspondence:

Hans J. Stauss
h.stauss@ucl.ac.uk

[†]Rebecca Pike and Niclas Thomas
were joint first authors.

[‡]Benny Chain and Hans J. Stauss
were joint senior authors.

Specialty section:

This article was submitted to
Alloimmunity and Transplantation,
a section of the journal
Frontiers in Immunology

Received: 22 January 2016

Accepted: 21 March 2016

Published: 11 April 2016

Citation:

Pike R, Thomas N, Workman S,
Ambrose L, Guzman D,
Sivakumaran S, Johnson M,
Thorburn D, Harber M, Chain B and
Stauss HJ (2016) PD1-Expressing T
Cell Subsets Modify the Rejection
Risk in Renal Transplant Patients.
Front. Immunol. 7:126.
doi: 10.3389/fimmu.2016.00126

We tested whether multi-parameter immune phenotyping before or after renal transplantation can predict the risk of rejection episodes. Blood samples collected before and weekly for 3 months after transplantation were analyzed by multi-parameter flow cytometry to define 52 T cell and 13 innate lymphocyte subsets in each sample, producing more than 11,000 data points that defined the immune status of the 28 patients included in this study. Principle component analysis suggested that the patients with histologically confirmed rejection episodes segregated from those without rejection. Protein death 1 (PD-1)-expressing subpopulations of regulatory and conventional T cells had the greatest influence on the principal component segregation. We constructed a statistical tool to predict rejection using a support vector machine algorithm. The algorithm correctly identified 7 out of 9 patients with rejection, and 14 out of 17 patients without rejection. The immune profile before transplantation was most accurate in determining the risk of rejection, while changes of immune parameters after transplantation were less accurate in discriminating rejection from non-rejection. The data indicate that pretransplant immune subset analysis has the potential to identify patients at risk of developing rejection episodes, and suggests that the proportion of PD1-expressing T cell subsets may be a key indicator of rejection risk.

Keywords: transplantation, rejection, T cells, protein death 1, risk factor

INTRODUCTION

Transplantation remains a life saving treatment for patients with kidney failure. Due to improvement in organ preservation, advances in surgical technologies, and the use of potent immune suppressive treatment regimens, the incidence of acute rejection has dramatically decreased in the recent past. However, despite potent immune suppression, approximately 20% of patients still develop acute rejection episodes (1). Such episodes predispose to chronic antibody-mediated rejection, tubule-interstitial fibrosis, and atrophy, resulting in irreversible damage and failure of the transplanted kidney. A registry study of 63,045 renal transplant patients showed that acute rejection episodes were the single most important predictor of chronic allograft nephropathy, increasing the risk of graft failure by 5.2-fold compared to patients without episodes of acute rejection (2). The loss or damage of a renal

transplant secondary to rejection has substantial consequences for patients in terms of increased all cause mortality. Acute rejection episodes result in an increased burden of immunosuppression contributing to the high rate of infectious and cancer-related deaths in the transplant population. Furthermore, graft loss has very substantial financial repercussions, as the annual cost of providing dialysis is approximately six times that of supporting a stable transplant.

Because of the importance of avoiding rejection and the consequences of unnecessary over-immunosuppression there is an ongoing search for biomarkers, which can identify the risk of rejection. Preexisting antibodies to donor HLA are an established risk factor for acute rejection (3). Soluble CD30, a member of the TNF receptor superfamily, which is expressed on T cells and shed into blood, has received considerable attention, but the predictive power of this marker is still not clear (4). More recently, a transcriptomic analysis has identified a panel of 17 genes whose expression can identify rejection episodes without the need for biopsy, and can predict rejection episodes up to 3 months before rejection can be observed histologically (5). The screening for expression of a set of five genes has been similarly used to identify patients with episodes of acute rejection (6). We were particularly interested in exploring whether pre-transplantation immune-profiling might provide a tool to predict those patients at risk of rejection, which would inform patient management and allow clinicians to adjust the dosing parameters of immunosuppressive medication accordingly.

Hence, we have performed a multi-parameter flow cytometry analysis of adaptive and innate lymphocyte subsets in the peripheral blood of renal transplant patients before and in the first 12 weeks after transplantation. Using statistical machine learning algorithms to analyze this complex data set, we find that the pretransplant immune-phenotype predicts the risk of acute rejection episodes, and that the proportion of PD1-expressing regulatory and conventional T cells is a key component of the predictive signature. These results suggest a strategy for developing personalized immune suppressive regimes according to the predicted rejection risk assessed prior to transplantation.

MATERIALS AND METHODS

Patients

The Immune Monitoring Study was conducted at the Royal Free Hospital, London, between May 2011 and October 2014. The study protocol was approved by the National Research Ethics Committee. All patients ($n = 28$) had given written informed consent to participate in the study, and participants were of diverse age and ethnicity. Clinical details and patient demographics are shown in **Table 1**. Blood samples were collected from patients pretransplant and posttransplant. For live donor organ recipients, pretransplant samples were taken before immunosuppression was started, and on the day of transplant. For cadaveric donor organ recipients, pretransplant samples were taken before immunosuppression on the day of transplant. After transplant, weekly samples were taken until week 12 posttransplant for all patients. All samples were taken before starting immunosuppression.

Patients received the following immunosuppressive medications: 20 mg Basiliximab monoclonal antibody (anti-CD25) therapy on the day of transplant and on day 4 after transplant. Five hundred milligram intravenous methylprednisolone on the day of transplant followed by 40 mg intravenous methylprednisolone for 3 days after transplant, then 20 mg of oral prednisolone for 7 days, followed by 7 days of 5 mg oral prednisolone. Tacrolimus was given with dose adjusted according to plasma levels. 1 g of Mycophenolate Mofetil for 1 month, 750 mg for a further 2 months, reduced to 500 g by 3 months posttransplant. Live donor recipients received both Tacrolimus and Mycophenolate Mofetil from ~2 weeks before transplant, while cadaveric donor recipients received these from the day of transplant. Both groups of patients continue with these medications indefinitely.

Rejection

In cases of unexplained increased serum creatinine levels, patients underwent kidney biopsy, and rejection of the kidney allograft was confirmed by histological analysis. Rejection was either cell-mediated (characterized by infiltration of lymphocytes and inflammatory cells into the organ) or antibody-mediated (characterized by C4d deposition in the organ and circulating donor-specific antibodies). Rejection was treated with steroids and/or modification of maintenance immunosuppression.

Blood Samples

Peripheral blood mononuclear cells (PBMCs) were separated from whole blood by means of density gradient centrifugation, and were stored at -180°C in vapor-phase nitrogen in the UCL-RFH Biobank. Samples were analyzed for flow cytometry no more than 3 years after storage.

Flow Cytometry

Multi-parametric flow cytometry was used for immunophenotyping. PBMC (1×10^6) were stained with a T-cell panel, an innate lymphoid panel or with an isotype control panel. Before antibody labeling, cells were incubated with purified human IgG (Sigma) to reduce non-specific binding. Cells were stained with mAbs against CD3-PE Cy7 (clone SK7), CD4-BD Horizon v500 (clone RPA-T4), CD8-BD Horizon v450 (clone RPA-T8), CD45R0-PECF594 (clone UCHL1), CD62L-APC (clone DREG-56), CD25-APC Cy7 (clone M-A251), CD127-FITC (clone HIL-7R-M21), CD279-PE (clone EH12.2H7) (Biolegend), HLA-DR-PerCP Cy5.5 (clone LN3) (eBioscience), CD16-APC H7 (clone 3G8), CD56-APC (clone NCAM 16.2), iNKT-PE (6B11), V82-FITC (clone B6), IgG1k-APC Cy7 (clone MOPC-21), IgG1k-APC (clone MOPC-21) (Biolegend), IgG1k-FITC (clone MOPC-21) (Biolegend), IgG1k-PE (clone MOPC-21) (Biolegend), and IgG2b-PerCP Cy5.5 (clone N/S) (eBioscience). Antibodies were from BD Biosciences unless stated otherwise.

Flow Cytometric Analysis

Flow cytometric analysis was carried out using a BD LSRFortessa™ cytometer with BD FACSDiva™ software v.6.0.1 (BD Biosciences). The data were analyzed using FlowJo v7.6.5 software (Treestar Inc.). Gates for CD25⁺, CD127⁺, PD-1⁺, and

TABLE 1 | Further clinical details and demographic of patients included in this study.

No.	Donor	Age	Ethnicity	CMV status	HLA mis-match	Original disease	Dialysis or not	Sensitization	Post-tx CMV viremia	Rejection	Other information
1	Live	33	White	D+ R-	111	Dialysis	Donor specific Abs: low level DQ2	Yes	Yes, cellular, 6 months		
2	Cadaveric	51	White	D+ R+	121	ADPKD	Dialysis	Not sensitized	Yes, D7	Yes, cellular, W1–2	
3	Live	49	White	D– R–	112	Familial Hyperuricaemic nephropathy	Predialysis	Not sensitized	No	Yes, cellular, W9	
4	Cadaveric	72	Black African	D+ R+	121	Small kidneys	Dialysis	Not sensitized	Yes, W4–6	Yes, cellular, W2	
5	Cadaveric	49	White	D– R+	110	MPGN	Dialysis	Not sensitized	No	Yes, cellular, W2 and W18	
6	Live	63	White	D+ R+	000	Small kidneys	Dialysis	Not sensitized	No	Yes, cellular, 12 months	
7	Cadaveric	25	Black African	D+ R+	111	Reduced nephron mass and hypertension	Dialysis	Not sensitized	No	Yes, cellular, 2 years	ABO _i , baseline postimmunosuppression
8	Live	52	White	D+ R+	122	ADPKD	Predialysis	Sensitized B8, B16, B35, A33 No DSA	No	Yes, cellular, 2 months	
9	Cadaveric	40	White	D+ R+	022	Proliferative glomerulonephritis	Dialysis	Not sensitized	Yes, low	Yes, cellular, W2	
10	Live	46	White and Black Car.	D+ R–	121	AA amyloid	Predialysis	Not sensitized	No	Yes, Ab-mediated, W1–3	HCV ⁺
11	Live	50	Black African	D+ R+	011	Type-2 diabetes	Dialysis	Not sensitized	Yes	Yes, cellular, W1	
12	Live	39	White	D+ R–	011	ADPKD	Predialysis	DSA low level DR1	Yes	No	
13	Live	33	White	D+ R+	111	Small kidneys	Predialysis	Not sensitized	No	No	HBV ⁺
14	Cadaveric	57	White	D+ R+	211	Small kidneys	Dialysis	Not sensitized	Yes, W7–9	No	
15	Live	33	Black African	D+ R+	111	Small kidneys	Dialysis	Sensitized cw5, cw7, B8. No DSA	No	No	
16	Live	65	Black	D– R+	011	Ischemic nephropathy	Dialysis	Sensitized B82, B81, B55, B54, B42. No DSA	Yes	No	
17	Live	26	White	D– R–	111	HSP	Predialysis	Not sensitized	No	No	
18	Live	46	Asian	D+ R+	222	IgA nephropathy	Predialysis	Not sensitized	Yes, W10–12	No	
19	Live	31	Asian	D– R–	110	Small kidneys	Predialysis	Sensitized A34 No DSA	No	No	
20	Cadaveric	53	Asian Indian	D+ R+	111	Renovascular disease	Dialysis	Not sensitized	No	No	

(Continued)

TABLE 1 | Continued

No.	Donor	Age	Ethnicity	CMV status	HLA mis-match	Original disease	Dialysis or not	Sensitization	Post-transplant CMV viremia	Rejection	Other information
21	Live	38	Mixed	D-R+	210	IgA nephropathy	Predialysis	Not sensitized	No	No	
22	Live	23	White	D+R-	000	Renal dysplasia	Dialysis	Sensitized B45, B76, B82, B44, A1	Yes, W7-9	No	
23	Cadaveric	40	Black African	D-R+	220	Hypertension	Predialysis	Sensitized B52, B45	No	No	
24	Live	33	White British	D-R-	111	Type 1 diabetes	Dialysis	Not sensitized	No	No	
25	Live	46	Any other white British	D+R+	111	HSP	Dialysis	Sensitized A11	No	No	
26	Live	23	Black African	D+R+	000	Vasculitis	Predialysis	Not sensitized	No	No	
27	Live	46	Any other black	D+R+	001	Hypertension	Predialysis	Not sensitized	No	No	
28	Live	38	Other—not stated	D+R+	110	IgA nephropathy	Predialysis	Not sensitized	No	No	

W, week; D, day; ABO, ABO incompatible; HCV, hepatitis C virus; HBV, hepatitis B virus; HIV, human immunodeficiency virus; Car, Caribbean; DSA, donor-specific antibody; ADPKD, autosomal dominant polycystic kidney disease; HSP, Henoch-Schönlein Purpura; MPGN, membranoproliferative glomerulonephritis; CMV, Cytomegalovirus. Patients 1–23 were used as the initial test cohort, and patients 23–28 were included in the validation cohort.

HLA-DR⁺ CD4⁺ and CD8⁺ T cell populations were set using the isotype control stained samples for each patient to define the negative population.

Principal Component Analysis

Principal component analysis (PCA) is an exploratory technique that is used to visualize high-dimensional data by projecting the data into a new smaller set of dimensions called principal components (PC), which contain most of the information within the data set. The first dimension of the new data is made up of a linear combination of all the measured dimensions of the data, with the coefficients chosen such as to maximize the variance of the dimension across all the samples. Subsequent PCs contain progressively less of the variance. Each PC is linearly independent uncorrelated to all other PC. Typically most variance is contained within a few PCs, which can be visualized in a series of two-dimensional plots. Since the mapping into the new coordinate system is given by a weighted linear sum of all original input variables (i.e., T cell subset frequencies in peripheral blood), the contribution of each original variable to each PC is reflected by the size of the corresponding weight coefficients.

Support Vector Machines

Support vector machines (SVM) are supervised binary classification tools (7). Given a set of training data, an SVM seeks an optimal separating hyperplane to split data points from two classes (e.g., rejection vs. no rejection). In order to accommodate non-linear boundaries between the data, a kernel function can be used to transform the original input space into a higher dimension feature space, where linear structure may be found. We initially compared the results of using untransformed data with a radial Gaussian kernel when constructing the SVM. No difference in classification accuracy was observed and all results shown use untransformed data.

The SVM algorithm learns the separating hyperplane such that the distance between the plane and the nearest points from each class, the margin, is maximized, subject to a cost (governed by a tuning parameter C), which penalizes points that falls on the wrong side of the margin. The value of the cost parameter, C, was determined by optimizing model accuracy over a range of values.

The algorithm, which yields the optimal separating hyperplane, is defined by a linear combination of the data dimensions. The linear coefficients defining the hyperplane can be considered as a set of weights, which identify those dimensions of the data with the greatest influence on the classification.

Additionally, the probability of class membership (e.g., rejection vs. no rejection) can be calculated by fitting a logistic regression model to the decision values that are output from the SVM (8). The decision values are the Euclidean distances that define how far each patient sample lies from the optimal separating hyperplane. Loosely speaking, the further sample lies from the boundary, the greater the probability that the sample belongs to its predicted class.

Validation

A key element to evaluate the power of any statistical model in classification is validation. In order to maximize the statistical

power from our initial patient sample size ($n = 23$), we evaluated the model using leave-one-out validation. In this approach, one patient is selected, and all results from that patient are removed from the data set. The SVM model is then optimized using the data from the remaining 22 patients, together with their known classification labels (i.e., reject/non-reject). The model is then used to predict the classification of the sample, which had been left out. In this way, the classification algorithm is built without including any knowledge from the patient who is being tested, and this patient serves as an unbiased validation case. The procedure is repeated for each individual patient, and the success rate of the classification is measured over all 23 patient data sets. We also used more traditional train/test strategy. An additional 5 patients were included into our study and independently analyzed by flow cytometry by a scientist who was not involved with the analyses of the initial 23 patients. A repeat flow analysis of a previously studied patient was also included to test reproducibility. The SVM algorithm trained on the initial 23 patients was used to assess the rejection risk of the 6 independently analyzed patients.

All analyzes were performed using statistical programming language R. SVM were implemented using the package e1071, while PCA and hierarchical clustering were performed using the heatmap.2 and prcomp functions in the core library.

Traditional statistical tests for significance were carried out using Mann–Whitney tests with Bonferroni test for multiple testing where required.

RESULTS

Table 1 shows a summary of the patient cohort included in this study. Of the 28 patients, histologically confirmed rejection was seen in 11 patients and 17 did not show signs of rejection. The CMV status and the percentage of patients with live and cadaveric donor organs were similar in the two subgroups. We did not see an increased incidence of CMV reactivation and viremia in the patients who had rejection episodes. BK infection was not detected in any of the patients.

The antibodies used in our T cell panel were specific for nine molecules that allowed us to define distinct T cell subsets, and quantify the proportion of activated cells (using CD25 and HLA-DR) and exhausted cells (using PD-1) within each subset. FlowJo analysis of the flow cytometry data was used to extract quantitative data on 52 T cell phenotypes each defined by expression of a particular combination of markers (see Table S1 in Supplementary Material for full list). **Figure 1** shows a representative flow cytometry profile obtained after staining with our T cell panel and indicates some of the T cell subsets that were included in the bioinformatics analysis. We used the expression pattern of CD45RO and CD62L to define T cells that were phenotypically defined as naive (N), central memory (CM), effector memory (EM), or end-stage (ES) effector cells (**Figures 2B,C**). We also used a cocktail of nine antibodies to define subsets of NK, iNKT, and γ/δ T cells. In this case, the bioinformatic analysis included 13 distinct phenotypes (see Table S2 in Supplementary Material for full list). Figure S1 in Supplementary Material shows a representative plot of this panel and some of the subsets identified. In total,

multi-color flow cytometry was initially performed on 23 patients using >150 samples collected at six- to eight-time points pre- and post-transplantation. An additional 5 patients were included in our study and independently analyzed to validate the prediction tool derived from the analysis of the first 23 patients.

We employed PCA as a powerful exploratory tool for revealing potential structure within the data set of the 23 patient cohort. The first few principal components often capture most of the information in the data and are therefore a very effective way to reduce the dimensionality of a high-dimensional data set. We initially based our analysis on the adaptive immune panel. **Figure 2A** shows a PCA based on T cell subset frequencies, as determined by our adaptive immune panel. Strikingly, patients who experienced rejection tend to cluster toward the left hand side, with PC1 scores <0. Conversely, patients who did not present with any signs of clinical rejection tend to have positive PC1 scores. Interestingly, the distinction between graft rejection and tolerance was lost when patient subset frequencies were normalized to pretransplant baseline measurements (**Figure 2B**). Differences between patients at baseline are therefore more important than relative differences post transplant in predicting graft prognosis post transplantation.

In contrast to the results obtained with the T cell panel, no clear stratification of rejection and tolerance was evident when the data obtained with the NK, iNKT, and γ/δ T immune panel were analyzed (**Figure 2C**). The frequency of the subsets identified by this panel therefore had no detectable predictive power for the development of rejection episodes in our cohort.

The first PCA component of the T cell panel suggested differential clustering of patients with and without rejection episodes. We therefore went on to investigate which T cell subsets were most important in driving this segregation. PCA allocates a “loading” to each dimension of the data (i.e., each T cell subset analyzed), which lie between –1 and 1. We identified those subsets with the largest, negative PC1 loadings (**Table 2**) to determine which subsets were implicated in predicting graft rejection. A common feature of all the largest loadings was the expression of PD1 in the identified T cell subsets. The largest negative loading in the CD8⁺ T cell population was seen in the PD1-expressing ES effector cells (CD45RO[−]/CD62L[−]). The negative loading in the CD4⁺ T cell population was similar in the N subset (CD45RO[−]/CD62L⁺), and in Treg cells (identified as CD25⁺ CD127 dull) with the ES (CD45RO[−]/CD62L[−]) phenotype.

On the basis of these results, we examined in more detail the expression of PD1 in the CD4⁺ and CD8⁺ T cell subpopulations in patients who had rejection episodes, compared to those who did not. **Figure 3A** shows flow cytometry plots of PD1 expression in a representative patient of each class. As predicted from the PCA analysis, the comparison of the flow cytometry plots showed that increased expression levels of PD1 was associated with rejection episodes. The summary of the PD1-expressing T cell subsets in all patient samples analyzed is shown in **Figure 3B**.

While PCA suggests that immune-phenotyping data can stratify patients with risk of transplant rejection, it is not designed to provide accurate predictions from new data. SVM are a class of very well-studied machine learning classification tools (see Materials and Methods). We constructed SVM classifiers based

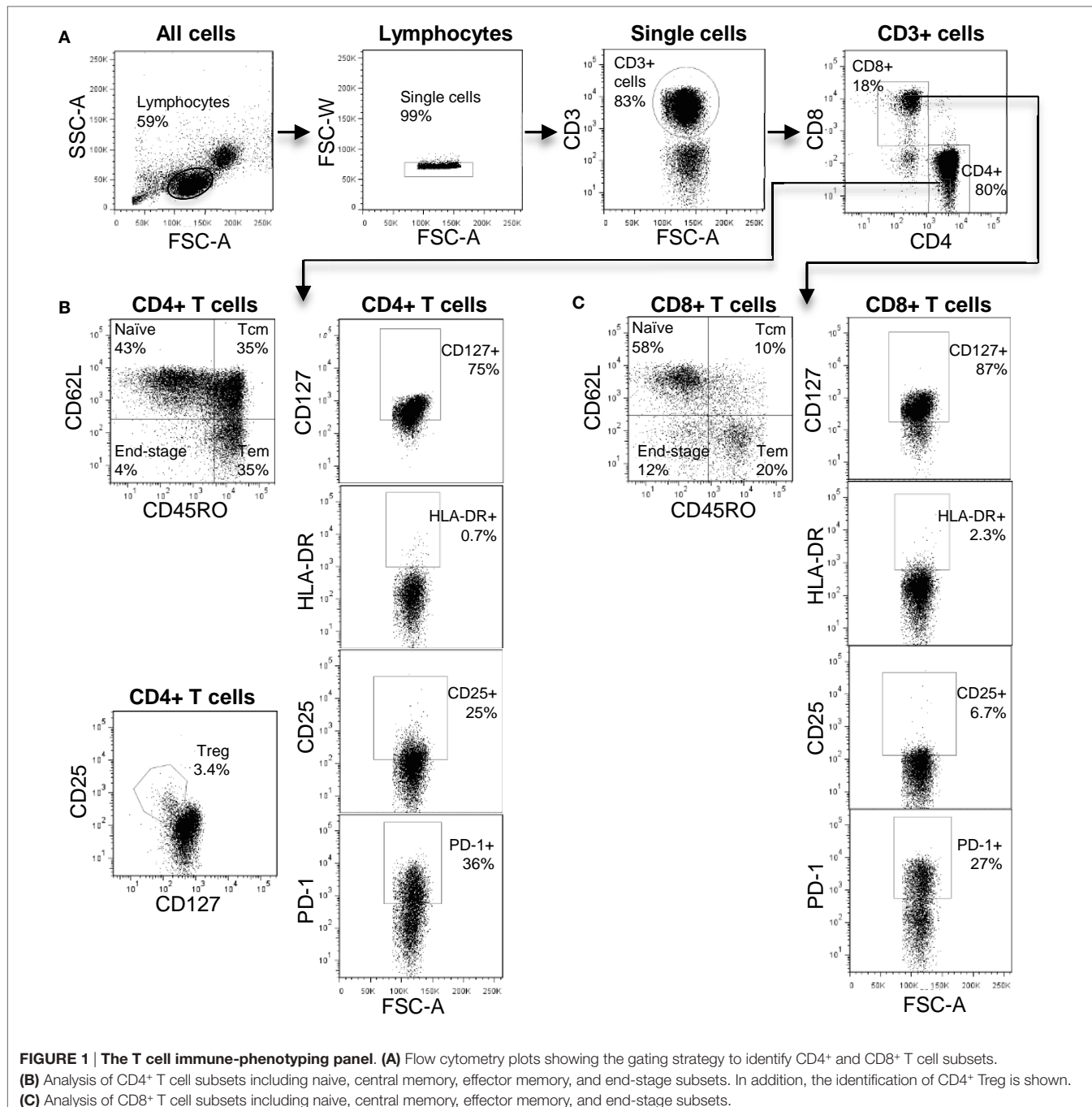


FIGURE 1 | The T cell immune-phenotyping panel. (A) Flow cytometry plots showing the gating strategy to identify CD4⁺ and CD8⁺ T cell subsets. **(B)** Analysis of CD4⁺ T cell subsets including naïve, central memory, effector memory, and end-stage subsets. In addition, the identification of CD4⁺ Treg is shown. **(C)** Analysis of CD8⁺ T cell subsets including naïve, central memory, effector memory, and end-stage subsets.

on data from three distinct time points during the course of renal transplantation: baseline, mid (between 4 and 6 weeks post-tx), and late (9–12 weeks post-tx). Using leave-one-out validation, we observed that baseline and midtime points correctly predicted the rejection status in 77 and 82% of the samples, respectively. The SVM based on later time points showed a poorer ability to discriminate, correctly predicting 68% of the samples. The SVM risk score (see Material and Methods) based on baseline/pre-transplant phenotype alone (which was available for 20 patients, 9 rejectors, and 12 non-rejectors) is shown in Figure 4A. A SVM

risk score of >0.5 suggests that the patient is more likely to exhibit a rejection episode, while a score of <0.5 suggests the patient is more likely not to show a rejection score. The further the risk score is from 0.5, the greater the confidence of the prediction.

We initially used leave-one-out validation because this provides the most powerful way to analyze the relatively small number of patients available for this study. However, we also used the more traditional train/test strategy. We selected the first (by date order of transplant) seven rejector and non-rejector data sets (in order to have a balanced data set) and used the data from these patients

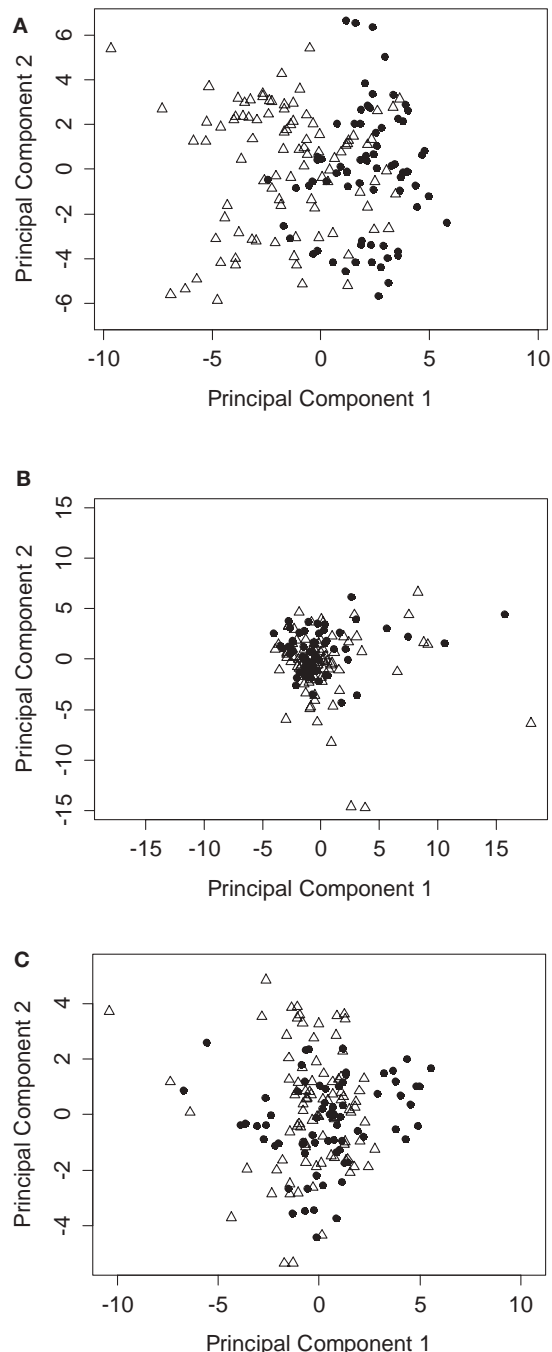


FIGURE 2 | PCA analysis of immunophenotyping data segregates between patients with or without rejection episodes. **(A)** PCA using all data points from the T cell immunophenotyping panel, showing the coordinates of samples from patients who reject (triangles) compared to those who do not reject (circles). **(B)** As for **(A)**, but all data points are normalized to pretransplant baseline values. **(C)** As for **(A)**, but using the NK, iNKT, and γ/δ T cell immunophenotyping panel.

to build an SVM. We then used this SVM to predict the outcome of the remaining 10 patients. The SVM correctly predicted 7/10 of the remaining patients even using this small training set, providing

TABLE 2 | The five largest negative loadings (predictive of rejection) obtained from PCA of T cell subset frequencies.

T Cell subset	Loading
CD8 ⁺ CD45RO ⁻ CD62L ⁻ PD1 ⁺	-0.28
CD8 ⁺ PD1 ⁺	-0.25
CD4 ⁺ PD1 ⁺	-0.23
CD4 ⁺ CD25 ⁺ CD127 ⁻ CD45RO ⁻ CD62L ⁻ PD1 ⁺	-0.22
CD4 ⁺ CD45RO ⁻ CD62L ⁺ PD1 ⁺	-0.22

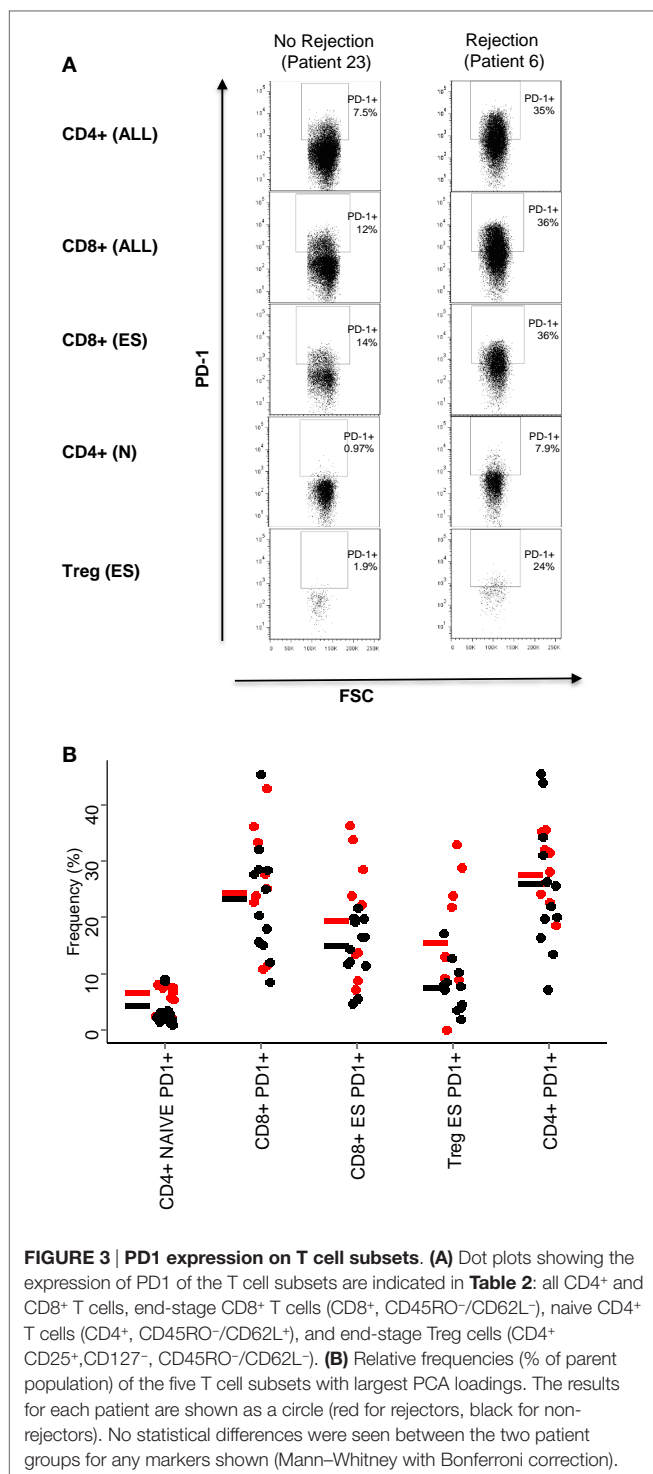
further support for the robustness of the predictions. Finally, we used the SVM built on the first set of 23 patients analyzed to predict the rejection status of five further patients for whom baseline pre-transplant samples were available and independently analyzed by a scientist who was not involved with the first cohort analysis. As a control for reproducibility, we included one sample of a patient of the first cohort in this independent analysis. All analyzed patients were correctly predicted to be non-rejectors (**Figure 4B**).

The SVM generates a set of weights (between -1 and 1) equivalent to those generated by the PCA weights and corresponds to “loadings” given to each dimension of the data (i.e., each T cell subset analyzed) when generating the classifying hyperplane. We analyzed the weights given to each data subset by the optimized SVM. In agreement with the results of the PCA, three of the five subsets with the largest coefficients included PD1 (**Table 3**). The remaining two subsets consisted of CD8 and CD4 EM T cells expressing CD25 and CD127, respectively. The mean frequency (as a proportion of parent) of each of all five subsets is shown in **Figure 5A**, and flow cytometry plots of PD1 expression in three representative patients with and without rejection episodes are shown in **Figure 5B**.

In addition to prediction of rejection prior to transplantation, it would be useful to use non-invasive screening to identify rejection post-transplantation without the need for biopsy. We therefore examined whether the immune-phenotype could identify rejection episodes using the SVM-derived probabilities of class membership (see Materials and Methods). We calculated the risk of rejection episodes over the 12-week period post-tx for each time point when a blood sample was collected and analyzed. **Figure 6A** shows the projected risk of rejection for each of the 11 patients who clinically presented with either cell- or antibody-mediated rejection; the time of rejection episodes is indicated with diamonds. In patients 1, 6, and 7, the rejection occurred after 12 weeks (see **Table 1**), which was outside the time period of collecting samples for this study. All but one of the remaining seven patients had a risk score >0.5, and five of the seven patients had a risk score greater than 0.75 at the time point when rejection episodes occurred. In contrast, only 4 out of 12 patients without rejection episodes had a risk score of more than 0.75 at any time point during the 12-week observation period (**Figure 6B**).

DISCUSSION

The major conclusion of our study is that the immune-phenotype of the peripheral blood T cell compartment contains information, which can predict the risk of a rejection episode following renal transplantation. In contrast, the panel defining NK, iNKT,



and γ/δ T cells did not identify a phenotype, which segregated between rejection and non-rejection. This may reflect a dominant role of α/β T cells in acute graft rejection, but it is also possible that our “innate lymphoid” flow cytometry panel did not include markers that might identify subsets involved in regulating transplant tolerance or rejection. It should be noted that we have used a limited number of markers to identify the T cell subsets and

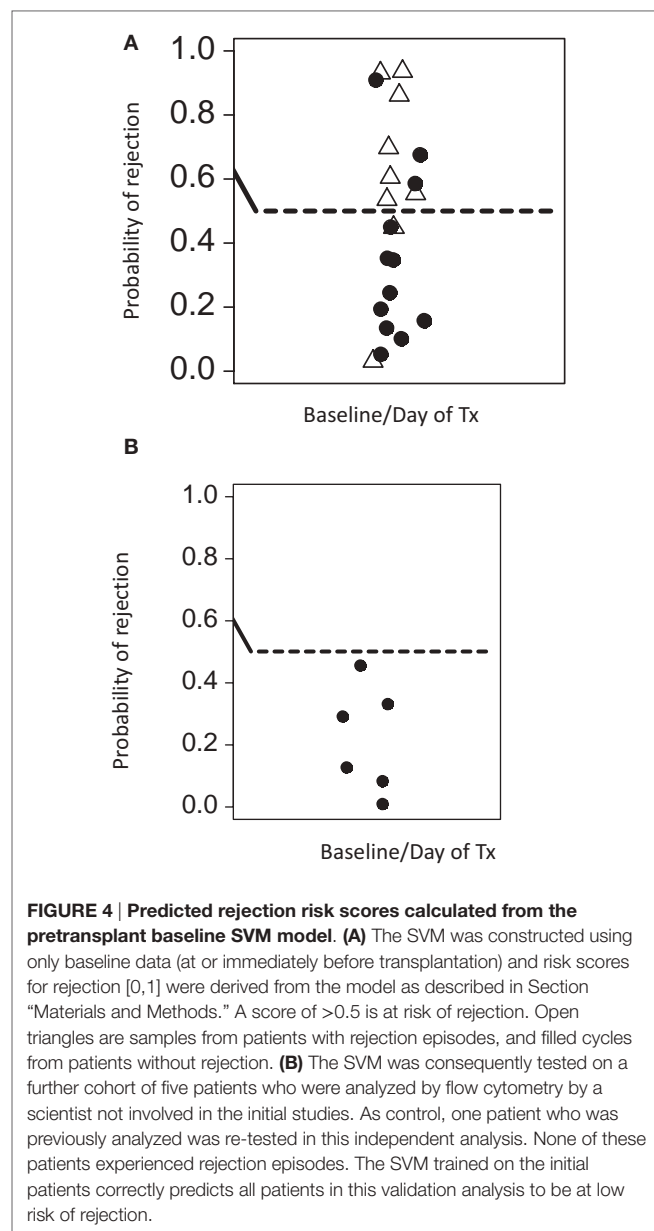


TABLE 3 | The five largest positive loadings (predictive of rejection) obtained from SVM classification of T cell subset frequencies.

T cell subset	Loading
CD4 ⁺ CD25 ⁺ CD127 ⁻ CD45RO ⁻ CD62L ⁺ PD1 ⁺	0.079
CD8 ⁺ CD45RO ⁺ CD62L ⁻ CD25 ⁺	0.076
CD8 ⁺ CD45RO ⁺ CD62L ⁻ PD1 ⁺	0.072
CD4 ⁺ CD25 ⁺ CD127 ⁻ CD45RO ⁻ CD62L ⁻ PD1 ⁺	0.066
CD4 ⁺ CD45RO ⁺ CD62L ⁻ CD127 ⁺	0.065

the expression of activation and exhaustion markers. It is possible that revised panels that include additional markers might improve the ability to identify patients at risk of rejection. In this study, we have not explored the risk factors of antibody-mediated

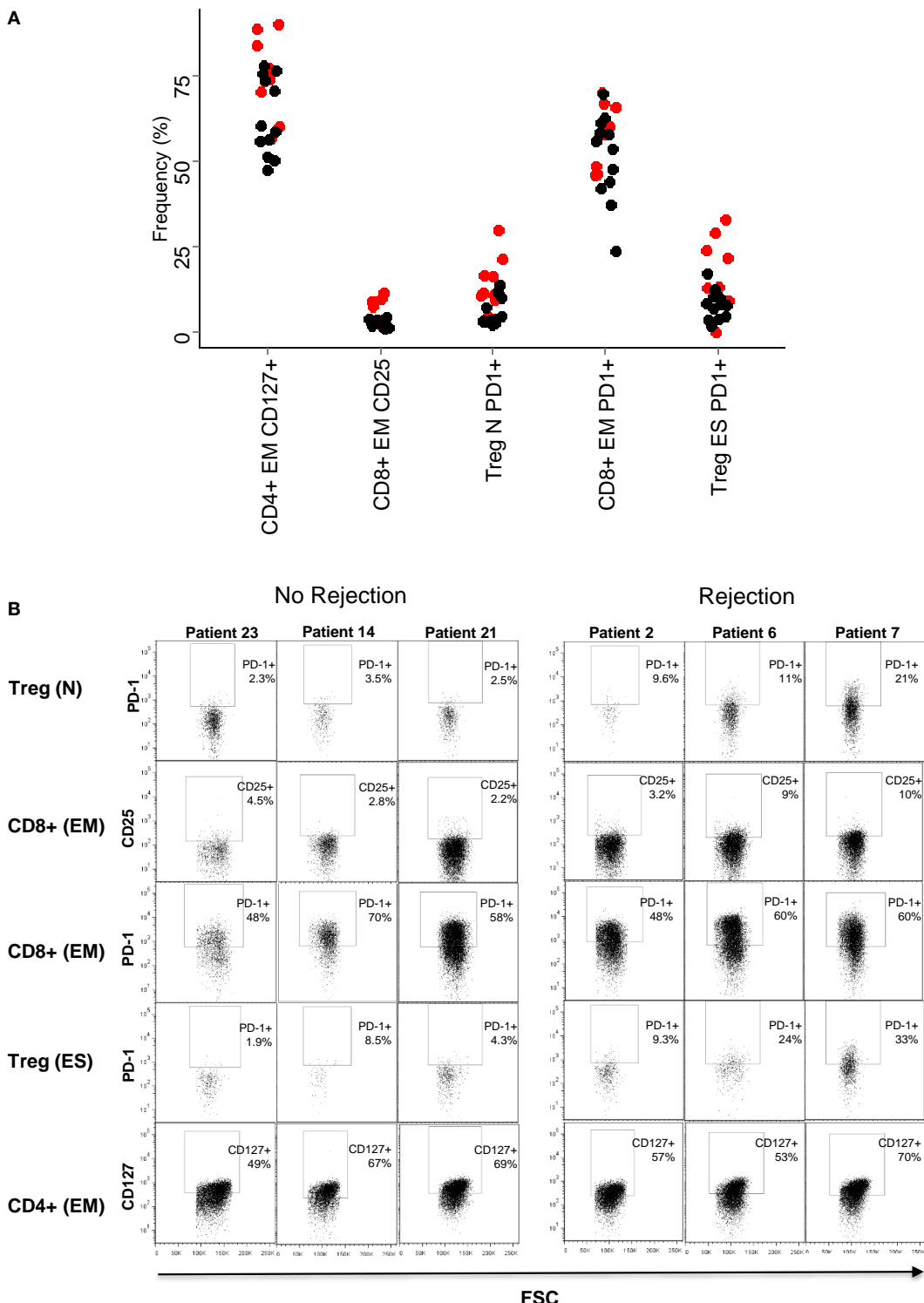


FIGURE 5 | Baseline frequencies and flow cytometry profiles of the subsets with largest coefficients in the SVM. (A) Relative frequencies (% of parent population) of the five T cell subsets with largest SVM coefficients. The result for each patient is shown as a circle (red for rejectors, black for non-rejectors). Significance values (Mann–Whitney with Bonferroni correction) for the five subsets are: PD1+ naive Treg (CD4+ CD25+, CD127-, CD45RO-/CD62L+, PD1+) $p = 0.02$, CD25+ effector memory CD8+ T cells (CD8+, CD45RO+/CD62L-, CD25+) $p > 0.1$, PD1+ effector memory CD8+ T cells (CD8+, CD45RO+/CD62L-, PD1+) $p > 0.1$, PD1+ end-stage Treg (CD4+ CD25+, CD127-, CD45RO-/CD62L-, PD1+) $p = 0.1$, and CD127+ effector memory CD4+ T cells (CD4+, CD45RO+/CD62L-, CD127+) $p > 0.1$. **(B)** Dotplots showing PD1 (y axis) and FSC (x axis) expression in the five T cell subsets are described in **(A)**, in three representative patients that did not reject, and three representative patients that did reject.

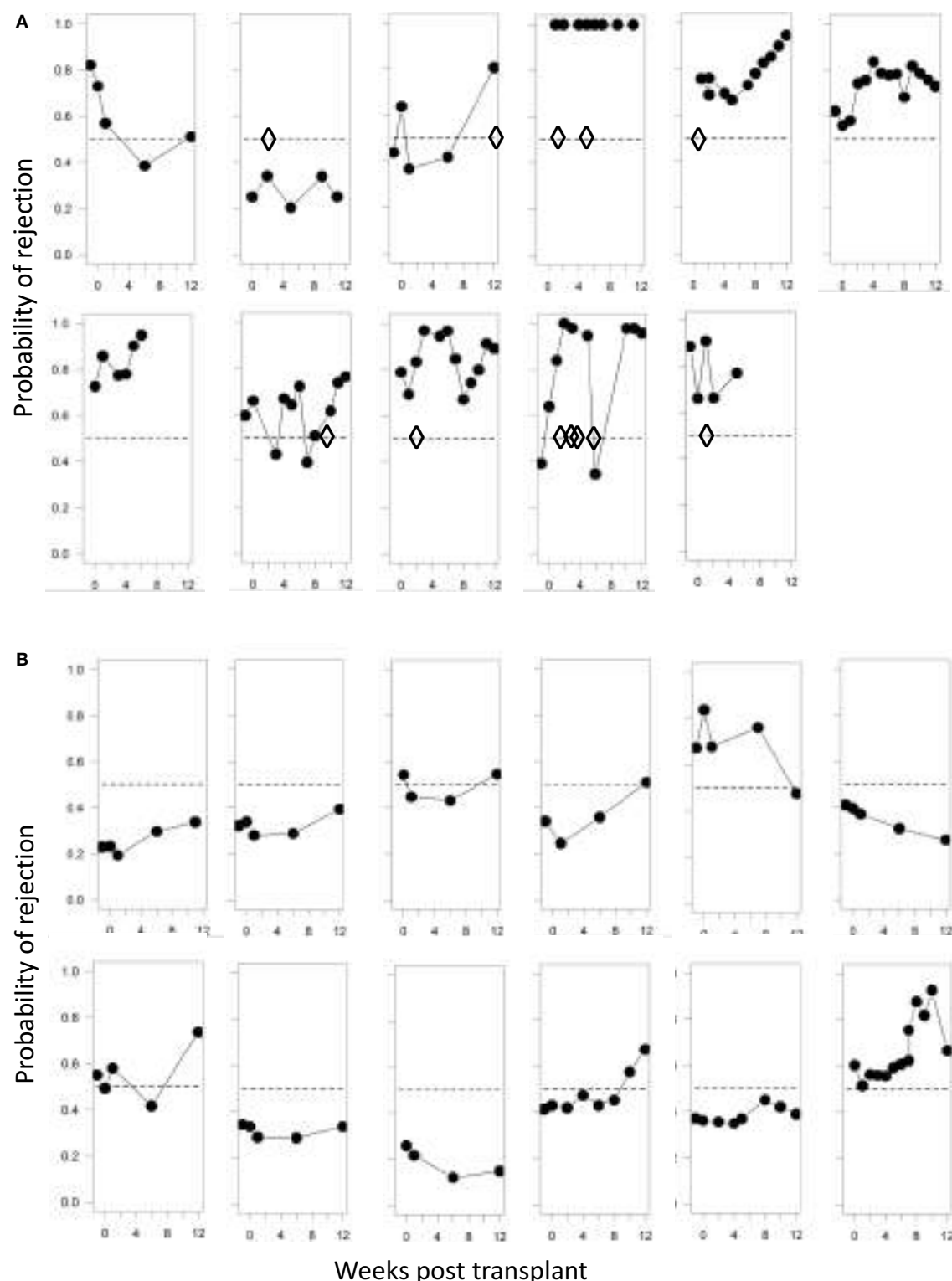


FIGURE 6 | Probabilities of identifying a rejection episode calculated from the SVM model. (A) Trajectories of the probability of rejection determined by SVM for each patient who clinically presented with rejection. Diamonds represent each clinically observed rejection episode. In panel 1 rejection occurred at 6 months; in panel 6 at 12 months, and in panel 7 at 24 months. **(B)** Trajectories of the probability of rejection determined by SVM for patient number 12–23 (Table 1), who presented with no clinical signs of rejection. The SVM is trained solely on baseline samples and evaluated using leave-one-out cross-validation.

rejection, which is mediated by donor-specific antibodies that are present in patients before transplantation.

Advances in multi-color flow cytometry have led to a continual increase in the complexity of immune-phenotyping. The introduction of new technologies, such as mass-cytometry or single cell transcriptomics, has the potential to further increase the number of molecules that can be quantified (9, 10). However, the high cost and technical challenges of using these new technologies mean that flow cytometry remains the technique of choice for immune phenotyping in most clinical settings. In this study, we have used nine parameters, which generated a large number of possible combinations that cannot be comprehensively interrogated using manual approaches. In addition, there is an increasing awareness that a classification on the basis of a few defined phenotypes is a simplification of the underlying biology. Computational tools, which can efficiently mine the increasingly high-dimensional space of immune-phenotyping data, are therefore likely to become a key to future biomarker discovery and translation into the diagnostic laboratory.

We have used a hybrid approach, in which quantitative population frequency data is first collected using classical manual flow cytometry analysis and then analyzed using high-dimensional computational statistical tools. This combination of manual and computational analysis was used to define 52 different T cell subsets, many of which were nested in each other. The overall accuracy of the classification was >75% when using samples collected either before, at or within 6 weeks post transplant. These data provide a strong rationale for further immunophenotyping studies, with the dual objective of increasing the size of the training cohort and thus the power of the machine learning algorithm, and perhaps incorporating additional immunophenotyping markers, which might further dissect the intrinsic variation in the immune status of patients, and hence accurately predict the response to the transplant and the associated immunosuppression.

In addition to the ability to predict rejection episodes, two important further conclusions emerge from both the PCA and SVM analysis. The first is that the predictive power lies predominantly within the pretransplant immunophenotype, and that the phenotype predictive power becomes much weaker at later times. In the first few weeks after transplantation, there is remarkably little change in the immune phenotype, but as time progresses the phenotype of different patients seems to converge. This unexpected finding provides a rationale to potentially use the pretransplant immune phenotype to identify patients at risk of developing rejection episodes, and then increase immune suppressive medication during the early phase after transplantation.

The second finding is that high PD1 expression in several T cell subsets predicts a higher rate of rejection. The function of PD1 has been studied extensively (11), although its role in Treg is less well understood (12). PD1 up-regulation has been observed in murine models of chronic viral infection and was found to identify exhausted T cells with reduced function (13). Similar observations have been made in cancer patients, and the treatment with anti-PD1 antibodies has reversed T cell dysfunction and resulted in impressive clinical benefits for patients (14). Recent experiments have indicated that the PD1/PD-L1 pathway is involved in Treg-mediated suppression of autoreactive B cell

responses (15). However, this did not involve PD1-positive Treg, as the suppression was mediated by PD-L1 expressed by Treg binding to PD1 expressed by the autoreactive B cells. Maybe more relevant for our observation is a recent study that demonstrated increased numbers of PD1-expressing Treg in the blood of patients suffering from an autoimmune condition that results in generalized vitiligo (16). Interestingly, upregulation of PD1 in Treg was also found in patients with chronic hepatitis C infection, and the observation that blockade of PD1 improved Treg function suggested that PD1 acted as negative regulator of Tregs in this setting (17). Together, these studies suggest that chronic immune activation (autoimmune or chronic infection) can result in the accumulation of PD1-expressing Treg with impaired functional activity. In our case, increased PD1 expression before transplantation might identify patients with a history of chronic immune activation combined with impaired Treg function, which together might enhance the potential of mounting damaging T cell responses against the transplanted kidney. This is in keeping with the recent demonstration that variations in the immune response profile of humans are strongly affected by environmental factors (18). It is possible that dialysis, age, and increased pathogen exposure might impact on the number of PD1-expressing Treg; in our cohort more patients were on dialysis and had a higher median age in the rejection group compared to the group without rejection. We note that an mRNA expression study in the peripheral blood of renal transplant patients showed that increased levels of PD1 mRNA was associated with acute rejection episodes (19). In this study, we have not analyzed the expression profile of CD57, a marker that has been linked to the resistance of renal transplant patients to respond to treatment with recombinant proteins that inhibit CD28 costimulation (20).

In conclusion, our study shows how computational tools, which are able to analyze the increasingly high-dimensional immunophenotyping data available, can be used to generate biomarkers useful for patient stratification, and to identify new biological features underlying a complex process such as transplant rejection. Validation of these results on a larger cohort is required, but this study suggests that immune-phenotyping may be useful in guiding patient management and may provide a strategy for developing personalized immune suppressive regimes according to the predicted rejection risk assessed prior to transplantation.

AUTHOR CONTRIBUTIONS

HS conceived and designed the work and wrote the paper. RP designed the work, acquired and analyzed data, and read and approved the paper. NT contributed to the design the work, analyzed data, read and approved the paper. SW contributed to the design the work, and read and approved the paper. LA contributed to the design the work and read and approved the paper. DG contributed to the design the work and read and approved the paper. SS acquired and analyzed data and read and approved the paper. MJ contributed to the design the work and read and approved the paper. MH, BC, and DT contributed to the design the work, analyzed data, and read and approved the paper. All authors agree to be accountable for all aspects of the work in

ensuring that questions related to the accuracy or integrity of any part of the work are appropriately investigated and resolved.

FUNDING

This work was supported by grants from Bloodwise UK, Cancer Research UK, Medical Research Council, National Institute of

Health Research, UCLH Biomedical Research Centre and Royal Free Charity.

SUPPLEMENTARY MATERIAL

The Supplementary Material for this article can be found online at <http://journal.frontiersin.org/article/10.3389/fimmu.2016.00126>

REFERENCES

- Meier-Kriesche HU, Schold JD, Srinivas TR, Kaplan B. Lack of improvement in renal allograft survival despite a marked decrease in acute rejection rates over the most recent era. *Am J Transplant* (2004) **4**:378–83. doi:10.1111/j.1600-6143.2004.00332.x
- Meier-Kriesche HU, Ojo AO, Hanson JA, Cibrik DM, Punch JD, Leichtman AB, et al. Increased impact of acute rejection on chronic allograft failure in recent era. *Transplantation* (2000) **70**:1098–100. doi:10.1097/00007890-200010150-00018
- Malheiro J, Tafulo S, Dias L, Martins LS, Fonseca I, Beirao I, et al. Analysis of preformed donor-specific anti-HLA antibodies characteristics for prediction of antibody-mediated rejection in kidney transplantation. *Transpl Immunol* (2015) **32**:66–71. doi:10.1016/j.trim.2015.01.002
- Chen Y, Tai Q, Hong S, Kong Y, Shang Y, Liang W, et al. Pretransplantation soluble CD30 level as a predictor of acute rejection in kidney transplantation: a meta-analysis. *Transplantation* (2012) **94**:911–8. doi:10.1097/TP.0b013e31826784ad
- Roedder S, Sigdel T, Salomonis N, Hsieh S, Dai H, Bestard O, et al. The kSORT assay to detect renal transplant patients at high risk for acute rejection: results of the multicenter AART study. *PLoS Med* (2014) **11**:e1001759. doi:10.1371/journal.pmed.1001759
- Lee A, Jeong JC, Choi YW, Seok HY, Kim YG, Jeong KH, et al. Validation study of peripheral blood diagnostic test for acute rejection in kidney transplantation. *Transplantation* (2014) **98**:760–5. doi:10.1097/TP.0000000000000138
- Pisanski T, Shawe-Taylor J. Characterizing graph drawing with eigenvectors. *J Chem Inf Comput Sci* (2000) **40**:567–71. doi:10.1021/ci9000938
- Platt RW, Leroux BG, Breslow N. Generalized linear mixed models for meta-analysis. *Stat Med* (1999) **18**:643–54. doi:10.1002/(SICI)1097-0258(19990330)18:6<643::AID-SIM76>3.0.CO;2-M
- Bodenmiller B, Zunder ER, Finck R, Chen TJ, Savic ES, Bruggner RV, et al. Multiplexed mass cytometry profiling of cellular states perturbed by small-molecule regulators. *Nat Biotechnol* (2012) **30**:858–67. doi:10.1038/nbt.2317
- Jaitin DA, Kenigsberg E, Keren-Shaul H, Elefant N, Paul F, Zaretsky I, et al. Massively parallel single-cell RNA-seq for marker-free decomposition of tissues into cell types. *Science* (2014) **343**:776–9. doi:10.1126/science.1247651
- Keir ME, Butte MJ, Freeman GJ, Sharpe AH. PD-1 and its ligands in tolerance and immunity. *Annu Rev Immunol* (2008) **26**:677–704. doi:10.1146/annurev.immunol.26.021607.090331
- Baecker-Allan C, Brown JA, Freeman GJ, Hafler DA. CD4+CD25+ regulatory cells from human peripheral blood express very high levels of CD25
- ex vivo. *Novartis Found Symp* (2003) **252**:67–88;discussion88–91,106–114. doi:10.1002/0470871628.ch6
- Barber DL, Wherry EJ, Masopust D, Zhu B, Allison JP, Sharpe AH, et al. Restoring function in exhausted CD8 T cells during chronic viral infection. *Nature* (2006) **439**:682–7. doi:10.1038/nature04444
- Brahmer JR, Tykodi SS, Chow LQ, Hwu WJ, Topalian SL, Hwu P, et al. Safety and activity of anti-PD-L1 antibody in patients with advanced cancer. *N Engl J Med* (2012) **366**:2455–65. doi:10.1056/NEJMoa1200694
- Gotot J, Gottschalk C, Leopold S, Knolle PA, Yagita H, Kurts C, et al. Regulatory T cells use programmed death 1 ligands to directly suppress autoreactive B cells in vivo. *Proc Natl Acad Sci U S A* (2012) **109**:10468–73. doi:10.1073/pnas.1201131109
- Tembhare MK, Parihar AS, Sharma VK, Sharma A, Chattopadhyay P, Gupta S. Alteration in regulatory T cells and programmed cell death 1-expressing regulatory T cells in active generalized vitiligo and their clinical correlation. *Br J Dermatol* (2015) **172**:940–50. doi:10.1111/bjd.13511
- Franceschini D, Paroli M, Francavilla V, Videtta M, Morrone S, Labbadia G, et al. PD-L1 negatively regulates CD4+CD25+Foxp3+ Tregs by limiting STAT-5 phosphorylation in patients chronically infected with HCV. *J Clin Invest* (2009) **119**:551–64. doi:10.1172/JCI36604
- Brodin P, Jojic V, Gao T, Bhattacharya S, Angel CJ, Furman D, et al. Variation in the human immune system is largely driven by non-heritable influences. *Cell* (2015) **160**:37–47. doi:10.1016/j.cell.2014.12.020
- Wang YW, Wang Z, Shi BY. Programmed death 1 mRNA in peripheral blood as biomarker of acute renal allograft rejection. *Chin Med J (Engl)* (2011) **124**:674–8.
- Espinosa J, Herr F, Tharp G, Bosinger S, Song M, Farris AB III, et al. CD57 CD4 T cells underlie belatacept-resistant allograft rejection. *Am J Transplant* (2016) **16**:1102–12. doi:10.1111/ajt.13613

Conflict of Interest Statement: HS is consultant for Cell Medica and hold shares in this company. The remaining authors declare that the research was conducted in the absence of any commercial or financial relationships that could be construed as a potential conflict of interest.

Copyright © 2016 Pike, Thomas, Workman, Ambrose, Guzman, Sivakumaran, Johnson, Thorburn, Harber, Chain and Stauss. This is an open-access article distributed under the terms of the Creative Commons Attribution License (CC BY). The use, distribution or reproduction in other forums is permitted, provided the original author(s) or licensor are credited and that the original publication in this journal is cited, in accordance with accepted academic practice. No use, distribution or reproduction is permitted which does not comply with these terms.



Precision subtypes of T cell-mediated rejection identified by molecular profiles

Paul Ostrom Kadota¹, Zahraa Hajjiri², Patricia W. Finn³ and David L. Perkins^{3,4*}

¹ Finn-Perkins Laboratory, Department of Medicine, University of Illinois-Chicago, Chicago, IL, USA, ² Finn-Perkins Laboratory, Department of Internal Medicine, Division of Nephrology, University of Illinois-Chicago, Chicago, IL, USA, ³ Department of Medicine, University of Illinois-Chicago, Chicago, IL, USA, ⁴ Department of Surgery, University of Illinois-Chicago, Chicago, IL, USA

OPEN ACCESS

Edited by:

Giorgio Raimondi,
Johns Hopkins School of Medicine,
USA

Reviewed by:

Minnie M. Sarwal,
University of California, San
Francisco, USA
Sheri M. Krams,
Stanford University, USA

*Correspondence:

David L. Perkins
perkinsd@uic.edu

Specialty section:

This article was submitted to
Alloimmunity and Transplantation,
a section of the journal
Frontiers in Immunology

Received: 01 July 2015

Accepted: 05 October 2015

Published: 06 November 2015

Citation:

Kadota PO, Hajjiri Z, Finn PW and
Perkins DL (2015) Precision subtypes
of T cell-mediated rejection identified
by molecular profiles.
Front. Immunol. 6:536.

doi: 10.3389/fimmu.2015.00536

Among kidney transplant recipients, the treatment of choice for acute T cell-mediated rejection (TCMR) with pulse steroids or antibody protocols has variable outcomes. Some rejection episodes are resistant to an initial steroid pulse, but respond to subsequent antibody protocols. The biological mechanisms causing the different therapeutic responses are not currently understood. Histological examination of the renal allograft is considered the gold standard in the diagnosis of acute rejection. The Banff Classification System was established to standardize the histopathological diagnosis and to direct therapy. Although widely used, it shows variability among pathologists and lacks criteria to guide precision individualized therapy. The analysis of the transcriptome in allograft biopsies, which we analyzed in this study, provides a strategy to develop molecular diagnoses that would have increased diagnostic precision and assist the development of individualized treatment. Our hypothesis is that the histological classification of TCMR contains multiple subtypes of rejection. Using R language algorithms to determine statistical significance, multidimensional scaling, and hierarchical, we analyzed differential gene expression based on microarray data from biopsies classified as TCMR. Next, we identified KEGG functions, protein–protein interaction networks, gene regulatory networks, and predicted therapeutic targets using the integrated database ConsensusPathDB (CPDB). Based on our analysis, two distinct clusters of biopsies termed TCMR01 and TCMR02 were identified. Despite having the same Banff classification, we identified 1933 differentially expressed genes between the two clusters. These genes were further divided into three major groups: a core group contained within both the TCMR01 and TCMR02 subtypes, as well as genes unique to TCMR01 or TCMR02. The subtypes of TCMR utilized different biological pathways, different regulatory networks and were predicted to respond to different therapeutic agents. Our results suggest approaches to identify more precise molecular diagnoses of TCMR, which could form the basis for personalized treatments.

Keywords: TCMR, precision medicine, personalized medicine, kidney transplant, systems biology

INTRODUCTION

An important goal in medicine is to develop precision therapies specific to each individual to deliver personalized medicine. As eloquently stated by Sir William Osler over 100 years ago, “variability is the law of life, and as no two faces are the same, so no two bodies are alike, and no two individuals react alike and behave alike under the abnormal conditions we know as disease.” Since the introduction of cyclosporine in the late 1980s, the therapeutic protocols for many patients in clinical transplantation have been based on three types of immunosuppressive drugs: a calcineurin inhibitor, an antimetabolite, and a steroid. More recently, an array of new agents including biological agents have emerged or are entering investigational study. In addition, protocols that are calcineurin inhibitor free or steroid sparing have also been developed. Given the increasing number of therapeutic agents and potential protocols and the limited number of transplant patients, it is not tractable to evaluate all of the potential therapeutic permutations in prospective clinical trials. Furthermore, a strategy is needed to precisely identify the optimal therapy to apply personalized medicine for each individual patient based on each patient’s genotype and phenotype (1–7).

Since its development in 1993, the Banff Classification has served as a valuable tool in the diagnosis of allograft rejection and a guide for clinical management. The first Banff classification standardized the histopathological criteria to diagnose rejection into six major categories based on the histopathological findings (8): (1) normal, (2) hyperacute, (3) borderline mild tubulitis, (4) acute rejection, (5) chronic allograft nephropathy (CAN), (6) other changes not due to rejection. A numerical grading was introduced for each of the renal compartments. This classification created a framework for further changes and modifications in subsequent updates of the Banff classification. Despite the success and huge positive impact this classification had on transplant medicine, it also had limitations. The major weaknesses are the substantial variability among pathologists and the lack of an external validation tool (9). The reproducibility of the Banff classification was assessed with a Kappa statistics scoring system (10–12). These studies showed a moderate reproducibility score for diagnostic classification, whereas the numerical grading of tubulitis had an extremely low kappa score indicating low reproducibility (10). Identifying a correlation between the Banff classification and graft survival has also been a challenge. In 2015, Krisl et al. followed 182 patients who developed a rejection episode for a median of 527 days. They noted no difference in death censored graft survival in the first 6 months after transplantation between the acute cellular rejection grades IA, IB, IIA, and IIB. They also noted no difference between the early and late Banff IA or IB classifications. However, the same histological classification of IIA had a significant difference in graft survival if it occurred late (after 6 months) versus early (13). These differences suggest that the different subtypes do not represent a graded severity score that correlates with graft survival, but rather a different type of rejection. In another study, Wu et al. followed 270 patients with rejection and noted no significant difference in the graft survival between TCMR I, II, or III. However, they noted worse graft outcomes in patients with vascular involvement regardless

of the degree of the timing or the degree of interstitial or tubular involvement (14). Again, this analysis suggests different subtypes of TCMR that are not precisely captured by the Banff classifications. In summary, these studies demonstrate the limitations of the Banff classification in grading the severity of rejection and in predicting outcomes.

Our overall hypothesis is that the histological diagnosis of TCMR as defined by the Banff classification of kidney transplant biopsies contains multiple subtypes of rejection involving different biological pathways and functions. To address these goals, in this report, we use a systems biology approach to provide a proof of principle analysis that identifies potential therapeutic agents that target specific subtypes of T cell-mediated rejection (TCMR).

The basis of our approach is the analysis of the transcriptome in allograft biopsies. The analysis of differential expression of mRNA has several advantages. First, genome wide assays of the transcriptome are relatively quick, quantitative, and reproducible. In contrast, other “omic” technologies, in particular proteomics and metabolomics can be technically more challenging and not genome wide. Second, the level of gene expression quantitated in the transcriptome reflects multiple effects including genomic, epigenetic, metagenomic, and environmental influences and thus integrates the effect of multiple biological regulatory mechanisms. Based on these considerations, analysis of the transcriptome, which is utilized in this study, is a quantitative, reproducible, and cost-effective approach to assay a genome wide response.

To interpret genome wide data, the application of systems biology methods that analyze pathways and networks of molecules in an “interactome” increases confidence in functional biological interpretations compared with the reductionist approach of analysis of isolated molecular interactions. In our analysis, we first identified the significant changes in the transcriptome of microarray data in a public database of kidney transplant biopsies that were classified as TCMR or control. After excluding outliers using multidimensional scaling (MDS), which is an essential step that supports precision analysis, we identified subtypes of TCMR using unsupervised hierarchical clustering. For each subtype, we constructed a protein–protein interaction (PPI) network, a gene regulatory network, and a KEGG pathway analysis, which illuminated interaction networks, signaling pathways, and regulatory mechanisms. In addition, we analyzed the DrugBank database of candidate drugs to identify putative therapeutic agents that would be specific for each subtype of TCMR.

MATERIALS AND METHODS

Data

The data files were downloaded from NCBI through R, version 3.10, using a *Bioconductor* package, GEOquery (15, 16). The dataset contains the microarray expression from an HG-U133_Plus_2 Affymetrix Human Genome array. Gene expression was given as log₂ fold change against controls. The dataset included 202 kidney biopsies taken from renal transplant patients undergoing biopsies for cause (17). The expression and phenotypic data can be found on the Gene Expression Omnibus (GEO) database, using GEO ascension number (GSE21374) (18).

The initial data set of 202 kidney biopsies included eleven diagnoses based upon pathology report. These biopsies included rejection diagnoses of antibody-mediated rejection (ABMR), acute tubular necrosis (ATN), BK virus, borderline, CAN, calcineurin inhibitor toxicity (CNIT), glomerulonephritis (GN), tubular atrophy/interstitial fibrosis (TAIF), T cell-mediated rejection (TCMR), and transplant glomerulopathy (TGP). There were 143 samples taken from 85 patients that underwent renal transplant. Eight additional kidney biopsies were taken from normal, native kidneys from patients undergoing nephrectomy for renal cell carcinoma. Finally, 51 additional transplant biopsies were added as a validation set. We focused on the largest cohort, TCMR, using the renal nephrectomy samples as a baseline control.

Statistical Methods

An analysis pipeline was created in the R language statistical and graphing environment (19). First, we normalized the 54,675 Affymetrix probe sets by Z-score and filtered the data based on the scaled expression level >0.12 and coefficient of variation (CV), which selected 6,473 genes that showed high expression and high CV. Next, we identified outlier samples using MDS. Samples with an intracentroid distance >2 SD greater than the mean were classified as outliers and removed from further analysis. To identify subtypes of TCMR, we performed unsupervised hierarchical clustering using the stats package. The clusters were evaluated by connectivity, Dunn, and Silhouette index, which identified two subtypes of TCMR. Differential gene expression was determined by student's *t* test ($p < 0.05$). Correction for multiple testing was performed by false discovery rate algorithm ($fdr < 0.05$).

Molecular Interaction Analysis

We used the ConsensusPathDB (CPDB), hosted by the Max Plank Institute of Molecular Genetics (20). CPDB combines 32 public resources for biological interactions including the KEGG, BIND, DrugBank and MINT databases. For each database, we analyzed TCMR01, TCMR02, and core gene list independently.

Over-representation analysis was performed in CPDB for KEGG pathways. The resulting enriched pathway-based sets included a minimum of two input genes with a hypergeometric test *p*-value of 0.01. Edges between KEGG pathways included at least a 30% overlap between connecting nodes.

We used CPDB induced network module analysis of high-confidence PPI, gene regulatory interactions, and drug-target interactions.

Network Visualization

Network data were visualized with the imaging platform Cytoscape (21).

RESULTS

Defining Subtypes of T Cell-Mediated Rejection

To identify subtypes of TCMR rejection in kidney allografts, we analyzed all samples classified as TCMR rejection (and nephrectomy controls) using the Banff histological classification

of rejection in a database of kidney transplant biopsies (GSE 21374). First, we filtered microarray expression data based on the $CV > 0.12$. Next, we analyzed the 31 samples classified as TCMR using MDS to identify statistical outliers among the samples (Figure 1). We defined samples as outliers that were more than two SD from the medoid. Based on this criterion, we classified three samples (T.31, T.22, and T.13) as outliers. The remaining samples were analyzed by hierarchical clustering using stats Package in R language (Figure 2B). To determine the optimal number of clusters, we analyzed the dendrogram based on connectivity, Dunn Index, and Silhouette Index (Table S1 in Supplementary Material). All three methods supported partitioning the results into two distinct clusters that we termed "TCMR01" and "TCMR02."

Hierarchical Clustering Based on Molecular Heterogeneity

Next, we calculated the mean expression levels of genes in TCMR01, TCMR02, NEPH01 (nephrectomy control), and NORM01 (biopsies pathologically classified as normal) and analyzed the subtypes with hierarchical clustering (Figure 2A). NEPH01 and NORM01 were similar based on proximity in the dendrogram. Interestingly, TCMR01 was more dissimilar than TCMR02 from the NEPH01 and NORM01 subtypes suggesting that TCMR01 exhibited the more extreme subtype. To determine if the two clusters contained differentially expressed genes, we performed *t*-tests between TCMR01 and TCMR02, which identified 1933 genes that were significantly differentially expressed ($fdr < 0.05$) (Table S2 in Supplementary Material). Thus, although the TCMR01 and TCMR02 subtypes of rejection had similar histological diagnoses, they were markedly heterogeneous at the molecular level of gene expression.

Functional Differences Between Subtypes of T Cell-Mediated Rejection

Based on the large number of differentially expressed genes in the TCMR01 and TCMR02 subtypes, we investigated whether the two subtypes had different biological functions. We selected three groups of differentially expressed genes: a core group that was differentially expressed in both subtypes and groups that were uniquely differentially expressed in either TCMR01 or TCMR02. Next, we identified the KEGG pathways that were significantly associated with each group of genes (Figure 3; Table S3 in Supplementary Material). In the core group, defined as the genes common to both TCMR01 and TCMR02, the pathway with the highest significance was "allograft rejection" ($q < 9.67E-16$), which supported the validity of our approach. Additional highly significant pathways included "graft-versus-host disease" ($q < 2.10E-15$), "antigen processing and presentation" ($q < 2.10E-15$), "type I diabetes mellitus" ($q < 2.90E-15$), "autoimmune thyroid disease" ($q < 4.75E-14$), "viral myocarditis" ($q < 9.44E-14$), "phagosome" ($q < 1.27E-10$), and "cell adhesion molecules" ($q < 3.37E-09$). All of the significant pathways share a strong pathological immune response and the emergence of pathways associated with autoimmunity, allergy and infections in addition to alloimmunity are due to the overlap in the genes involved in these immune processes. Importantly, it is notable that the significance level of "allograft

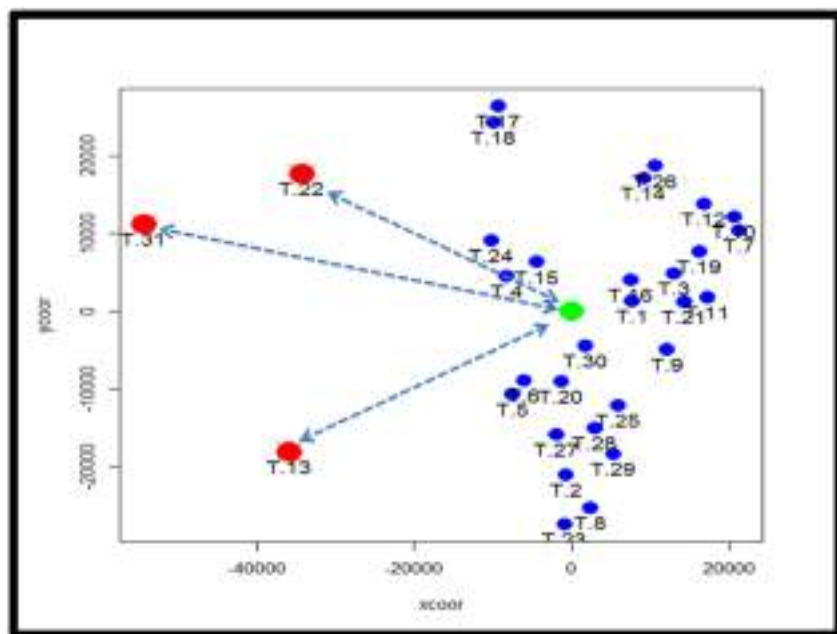


FIGURE 1 | Analysis of potential sample outliers with multidimensional scaling (MDS). We analyzed 31 samples with a pathological diagnosis of T cell-mediated rejection (TCMR) in the kidney transplant database (GSE21374). Using multidimensional scaling of the gene expression data, we identified samples with an intracentroid distance z-score > 2 (represented by the dashed lines) which included three samples (T13, T22 and T31).

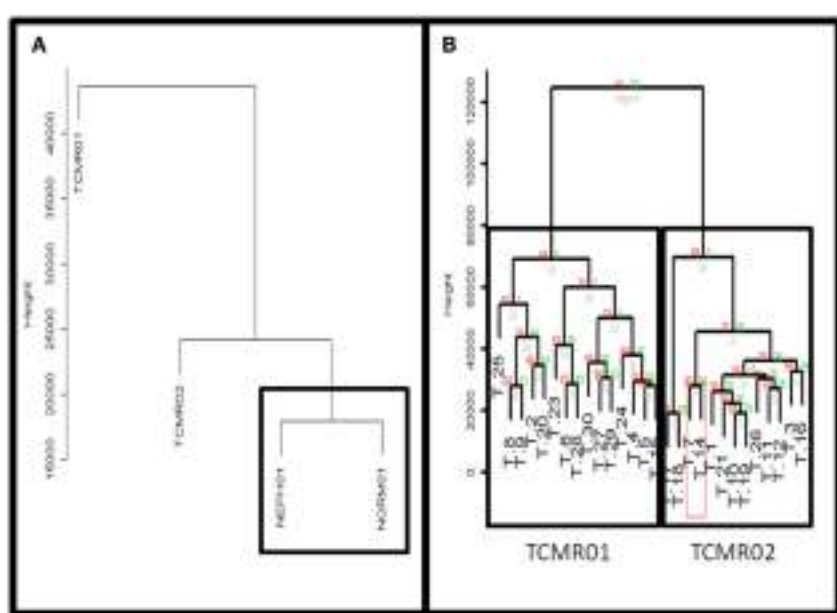
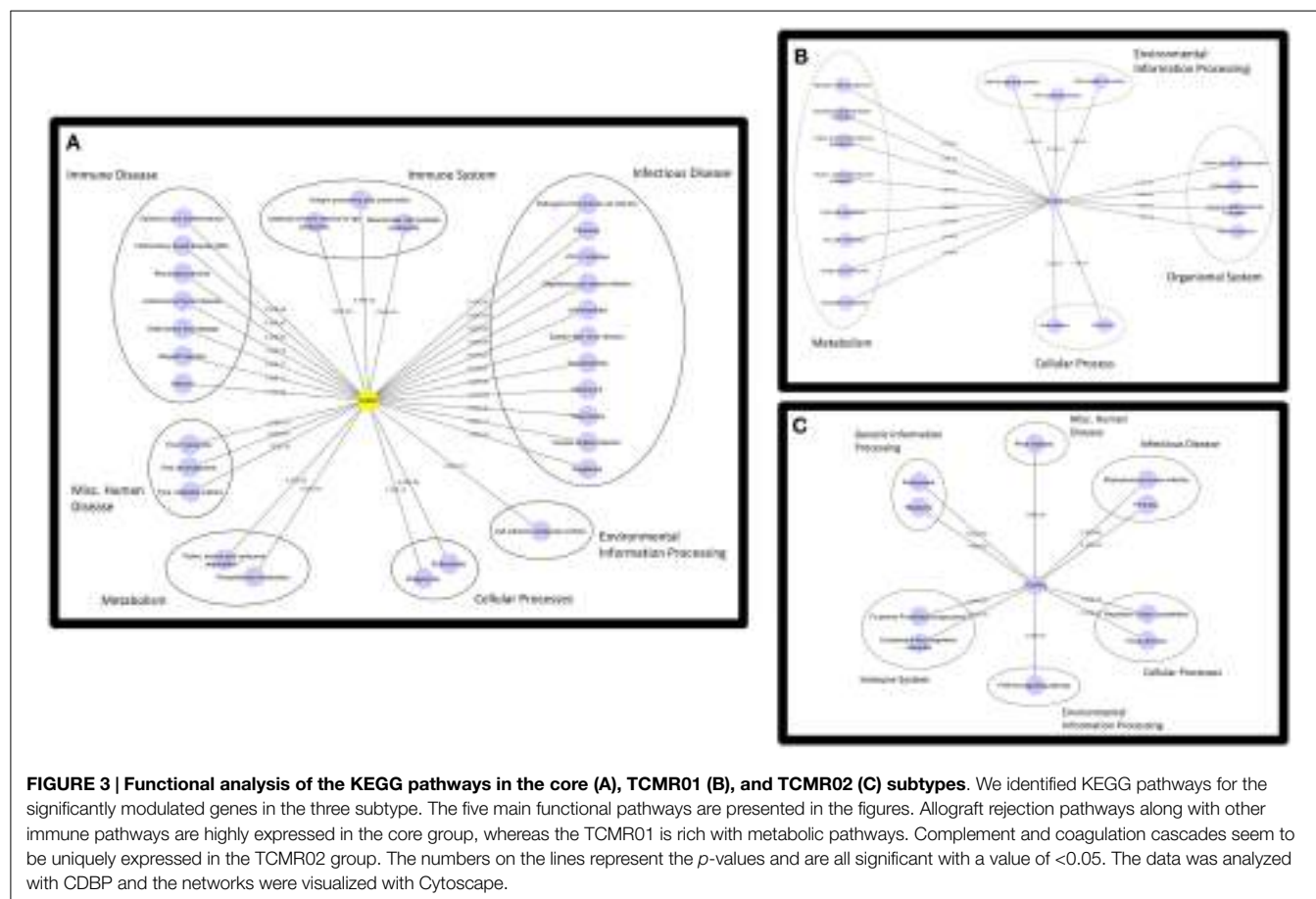


FIGURE 2 | (A) Comparison of TCMR01 and TCMR02 with the normal and nephrectomy controls. Unsupervised hierarchical clustering of TCMR01, TCMR02, NEPH01 (nephrectomy) and NORM01 (normal biopsy samples). **(B)** The subtypes of T cell-mediated rejection (TCMR) classified by unsupervised hierarchical clustering. After filtering the initial 54,675 Affymetrix probe sets based upon scaled expression and coefficient of variation, we identified two distinct groups of T cell-Mediated Rejection: TCMR01 (left) and TCMR02 (right). The two sub-diagnoses were differentiated by 1933 significant genes based upon false-discovery rate corrected p -values of 0.05.

rejection” is more than an order of magnitude more significant than the other pathways. In addition to immune processes, we also detected significant metabolic pathways including “tryptophan metabolism” ($q < 0.000152$), “histidine metabolism”

($q < 0.000194$), “glycine, serine, and threonine metabolism” ($q < 0.00154$), “fatty acid degradation” ($q < 0.00242$), “valine, leucine, and isoleucine degradation” ($q < 0.00285$), “arginine and proline metabolism” ($q < 0.0074$), and “fructose and mannose



metabolism” ($q < 0.00864$) that may be important in modulating the immune response and could potentially serve as novel therapeutic targets. In contrast to the core response, the pathways associated with the TCMR01 subtype predominantly involved metabolism. The pathways represented a diverse array of metabolic functions ranging from the citrate cycle to amino acid metabolism to glyoxylate metabolism to extracellular matrix interaction. The TCMR01 subtype did not contain any significant pathways directly involving immune functions, whereas the TCMR02 included a number of immune responses associated with infections, complement and coagulation cascades and natural killer cell-mediated cytotoxicity. Based on the KEGG pathway analysis, our data indicate that the TCMR01 and TCMR02 subtypes of rejection, in addition to differential gene expression, have different biological functions.

Protein Interactions

To investigate the mechanisms regulating the different biological functions in the different subtypes of rejection, we constructed PIP graphs (Figure 4). Overall, it is apparent that the PIPs include subnetworks involved a diverse array of biological processes. For example, the core genes common to both subtypes mediated upregulation of HLA class I and II molecules, expression of cytoskeletal molecules including tubulin, fibulin,

and actin-binding proteins, proteasome components, IFN γ receptor, and interferon response factors and regulators of stress and energy production. The TCMR01 subtype upregulated collagen and metabolic enzymes. In contrast, the TCMR02 subtype had increased expression of RANTES, complement components of C1q, matrix protein keratin 19, cytoskeletal components of actin and tropomyosin, proteasome components, and GTP-binding proteins.

Transcription Factors

Next, we analyzed the mechanisms regulating the differential gene expression by focusing on the regulation of gene expression by transcription factors (Figure 5). In the core genes, we detected STAT1, JUND, HNF1, and IKB. In contrast, transcription factors unique to the TCMR01 subtype include STAT3, FRA, JUNB, MYC, GR, and ZIC1, whereas transcription factors unique to the TCMR02 subtype include STAT2, MAFB, Kaiso, EGR1, and CEBPD. In addition, FKBP5, which is a *cis-trans* prolyl isomerase that mediates calcineurin inhibition and binds the immunosuppressants, FK506 and rapamycin is upregulated in TCMR02. The differential abundance of transcription factors, which are known to be regulated by different cytokines and growth factors, suggest the activation of different signal transduction pathways in the two rejection subtypes.

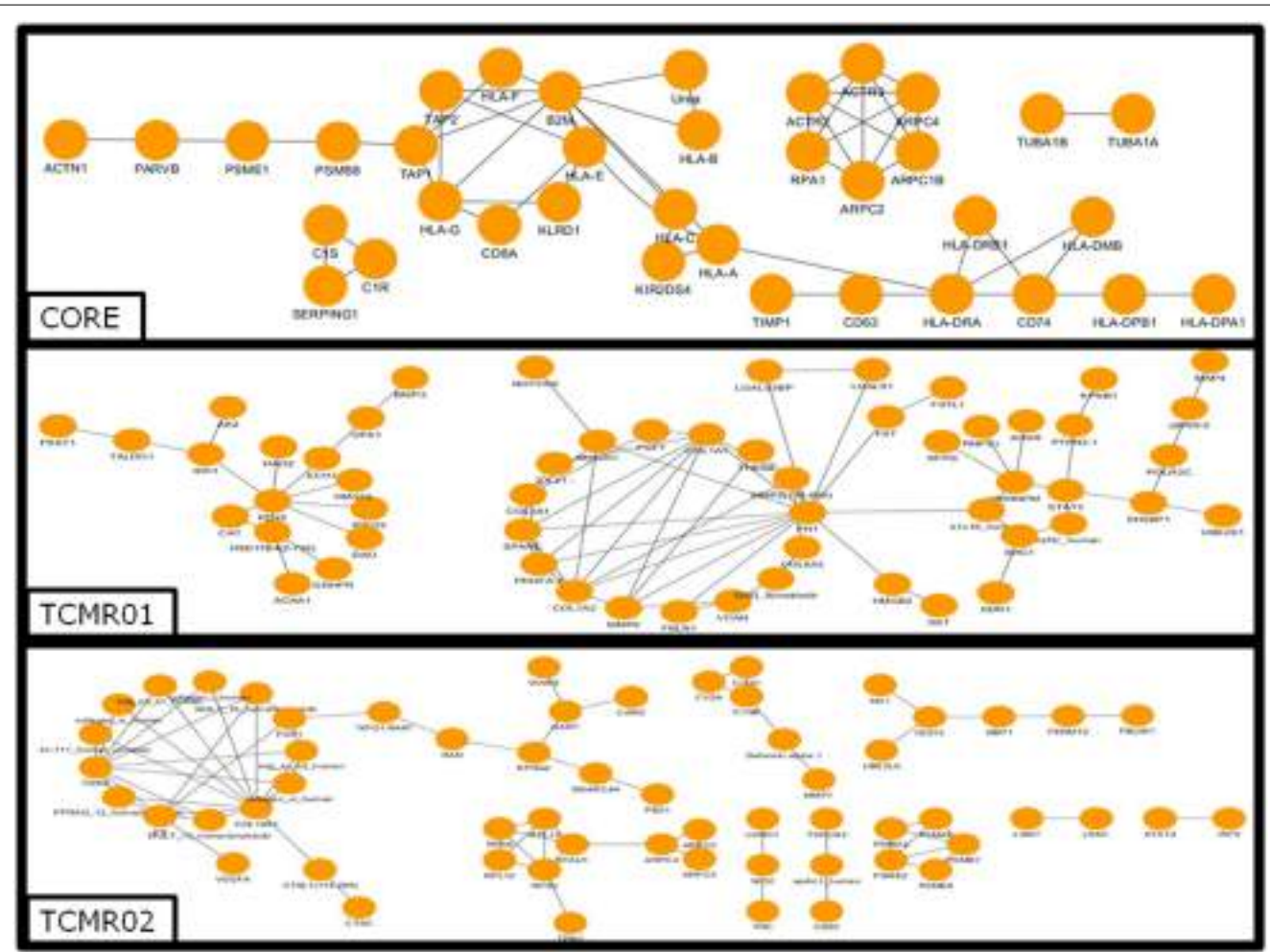


FIGURE 4 | Analysis of the protein–protein interaction networks in the core, TCMR01 and TCMR02 subtypes. We identified the protein–protein interaction networks of the significantly modulated genes for the core, TCMR01 and TCMR02. Each node represents a protein from the input gene list, and each edge shows a high-confidence protein–protein interaction (PPI). The three subnetworks show how the TCMR subtypes are vastly different on a molecular level. The data was analyzed with CDBP and the networks were visualized with Cytoscape.

Drug–Target Interactions

Given the different transcription factor and effector mechanisms functioning in the different subtypes, we investigated the notion that different treatment modalities would be more precise for each subtype of rejection. An analysis of the potential therapeutic drugs effective against the core genes containing both TCMR01 and TCMR02 phenotypes identifies multiple drugs that have been studied in clinical trials or FDA approved as treatment for transplantation including Muromonab (OKT3), Epothilone B, Epothilone D, Gemtuzumab ozogamicin, Ibritumomab, PDX, Fucose, Sulfasalazine, and TNRF2 (cleaved) (Figure 6). In an analysis of drugs that may be more precisely targeted to each subtype, we identified, as expected based on the PIP, drugs targeted to metabolic processes in TCMR01. In contrast, among the drugs targeted to TCMR02, we detected 15 agents in clinical use or that have undergone clinical trials including Alemtuzumab, Alefacept, and Gemtuzumab. In addition, several potential cancer drugs had potential targets in the TCMR02 subtype. These results suggest that our analytical methods may identify therapeutic

drugs that would be more precise in the treatment of subtypes of TCMR.

DISCUSSION

In this study, we investigated the hypothesis that the histological classification of TCMR contained multiple subtypes of rejection involving different biological pathways and functions. Our analysis using systems biology approaches identified two distinct subtypes of rejection, TCMR01 and TCMR02. We confirmed the validity of the clusters by three criteria (connectivity, Dunn index, and Silhouette index). A direct comparison of gene expression between the two subtypes identified 1933 genes that were significantly differentially expressed ($fdr < 0.05$) despite the fact that all samples had a similar histological diagnosis. We suggest that the significance of our study is the demonstration of the proof of principle that analysis of the transcriptome may be a more precise classifier than current histological diagnoses.

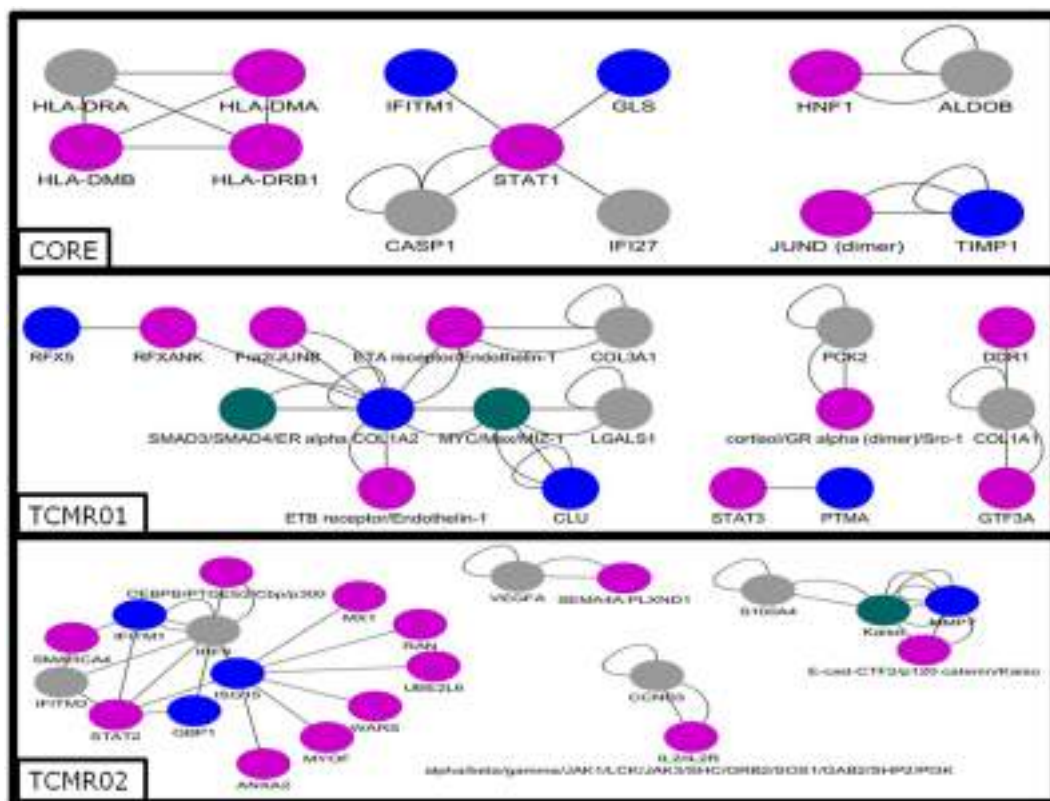


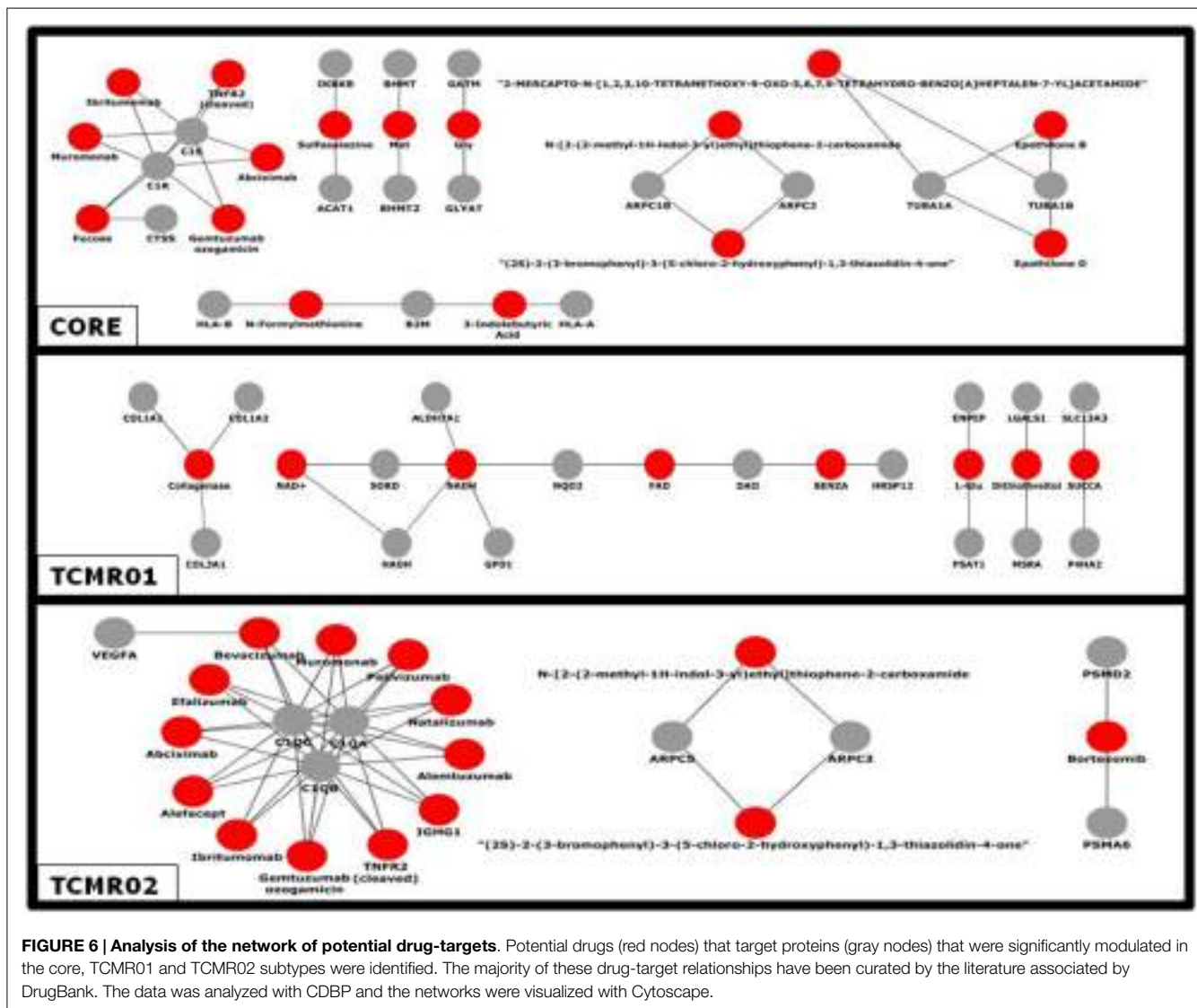
FIGURE 5 | Analysis of the gene regulatory interaction networks in the core, TCMR01 and TCMR02 subtypes. We identified putative gene regulatory networks in the core, TCMR01 and TCMR02 based on the significantly modulated genes (blue nodes). The contrasting elements in the two subnetworks show that the TCMR subtypes are different on the level of transcriptional regulation. The data was analyzed with CDBP and the networks. Gray nodes represent products. Purple nodes represent transcription factors. Green nodes represent repressors.

We identified three groups of differentially expressed genes that composed the core response defined as the genes common to both subtypes and groups unique to each subtype of rejection. A functional analysis of gene expression data using the KEGG database identified different functions for each group (18). For example, the core functions that were based on genes differentially expressed in both subtypes included immune functions involved in alloimmune responses. In fact, the most significant pathway was “allograft rejection,” which strongly supports the validity of our analysis. In contrast, the KEGG pathways associated with the unique genes in TCMR01 included predominantly metabolic functions (e.g., glyoxylate metabolism, amino acid metabolism, and citrate cycle), which may indicate parenchymal damage to the graft. The pathways unique in TCMR02 included complement and coagulation cascades and natural killer cell cytotoxicity. Thus, at the functional level our analysis demonstrated core functions common to both subtypes as well as unique functions specific for either TCMR01 or TCMR02. The unique functions suggest potential strategies to develop precision treatments, potentially applicable to transplant rejection.

We analyzed the KEGG database, which is collated on current knowledge (22). It is notable that multiple pathways activated in the core genes were either immune or metabolic processes. For example, another immune pathway was graft-versus-host disease;

however, the patients did not have clinical evidence of graft-versus-host disease. Importantly, this pathway was more than one order of magnitude less significant than allograft rejection and a manual inspection of the relevant genes in these pathways shows that the identical genes can participate in multiple broad disease focused KEGG pathways, such as allograft rejection or GVHD. Thus, when evaluating these disease pathways, it is essential to include additional criteria such as clinical correlates or metadata. When considering the more biologically fundamental pathways (e.g., phagosome, histidine metabolism, proteasome, fatty acid degradation, valine degradation, endocytosis, natural killer cell cytotoxicity, arginine metabolism, and fructose metabolism), we observed that the relevant genes are activated.

We also investigated potential mechanisms that mediated the disease processes identified by KEGG pathways. At the level of protein interactions, the core response includes anticipated immune molecules including HLA Class I and II, CD8, and complement receptors. In addition, we identified antigen processing and presenting molecules (HLA-DM β , proteasome, and CD74) cytoskeletal proteins (tubulin, actin). In contrast, the TCMR01-specific proteins included numerous metabolic mediators and collagen proteins suggesting possible wound healing and fibrosis. The TCMR02-specific proteins included C1q complement proteins, FKBP, RANTES, and cathepsin O. At the level of differential



expression of transaction factors, there were differences among the three groups. Interestingly, an analysis of the STAT molecules showed that the core response included STAT1, TCMR01 included STAT3, and TCMR02 included STAT2 indicating the activation of different signal transduction pathways in each group.

Considered as a whole, we emphasize that the most compelling observation of our systems biology approach is the demonstration that diverse biological mechanisms are coordinated in an integrated response in allograft rejection. As expected, multiple immune mechanisms are identified (e.g., MHC Class I and II, complement pathways, cytokines, and chemokines). In addition, genes involved in regulation of the cytoskeleton, extracellular matrix, metabolism, gene regulation, apoptosis, signal transduction, and stress response were identified. Importantly, diverse regulatory mechanisms that could potentially coordinate the regulation of these mechanisms were also identified including regulators of transcription, RNA processing, splicing and stability, translation, nuclear transport, chromatin remodeling and epigenetic modifications. The subnetworks and pathways depicted in

our analyses identify some of the molecular interactions that may regulate and coordinate the biological systems in TCMR.

Bunnag et al. analyzed the relationship between the molecular expression, histopathology, and renal function in kidney transplant biopsies with low GFR using microarray technology. They analyzed transcripts differentially expressed in patients with low versus high GFR. They noted that the highest expressed were tissue injury transcripts, whereas the lowest expressed were the kidney parenchyma transcripts (23). Genes which were highly expressed in the tissue injury pathway included integrins, keratin genes and a metalloproteinase gene (MMP7) were noted in our TCMR02 group. This indicates that our analysis of rejection subtypes identifies some of the same genes. A major difference between the studies is that the study population analyzed by Bunnag et al. only included 13% biopsy proven TCMR. Einecke et al. investigated whether there is a specific transcriptome indicative of organ failure when the biopsy is performed 1 year after transplantation. A direct analysis between our gene data set and their gene data set shows a 50% shared genes in the core and TCMR01 groups

and 37% with the TCMR02 group (Supplementary Material) (17). Their study population had multiple causes of graft failure and only 13% had TCMR. The authors developed a gene expression risk score which was predictive of graft failure in biopsies of kidney transplants greater than 1 year after transplantation. Their analysis differs from ours as they did not focus on TCMR but rather analyzed all biopsies with graft dysfunction. As expected, the genes associated with graft failure had functions related to tissue injury. Sarwal et al. analyzed microarray data from 59 pediatric renal allograft biopsies with poor function. They identified three different signatures of the transcriptome although the samples were indistinguishable by light microscopy (24). Their study re-emphasizes the need to establish a genetic classification which will aid in the management of TCMR, which is the problem our study addressed. We analyzed microarray data of only TCMR biopsies and classified the results into two major subtypes according to their functional pathways. Our detailed approach allowed us to identify specific pathways, which may be targeted in the future with specific therapies for TCMR01 or TCMR02 subtype of rejection. This new classification could provide specific therapeutic targets for personalized treatment.

Our study identified two specific subtypes of rejection, TCMR01 or TCMR02. As expected, we also identified drugs that had putative targets in both subtypes. Interestingly, a number of the drugs that were potential therapies are either current or previous therapies (Muromonab, Alemtuzumab, and Alefacept), are in clinical trials or are treatments for other diseases including cancer (Abciximab, Gemtuzumab ozogamicin, Ibritumomab, sunitinib, Bevacizumab, CPG52364, mc0457,

mln518, ptk787, Ranibizumab, PDX, Efalizumab, and Natalizumab) (25–40). The fact that some of these agents have been clinically effective in the treatment of rejection (e.g., Muromonab) supports the validity of the analysis and suggests that it could be informative to develop clinical trials that link therapeutic agents with a specific molecular classification, either TCMR01 or TCMR02. In addition, future studies that combine integrated omics analyses, e.g., combining proteomics, metabolomics, etc., with transcriptomics could increase the power of a systems analysis.

AUTHOR CONTRIBUTIONS

DP designed the systems biology approach of the project. PF and DP provided direction for the analyses and interpretation of the data. ZH, PF and DP provided clinical insights to genetic output. PK implemented the statistical calculations and created the network visualizations.

ACKNOWLEDGMENTS

This research was made possible by an NIH RO1 Grant (RO1AI075317).

SUPPLEMENTARY MATERIAL

The Supplementary Material for this article can be found online at <http://journal.frontiersin.org/article/10.3389/fimmu.2015.00536>

REFERENCES

- Chong AS, Perkins DL. Transplantation: molecular phenotyping of T-cell-mediated rejection. *Nat Rev Nephrol* (2014) **10**(12):678–80. doi:10.1038/nrneph.2014.197
- Halloran PE. T cell-mediated rejection of kidney transplants: a personal viewpoint. *Am J Transplant* (2010) **10**(5):1126–34. doi:10.1111/j.1600-6143.2010.03053.x
- Saint-Mezard P, Berthier CC, Zhang H, Hertig A, Kaiser S, Schumacher M, et al. Analysis of independent microarray datasets of renal biopsies identifies a robust transcript signature of acute allograft rejection. *Transpl Int* (2009) **22**(3):293–302. doi:10.1111/j.1432-2277.2008.00790.x
- Reeve J, Sellarés J, Mengel M, Sis B, Skene A, Hidalgo L, et al. Molecular diagnosis of T cell-mediated rejection in human kidney transplant biopsies. *Am J Transplant* (2013) **13**(3):645–55. doi:10.1111/ajt.12079
- Halloran PE, Pereira AB, Chang J, Matas A, Picton M, De Freitas D, et al. Potential impact of microarray diagnosis of T cell-mediated rejection in kidney transplants: the INTERCOM study. *Am J Transplant* (2013) **13**(9):2352–63. doi:10.1111/ajt.12387
- Famulski KS, Einecke G, Sis B, Mengel M, Hidalgo LG, Kaplan B, et al. Defining the canonical form of T-cell-mediated rejection in human kidney transplants. *Am J Transplant* (2010) **10**(4):810–20. doi:10.1111/j.1600-6143.2009.03007.x
- Venner JM, Famulski KS, Badr D, Hidalgo LG, Chang J, Halloran PE. Molecular landscape of T cell-mediated rejection in human kidney transplants: prominence of CTLA4 and PD ligands. *Am J Transplant* (2014) **14**(11):2565–76. doi:10.1111/ajt.12946
- Bhowmik DM, Dinda AK, Mahanta P, Agarwal SK. The evolution of the Banff classification schema for diagnosing renal allograft rejection and its implications for clinicians. *Indian J Nephrol* (2010) **20**(1):2–8. doi:10.4103/0971-4065.62086
- Mengel M, Sis B, Halloran PE. SWOT analysis of Banff: strengths, weaknesses, opportunities and threats of the international Banff consensus process and classification system for renal allograft pathology. *Am J Transplant* (2007) **7**(10):2221–6. doi:10.1111/j.1600-6143.2007.01924.x
- Furness PN, Taub N. International variation in the interpretation of renal transplant biopsies: report of the CERTPAP project1. *Kidney Int* (2001) **60**(5):1998–2012. doi:10.1046/j.1523-1755.2001.00030.x
- Gough J, Rush D, Jeffery J, Nickerson P, McKenna R, Solez K, et al. Reproducibility of the Banff schema in reporting protocol biopsies of stable renal allografts. *Nephrol Dial Transplant* (2002) **17**(6):1081–4. doi:10.1093/ndt/17.6.1081
- Marcussen N, Olsen TS, Benediktsson H, Racusen L, Solez K. Reproducibility of the Banff classification of renal allograft pathology: inter- and intraobserver variation. *Transplantation* (1995) **60**(10):1083–9. doi:10.1097/00007890-19951270-00004
- Krisl JC, Alloway RR, Shield AR, Govil A, Mogilishetty G, Cardi M, et al. Acute rejection clinically defined phenotypes correlate with long-term renal allograft survival. *Transplantation* (2015) **99**(10):2167–73. doi:10.1097/TP.0000000000000706
- Wu K, Budde K, Lu H, Schmidt D, Liefeldt L, Glander P, et al. The severity of acute cellular rejection defined by Banff classification is associated with kidney allograft outcomes. *Transplantation* (2014) **97**(11):1146–54. doi:10.1097/01.TP.0000441094.32217.05
- Gentleman RC, Carey VJ, Bates DM, Bolstad B, Dettling M, Dudoit S, et al. Bioconductor: open software development for computational biology and bioinformatics. *Genome Biol* (2004) **5**(10):R80. doi:10.1186/gb-2004-5-10-r80
- Davis S, Meltzer PS. GEOquery: a bridge between the gene expression omnibus (GEO) and bioconductor. *Bioinformatics* (2007) **23**(14):1846–7. doi:10.1093/bioinformatics/btm254
- Einecke G, Reeve J, Sis B, Mengel M, Hidalgo L, Famulski KS, et al. A molecular classifier for predicting future graft loss in late kidney transplant biopsies. *J Clin Invest* (2010) **120**(6):1862–72. doi:10.1172/JCI41789

18. Edgar R, Domrachev M, Lash AE. Gene expression omnibus: NCBI gene expression and hybridization array data repository. *Nucleic Acids Res* (2002) **30**(1):207–10. doi:10.1093/nar/30.1.207
19. R Development Core Team. *R: A Language for Statistical Computing*. Vienna: R Foundation for Statistical Computing (2010).
20. Kamburov A, Pentchev K, Galicka H, Wierling C, Lehrach H, Herwig R. ConsensusPathDB: toward a more complete picture of cell biology. *Nucleic Acids Res* (2011) **39**(Database issue):D712–7. doi:10.1093/nar/gkq1156
21. Shannon P, Markiel A, Ozier O, Baliga NS, Wang JT, Ramage D, et al. Cytoscape: a software environment for integrated models of biomolecular interaction networks. *Genome Res* (2003) **13**(11):2498–504. doi:10.1101/gr.123930
22. Ogata H, Goto S, Sato K, Fujibuchi W, Bono H, Kanehisa M. KEGG: Kyoto encyclopedia of genes and genomes. *Nucleic Acids Res* (1999) **27**(1):29–34. doi:10.1093/nar/27.1.29
23. Bunnag S, Einecke G, Reeve J, Jhangri GS, Mueller TF, Sis B, et al. Molecular correlates of renal function in kidney transplant biopsies. *J Am Soc Nephrol* (2009) **20**(5):1149–60. doi:10.1681/ASN.2008080863
24. Sarwal M, Chua MS, Kambham N, Hsieh SC, Satterwhite T, Masek M, et al. Molecular heterogeneity in acute renal allograft rejection identified by DNA microarray profiling. *N Engl J Med* (2003) **349**(2):125–38. doi:10.1056/NEJMoa035588
25. Smith SL. Ten years of orthoclone OKT3 (muromonab-CD3): a review. *J Transl Coord* (1996) **6**(3):109–19. doi:10.7182/prtr.1.6.3.8145l3u185493182
26. Hanaway MJ, Woodle ES, Mulgaonkar S, Peddi VR, Kaufman DB, First MR, et al. Alemtuzumab induction in renal transplantation. *N Engl J Med* (2011) **364**(20):1909–19. doi:10.1056/NEJMoa1009546
27. Bashir SJ, Maibach HI. Alefacept (Biogen). *Curr Opin Investig Drugs* (2001) **2**(5):631–4.
28. Best PJ, Lennon R, Gersh BJ, Ting HH, Rihal CS, Bell MR, et al. Safety of abciximab in patients with chronic renal insufficiency who are undergoing percutaneous coronary interventions. *Am Heart J* (2003) **146**(2):345–50. doi:10.1016/S0002-8703(03)00231-X
29. Bross PF, Beitz J, Chen G, Chen XH, Duffy E, Kieffer L, et al. Approval summary: gemtuzumab ozogamicin in relapsed acute myeloid leukemia. *Clin Cancer Res* (2001) **7**(6):1490–6.
30. Witzig TE. The use of ibritumomab tiuxetan radioimmunotherapy for patients with relapsed B-cell non-Hodgkin's lymphoma. *Semin Oncol* (2000) **27**(6 Suppl 12):74–8.
31. Motzer RJ, Hutson TE, Tomczak P, Michaelson MD, Bukowski RM, Rixe O, et al. Sunitinib versus interferon alfa in metastatic renal-cell carcinoma. *N Engl J Med* (2007) **356**(2):115–24. doi:10.1056/NEJMoa065044
32. Shih T, Lindley C. Bevacizumab: an angiogenesis inhibitor for the treatment of solid malignancies. *Clin Ther* (2006) **28**(11):1779–802. doi:10.1016/j.clinthera.2006.11.015
33. Ponzio NM, Cutro S, Hu J, Marzouk A, Marshall JD. CpG oligodeoxynucleotide-induced immunity prevents growth of germinal center-derived B lymphoma cells. *Int Immunopharmacol* (2006) **6**(13–14):2057–68. doi:10.1016/j.intimp.2006.08.008
34. Li Y, Zhang ZF, Chen J, Huang D, Ding Y, Tan MH, et al. VX680/MK-0457, a potent and selective Aurora kinase inhibitor, targets both tumor and endothelial cells in clear cell renal cell carcinoma. *Am J Transl Res* (2010) **2**(3):296–308.
35. DeAngelo DJ, Stone RM, Heaney ML, Nimer SD, Paquette RL, Klisovic RB, et al. Phase 1 clinical results with tandutinib (MLN518), a novel FLT3 antagonist, in patients with acute myelogenous leukemia or high-risk myelodysplastic syndrome: safety, pharmacokinetics, and pharmacodynamics. *Blood* (2006) **108**(12):3674–81. doi:10.1182/blood-2006-02-005702
36. Yamamoto A, Watanabe H, Sueki H, Nakanishi T, Yasuhara H, Iijima M. Vascular endothelial growth factor receptor tyrosine kinase inhibitor PTK787/ZK 222584 inhibits both the induction and elicitation phases of contact hypersensitivity. *J Dermatol* (2007) **34**(7):419–29. doi:10.1111/j.1346-8138.2007.00304.x
37. Gaudreault J, Fei D, Beyer JC, Ryan A, Rangell L, Shiu V, et al. Pharmacokinetics and retinal distribution of ranibizumab, a humanized antibody fragment directed against VEGF-A, following intravitreal administration in rabbits. *Retina* (2007) **27**(9):1260–6. doi:10.1097/IAE.0b013e318134eecc
38. Shimanovsky A, Dasanu CA. Pralatrexate: evaluation of clinical efficacy and toxicity in T-cell lymphoma. *Expert Opin Pharmacother* (2013) **14**(4):515–23. doi:10.1517/14656566.2013.770474
39. Koszik F, Stary G, Selenko-Gebauer N, Stingl G. Efalizumab modulates T cell function both in vivo and in vitro. *J Dermatol Sci* (2010) **60**(3):159–66. doi:10.1016/j.jdermsci.2010.10.003
40. Ghosh S, Goldin E, Gordon FH, Malchow HA, Rask-Madsen J, Rutgeerts P, et al. Natalizumab for active Crohn's disease. *N Engl J Med* (2003) **348**(1):24–32. doi:10.1056/NEJMoa020732

Conflict of Interest Statement: The authors declare that the research was conducted in the absence of any commercial or financial relationships that could be construed as a potential conflict of interest.

Copyright © 2015 Kadota, Hajjiri, Finn and Perkins. This is an open-access article distributed under the terms of the Creative Commons Attribution License (CC BY). The use, distribution or reproduction in other forums is permitted, provided the original author(s) or licensor are credited and that the original publication in this journal is cited, in accordance with accepted academic practice. No use, distribution or reproduction is permitted which does not comply with these terms.



Cardiac Arrest Disrupts Caspase-1 and Patterns of Inflammatory Mediators Differently in Skin and Muscle Following Localized Tissue Injury in Rats: Insights from Data-Driven Modeling

Ravi Starzl^{1,2,3*}, Dolores Wolfram⁴, Ruben Zamora^{5,6}, Bahiyyah Jefferson⁵, Derek Barclay⁵, Chien Ho⁷, Vijay Gorantla², Gerald Brandacher³, Stefan Schneeberger³, W. P. Andrew Lee³, Jaime Carbonell¹ and Yoram Vodovotz^{5,6}

OPEN ACCESS

Edited by:

Julia Arciero,
Indiana University-Purdue University
Indianapolis, USA

Reviewed by:

Carson C. Chow,
National Institutes of Health, USA
David L. Perkins,
UIC, USA

*Correspondence:

Ravi Starzl
rstarzl@cs.cmu.edu

Specialty section:

This article was submitted to
Alloimmunity and Transplantation,
a section of the journal
Frontiers in Immunology

Received: 01 May 2015

Accepted: 02 November 2015

Published: 20 November 2015

Citation:

Starzl R, Wolfram D, Zamora R, Jefferson B, Barclay D, Ho C, Gorantla V, Brandacher G, Schneeberger S, Andrew Lee WP, Carbonell J and Vodovotz Y (2015) Cardiac Arrest Disrupts Caspase-1 and Patterns of Inflammatory Mediators Differently in Skin and Muscle Following Localized Tissue Injury in Rats: Insights from Data-Driven Modeling. *Front. Immunol.* 6:587.
doi: 10.3389/fimmu.2015.00587

¹Language Technologies Institute, Carnegie Mellon University, Pittsburgh, PA, USA, ²Department of Plastic and Reconstructive Surgery, University of Pittsburgh, Pittsburgh, PA, USA, ³Department of Plastic and Reconstructive Surgery, Johns Hopkins Medicine, Baltimore, MD, USA, ⁴Department of Plastic and Reconstructive Surgery, Innsbruck Medical University, Innsbruck, Austria, ⁵Department of Surgery, University of Pittsburgh, Pittsburgh, PA, USA, ⁶Center for Inflammation and Regenerative Modeling, McGowan Institute for Regenerative Medicine, University of Pittsburgh, Pittsburgh, PA, USA, ⁷Department of Biological Sciences, Carnegie Mellon University, Pittsburgh, PA, USA

Background: Trauma often cooccurs with cardiac arrest and hemorrhagic shock. Skin and muscle injuries often lead to significant inflammation in the affected tissue. The primary mechanism by which inflammation is initiated, sustained, and terminated is cytokine-mediated immune signaling, but this signaling can be altered by cardiac arrest. The complexity and context sensitivity of immune signaling in general has stymied a clear understanding of these signaling dynamics.

Methodology/principal findings: We hypothesized that advanced numerical and biological function analysis methods would help elucidate the inflammatory response to skin and muscle wounds in rats, both with and without concomitant shock. Based on the multiplexed analysis of inflammatory mediators, we discerned a differential interleukin (IL)-1 α and IL-18 signature in skin vs. muscle, which was suggestive of inflammasome activation in the skin. Immunoblotting revealed caspase-1 activation in skin but not muscle. Notably, IL-1 α and IL-18, along with caspase-1, were greatly elevated in the skin following cardiac arrest, consistent with differential inflammasome activation.

Conclusion/significance: Tissue-specific activation of caspase-1 and the NLRP3 inflammasome appear to be key factors in determining the type and severity of the

Abbreviations: BRD, band relative density; CTA, composite tissue allotransplantation; df, degrees of freedom; F, F-statistic (ratio of the between-group and within-group mean squares); FAN, confirmatory factor analysis; “injury only,” excisional wound group; LPS, lipopolysaccharide; MS, mean squares (the ratio SS/df); NMR, nuclear magnetic resonance; PCA, principal component analysis; PMN, polymorphonuclear neutrophil; “shock associated with cardiac arrest,” cardiac arrest group; SS, sum of squares.

inflammatory response to tissue injury, especially in the presence of severe shock, as suggested via data-driven modeling.

Keywords: Inflammasome, inflammatory mediators, computational modeling, data driven modeling, cardiac arrest and trauma, immunoregulatory, localized tissue injury, hemorrhagic shock

INTRODUCTION

Healthy skin and muscle tissue exist in a steady-state equilibrium that is characterized in large part by the absence of acute inflammation (1). When injured, the tissue's steady state is upset, inducing a cascade of responses that include inflammation, repair, and remodeling of the affected region. The inflammatory response is an essential part of successful wound healing and sets the stage for effective repair and remodeling (2). The composition of the underlying inflammatory/immune signaling that drives the inflammatory response to injury is therefore critical in determining whether the inflammation ultimately leads to successful healing or instead leads to additional damage and dysfunctional tissue healing. However, when inflammatory signaling proportional to an injury is altered, the inflammatory response does not successfully transition to subsequent stages of tissue healing (3). Significant systemic insults, such as cardiac arrest, have the potential to drastically alter local immune signaling activity and possibly disrupt wound healing. To the best of our knowledge, the effect of cardiac arrest on these local wound-healing-associated immune signaling processes has not been elucidated.

In the setting of both civilian and military trauma, severe local tissue injury can often be accompanied by cardiac arrest (4–7). Cardiac arrest affects numerous physiological processes, as well as setting in motion systemic inflammation (8–11). Although short-term hypoxia may be an important part of stimulating wound healing (12), severe or extended disruption of oxygen supply interferes with successful wound healing (13). We hypothesize that the specific local inflammatory mediator network patterns expressed during the initial inflammatory response contain information about how the immune system is responding to a localized injury, and whether the response is leading to successful or dysfunctional healing outcome.

Cardiac arrest, even with eventual sudden restoration of blood flow, is known to cause significant cellular stress, the buildup of toxins, and the release of endogenous danger signals that can promote inflammation. In the neurological context, cardiac arrest is particularly well understood to cause a great deal of damage to nerves. Therefore, we further hypothesize that the eventual sudden restoration of blood flow will in essence create an ischemia/reperfusion milieu characterized by the further release of inflammatory mediators, which will have a further deleterious effect on properly localized and moderated wound healing.

The domain of wound healing has been extensively studied with many excellent articles and reviews that provide an overview of the phases, cellular processes, and molecular signals that have been observed in various wound-healing settings (2, 14–18). The effect of the insult of cardiac arrest on patient outcomes has been studied with respect to the impact on patient survival and

neurological damage, with significant focus on the potential protective effects of induced mild hypothermia (19–22). However, to the best of our knowledge, no prior studies examine the effect that cardiac arrest may have on the local immune signaling processes essential to inflammation and wound healing.

Analysis and interpretation of the immune signaling process that drives inflammation is challenging because of the complex interplay among inflammatory mediators and their sensitive dependence on local and systemic conditions. Consequently, analysis of the progression of inflammation must leverage analytic methods and the insights that are capable of robustly assessing multiple dimensions of variance simultaneously, and of obtaining relevant information from high-dimensional data matrices (23).

A variety of data analysis methods suitable to exposing the internal structure of such noisy, high-dimensional data have been developed and utilized extensively for the analysis of complex systems in areas such as computational linguistics and machine learning (24). We and others have suggested the need to employ data-driven computational modeling in order to derive insights from the types of high-dimensional datasets obtained when studying complex biological system, such as the inflammatory response (25–27). We have explored multiple techniques for visualizing and enumerating salient features of acute inflammation in both preclinical and clinical settings, thus providing some insight into the types of analytic methods likely to be effective in elucidating key aspects of the observed inflammatory response (25, 28–37).

In the present study, we investigated patterns of immune signaling induced *in vivo* in rat skin and muscle following tissue injury in the form of excisional wounding. We then carried out *in silico* analyses to define principal drivers of local inflammatory responses, in the presence or absence of cardiac arrest. We demonstrate that tissue-specific immune signaling patterns are modified by cardiac arrest (also a paradigm of severe hemorrhagic shock) and suggest that inflammasome activity may govern the type of inflammation initiated.

MATERIALS AND METHODS

Rat Model of Tissue Injury

To simulate tissue injury, we carried out deep tissue excisional biopsies of skin and muscle (38, 39). All animal procedures, care, and housing were reviewed and approved by the University of Pittsburgh Institutional Animal Care and Use Committee and followed the National Institutes of Health guidelines for the care and use of laboratory animals. We divided the study into two experimental groups: injury only (injury group) and injury with cardiac arrest (cardiac arrest group). In the “injury group,” four Lewis rats were anesthetized, and an excision biopsy was taken

from the lateral aspect of the thigh on one of the hind limbs in each of the rats. Tissue was drawn away from the body and held in forceps while surgical scissors cut 15 mm × 10 mm of tissue from the lateral aspect of the thigh. In the “cardiac arrest group,” four Lewis rats were sacrificed with a fatal sodium pentobarbital (Lundbeck Inc., Deerfield, IL, USA) overdose, and excision biopsy taken 15–30 s after cessation of heartbeat.

Protein Isolation and Sample Preparation

We have previously shown the preservation of animal and human tissues in RNALater™ (Ambion, Austin, TX, USA) is a method compatible with subsequent Luminex™ analysis (40–42). Accordingly, all tissue samples were sectioned into ≤0.5 cm³ pieces and placed into individual sample tubes filled with RNALater™ and stored as per manufacturer instructions and as determined empirically in our prior study (40). For tissue processing, approximately 50 mg of the tissue was transferred to a 2-ml microcentrifuge tube containing 0.6 ml of 1× BioSource™ (Invitrogen, San Diego, CA, USA) tissue extraction reagent supplemented with 10 µl of 100mM phenylmethanesulfonyl fluoride in ethanol as a protease inhibitor. The tissues were then homogenized using a tissue homogenizer, then centrifuged at 4°C for 10 min at 10,000 × g. After centrifugation, the supernatant were collected and assayed for protein content using the bicinchoninic acid (BCA) protein assay (Pierce, Rockford, IL, USA) as per manufacturer’s protocol.

Assays for Inflammation Biomarkers

All samples were assayed for inflammatory cytokines and chemokines using the Luminex™ multiplexing platform (100 IS; MiraiBio, Alameda, CA, USA) and a Millipore™ 14-plex rat cytokine bead set (Millipore, Billerica, MA, USA) that included interferon (IFN) γ, interleukin (IL)-1α, IL-1β, IL-2, IL-4, IL-5, IL-6, IL-10, IL-12p70, IL-18, monocyte chemotactic protein (MCP-1), GRO/KC, TNFα, and granulocyte-macrophage colony-stimulating factor (GM-CSF). Results were read in picogram per milliliter, then subsequently normalized to total mass of sample protein (picogram of cytokine/milligram of protein) for each of the 14 cytokines by the formula $x = (a/b) \times 1000$, where x = (picogram of cytokine/milligram of protein), a = (picogram per milliliter of cytokine), and b = (microgram per milliliter of protein).

For immunodetection of caspase-1, protein samples (25 µg) were separated on 12% SDS-polyacrylamide gels, and the gels were electroblotted onto PVDF membranes. After overnight blocking, the membranes were incubated overnight with a rabbit polyclonal antibody from Abcam (Cambridge, MA, USA) at 4°C followed by 1 h incubation with a goat antirabbit secondary antibody from Pierce (Rockford, IL, USA) at room temperature. Bands were detected using the Supersignal™ West Dura Extended Duration Substrate Chemiluminescent kit as per the manufacturer instructions. All readings are for active caspase-1 (20 kDa).

For Coomassie blue staining, the same procedure was followed as for acrylamide gels (4–15%), then stained with Bio-safe™ (BioRad, Hercules, CA, USA) stain. After washing, 50 ml of Bio-safe™ Coomassie stain was added. After shaking for 1 h, the protein bands became visible within 20 min and reached maximum

intensity within 1 h. Skin to muscle caspase-1 expression was calculated by dividing the measured band relative density (BRD) ratio of skin with the measured BRD ratio of muscle: $r = s/m$, where s = skin BRD, m = muscle BRD, and r = ratio of skin BRD to muscle BRD. SEM was calculated for each group.

Statistical and Computational Analyses

Statistical analyses were performed using Math Works MatLab™, Microsoft Excel™, and SAS Stat View™. Western blot quantifications were compared using a balanced one-way ANOVA with 5% significance. Cytokine quantifications were compared utilizing an unpaired one-tailed heteroscedastic *t*-test, again with a 5% significance level.

Principal component analysis (PCA) (26) was used to help discern which of the 14 proinflammatory cytokines and chemokines measured by Luminex™ are the most informative with regards to the observed immune response, similar to methodology we have used previously in the context of murine trauma/hemorrhage (25). Data were grouped by tissue (all skin samples and all muscle samples), and linear combinations of the original 14 dimensions (cytokines/chemokines) in each group were created in order to produce synthesized latent variables that explain >95% of the variance observed. The strength of each inflammatory mediator’s contribution to each of the principal components was also examined, in order to provide additional evidence for determining which cytokines/chemokines could be considered to be driving the observed immune reactions (25).

Immune signaling is driven to a large extent by the local inflammatory mediator milieu. While methods, such as PCA, are able to identify mediators that contribute the most variance to the observed immune response, it is essential to place these numerical results in biological context. Therefore, the PCA was combined with a confirmatory factor analysis (FAN) to elucidate the relevant pathways of the observed immune response. As a part of the FAN, the published literature was examined for descriptions of the similarities and differences in the known biological properties of the cytokines identified through PCA, in order to find common or complimentary patterns of function. Groupings of inflammatory mediator contributions to components one and two in the PCA were interpreted as latent factors and used as the basis for FAN. FAN seeks to model the observed variables as linear combinations of the provided potential factors. This form of analysis is based on regression modeling, and therefore provides additional weight to similar evidence found through PCA when there is similarity in the results.

While factor analysis is related to PCA, the two analyses are not identical. PCA takes a linear combination of the observed variables to derive synthesized latent variables; however, factor analysis takes the conceptually opposite approach. Using regression techniques, this method models the observed variables through linear combinations of potential latent variables that are provided. When the two methods produce models that are in agreement or similar, we interpret this as suggestive evidence that the latent variables are indeed playing an influential role in the observed pathology.

The literature-based analysis is a process by which we have utilized previously published studies that elucidate the mechanisms or behaviors of the signaling proteins under analysis. We extract the biological functions described as associated with the proteins and use those functions as labels in our feature transformation and factor analysis work. We believe that this is an efficient evidence-based method to describe what signaling proteins the transformation and factor analysis methods are emphasizing as important and putting them into a narrative that describes what role they are likely fulfilling in context.

RESULTS

As a paradigm of localized tissue injury, excisional biopsies were made on the lateral aspect of the thigh on Lewis rat hind limbs, as described in Section “Materials and Methods.” To elucidate changes in the immune signaling profile that occur at the cessation of heartbeat, cardiac arrest was induced as described in Section “Materials and Methods.” The testing of the second hypothesis stated in the introduction is through samples collected within 30 s of cardiac arrest, within a timeframe that is common in trauma-associated cardiac arrest events.

Samples taken from the wounded areas of skin and muscle were found to have significantly different levels and patterns of inflammatory mediator expression. These differences were evident across groups as well as across tissue.

In skin, the levels of IL-18 and IL-1 α present in “cardiac arrest group” animals (**Figure 1A**) were much higher than those seen in any other groups. MCP-1, GM-CSF, IL-10, IL-6, and IL-1 β were all also elevated in the “injury group” animals (**Figure 1B**). In muscle, similar differences between “cardiac arrest group” animals (**Figure 1C**) and “injury group” (**Figure 1D**) were also seen, along with marked increases in IL-18, IL-1 α , IL-6, IFN γ , and MCP-1.

The presence of IL-18 and IL-1 β led us to hypothesize the presence and activation of the NLRP3 inflammasome in response to localized tissue injury and cardiac arrest. To test this hypothesis, we examined the expression of caspase-1, which is required for inflammasome activity (43). As determined by Western blotting analysis, caspase-1 was present in both skin and muscle in all study groups (**Figures 2A,B**). This finding, in combination with the presence of IL-18 and IL-1 β , strongly indicates NLRP3 inflammasome activity. Similar levels of caspase-1 expression were found in both the skin (**Figure 2C**) and muscle (**Figure 2D**) of “injury group” animals, implying relatively equal levels of inflammasome activation. In contrast, “cardiac arrest group” animals expressed significantly more caspase-1 in skin than muscle, by approximately a factor of 12.

“Cardiac arrest group” skin was associated with elevated levels of caspase-1 and IL-18. In “cardiac arrest group” muscle, IL-18 levels were also markedly increased; however, caspase-1 levels were lower than in “injury group” muscle.

Whereas significant inflammatory mediator concentration differences in the skin were observed between the “injury group” and “cardiac arrest group,” the levels were consistently higher in the “cardiac arrest group” animals (**Figures 3B–G**). The single exception was GM-CSF, which was present at a much higher

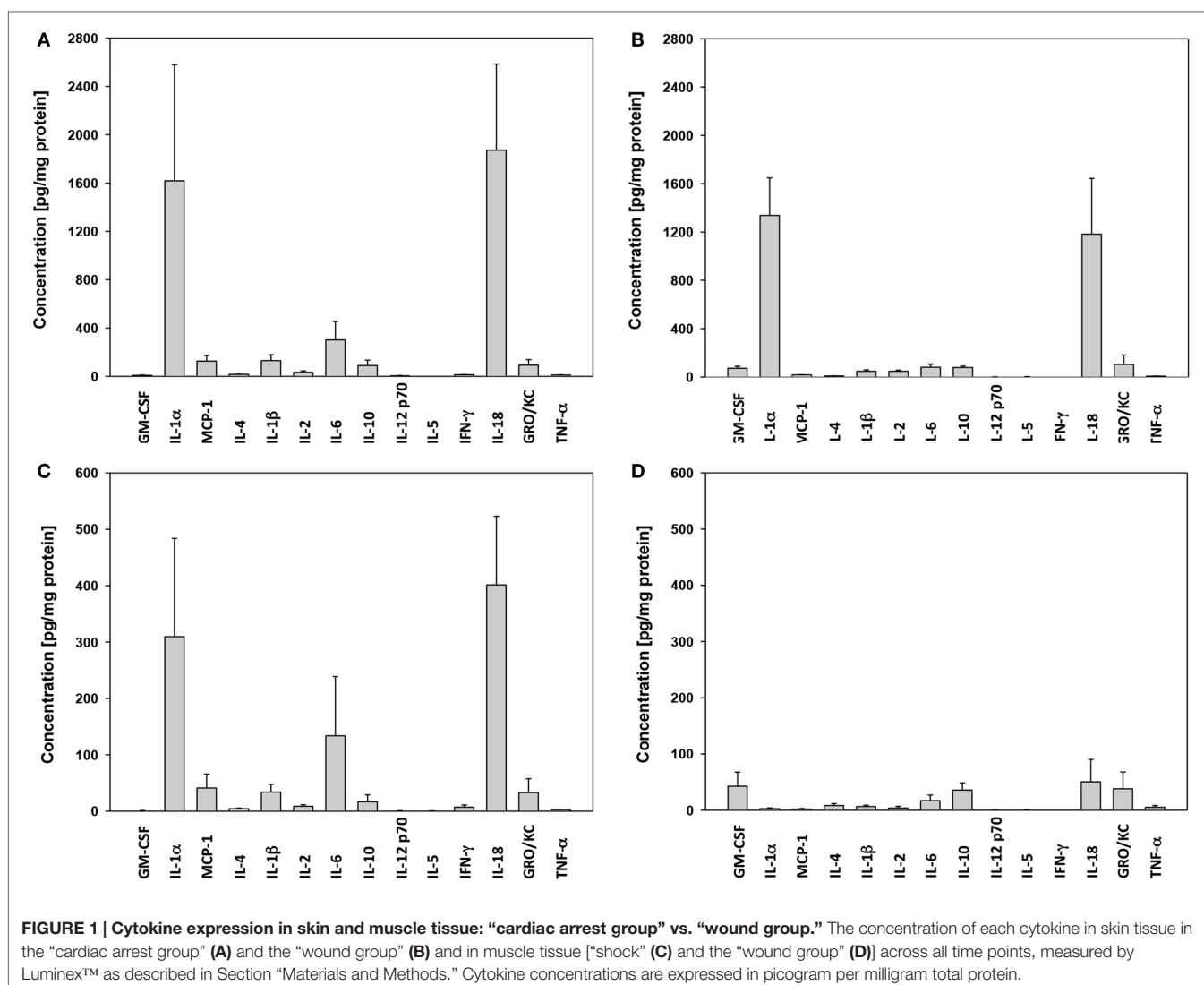
concentration in the skin of “injury group” animals (**Figure 3A**). In “cardiac arrest group” animals, the cytokine with the highest differential elevation relative to “injury group” animals was IFN γ . The only cytokine elevated differentially between groups within muscle tissue was IL-18, whose expression was considerably higher in “cardiac arrest group” animals (**Figure 3N**).

Also notable was the contrast between skin and muscle tissue inflammatory mediator profiles, particularly within the “injury group” (**Figures 3H–Q**). Interestingly, the “injury group” animals displayed a much wider range of statistically significant differences in the expression of cytokines and chemokines between skin and muscle tissue as compared to “cardiac arrest group” animals. Although the concentration of many of these inflammatory mediators was actually higher in “cardiac arrest group” animals, the difference between skin and muscle tissue expression of each cytokine was much smaller. IL-4, IL-12p70, and TNF α were expressed at significantly different levels between skin and muscle tissues within the “cardiac arrest group” animals (**Figures 3O–Q**). These expression levels are also distinct from any inflammatory mediators within the “injury group,” revealing distinct immune signaling patterns in the two groups.

Principal component analysis synthesized two latent variables in skin (**Figure 4A**) and in muscle (**Figure 4B**). In skin, the first principal component was comprised mostly of IL-18 and IL-1 α , while the second component was comprised of IL-18, IL-6, MCP-1, IL-1 β , and GRO/KC (**Figure 4C**). The first principal component of muscle was also primarily made up of IL-18 and IL-1 α , whereas the second principal component was mostly comprised of IL-6, IL-18, MCP-1, and GRO-KC (**Figure 4D**). TNF α and IL-4 were identified as important cytokines in both “cardiac arrest group” skin and muscle and are known to play a role in many immune regulation or intercellular signaling contexts (44–46). Although the contribution of each of these cytokines is similar in the first principal component, their contributions were substantially different in the second principal component. This finding suggests that the cytokines are complementary in some respects but have distinct roles in the inflammatory mediator network.

Principal component analysis suggested a potential role for GM-CSF in tissue injury (but not shock) skin. The converse was observed in the case of the chemokine MCP-1 (CCL2), which was highly expressed in the skin of “cardiac arrest group” animals, but expressed at far lower levels in the skin of the “injury group” animals. Furthermore, high levels of IFN γ were observed in the “cardiac arrest group” animals, while IFN γ was entirely absent from the “injury group” animals.

Two-factor analysis of the skin generated a model of cytokine/chemokine contributions to the latent variables that was very similar to the representation derived by PCA (**Figure 5A**). Two-factor analysis of the muscle yielded a model that has similarities with the model derived by PCA; however, the overall agreement of the two models is not as strong as found in skin (**Figure 5B**). The functions of inflammatory mediators most heavily influencing each factor were correlated with descriptions of their biological function from the literature, and through this analysis labels for the latent variables, which were established as “macrophage activation” and “cell-mediated cytotoxic response.”



DISCUSSION

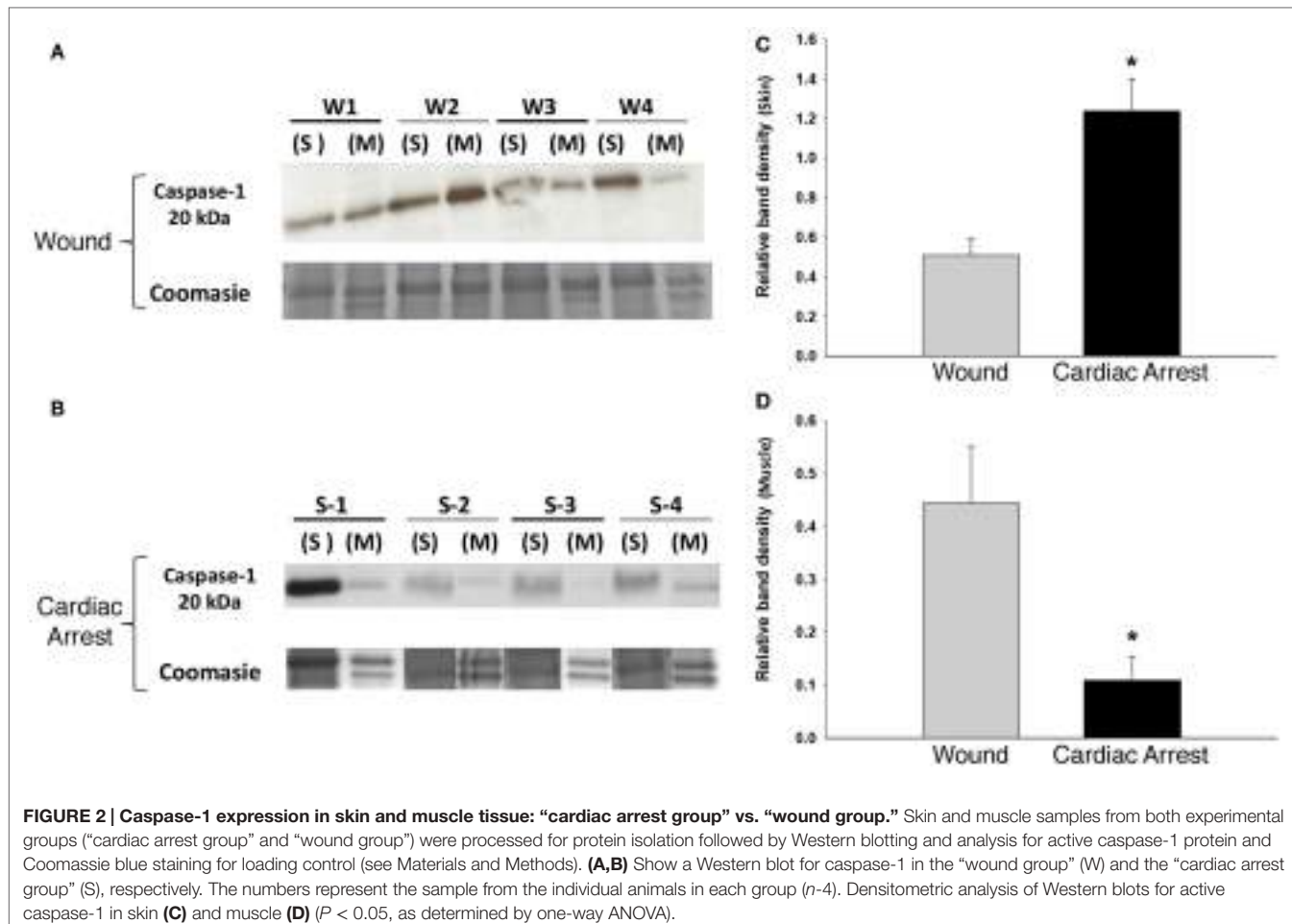
Inferring Inflammasome-Driven Networks from Data-Driven Modeling

In the present study, we sought to elucidate immune/inflammatory signaling patterns in the response to skin and muscle damages, in the presence or absence of cardiac arrest. We reasoned that this would represent an important step in understanding the potential mechanisms that drive immunological responses to tissue damage at the earliest stages in the settings of complex injury.

In the present study, we hypothesized that application of high-dimensional feature transformation methods, combined with biological knowledge from reports in the literature, can provide a deeper understanding of the immune signaling processes that underlie injury-associated inflammation. Based on the multiplexed analysis of inflammation biomarkers coupled with data-driven modeling, we suggest that tissue injury leads to the differential induction of IL-1 α and IL-18 in skin vs. muscle. This inflammatory profile is associated with elevated caspase-1

immunoblotting in skin but not muscle. Cardiac arrest greatly elevates IL-1 α , IL-18, and caspase-1 in the skin. Thus, inflammasome activity appears to be central to the type and severity of the inflammatory response to local tissue injury, and this activity appears to be augmented greatly in the presence of cardiac arrest.

We utilized PCA in the current study, because this method is capable of quantifying the amount of information contributed by individual cytokines to the observed inflammation (25, 47, 48). Because this method evaluates the contribution of new information derived from each inflammatory mediator to each of the inflammatory processes observed, PCA assigns the highest scoring to cytokines most correlated with a specific inflammatory response. As utilized herein, PCA seeks to find the linear combination of the original 14 inflammatory mediators that captures the most variance in the smallest number of synthesized variables. Thus, since PCA can show which combination of inflammatory mediators lies in a particular principal component, this method can suggest inflammatory networks which interact together to drive a particular facet of the overall response.



Although a well-established numerical analysis method, additional evidence to support the interpretation of PCA results is desirable and can be provided by FAN (49–51). PCA and FAN are related methods and can intuitively be understood as providing confirmatory analysis. While PCA is based on variance, FAN takes as the input the number of hypothesized factors driving the observed process and then seeks to find the optimal linear coefficients for each cytokine to project from the hypothesized factors back to the original values measured for each cytokine. In short, PCA reduces the dimensionality of a given dataset, while FAN expands that dimensionality. In both cases, the effect is to expose the orthogonal aspects of the data in order to gain a better perspective of what measured parameters are most responsible for driving the observed process, which in the present study is inflammation. When the two methods produce coefficient scores for the inflammatory mediators that are similar to each other, this can be interpreted as evidence in support of the hypothesis that inflammation is, to some degree, driven by those particular mediators. However, if the two methods produce coefficient scores that do not agree, it is likely that the number of hypothesized factors is insufficient to capture the complexity of the inflammatory process.

Using such dimensionality reduction methods, we have previously inferred principal characteristics or drivers of inflammation in mice subjected to surgical trauma alone vs. that same trauma in combination with hemorrhagic shock (25). More recently, we have utilized PCA to suggest a key module in a multicompartment mechanistic mathematical model of inflammation and organ pathophysiology in endotoxemic swine (48), to suggest key physiologic effects of peritoneal suction as a therapy for sepsis (32), to connect *in vitro* and *in vivo* outcomes in the inflammatory response to implanted biomaterials (28), as well as suggesting key changes in metabolism that occur in the setting of pulsatile perfusion of livers prior to transplantation (29). Importantly, we have recently used these methods to suggest a role for the inflammasome (including elevated IL-18 and caspase-1) in a rat model of chronic neuropathic pain (42).

To better understand the observed immune signaling activity, we investigated two classes of insult: tissue injury only and tissue injury with shock. In the first model, the inflammatory response to surgically excised wounds in skin and muscle tissue without any secondary contaminants reveals immune signaling patterns primarily associated with wound healing. In the model of injury with shock, changes in the patterns of the inflammatory response

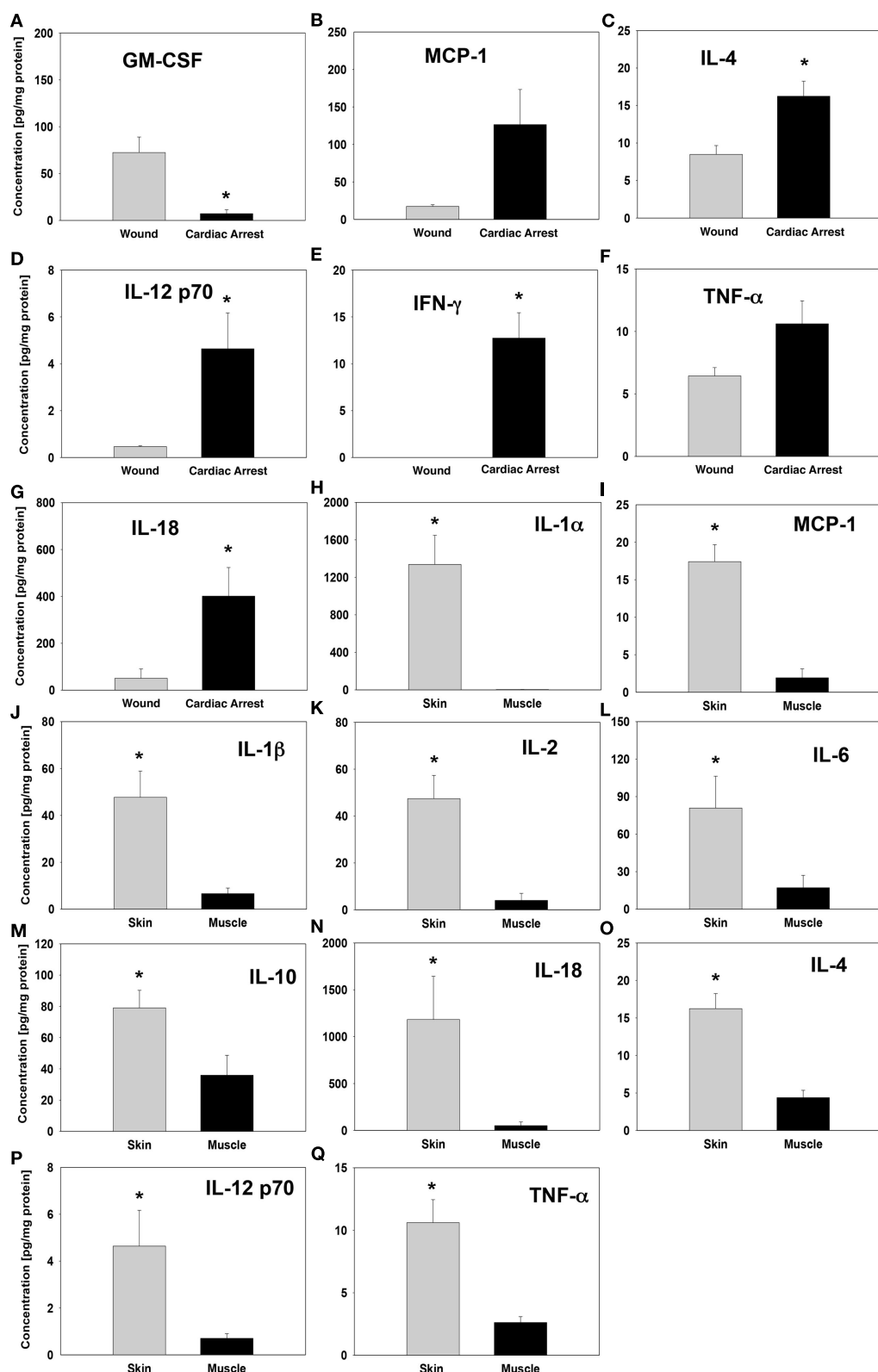


FIGURE 3 | Cytokine levels in “wound group” vs. “cardiac arrest group” and in skin vs. muscle tissue. Tissue protein-normalized cytokine concentrations in “wound group” vs. “cardiac arrest group” (A–G) and in skin vs. muscle tissue (H–Q). The concentrations of each cytokine were measured by Luminex™ as described in Section “Materials and Methods” and are expressed in picogram per milligram total protein. * $P < 0.05$ by one-tail heteroscedastic t -test.

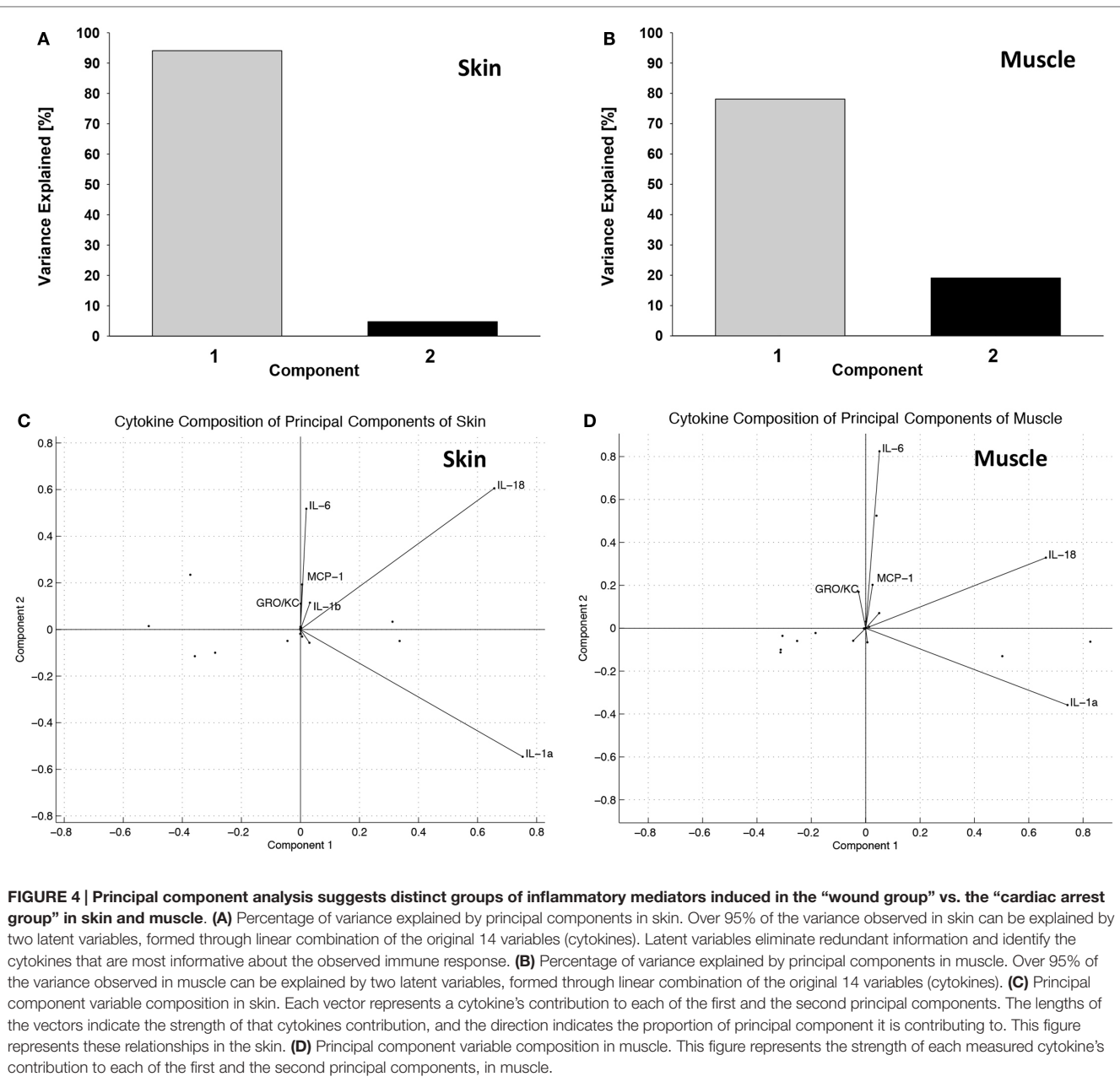


FIGURE 4 | Principal component analysis suggests distinct groups of inflammatory mediators induced in the “wound group” vs. the “cardiac arrest group” in skin and muscle. (A) Percentage of variance explained by principal components in skin. Over 95% of the variance observed in skin can be explained by two latent variables, formed through linear combination of the original 14 variables (cytokines). Latent variables eliminate redundant information and identify the cytokines that are most informative about the observed immune response. **(B)** Percentage of variance explained by principal components in muscle. Over 95% of the variance observed in muscle can be explained by two latent variables, formed through linear combination of the original 14 variables (cytokines). **(C)** Principal component variable composition in skin. Each vector represents a cytokine's contribution to each of the first and the second principal components. The lengths of the vectors indicate the strength of that cytokine's contribution, and the direction indicates the proportion of principal component it is contributing to. This figure represents these relationships in the skin. **(D)** Principal component variable composition in muscle. This figure represents the strength of each measured cytokine's contribution to each of the first and the second principal components, in muscle.

to surgically incised wounds under conditions of cardiac arrest represent the disruptive effect of a disruption in blood flow and the associated stresses have on wound-healing signaling. Changes in immune signaling under these circumstances are caused by metabolic stress and other factors accompanying shock.

In the present study, we observed elevations in a wide range of proinflammatory mediators, including IL-1 α , IL-1 β , IL-4, IL-6, IL-12, IL-18, MCP-1, and TNF α . These networks of inflammatory mediators, observed in both the “injury group” and the “cardiac arrest group” are indicative of highly activated immune cells, such as dendritic cells, mast cells, and neutrophils. Dendritic cells are known as sensitive and potent pathogen presentation cells, but they are also becoming recognized as important in wound

detection and healing in a variety of contexts (52–54). The specific role of these immune cells in a tissue is affected by the cytokine milieu present (23, 55). Importantly, most of these mediators have been implicated in the response to trauma/hemorrhage, in prior studies, especially TNF α (56–59) and MCP-1 (31, 35).

Although the specific milieu of the “injury group” and “cardiac arrest group” animals appeared distinct, PCA and FAN suggested a central role for IL-1 α and IL-18, leading us to hypothesize and confirm the concomitantly elevated expression of activated caspase-1 as evidence for strong inflammasome activation in these tissues. As cells are killed, are damaged, or are induced into apoptosis by the wounding process, they release endogenous damage-associated molecular pattern (DAMP) molecules, such as uric acid crystals

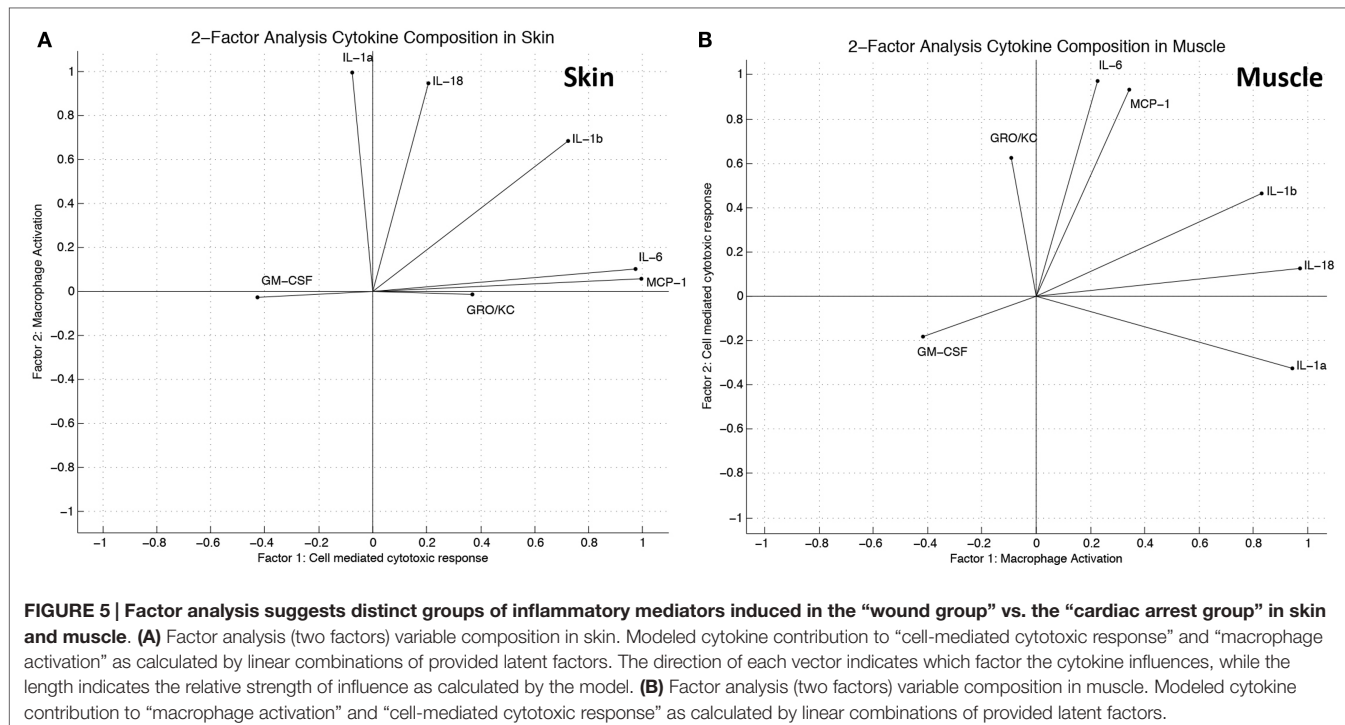


FIGURE 5 | Factor analysis suggests distinct groups of inflammatory mediators induced in the “wound group” vs. the “cardiac arrest group” in skin and muscle. (A) Factor analysis (two factors) variable composition in skin. Modeled cytokine contribution to “cell-mediated cytotoxic response” and “macrophage activation” as calculated by linear combinations of provided latent factors. The direction of each vector indicates which factor the cytokine influences, while the length indicates the relative strength of influence as calculated by the model. **(B)** Factor analysis (two factors) variable composition in muscle. Modeled cytokine contribution to “macrophage activation” and “cell-mediated cytotoxic response” as calculated by linear combinations of provided latent factors.

and high-mobility group protein B1 (HMGB1), molecules that trigger inflammatory response mechanisms (60–64). One DAMP-induced mechanism of particular relevance to the inflammatory signaling profile observed in this study involves the activation of the NLRP3 inflammasome (65), which is one of several multiprotein complexes that play important roles in inflammation and cell death (66). Deficiency or overactivation of these cytoplasm-based protein assemblies has been implicated in inflammation-associated damage in a variety of disorders (67), and inflammasome activation is widely regarded as critical in the initiation of the innate immune response. NLRP3 responds to DAMPs and involves a spontaneous protein assembly that forms primarily in the cytoplasm of macrophages, monocytes, some keratinocytes (65), and mast cells (68). The NLRP3 inflammasome is known to respond to cytokines as well as DAMPs including HMGB1 and uric acid crystals (69). The inflammasome, in turn, produces and secretes bioactive proinflammatory cytokines. This process initiates an inflammation and wound-healing cycle that may moderate and conclude successfully with functional wound healing or may lead to runaway inflammation resulting in dysfunctional wound healing (68).

Although all classes of inflammasome produce proinflammatory cytokines, each assembly only forms in response to specific stimuli. In the present study, we found evidence for the activation of NLRP3 (crysopyrin, NALP3) inflammasome. This inflammasome forms specifically in response to the types of DAMPs released in wounding and shock, as well as pathogen-associated molecular patterns (PAMPs) (70, 71). This class of inflammasomes leads to the recruitment of caspase-1 and the cleavage of pro-IL-1 β and pro-IL-18 to yield the bioactive, proinflammatory cytokines IL-1 β and IL-18. These cytokines are able to induce degranulation in polymorphonuclear neutrophil (PMN)

leukocytes (72). Importantly, caspase-1 activity appears to be essential for the innate immune response, given that caspase-1-deficient mice are resistant to developing shock in response to PAMPs, such as LPS (73).

NLRP3-depleted mice produce neither IL-1 β nor IL-18 but are still able to express IL-1 α , IL-12p40, and TNF α (74). In the present study, we found large quantities of IL-1 α in wounded skin across all groups, suggesting that the observed immune response may in fact be comprised of several components that are driven by different activation and signaling pathways. Furthermore, we observed larger quantities of IL-18 vs. IL-1 β , in line with reported requirement for prestimulation, for example with LPS, for the detection of large quantities of IL-1 β (73). These findings are also in line with our recent studies in a rat model of chronic constriction injury and neuropathic pain (42).

In addition to inflammasome-derived cytokines, analysis of the biological functions of the cytokines identified by PCA suggested other potential mechanisms of inflammation induced by skin injury and cardiac arrest. For example, GM-CSF was highly expressed in skin in the “injury group” animals, while this cytokine was relatively absent in the “cardiac arrest group” animals. Since GM-CSF is an important regulator of macrophage and granulocyte populations and has been shown to play an important role in the onset and propagation of inflammation (75, 76), its presence indicates strong macrophage recruitment and host defense or inflammatory activity. Thus, we hypothesize that GM-CSF plays a key role in the phenotype of the skin of the “injury group,” a role which we hypothesize is supported by cytokines, such as TNF α and IL-4. Numerous reports on the healing properties of GM-CSF in the literature support our PCA-derived hypothesis for the role of GM-CSF in the “injury group” (77–82).

In muscle, IL-6, IL-18, and IL-1 α shared both direction and strength of influence in both PCA and FAN models of muscle. Interestingly, we have suggested that MCP-1 in some way controls IL-6 expression (31), and it was notable that MCP-1 figured in both PCA and FAN. Additionally, GM-CSF and IL-1 β were influential variables in PCA but were not highly influential in FAN. These findings suggest that the muscle response to injury, both with and without shock, is likely driven by a larger number of latent factors than in skin.

The high concentrations of MCP-1 seen in the “cardiac arrest group” may possibly be caused by the cellular metabolic stress associated with cardiac arrest, resulting in insufficient cellular perfusion that would then lead to vasodilation, shock, and widespread degranulation of mast cells (83, 84). This chemokine helps recruit monocytes, dendritic cells, and memory T cells to sites of inflammation. Perhaps more significantly, MCP-1 exerts an important role in the degranulation of basophils and mast cells, facilitating the release of serine proteases, histamine, serotonin, and proteoglycans (70). In turn, mast cell and neutrophil degranulation induced by chemokines, such as MCP-1, and cytokines, such as IL-18, releases TNF α , eosinophil chemotactic factor, histamine, and a number of other factors (85, 86). This release alerts other nearby cells of injury and is a part of the cascade that begins the immune response to the injury. This hypothesis is supported by evidence that the mast cells are required for optimal migration of dendritic cells, swelling, neutrophil infiltration, and other effects associated with wound healing (87). We have recently suggested, through combined *in vitro*, *in silico*, and clinical studies that liver-derived MCP-1 is a central mediator in dynamic networks of inflammation in trauma (31).

In the “cardiac arrest group,” it is likely that the release of TNF α as a proapoptotic cytokine was triggered, leading to higher concentrations of TNF α in the skin of the “cardiac arrest group.” However, the role of TNF α is varied and dependent on a wide range of factors, including receptor binding (TNF-R1 vs. TNF-R2), the local cytokine milieu, the presence of reactive oxygen species, as well as many additional factors (88, 89). It is therefore not surprising that TNF α is seen also seen in the “injury group” although not in as primary a role as in the “cardiac arrest group.”

TNF α also plays a potentially important role as a costimulator of IFN γ production with IL-12 (IL-12p70) (90–92). Levels of IFN γ in the skin of the “cardiac arrest group” suggest this as an important role of IL-12 in this context but is also capable of a variety of immunological capabilities, including stimulating proliferation in resting peripheral cells, promoting the generation of lymphokine-activated killer cells (LAK cells), and augmenting the cytolytic activity of natural killer cells (NK cells) (93–96).

Another prominent cytokine observed in our studies was IL-4, which is known to stimulate IgE B cell differentiation as well as alternative activation of macrophages into M2 repair cells (97), suggesting that IL-4 may be supporting a wound-healing pattern in the “injury group.” However, in the “cardiac arrest group,” significantly higher concentrations of IL-4, as well as the increased presence of additional cytokines that are associated with shock, suggest that in this context IL-4 may be acting as a promoter of IgE synthesis, contributing to the shock reaction and promoting widespread rapid degranulation of PMN leukocytes. Importantly,

in the “injury group,” high levels of GM-CSF are seen along with moderate amounts of IL-4. This same combination of cytokines has been shown to enable the maturation of monocytes into dendritic cells *in vitro* (98).

Limitations

There are several challenges and limitations in this study. This study focuses on the early inflammatory phase following injury and therefore does not follow wounds through full healing. Although statistically significant differences in the expression levels of multiple inflammatory mediators were found between groups, the study size was limited to eight animals (four in the “injury group” and four in the “cardiac arrest group”). Additionally, a single time point proximal to the time of injury was studied. Future studies would ideally extend the findings reported here with larger study groups, sampled at multiple longitudinal time points. Our focus on the inflammasome was derived from an analysis of a limited number of inflammatory mediators. Thus, it is possible that (1) others, unmeasured inflammatory mediators play key roles in postinjury inflammation and (2) that our analysis methods were insufficient to inform our hypotheses. With regard to the former, we attempted to focus our analysis on mediators that have been studied previously in wound biology. With regard to the latter, we attempted to use corroborative methodologies (PCA and FAN) to gain confidence in our conclusions. In skin, the agreement between PCA and FAN models was high across all measured mediators, providing additional evidence that two factors are explanatory. Nonetheless, confirmation of this hypothesis requires studies in which the inflammasome, caspase-1, IL-1 α , and/or IL-18 is antagonized.

CONCLUSION

The inflammasome appears to govern the early inflammatory response to tissue injury in the skin, releasing proinflammatory factors likely to initiate host defense and clearance of debris. Normal wound healing is characterized and regulated by characteristic immune signaling patterns, reflected in characteristic cytokine and chemokine profiles of skin and muscle (17, 99–102). The mediator profile characteristic of an early inflammatory response to tissue injury is modified extensively as a result of cellular stress induced by shock, likely interfering with eventual wound repair and regeneration. Moreover, the inflammatory network characteristics of skin and muscle injury responses (both with and without severe shock) are recognized as distinct from each other, as inferred from data-driven computational analyses. These findings support the use of feature transformation methods, in combination with literature-based analysis of the underlying biological functions, as a method to separate relevant biological processes from irrelevant homeostatic processes, or other background functions.

ACKNOWLEDGMENTS

This work was supported by NIH grant P50-GM-53789. The authors would like to thank Dr. Qing Ye from Carnegie Mellon University’s NMR Center, Mr. Ed Gray, and Mr. Tim Starzl for their invaluable insight and suggestions on how to improve this work.

REFERENCES

- Stadelmann WK, Digenis AG, Tobin GR. Physiology and healing dynamics of chronic cutaneous wounds. *Am J Surg* (1998) **176**(2A Suppl):26S–38S. doi:10.1016/S0002-9610(98)00183-4
- Singer AJ, Clark RA. Cutaneous wound healing. *N Engl J Med* (1999) **341**(10):738–46. doi:10.1056/NEJM199909023411006
- Fahey TJ III, Sadaty A, Jones WG II, Barber A, Smoller B, Shires GT. Diabetes impairs the late inflammatory response to wound healing. *J Surg Res* (1991) **50**(4):308–13. doi:10.1016/0022-4804(91)90196-S
- 2005 American Heart Association Guidelines for Cardiopulmonary Resuscitation and Emergency Cardiovascular Care. Part 10.7: cardiac arrest associated with trauma. *Circulation* (2005) **112**(24_Suppl):IV-146–IV-149. doi:10.1161/CIRCULATIONAHA.105.166569
- Battistella FD, Nugent W, Owings JT, Anderson JT. Field triage of the pulseless trauma patient. *Arch Surg* (1999) **134**(7):742–5. doi:10.1001/archsurg.134.7.742
- Rosemurgy AS, Norris PA, Olson SM, Hurst JM, Albrink MH. Prehospital traumatic cardiac arrest: the cost of futility. *J Trauma* (1993) **35**(3):468–73. doi:10.1097/000005373-199309000-00022
- Cera SM, Mostafa G, Sing RF, Sarafin JL, Matthews BD, Heniford BT. Physiologic predictors of survival in post-traumatic arrest. *Am Surg* (2003) **69**(2):140–4.
- Scolletta S, Donadello K, Santonocito C, Franchi F, Taccone FS. Biomarkers as predictors of outcome after cardiac arrest. *Expert Rev Clin Pharmacol* (2012) **5**(6):687–99. doi:10.1586/ecp.12.64
- Adrie C, Laurent I, Monchi M, Cariou A, Dhainau JF, Spaulding C. Postresuscitation disease after cardiac arrest: a sepsis-like syndrome? *Curr Opin Crit Care* (2004) **10**(3):208–12. doi:10.1097/01.ccx.0000126090.06275.fe
- Bro-Jeppesen J, Kjaergaard J, Wanscher M, Nielsen N, Friberg H, Bjerre M, et al. The inflammatory response after out-of-hospital cardiac arrest is not modified by targeted temperature management at 33 degrees C or 36 degrees C. *Resuscitation* (2014) **85**(11):1480–7. doi:10.1016/j.resuscitation.2014.08.007
- Segel GB, Halterman MW, Lichtman MA. The paradox of the neutrophil's role in tissue injury. *J Leukoc Biol* (2011) **89**(3):359–72. doi:10.1189/jlb.0910538
- Knighton DR, Silver IA, Hunt TK. Regulation of wound-healing angiogenesis—effect of oxygen gradients and inspired oxygen concentration. *Surgery* (1981) **90**(2):262–70.
- Berghe GV, Zegher FD, Bouillon R. Acute and prolonged critical illness as different neuroendocrine paradigms. *J Clin Endocrinol Metab* (1998) **83**(6):1827–34. doi:10.1210/jc.83.6.1827
- Martin P. Wound healing – aiming for perfect skin regeneration. *Science* (1997) **276**(5309):75–81. doi:10.1126/science.276.5309.75
- Leoni G, Neumann PA, Sumagin R, Denning TL, Nusrat A. Wound repair: role of immune-epithelial interactions. *Mucosal Immunol* (2015) **8**:959–68. doi:10.1038/mi.2015.63
- Broughton G II, Janis JE, Attinger CE. The basic science of wound healing. *Plast Reconstr Surg* (2006) **117**(7 Suppl):12S–34S. doi:10.1097/01.prs.0000225430.42531.c2
- Werner S, Grose R. Regulation of wound healing by growth factors and cytokines. *Physiol Rev* (2003) **83**(3):835–70. doi:10.1152/physrev.00032.2002
- Diegelmann RF, Evans MC. Wound healing: an overview of acute, fibrotic and delayed healing. *Front Biosci* (2004) **9**:283–9. doi:10.2741/1184
- Tuma MA, Stansbury LG, Stein DM, McQuillan KA, Scalea TM. Induced hypothermia after cardiac arrest in trauma patients: a case series. *J Trauma* (2011) **71**(6):1524–7. doi:10.1097/TA.0b013e31823c5a06
- Lundby JB, Rai M, Ramu B, Hosseini-Khalili A, Li D, Slim HB, et al. Therapeutic hypothermia is associated with improved neurologic outcome and survival in cardiac arrest survivors of non-shockable rhythms. *Resuscitation* (2012) **83**(2):202–7. doi:10.1016/j.resuscitation.2011.08.005
- Sagalyn E, Band RA, Gaieski DF, Abella BS. Therapeutic hypothermia after cardiac arrest in clinical practice: review and compilation of recent experiences. *Crit Care Med* (2009) **37**(7 Suppl):S223–6. doi:10.1097/CCM.0b013e3181aa5c7c
- Ondo M, Schaller MD, Feihl F, Ribordy V, Liaudet L. From evidence to clinical practice: effective implementation of therapeutic hypothermia to improve patient outcome after cardiac arrest. *Crit Care Med* (2006) **34**(7):1865–73. doi:10.1097/01.CCM.0000221922.08878.49
- Nathan C, Sporn M. Cytokines in context. *J Cell Biol* (1991) **113**(5):981–6. doi:10.1083/jcb.113.5.981
- Donoho DL. High-dimensional data analysis: the curses and blessings of dimensionality. *AMS Math Challenges Lecture* (2000) 1–32.
- Mi Q, Constantine G, Ziraldo C, Solovyev A, Torres A, Namas R, et al. A dynamic view of trauma/hemorrhage-induced inflammation in mice: principal drivers and networks. *PLoS One* (2011) **6**(5):e19424. doi:10.1371/journal.pone.0019424
- Janes KA, Yaffe MB. Data-driven modelling of signal-transduction networks. *Nat Rev Mol Cell Biol* (2006) **7**(11):820–8. doi:10.1038/nrm2041
- An G, Nieman G, Vodovotz Y. Computational and systems biology in trauma and sepsis: current state and future perspectives. *Int J Burns Trauma* (2012) **2**(1):1–10.
- Wolf MT, Vodovotz Y, Tottey S, Brown BN, Badylak SF. Predicting in vivo responses to biomaterials via combined in vitro and in silico analysis. *Tissue Eng Part C Methods* (2015) **21**(2):148–59. doi:10.1089/ten.TEC.2014.0167
- Fontes P, Lopez R, van der Plaats A, Vodovotz Y, Minervini M, Scott V, et al. Liver preservation with machine perfusion and a newly developed cell-free oxygen carrier solution under subnormothermic conditions. *Am J Transplant* (2015) **15**(2):381–94. doi:10.1111/ajt.12991
- Azhar N, Ziraldo C, Barclay D, Rudnick DA, Squires RH, Vodovotz Y, et al. Analysis of serum inflammatory mediators identifies unique dynamic networks associated with death and spontaneous survival in pediatric acute liver failure. *PLoS One* (2013) **8**(11):e78202. doi:10.1371/journal.pone.0078202
- Ziraldo C, Vodovotz Y, Namas RA, Almahmoud K, Tapias V, Mi Q, et al. Central role for MCP-1/CCL2 in injury-induced inflammation revealed by in vitro, in silico, and clinical studies. *PLoS One* (2013) **8**(12):e79804. doi:10.1371/journal.pone.0079804
- Emr B, Sadowsky D, Azhar N, Gatto LA, An G, Nieman GF, et al. Removal of inflammatory ascites is associated with dynamic modification of local and systemic inflammation along with prevention of acute lung injury: in vivo and in silico studies. *Shock* (2014) **41**(4):317–23. doi:10.1097/SHK.0000000000000121
- Zaaqoq AM, Namas R, Almahmoud K, Azhar N, Mi Q, Zamora R, et al. Inducible protein-10, a potential driver of neurally controlled interleukin-10 and morbidity in human blunt trauma. *Crit Care Med* (2014) **42**(6):1487–97. doi:10.1097/CCM.0000000000000248
- Wolfram D, Morandi EM, Eberhart N, Hautz T, Hackl H, Zelger B, et al. Differentiation between acute skin rejection in allotransplantation and T-cell mediated skin inflammation based on gene expression analysis. *Biomed Res Int* (2015) **2015**:259160. doi:10.1155/2015/259160
- Namas RA, et al. Temporal patterns of circulating inflammation biomarker networks differentiate susceptibility to nosocomial infection following blunt trauma in humans. *Ann Surg* (2014). doi:10.1097/SLA.0000000000001001
- Almahmoud K, Namas RA, Zaaqoq AM, Abdul-Malak O, Namas R, Zamora R, et al. Pre-hospital hypotension is associated with altered inflammation dynamics and worse outcomes following blunt trauma in humans. *Crit Care Med* (2015) **43**(7):1395–404. doi:10.1097/CCM.0000000000000964
- Sadowsky D, Nieman G, Barclay D, Mi Q, Zamora R, Constantine G, et al. Impact of chemically-modified tetracycline 3 on intertwined physiological, biochemical, and inflammatory networks in porcine sepsis/ARDS. *Int J Burns Trauma* (2015) **5**(1):22–35.
- Dorsett-Martin WA. Rat models of skin wound healing: a review. *Wound Repair Regen* (2004) **12**(6):591–9. doi:10.1111/j.1067-1927.2004.12601.x
- Lindblad WJ. Considerations for selecting the correct animal model for dermal wound-healing studies. *J Biomater Sci Polym Ed* (2008) **19**(8):1087–96. doi:10.1163/156856208784909390
- Barclay D, Zamora R, Torres A, Namas R, Steed D, Vodovotz Y. A simple, rapid, and convenient Luminex-compatible method of tissue isolation. *J Clin Lab Anal* (2008) **22**(4):278–81. doi:10.1002/jcl.a.20253
- Wolfram D, Starzl R, Hackl H, Barclay D, Hautz T, Zelger B, et al. Profiling inflammatory cytokines mediating acute rejection after vascularized composite allotransplantation in a rat limb transplant model. *PLoS One* (2014) **9**:e99926. doi:10.1371/journal.pone.0099926

42. Vasudeva K, Azhar N, Barclay D, Janjic JM, Pollock JA. In vivo and systems biology studies implicate interleukin-18 as a central mediator in chronic pain. *J Neuroimmunol* (2015) **283**: 43–9. doi:10.1016/j.jneuroim.2015.04.012
43. Martinon F, Burns K, Tschopp J. The inflammasome: a molecular platform triggering activation of inflammatory caspases and processing of proIL-beta. *Mol Cell* (2002) **10**(2):417–26. doi:10.1016/S1097-2765(02)00599-3
44. Nelms K, Keegan AD, Zamorano J, Ryan JJ, Paul WE. The IL-4 receptor: signaling mechanisms and biologic functions. *Annu Rev Immunol* (1999) **17**:701–38. doi:10.1146/annurev.immunol.17.1.701
45. Tracey KJ, Cerami A. Tumor necrosis factor: an updated review of its biology. *Crit Care Med* (1993) **21**(10 Suppl):S415–22. doi:10.1097/00003246-199310001-00002
46. Kresina TF. *Immune Modulating Agents*. 1 ed. New York, NY: CRC Press (1997). 576 p.
47. Jolliffe IT. Principal component analysis. 2nd ed. *Springer Series in Statistics*. New York: Springer (2002).
48. Nieman G, Brown D, Sarkar J, Kubiak B, Ziraldo C, Dutta-Moscato J, et al. A two-compartment mathematical model of endotoxin-induced inflammatory and physiologic alterations in swine. *Crit Care Med* (2012) **40**:1052–63. doi:10.1097/CCM.0b013e31823e986a
49. Brown TA. *Confirmatory Factor Analysis for Applied Research* 2nd ed. Guilford Publications (2015).
50. Thompson B. *Exploratory and Confirmatory Factor Analysis: Understanding Concepts and Applications*. Washington, DC: American Psychological Association (2004). 195 p.
51. Kim J-O, Mueller CW. *Factor Analysis: Statistical Methods and Practical Issues*. Vol. 14. Newbury Park, CA: SAGE (1978).
52. Gregorio J, Meller S, Conrad C, Di Nardo A, Homey B, Lauerman A, et al. Plasmacytoid dendritic cells sense skin injury and promote wound healing through type I interferons. *J Exp Med* (2010) **207**(13):2921–30. doi:10.1084/jem.20101102
53. Trautmann A, Toksoy A, Engelhardt E, Bröcker EB, Gillitzer R. Mast cell involvement in normal human skin wound healing: expression of monocyte chemoattractant protein-1 is correlated with recruitment of mast cells which synthesize interleukin-4 in vivo. *J Pathol* (2000) **190**(1):100–6. doi:10.1002/(SICI)1096-9896(200001)190:1<100::AID-PATH496>3.0.CO;2-Q
54. Pruthi D, Munick ED, Fu Q, McGarr R, Moodie K. Critical role of dendritic cells in wound healing after myocardial infarction in CD11c-DTR-GFP mice. *FASEB J* (2009) **23**.
55. Nathan C. Points of control in inflammation. *Nature* (2002) **420**(6917):846–52. doi:10.1038/nature01320
56. Spielmann S, Kerner T, Ahlers O, Keh D, Gerlach M, Gerlach H. Early detection of increased tumour necrosis factor alpha (TNFalpha) and soluble TNF receptor protein plasma levels after trauma reveals associations with the clinical course. *Acta Anaesthesiol Scand* (2001) **45**:364–70. doi:10.1034/j.1399-6576.2001.045003364.x
57. Sailhamer EA, Li Y, Smith EJ, Shuja F, Shults C, Liu B, et al. Acetylation: a novel method for modulation of the immune response following trauma/hemorrhage and inflammatory second hit in animals and humans. *Surgery* (2008) **144**(2):204–16. doi:10.1016/j.surg.2008.03.034
58. Li S, Tao L, Jiao X, Liu H, Cao Y, Lopez B, et al. TNFalpha-initiated oxidative/nitritative stress mediates cardiomyocyte apoptosis in traumatic animals. *Apoptosis* (2007) **12**(10):1795–802. doi:10.1007/s10495-007-0108-2
59. Foex BA. Systemic responses to trauma. *Br Med Bull* (1999) **55**(4):726–43. doi:10.1258/0007142991902745
60. Kono H, Rock KL. How dying cells alert the immune system to danger. *Nat Rev Immunol* (2008) **8**(4):279–89. doi:10.1038/nri2215
61. Straino S, Di Carlo A, Mangoni A, De Mori R, Guerra L, Maurelli R, et al. High-mobility group box 1 protein in human and murine skin: involvement in wound healing. *J Invest Dermatol* (2008) **128**(6):1545–53. doi:10.1038/sj.jid.5701212
62. Ranzato E, Patrone M, Pedrazzi M, Burlando B. HMGB1 promotes scratch wound closure of HaCaT keratinocytes via ERK1/2 activation. *Mol Cell Biochem* (2009) **332**(1–2):199–205. doi:10.1007/s11010-009-0192-4
63. Zampell JC, Yan A, Avraham T, Andrade V, Malliaris S, Aschen S, et al. Temporal and spatial patterns of endogenous danger signal expression after wound healing and in response to lymphedema. *Am J Physiol Cell Physiol* (2011) **300**(5):C1107–21. doi:10.1152/ajpcell.00378.2010
64. Zhang Q, O'Hearn S, Kavalukas SL, Barbul A. Role of high mobility group box 1 (HMGB1) in wound healing. *J Surg Res* (2012) **176**(1):343–7. doi:10.1016/j.jss.2011.06.069
65. Kono H, Chen CJ, Ontiveros F, Rock KL. Uric acid promotes an acute inflammatory response to sterile cell death in mice. *J Clin Invest* (2010) **120**(6):1939–49. doi:10.1172/JCI40124
66. Thornberry NA, Bull HG, Calaycay JR, Chapman KT, Howard AD, Kostura MJ, et al. A novel heterodimeric cysteine protease is required for interleukin-1 beta processing in monocytes. *Nature* (1992) **356**(6372):768–74. doi:10.1038/356768a0
67. Becker CE, O'Neill LA. Inflammasomes in inflammatory disorders: the role of TLRs and their interactions with NLRs. *Semin Immunopathol* (2007) **29**(3):239–48. doi:10.1007/s00281-007-0081-4
68. Angele MK, Knöferl MW, Ayala A, Albina JE, Cioffi WG. Trauma-hemorrhage delays wound healing potentially by increasing pro-inflammatory cytokines at the wound site. *Surgery* (1999) **126**(2):279–85. doi:10.1016/S0039-6060(99)70166-2
69. Martinon F, Pétrilli V, Mayor A, Tardivel A, Tschopp J. Gout-associated uric acid crystals activate the NALP3 inflammasome. *Nature* (2006) **440**(7081):237–41. doi:10.1038/nature04516
70. Fujisawa T, Kato Y, Nagase H, Atsuta J, Terada A, Iguchi K, et al. Chemokines induce eosinophil degranulation through CCR-3. *J Allergy Clin Immunol* (2000) **106**(3):507–13. doi:10.1067/mai.2000.108311
71. Chenaud B, Tenu JP. Involvement of nitric oxide synthase in antiproliferative activity of macrophages: induction of the enzyme requires two different kinds of signal acting synergistically. *Int J Immunopharmacol* (1994) **16**(5–6):401–6. doi:10.1016/0192-0561(94)90028-0
72. Leung BP, Culshaw S, Gracie JA, Hunter D, Canetti CA, Campbell C, et al. A role for IL-18 in neutrophil activation. *J Immunol* (2001) **167**(5):2879–86. doi:10.4049/jimmunol.167.5.2879
73. Melnikov VY, Ecdter T, Fantuzzi G, Siegmund B, Lucia MS, Dinarello CA, et al. Impaired IL-18 processing protects caspase-1-deficient mice from ischemic acute renal failure. *J Clin Invest* (2001) **107**(9):1145–52. doi:10.1172/JCI12089
74. Walter K, Hölscher C, Tschopp J, Ehlers S. NALP3 is not necessary for early protection against experimental tuberculosis. *Immunobiology* (2010) **215**(9–10):804–11. doi:10.1016/j.imbio.2010.05.015
75. Hamilton JA. GM-CSF in inflammation and autoimmunity. *Trends Immunol* (2002) **23**:403–8. doi:10.1016/S1471-4906(02)02260-3
76. Hamilton JA, Anderson GP. GM-CSF Biology. *Growth Factors* (2004) **22**(4):225–31. doi:10.1080/08977190412331279881
77. Braunstein S, Kaplan G, Gottlieb AB, Schwartz M, Walsh G, Abalos RM, et al. GM-CSF activates regenerative epidermal growth and stimulates keratinocyte proliferation in human skin in vivo. *J Invest Dermatol* (1994) **103**(4):601–4. doi:10.1111/1523-1747.ep12396936
78. Castrogiovanni P, Ventimiglia P, Imbesi R. rHuGM-CSF: a possible therapeutic treatment in resistant chronic wound healing: our first observations. *Clin Ter* (2010) **161**(3):e101–4.
79. Zhang L, Chen J, Han C. A multicenter clinical trial of recombinant human GM-CSF hydrogel for the treatment of deep second-degree burns. *Wound Repair Regen* (2009) **17**(5):685–9. doi:10.1111/j.1524-475X.2009.00526.x
80. Bernasconi E, Favre L, Maillard MH, Bachmann D, Pythoud C, Bouzourene H, et al. Granulocyte-macrophage colony-stimulating factor elicits bone marrow-derived cells that promote efficient colonic mucosal healing. *Inflamm Bowel Dis* (2010) **16**(3):428–41. doi:10.1002/ibd.21072
81. Sutton TL, Pierpont YN, Robson MC, Payne WG. The use of growth factors and other humoral agents to accelerate and enhance burn wound healing. *Eplasty* (2011) **11**:e41.
82. Hu X, Sun H, Han C, Wang X, Yu W. Topically applied rhGM-CSF for the wound healing: a systematic review. *Burns* (2011) **37**(5):729–41. doi:10.1016/j.burns.2010.08.016
83. Sung FL, Zhu TY, Au-Yeung KK, Siow YL, O K. Enhanced MCP-1 expression during ischemia/reperfusion injury is mediated by oxidative stress and NF-kappaB. *Kidney Int* (2002) **62**(4):1160–70. doi:10.1111/j.1523-1755.2002.kid577.x
84. Hillenbrand A, Knippschild U, Weiss M, Schrezenmeier H, Henne-Bruns D, Huber-Lang M, et al. Sepsis induced changes of adipokines and cytokines

- septic patients compared to morbidly obese patients. *BMC Surg* (2010) **10**:26. doi:10.1186/1471-2482-10-26
85. Stone KD, Prussin C, Metcalfe DD. IgE, mast cells, basophils, and eosinophils. *J Allergy Clin Immunol* (2010) **125**(2):S73–80. doi:10.1016/j.jaci.2009.11.017
86. Yoshimoto T, Nakanishi K. Roles of IL-18 in basophils and mast cells. *Allergol Int* (2006) **55**(2):105–13. doi:10.2332/allergolint.55.105
87. Suto H, Nakae S, Kakurai M, Sedgwick JD, Tsai M, Galli SJ. Mast cell-associated TNF promotes dendritic cell migration. *J Immunol* (2006) **176**(7):4102–12. doi:10.4049/jimmunol.176.7.4102
88. Kamata H, Honda S, Maeda S, Chang L, Hirata H, Karin M. Reactive oxygen species promote TNF α -induced death and sustained JNK activation by inhibiting MAP kinase phosphatases. *Cell* (2005) **120**(5):649–61. doi:10.1016/j.cell.2004.12.041
89. Grell M, Zimmermann G, Gottfried E, Chen CM, Grünwald U, Huang DC, et al. Induction of cell death by tumour necrosis factor (TNF) receptor 2, CD40 and CD30: a role for TNF-R1 activation by endogenous membrane-anchored TNF. *EMBO J* (1999) **18**(11):3034–43. doi:10.1093/emboj/18.11.3034
90. Okamura H, Tsutsui H, Komatsu T, Yutsudo M, Hakura A, Tanimoto T, et al. Cloning of a new cytokine that induces IFN-gamma production by T cells. *Nature* (1995) **378**(6552):88–91. doi:10.1038/378088a0
91. Tripp CS, Unanue WS. ER Interleukin 12 and tumor necrosis factor alpha are costimulators of interferon gamma production by natural killer cells in severe combined immunodeficiency mice with listeriosis, and interleukin 10 is a physiologic antagonist. *Proc Natl Acad Sci U S A* (1993) **90**:3725–9. doi:10.1073/pnas.90.8.3725
92. Wherry JC, Schreiber RD, Unanue ER. Regulation of gamma interferon production by natural killer cells in scid mice: roles of tumor necrosis factor and bacterial stimuli. *Infect Immun* (1991) **59**(5):1709–15.
93. Bertagnolli MM, Lin BY, Young D, Herrmann SH. IL-12 augments antigen-dependent proliferation of activated T lymphocytes. *J Immunol* (1992) **149**(12):3778–83.
94. Chan SH, Perussia B, Gupta JW, Kobayashi M, Pospisil M, Young HA, et al. Induction of interferon gamma production by natural killer cell stimulatory factor: characterization of the responder cells and synergy with other inducers. *J Exp Med* (1991) **173**(4):869–79. doi:10.1084/jem.173.4.869
95. Magram J, Connaughton SE, Warrier RR, Carvajal DM, Wu CY, Ferrante J, et al. IL-12-deficient mice are defective in IFN gamma production and type 1 cytokine responses. *Immunity* (1996) **4**(5):471–81. doi:10.1016/S1074-7613(00)80413-6
96. Chehimi J, Starr SE, Frank I, Rengaraju M, Jackson SJ, Llanes C, et al. Natural killer (NK) cell stimulatory factor increases the cytotoxic activity of NK cells from both healthy donors and human immunodeficiency virus-infected patients. *J Exp Med* (1992) **175**(3):789–96. doi:10.1084/jem.175.3.789
97. Mantovani A, Sica A, Locati M. Macrophage polarization comes of age. *Immunity* (2005) **23**(4):344–6. doi:10.1016/j.immuni.2005.10.001
98. Sallusto F, Lanzavecchia A. Efficient presentation of soluble antigen by cultured human dendritic cells is maintained by granulocyte/macrophage colony-stimulating factor plus interleukin 4 and downregulated by tumor necrosis factor alpha. *J Exp Med* (1994) **179**(4):1109–18. doi:10.1084/jem.179.4.1109
99. Witte MB, Barbul A. General principles of wound healing. *Surg Clin North Am* (1997) **77**(3):509–28. doi:10.1016/S0039-6109(05)70566-1
100. Gillitzer R, Goebeler M. Chemokines in cutaneous wound healing. *J Leukoc Biol* (2001) **69**(4):513–21.
101. McKay IA, Leigh IM. Epidermal cytokines and their roles in cutaneous wound healing. *Br J Dermatol* (1991) **124**(6):513–8. doi:10.1111/j.1365-2133.1991.tb04942.x
102. Barrientos S, Stojadinovic O, Golinko MS, Brem H, Tomic-Canic M. Growth factors and cytokines in wound healing. *Wound Repair Regen* (2008) **16**(5):585–601. doi:10.1111/j.1524-475X.2008.00410.x

Conflict of Interest Statement: The authors declare that the research was conducted in the absence of any commercial or financial relationships that could be construed as a potential conflict of interest.

Copyright © 2015 Starzl, Wolfram, Zamora, Jefferson, Barclay, Ho, Gorantla, Brandacher, Schneeberger, Andrew Lee, Carbonell and Vodovotz. This is an open-access article distributed under the terms of the Creative Commons Attribution License (CC BY). The use, distribution or reproduction in other forums is permitted, provided the original author(s) or licensor are credited and that the original publication in this journal is cited, in accordance with accepted academic practice. No use, distribution or reproduction is permitted which does not comply with these terms.



Introduction of a framework for dynamic knowledge representation of the control structure of transplant immunology: employing the power of abstraction with a solid organ transplant agent-based model

Gary An*

Department of Surgery, University of Chicago, Chicago, IL, USA

OPEN ACCESS

Edited by:

Giorgio Raimondi,
Johns Hopkins School of
Medicine, USA

Reviewed by:

Julee Thakar,
University of Rochester, USA
Judy Day,
University of Tennessee, USA
Rebecca Segal,
Virginia Commonwealth University,
USA

***Correspondence:**

Gary An
docgca@gmail.com

Specialty section:

This article was submitted to
Alloimmunity and Transplantation,
a section of the
journal Frontiers in Immunology

Received: 05 May 2015

Accepted: 19 October 2015

Published: 06 November 2015

Citation:

An G (2015) Introduction of a framework for dynamic knowledge representation of the control structure of transplant immunology: employing the power of abstraction with a solid organ transplant agent-based model. *Front. Immunol.* 6:561.
doi: 10.3389/fimmu.2015.00561

Agent-based modeling has been used to characterize the nested control loops and non-linear dynamics associated with inflammatory and immune responses, particularly as a means of visualizing putative mechanistic hypotheses. This process is termed dynamic knowledge representation and serves a critical role in facilitating the ability to test and potentially falsify hypotheses in the current data- and hypothesis-rich biomedical research environment. Importantly, dynamic computational modeling aids in identifying useful abstractions, a fundamental scientific principle that pervades the physical sciences. Recognizing the critical scientific role of abstraction provides an intellectual and methodological counterweight to the tendency in biology to emphasize comprehensive description as the primary manifestation of biological knowledge. Transplant immunology represents yet another example of the challenge of identifying sufficient understanding of the inflammatory/immune response in order to develop and refine clinically effective interventions. Advances in immunosuppressive therapies have greatly improved solid organ transplant (SOT) outcomes, most notably by reducing and treating acute rejection. The end goal of these transplant immune strategies is to facilitate effective control of the balance between regulatory T cells and the effector/cytotoxic T-cell populations in order to generate, and ideally maintain, a tolerant phenotype. Characterizing the dynamics of immune cell populations and the interactive feedback loops that lead to graft rejection or tolerance is extremely challenging, but is necessary if rational modulation to induce transplant tolerance is to be accomplished. Herein is presented the solid organ agent-based model (SOTABM) as an initial example of an agent-based model (ABM) that abstractly reproduces the cellular and molecular components of the immune response to SOT. Despite its abstract nature, the SOTABM is able to qualitatively reproduce acute rejection and the suppression of acute rejection by immunosuppression to generate transplant tolerance. The SOTABM is intended as an initial example of how ABMs can be used to dynamically represent mechanistic knowledge concerning transplant immunology in a scalable and expandable form and can thus potentially serve as useful adjuncts to the investigation and development of control strategies to induce transplant tolerance.

Keywords: transplant immunology, agent-based modeling, immunosuppressive agents, mathematical modeling, discrete models, immune system modeling, immune system models, agent-based models

INTRODUCTION: THE ROLE OF DYNAMIC KNOWLEDGE REPRESENTATION TO ADDRESS THE TRANSLATIONAL DILEMMA

The central dilemma for the biomedical research community today can be described as a paradoxical challenge of dealing with an embarrassment of riches. Technological advances in experimental methodology have led to an unprecedented ability to probe deeply into the workings of biological systems and acquire information at a level of detail not previously imagined. Advances in computational capability, both in terms of storage and processing, have allowed the analysis of data sets at a fundamentally different scale. However, the challenges of interpreting this plethora of data are growing as quickly as the ability to acquire it. This condition is most evident in the ability to turn this increased basic biomedical knowledge into effective therapies to treat the diseases that most impact society today. The United States Food and Drug Administration report: "Innovation or Stagnation: Challenge and Opportunity on the Critical Path to New Medical Products" (1) clearly delineates a steadily increasing expenditure on Research and Development that is concurrent with a progressive decrease in the delivery of medical products to market; while this report is over a decade old, this trajectory has not substantively changed since the release of that report. This is the *Translational Dilemma* that faces biomedical research: the inability to effectively and efficiently translate basic mechanistic knowledge into clinically effective therapeutics, most apparent in attempts to understand and modulate "systems" processes/disorders, such as sepsis, cancer, wound healing, and immunomodulation (including transplantation). The current situation calls for a re-assessment of the scientific process as currently executed in biomedical research as an initial step toward identifying where and how the process can be augmented by technology. We have asserted that the primary bottleneck in the current biomedical research workflow is the ability to evaluate and falsify the vast sets of putative mechanistic hypotheses being generated from the data-rich environment and that the use of computational modeling for dynamic knowledge representation is the means by which this bottleneck, and the Translational Dilemma, can be addressed (2). With the specific goal of facilitating the computational representation of the mechanistic knowledge generated from basic biological research, agent-based modeling is a modeling method that is particularly well suited for this purpose.

DYNAMIC KNOWLEDGE REPRESENTATION WITH AGENT-BASED MODELING

Agent-based modeling is a discrete event, object-oriented, rule-based, and often spatially explicit method for dynamic computer modeling that represents systems as a series of interacting components (3–7). An agent-based model (ABM) is a computer program that generates populations of discrete computational objects (or *agents*) that correspond to the component-level at which the reference system is being examined. These computational agents

are organized into *agent classes* representing groupings of agents of a similar type defined by shared properties and characteristics. Agents are governed by *agent rules*, which are a series of instructions that allow the agent to be treated as an input–output object. ABM rules are often expressed as conditional statements ("if-then" statements), making ABMs an intuitive way for representing mechanisms identified from basic science research. Consider the following simple example. There is an agent class called cell-type-1 used to represent a particular cell type. That cell type is known to have a particular receptor, which is called receptor-A, which can bind to a ligand, ligand-A. The binding of ligand-A to receptor-A activates a signal transduction enzyme that is called ST-enzyme-B. This knowledge would be expressed in an ABM in the following manner:

Rule for agent-class cell-type-1:

*If ligand-A present, then bind to receptor-A
If receptor-A bound to ligand-A, then activate ST-enzyme-B...*

The general nature of a "rule" allows other types of mathematical or computational models (i.e., differential equation, stochastic, or network) to be used as rule systems (7–13). Individual agents incorporate the properties and rule structures of their parent agent class but are able to manifest diverging behavioral paths based on the differing local inputs that are possible through the ABM's spatially heterogeneous simulation environment. For instance, in the example presented earlier, it can be readily seen that the behavior of different individual computational agents of type cell-type-1 might now deviate from each other: those in the presence of ligand-A will behave differently from those not exposed to ligand-A. This is the key property of ABMs that allow them to behave "realistically," generating population/system level outputs from the heterogeneous behavioral trajectories of individual agent instances that embody lower-level knowledge and mechanisms. Thus, ABMs intrinsically cross scales of biological organization, utilizing behavioral rules (Scale #1) to determine individual agent behavior (Scale #2) and then aggregating individuals into population dynamics of the global system (Scale #3). The ability to generate distributions of population behavior is also enhanced by the common practice of adding stochastic components to the agents' rules: this stochasticity may reflect either apparent randomness associated with limitations of measurement, or actual stochastic processes present in the reference system (which may amount to the same thing).

Agent-based modeling has been used in multiple domains, particularly in those systems that can be viewed as involving the interactions between populations of components, such as ecology (14, 15), social/political science (16), microeconomics (17), and epidemiology (18). Agent-based modeling has also been increasingly and more extensively applied to biomedical systems, primarily in terms of characterizing multicellular interactions, such as in the study of sepsis (19–22), cancer (8, 23–26), cellular trafficking (27–31), host–microbe interactions (32, 33), gastrointestinal biology (34–36), and wound healing (12, 37, 38).

By virtue of their rule-based nature, ABMs are an intuitive means of dynamically representing the mechanisms and

hypotheses present in the biomedical literature, allowing them to serve as dynamic knowledge representations of mechanistic hypotheses (21, 39). The intrinsic multiscale nature of ABMs allows researchers to translate putative causal mechanisms to system level phenotypes, an essential function in dealing with the complexity of biological systems. Additionally, the non-prescribed nature of the rules embedded in an ABM, which facilitates the initial development of abstract models and the progressive addition of more detail as it becomes needed, makes agent-based modeling well suited as a scalable modular framework that can evolve with the state of knowledge about a particular system (7, 8, 13, 22, 40).

Agent-based models are related to and share many features of other spatially discrete modeling methods, most notably cellular automata. However, what distinguishes ABM from cellular automata and other types of discrete methods is the ease of the mapping between the reference system and the construction of the ABM. Importantly, ABMs facilitate *abstraction*. The process of abstraction is an essential step in the scientific process; it is only through abstraction that generalization is possible: the ability to extrapolate how one seemingly unique object/system can be treated as similar to another seemingly unique object/system. The process of generalization is the means by which science gains its explanatory power: now one thing learned about one object can be applied to another distinct yet related object. It is readily apparent that this principle of abstraction is embedded in the structure of ABMs through the relationship between the descriptions of a particular agent class and the behaviors of the individual instances of that class. Recognizing the essential role of abstraction in the scientific process leads to the driving concept of parsimony in the quest for explanation (i.e., hypothesis construction). Explanatory power is thus tied to an iterative process of evaluating and refining hypotheses that grow from a parsimonious root. The historical, philosophical, and logical bases for this understanding of the scientific process are reviewed and described in Ref. (41). This concept of parsimony also applies to the process of developing computational/mathematical models. As with all mathematical modeling methods, the initial construction of an ABM should keep the rules as simple as possible, often at the initial expense of mechanistic detail. What initially may seem to be a limitation is actually of considerable benefit, as ABMs representing incomplete and uncertain mechanisms can provide a mean of testing the plausibility of those mechanisms (14, 15). As such, the goal of simulation experiments is to provide sufficiently plausible model behavior given a particular ABM such that it is possible to state that the ABM has *face validity*. Face validity is the initial standard for validation as described in the modeling and simulation community and reflects the ability of a particular simulation to behave in a plausible and recognizable way (42, 43). Very often, this is reflected in the qualitative nature of the mapping between the simulation output and the real-world data, with an emphasis on having real-world behaviors targeted at multiple scales. This approach has been termed pattern-oriented modeling (POM) (14, 15) and has an established role in the biomedical application of ABMs (3, 6, 21). While initially developed for the use of agent-based modeling in ecology, the principles of POM, defined as "...the multi-criteria design, selection and calibration of models of complex systems" (14), can serve as a

useful framework for the development and use of ABMs in the biomedical context. POM contains three primary elements: (1) patterns used to determine model structure, 2) patterns used for model selection, and 3) patterns used for calibration. Each of these elements is treated with an iterative process that involves identification, instantiating, and refinement. As with all computational models, the greater fidelity of mapping between the ABM and its biological counterparts enhances the correlation between simulation results and the real-world behaviors, but it must be recognized that such increased fidelity can only be achieved through an iterative process of refinement arising from a necessarily parsimonious origin (6, 21).

The advantages of agent-based modeling are most evident when trying to integrate multiple populations of subcomponents (such as biological cells) that interact in a highly dynamic fashion. The multiple cell types and interactions present in transplant immunology represent exactly this type of system. Therefore, presented herein is an abstract representation of fundamental knowledge concerning the process of acute solid organ transplant (SOT) rejection incorporated into the solid organ transplant agent-based model (SOTABM). While there have been multiple prior ABMs of the immune response (as opposed to inflammation) (44–46) to our knowledge, there have been no prior published applications of agent-based modeling to SOT. The fundamental conceptual basis of the SOTABM is the view that effective transplantation centers around a "tipping point" between the proinflammatory aspects of the immune response aimed at eradicating non-self-cells (evolutionarily reflected in infection) versus the anti-inflammatory control mechanisms that prevent that immune response to damaging the host. More specifically, this tipping point is primarily governed by the cellular components that bridge the transition from the non-specific innate inflammatory immune response, which is the primary end effector for cellular/tissue/microbe damage, and the adaptive immune capability that focuses on partitioning response between self and non-self. The SOTABM is intended to provide an initial example of how a dynamic knowledge representation framework can be used to instantiate and replicate the general properties of transplant immunology with respect to acute rejection. As such, the SOTABM necessarily represents a simplified version of the real-world system, with its form the result of modeling choices made by the developer (as is the case with virtually any model, computational, or otherwise) governed by the principle of parsimony. Thus, there is no supposition that the SOTABM is a comprehensive representation of the sum total of knowledge concerning the cellular and molecular mechanisms of transplant immunology. Rather, the situation is quite the opposite, with the SOTABM intended to represent a basic and fundamental set of components and actions sufficient to explain core general behaviors associated with transplant immunology. Furthermore, the SOTABM represents one perspective (the modelers) of what these most basic and fundamental components and actions are. Given the goal of implementing canonical processes, initial models like the SOTABM draw heavily from literature reviews that present the best approximation of what is generally accepted within a scientific community. Therefore, the SOTABM is based on a series of literature reviews of transplant immunology, with

particular emphasis of the modeler's interpretation of Ref. (47) as the central reference text to provide the overall structure of the SOTABM. The exercise of developing the SOTABM as presented in this article is intended as an example of how such biomedical knowledge can be instantiated in an ABM, and in so doing demonstrate how such a process could be extended to incorporate greater mechanistic detail and a wider range of transplant pathophysiology.

Throughout the text we will attempt to clarify the distinction between the actual biological objects and the computational objects used to represent them by depicting the names of the computational objects in *courier font*.

METHODS

General Principles and Purpose of the Solid Organ Transplant ABM

As stated earlier, the intent of this presentation of the SOTABM is as a demonstration of how knowledge concerning transplant immunology could be initially incorporated into an ABM, with particular emphasis on the utilization of abstraction and qualitative pattern matching to enhance the understanding of biological systems. It is critical to emphasize the importance of looking at "model" in its verb form: "to model" as opposed to "a model." As such, one should not think of these models as end products, but rather as subjects for discourse in the iterative process that is science. Admittedly, this viewpoint is not the familiar one for biologists/experimentalists when dealing with "computation" in biomedicine. The far more common perspective is one of the computational modeling as an analysis service rooted in statistics and the identification of correlations: i.e., "Here are my results, tell me what this means using your fancy algorithms." Alternatively, the use of dynamic computational modeling as a form of knowledge representation and integration (which is how mathematical modeling is most powerfully used in the physical sciences) requires much more engagement on the part of the biologist, where the dynamic computational model is now a "conversation piece," subject to interactions where its explanatory power is assessed, its underpinnings challenged, and refinements applied, with the intent of moving toward a greater understanding of the system being studied. The SOTABM is very much intended to be the initial step in such an engagement. In reviewing the development and evaluation of the SOTABM presented in this article, the reader is encouraged to note the specific inclusions and omissions made (inherent in the modeling process) and consider how they would potentially address their perceived shortcomings/limitations of the SOTABM if they were to undertake such an exercise. At a fundamental level, dynamic models such as the SOTABM should not be viewed as end products, but rather as objects intended to generate discourse and simulate an iterative process of testing, falsification, and refinement.

A Note on Parameters

As with all computational models, ABMs require the use of multiple parameters (constants utilized in the model's rules). For

example, in the sample rule previously provided, its implementation would be:

If [some value of] ligand-A is present, then bind to receptor-A [to some degree].

If [some threshold value] of receptor-A is bound with ligand-A, the activate ST-enzyme-B [to some degree]

It should be immediately evident that the behavior of any model is heavily dependent upon the parameters chosen. As such, the issue of parameter selection holds particular importance in the development and use of computational models. Ideally, choosing parameters that are derived from experimentally available data substantially enhances the believability of a computational model (assuming it behaves plausibly with those parameters). However, the process of experimentally acquiring specific parameters is often extremely difficult, if not infeasible or impossible, given current experimental and sampling technologies. This latter condition, in fact, has substantially limited the adoption of dynamic computational models in biomedical research, where a very stringent and restrictive criteria for what constitutes a "believable model," dependent upon quantitative parameter and model behavior matching, substantially reduces the number of "believable models" that can actually be produced. Interestingly, it has been argued that such specifically detailed parameters can only be obtained in highly constrained and artificial experimental conditions, with the end result of a model "valid" for those experimental conditions, but of limited applicability beyond those conditions when more systems-level phenomena are being examined (6). This latter understanding is actually more in keeping with the traditional scientific goal of discovery and establishing generalizing principles, as opposed to the engineering paradigm of optimization and design that underlies many researchers' experience with modeling and simulation.

The demonstration of agent-based modeling with the SOTABM takes the generalizing, parsimonious approach. As noted earlier, one of the advantages of agent-based modeling is its embracement of abstraction as a means of dealing with incomplete knowledge. By utilizing population effects as their primary output metrics, ABMs allow the characterization of system behavior in a more qualitative fashion, at least in the initial stages of development. For this reason, POM (14, 15) and the use of face validity as assessment criteria (42, 43) are heavily utilized in the development and evaluation of ABMs. This shifts the utility of dynamic computational modeling from quantitative prediction or engineering optimization to explorations of plausible and recognizable behaviors; this shift in the goal of modeling influences the selection and determination of the parameters used in the SOTABM. As can be seen in the sample rule explained earlier, ABM rules can start off as logical statements; the addition of conditional reified modifiers turns these rules into expressions closer to arithmetic. This allows certain types of parameters, specifically those associated with processes with known time scales, to be derived arithmetically. Even though these rates are potentially extractable and knowable, within the context of the specific ABM, their actual values are not important. In fact, since the SOTABM utilizes an abstract representation

of space, an attempt to directly apply experimentally derived numerical values for those parameters could potentially foster the belief that the model is somehow more “real” than it actually is. Rather, the relationship certain parameters have to other connected parameters is what is crucial for determining the behavior of the model. The relative dependencies of these connected and related parameters can prove very challenging if one required quantitative fidelity, but given that the current modeling goal is determining and examining sets of overall system behaviors, this type of parameter representation is appropriate [and arguably more relevant to translating the findings of a model beyond its specific implementation (6)]. As such, the establishment of these parameter values often starts with an arbitrary range and is generally followed by a heuristic, hand-fitting process involving repeated runs of the ABM and adjustment based on plausible behavior. If such plausible behavior cannot be generated, then this points to a fundamental insufficiency in the model. This process is integral to the development and calibration of an ABM. However, note that this hand-fitting process of calibration occurs before the execution of the presented simulation experiments; there is no retrofitting of parameters based on the outcomes of the actual experimental simulations.

SOTABM Overview

SOTABM is an abstract representation of the inflammatory and immune components involved in the acute rejection process of a SOT. The SOTABM is implemented in the freeware agent-based modeling toolkit Netlogo (48). Netlogo is a self-contained toolkit for agent-based modeling and is specifically designed to allow non-computer programmers/mathematicians to create dynamic models of their systems of interest. Interested readers are directed to the Netlogo website (<https://ccl.northwestern.edu/netlogo/>) to see examples and download the toolkit for their own use. Cellular components are depicted by computational agents (“turtles” in Netlogo terminology): some of these cell types are able to move while others remain static. The background grid spaces (“patches” in Netlogo terminology) represent the extracellular environment of the model. Agents hold variables representing determinants of their internal state (i.e., molecular components of the cells), which in turn govern their state transition rules (i.e., behavior). Patches hold variables that represent extracellular mediators, which diffuse between discrete patches using Netlogo’s `diffuse` function [which takes the value of the variable on an individual patch and evenly distributes some fraction of that value to the surrounding eight patches; see Ref. (48)]. Interactions with the SOTABM take place through the standard Netlogo interface, consisting of various GUI buttons, switches, and sliders by which certain functions are called and parameters set. The stochasticity in the SOTABM is produced by the use of Netlogo’s random number generator to add probabilistic modifiers to the agents’ state transition rules; Netlogo uses the Mersenne Twister pseudorandom generator, one of the most commonly used pseudorandom number generators utilized in software design (48). Consistent with the general modeling strategy that it is necessary to represent the baseline healthy state with some degree of the system robustness and function present in the real-world reference system, the SOTABM is constructed to be able to utilize its inflammatory and immune

functions to deal with both sterile injury (i.e., tissue trauma) and an infectious insult. The SOTABM is available for download from http://bionetgen.org/SCAI-wiki/index.php/Main_Page.

Description of the Model World for the SOTABM

At its current level of abstraction the SOTABM does not explicitly represent tissue or organ architecture but instead utilizes an abstract representation of various tissue compartments where different cellular interactions occur. The SOTABM does not include the means to differentiate the various degrees of immunogenicity seen between renal, hepatic, and cardiac transplants. The primary interaction space in the host tissue is represented by a two-dimensional square grid where the edges “wrap,” making it topologically a torus. The size of the grid is 41×41 grid spaces; this size was arbitrarily chosen to trade off computational efficiency versus enough space to allow for distinct groupings of agents (see **Figure 1**). Each grid space is populated by an agent representing a generic host tissue cell (`self-cell`), and populations of immune cells move in a semi-Brownian fashion over this surface. The specific cell types and produced mediators represented in the SOTABM are described later in the respective Section “Methods.” The modeling choice was made to divide the overall world space of the SOTABM into four quadrants each representing a spatially distinct, but still connected, interaction space with different functions. Thus, the SOTABM has a distinct area in the left upper quadrant of the grid, which is intended to represent the intralymph node interaction space in a more spatially defined and limited area. Similarly, simulations of transplanted tissue, as well as remote tissue infection or injury, are localized in different quadrants of the grid (see **Figure 1**). Three different conditions are able to be applied to the system: Condition #1 sterile injury, Condition #2 localized infection, and Condition #3 solid tissue transplant. Conditions #1 and #2 can be varied in their size and are depicted as generally circular areas; Condition #3 is of fixed size consisting of 109 transplant cells in a roughly rectangular configuration. The size of the simulated transplant (109 cells) is semiarbitrary, decided upon primarily based on the size of the world grid (itself an arbitrary constraint) and the modeling decision to represent different body compartments/tissues in different quadrants of the world grid. As noted earlier, the current version of the SOTABM uses a generic “transplanted tissue,” and therefore does not distinguish between the different immunological properties seen between renal, hepatic, or cardiac tissues. In addition to depicting generic transplanted organ tissue, graft mesenchymal stromal/stem cells (`graft-MSCs`) are also included in the transplanted area. These cells were selected for inclusion based on their role in suppressing the generation of cytotoxic immune cells directed against the graft (see later). Other graft-associated immune cells, such as macrophages, dendritic cells, and T-cell subtypes residing in any graft lymphoid tissue, were not included since the intent at this stage is not to attempt to represent graft versus host disease. While it is potentially possible to have concurrent conditions within the SOTABM, such as simulating the tissue trauma of transplant followed by the transplanted organ itself, or the development of an

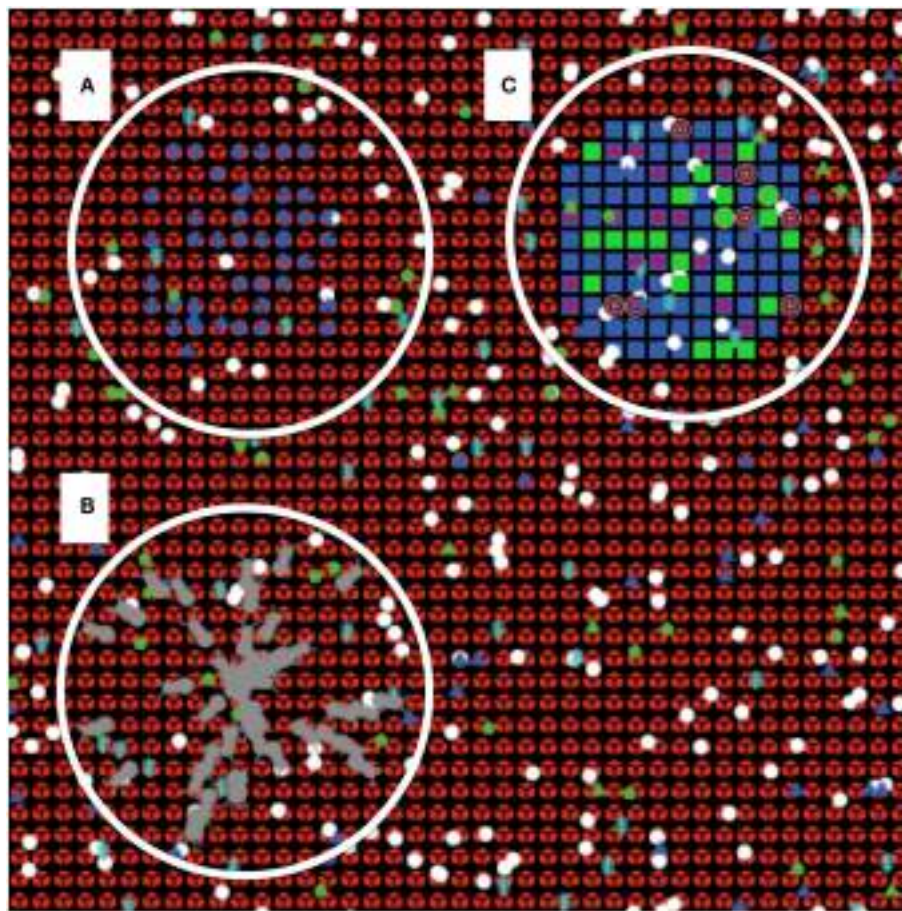


FIGURE 1 | Screenshot of the solid organ transplant agent-based model (SOTABM). This figure depicts the NetLogo graphical interface of the SOTABM. The model world consists of a two-dimensional square grid that is 41×41 grid spaces in size. Each grid space is populated by a self-cell (red), and multiple inflammatory/immune cells can be seen distributed over its surface. Letter **(A)** emphasizes the simulated lymph tissue area in the left upper quadrant of the SOTABM; naive-CD8-ts (blue dots) can be seen in this area. Letter **(B)** emphasizes the region where either infectious insult (here depicted as gray bugs) or tissue trauma (not shown) can be applied. Placement of the perturbation in this area constitutes a “remote” insult from the area of potential transplant. Letter **(C)** emphasizes the area where transplant tissue is applied in the right upper quadrant. Transplant cells can be seen as blue squares, with various other agents representing graft/donor macrophages and dendritic cells can be seen overlying the transplant tissue. Note that the concurrent presence of infection and transplant tissue is provided for depiction purposes only; in the simulation experiments presented for the SOTABM, there were no concurrent types of system perturbations performed.

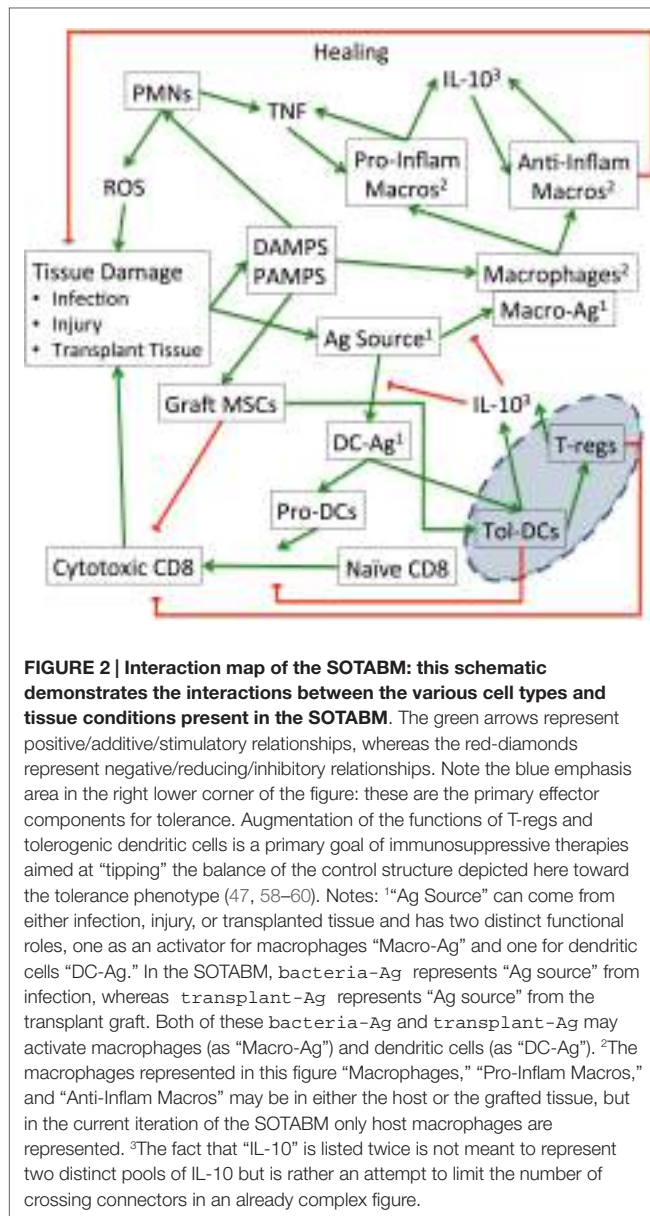
infection in a previously transplanted case, for purposes of this initial demonstration of the SOTABM it was elected not to add this complexity at this time.

Given the abstraction of the functions represented in the SOTABM, it is not precisely calibrated to time at a granular mechanistic level. Rather, the effects of the cellular-molecular events are simulated to take place with one cycle of the SOTABM (ticks in NetLogo terminology) approximating 15 min of real-world time.

Interaction and Control Structure of the SOTABM

As noted earlier, the primary goal of the SOTABM is to serve as an initial example of how to depict the general control structure of the transplant immune response, particularly pertaining to

acute rejection, in an ABM. A schematic of this control structure can be seen in **Figure 2**. Note that in order to not generate a completely uninterpretable figure, the exact model components utilized in the SOTABM (i.e., the names of all the agent classes) are not explicitly represented in **Figure 2**; rather representative labels are used to depict the main categories of cells and mediators chosen to be included in the SOTABM. Text contextualizing the specific model components to **Figure 2** is provided in the descriptions of those components in the sections later. As a general description, the initial components of the innate immune response represent the end effector of the system, being primarily responsible for interactions influencing tissue damage, microbial killing, and abstracted tissue reconstitution. The innate immune response incorporates both pro- and anti-inflammatory components, consistent with a self-contained control structure befitting its role as a highly evolutionarily



conserved, fundamental function of multicellular organisms. This component of the SOTABM is very similar to structure to our prior work modeling the acute inflammatory response (20, 22). The SOTABM also includes an additional layer of control representing the regulatory role of lymphocytes, primarily T-cell subtypes. It is noted again that as with all mathematical/computational models, the specific components included in the SOTABM are the result of choices made by the modeler. Given the intent to start from the most well-established and generally accepted components and mechanisms present, introductory ABMs such as the SOTABM often focus on utilizing the content of well-respected review articles for their initial structure. In this case, the initial version of the SOTABM takes the information reviewed in Ref. (47) as its primary source for its included components and mechanisms. While it is clearly evident both

from Ref. (47) and from other resources utilized for the development of the SOTABM (49–57) that there are multiple subtypes of regulatory T cells (T-reg), for simplicity’s sake this initial version of the SOTABM abstracts these into the general classes of effector/cytotoxic T cells and T-reg. This simplifying process utilizes the following general guidelines:

1. If a cell type or subtype has essentially the same set of input and output relationships as another cell type, then these were aggregated to a more general cell type description.
2. If a cell type did not have an output relationship that rendered it unique, it was not included.
3. If a cell type served as an intermediate pathway that was otherwise represented in the model using previously selected cell types, it was not included.
4. If a cell type had an output that did not fit into the existing level of functional representation of the SOTABM, such as ischemia–reperfusion, these cells were not included.
5. In general, specific secreted mediator/cytokine relationships were abstracted out if their action could be represented with a cell-to-cell influence/interaction. Note that this does not mean the interaction represented is an actual cell-to-cell physical event, but rather that the effect of the omitted mediator could be represented through a direct relationship.

For instance, comparing **Figure 2** with **Figures 1** and **2** from Ref. (47), **Figure 2** in this paper aggregates T-cell subtypes that have the same input/output or target into the more abstract grouping. This modeling decision is based on the assessment that the impact of the subtleties associated with the finer control provided by these T-cell subtypes is below the representational resolution of the current SOTABM. It is also assumed that there is essentially no lymphoid tissue in the transplanted graft; this is generally consistent with the most common types of SOTs (hepatic, renal, and cardiac) and is consistent with the previously noted decision not to model graft versus host disease at this stage. It is acknowledged that these abstractions may have an impact on the subsequent iterations of the SOTABM as it becomes more refined, but these are accepted possibilities intrinsic to the iterative nature of model development. Furthermore, recognition of these abstractions/omissions would be natural points for future expansion of the SOTABM.

Cell and Agent Types

The following sections describe the specific agent classes included in the SOTABM. As noted earlier, the overall relationships between the cellular components included are depicted in **Figure 2**, albeit with a generalization of the cellular subtypes necessary to facilitate depiction in the figure. The relationships and interaction rules for the agents are described later, with the recognition that the encoding of those rules in the SOTABM follows the process described in Section “*A Note on Parameters.” Since the actual values used in the SOTABM would have little meaning outside the context of the actual code, the entire SOTABM model is available for download from http://bionetgen.org/SCAI-wiki/index.php/Main_Page so that interested readers can view the interactions themselves.

Host Tissue (self-cells)

These cells represent the general tissue of the host. They do not move and occupy each intact grid space of the SOTABM at baseline. They contain a life variable, which determines their health state. Damage to the self-cells is reflected by a decrement of the life variable. When damaged beyond a certain threshold (arbitrarily set at <70% health, or $<\text{life} = 70$), the self-cells will produce damage-associated molecular pattern molecules (DAMPS) that will activate various inflammatory cells. Self-cells can be damaged by bacteria, or by the production of reactive oxygen species ($r\text{-oxy-s}$) from immune cells, or directly upon initialization in the sterile tissue injury mode. They are healed primarily by anti-inflammatory macrophage species (host-anti-inflam-macros), though also to a less or degree by proinflammatory macrophage species (host-pro-inflam-macros).

Simulated Bacteria (Bacteria-Present)

Ref. (20, 57) was used to develop the rules for bacterial infection in the SOTABM. Bacterial infection is simulated abstractly by using placeholder agents representing the presence of infection (bacteria-present), which themselves have a state variable representing the amount of bacteria present on a single patch (bacteria-count). As noted earlier, bacteria are introduced into the simulation at initialization at varying sizes of initial insult. The bacteria reduce the life of the self-cell present on their own patch, and when the life of that self-cell is reduced to 0, the bacterial colonies/clusters spread to an adjacent patch, where the subsequent value of bacteria-count on the target patch represents the magnitude of bacteria that have spread. The bacteria produce pathogen-associated molecular pattern molecules (PAMPS), which act analogously to DAMPS in terms of attracting and activating immune cells. Bacteria are killed by $r\text{-oxy-s}$, as well as by activated proinflammatory macrophages (host-pro-inflam-macros).

Transplanted Tissue (Transplant Cells)

Solid organ transplant is represented by the application of a solid section of 109 transplant cells in the right upper quadrant of the SOTABM (size arbitrarily set to 109 cells). Transplant cells perform all the functions of the self-cells in terms of keeping track of their health via the life variable and producing DAMPS if damaged. In addition, they also have a state variable for non-self antigen (transplant-Ag), which can be passed on to any host antigen-presenting cells [host macrophages (host-macros) and host-DCs] that come into contact with them. Also, in addition to being able to be damaged by bacteria or $r\text{-oxy-s}$, they can also be directly damaged by activated cytotoxic CD8⁺ T cells (cyto-CD8-ts).

Polymorphonuclear Neutrophil Cells

These are the most common type of inflammatory cells; the rules for polymorphonuclear neutrophil cells (PMNs) are drawn from Ref. (20, 52, 53, 57). They move randomly unless in the presence of their chemotactic triggers (DAMPS and PAMPS). When triggered, they follow the gradients of these molecules to the areas of injury or infection, where they undergo respiratory burst. This

results in the production of $r\text{-oxy-s}$, which kills bacteria and damages normal tissue.

Host Macrophages (Host-Macros)

Their interactions are depicted under boxes "Macrophages," "Pro-Inflam Macros," and "Anti-Inflam Macros" in Figure 2. The rules for host-macros and their subtypes are derived from Ref. (20, 47, 52, 53, 57, 61, 62). Similar to PMNs, these immune cells move randomly unless in the presence of threshold levels of their chemotactic triggers: a combination of DAMPS / PAMPS and tumor necrosis factor (TNF). They become activated into either a proinflammatory phenotype or an anti-inflammatory phenotype depending on their milieu. DAMPS, PAMPS, and TNF all favor the proinflammatory state, while interleukin-10 (IL-10) favors the anti-inflammatory state. Proinflammatory activated macrophages (host-pro-inflam-macros) will produce both TNF and IL-10 based on their level of stimulation by PAMPS and DAMPS. The effect of IL-10 is to decrease the responsiveness of host-DCs and host-macros to recognize antigen. They will also abstractly perform phagocytosis (by reducing the bacteria-count of bacteria-present on patches colocated with the host-macro), and weakly heal normal tissue. Anti-inflammatory activated macrophages (host-anti-inflam-macros) will produce IL-10 based on their level of stimulation by PAMPS, DAMPS, and TNF; they do not produce TNF. They are the primary healing cells in the SOTABM, representing this function abstractly by increasing the life of any self-cells present until they return to normal. Also, unactivated host-macros are able to recognize non-self antigens (transplant-Ag) when they come into contact with transplant cells. Once they carry transplant-Ag, they are able to convert any naïve CD8 T cells (naïve-CD8-ts) in the lymph node area of the SOTABM to cyto-CD8-ts, which can then migrate to the area of the transplant and damage it.

Host Dendritic Cells (host-DCs, pro-host-DCs, and tol-host-DCs)

These cells function similarly to unactivated host-macros, and rules for their behavior were derived from Ref. (47, 63, 64). If they come into contact with bacteria or transplant cells, they will pick up either bacteria-Ag or transplant-Ag. These activated dendritic cells have two distinct paths: either their default path as proinflammatory dendritic cells (pro-host-DCs) that are able to activate naïve-CD8-ts to their cytotoxic form (cyto-CD8-ts) through direct contact, or as tolerogenic dendritic cells (tol-host-DCs) that directly inhibit the generation of cyto-CD8-ts, as well as activating T-reggs and producing IL-10. This last function, the production of IL-10, is a negative feedback control mechanism that reduces the ability of host-DCs and host-macros to pick up antigen in the first place. The default trajectory of an antigen-activated host-DC is toward the pro-host-DC phenotype, but interaction with graft-MSCs will switch them to the tol-host-DC phenotype.

CD8⁺ T Cell Species (naïve-CD8-ts and cyto-CD8-ts)

Rules for T cells in this and the following sections were derived from Ref. (47, 49–53, 62, 63). These cells are initialized as

naïve-CD8-ts in the left upper quadrant of the SOTABM, simulating their baseline existence in lymph tissue. In their naïve form, they do not move, but if they are exposed to/colocated with host-macros or host-DCs that are positive for transplant-Ag, then they become activated to cyto-CD8-ts, which can then move to the area of transplant tissue. If they come into contact with transplant cells they will reduce their life, leading to the production of DAMPS and eventually killing the transplant cell.

Regulatory T Cells

This agent class is used to abstractly aggregate a large set of different subtypes of T cells (many of which are CD4⁺ but also includes CD8⁺ regulatory cells, double negative CD T cells, among others) (47, 49–53, 55, 63). While a plethora of these cell types exist, in general, they share many common features:

1. Their production and function are enhanced by IL-10.
2. Many produce IL-10.
3. They inhibit the generation of, function of, and promote the apoptosis of both effector T cells and non-tolerogenic dendritic cells.
4. They promote the generation and function of tolerogenic dendritic cells.

Therefore, the current version of the SOTABM aggregates these functions into a single abstract t-reg class. T-reg cells freely move, reflecting their initial peripheral location. They become activated through interactions with antigen-presenting cells (either host-macros or host-DCs with positive transplant-Ag); once activated, they produce IL-10. They are also able to induce apoptosis of antigen-presenting cells already activated with transplant-Ag.

Mesenchymal Stromal/Stem Cells

These are immature, multipotent cells initially derived from the bone marrow but present in virtually all organ tissue (including transplanted organs); rules for implementation of mesenchymal stromal/stem cells (MSCs) are drawn from Ref. (47, 54, 55, 58, 65–67). These cells are activated by inflammation, though not immediately or acutely, as would be seen in tissue trauma or bacterial infection. Rather, their function is more pronounced in the face of longer standing inflammation, as would be seen in chronic infections or persistent inflammation. MSCs have potent anti-inflammatory properties triggered by exposure to DAMPS, resulting in the downregulation of effector T cells. Their specific role in transplant immunology is not completely clear. The SOTABM focuses on the role of MSCs only in the graft tissue (graft-MSCs) because: (1) MSCs do not appear to be present in meaningful numbers in the circulation, (2) the apparent time course of MSC activity lies outside the time period where host-derived MSCs might affect acute rejection, and (3) MSCs are present in organs commonly transplanted (i.e., liver, kidney, and heart). Graft-MSCs become activated by DAMPS, deactivate cyto-CD8-ts, and promote the generation of tol-host-DCs.

Simulated Antirejection Immunosuppression

It is generally accepted that in the absence of immunosuppression, all non-identical genotype organ transplants will result in acute rejection (47). A primary goal of immunosuppressive therapy is to tip the balance from T-cell-mediated immunity and cytotoxicity toward a tolerogenic phenotype dominated by T-reg (59). The end effector targets of immunosuppression can be seen in the blue emphasis region in **Figure 2**. While there are many different specific targets for immunosuppressive drugs, this current paper is focused on evaluating the effects of reducing effector T-cell populations/function while attempting to spare the role of T-reg. The SOTABM simulates the following general classes of immunosuppression.

T-Cell Eradication Therapies

These therapies, which are primarily polyclonal or monoclonal antibodies directed against T cells, are used as induction modalities (60). They are traditionally thought to function by depleting the host's T-cell populations, reducing the initial adaptive immune cellular response to the graft, and favoring the generation of tolerogenic, T-reg populations, though they are more recently recognized as having additional effects related to interference with leukocyte–endothelial adhesion as well as reducing dendritic cell function (60). For simplicity's sake, this initial version of the SOTABM focuses on simulating only the effect of T-cell depletion and represents this effect by allowing for 90% percentage depletion of T cells from day 2 to day 14 following transplant (68).

Calcineurin Inhibition

Calcineurin is a phosphatase that dephosphorylates the transcription factor necessary for T-cell activation (nuclear factor for the activation of T cells or NFAT) and allowing its localization in the nucleus. Inhibition of calcineurin prevents this localization and limits the activation of T cells. The SOTABM uses data regarding two of the most commonly used calcineurin inhibitors, cyclosporine A and tacrolimus, as reference points for the simulation of calcineurin inhibition (69–72). While both of these compounds block T-cell activation arising from interleukin-2 (IL-2) responsiveness, in the interest of simplicity the dynamics of IL-2 are not explicitly modeled. As such, the SOTABM qualitatively simulates the effect of calcineurin inhibition by reducing the probability that both naïve-CD8-ts are converted to cyto-CD8-ts, as well as the activation of T-reg by tol-host-DCs.

Cell-Based Supplementation Therapies

There is increasing interest in providing organ transplant patients with supplementary populations of those cells believed to favor the tolerogenic phenotype. T-reg and regulatory macrophages have been employed in this fashion, with initially promising results (47). However, the scalability of these modalities is hampered by practical barriers in the collection/generation of sufficient populations of appropriately configured cells. Therefore, cell transfer research has naturally turned toward those cell types that may be more readily available. Specifically, mesenchymal stromal cells have

been employed, with varying results (47, 54, 58). The SOTABM simulates the effect of MSC transfer therapy by the addition of 100 MSCs to the simulation following application of the transplant.

SIMULATION EXPERIMENTS

As noted earlier, current version of the SOTABM is intended as an initial example of an ABM that can serve as a scalable framework for dynamic knowledge representation of transplant immunology. The goal of such initial simulation experiments is to provide face validity, i.e., sufficiently plausible model behavior reflected in the qualitative mapping between the simulation output and the real-world behavior (6, 42, 43). This modeling goal places the current version of the SOTABM in the earliest phases of the POM process (14, 15). It should be noted that there is not a presumption of “uniqueness” of this particular configuration of the SOTABM. Rather, achieving face validity with the current iteration of the SOTABM just demonstrates that there exists a configuration of model parameters such that these behaviors can be reproduced (3, 6, 21). As applied to the SOTABM, this approach leads to the execution of simulation experiments aimed at replicating the conditions listed below.

Simulation experiments utilize the stochastic nature of ABMs to generate simulated populations for each experiment performed with the SOTABM. The following experiments were performed with $N = 100$ incidences per condition:

- Baseline immune response to injury and infection: these simulations were performed to establish plausible behavior of the SOTABM in terms of its ability to recover initial perturbations involving just tissue damage (sterile injury) or infection. “Death” of the system was arbitrarily defined as when the simulation run reached a level $<20\%$ total system health (reflected by the summed `life` variables of all the `self-cells`). Simulations were performed reflecting 28 days of simulated time and consisted of a *parameter sweep* of the level of the initial insult. A parameter sweep consists of a series of simulation runs ($N = 100$) across a range of the selected parameter. In this case, the parameter is the initial amount of injury (initial injury number) or infection (initial infection number) applied to the SOTABM, and the parameter sweeps performed can be considered analogous to the dose-response range or generated mortality in the design of a particular wet-lab experimental model. Plausible behavior would be reflected by bounds on the ability of the system to survive based on the magnitude of the initial insult, below which where survival = 100% and above which survival = 0%. This is similar to the previously utilized method for evaluating the response of an ABM of systemic inflammation to injury and infection (19, 20).
- Baseline immune response to transplant: as opposed to the simulation experiments used to examine SOTABM response to injury and infection, which consisted of parameter sweeps of the magnitude of initial perturbation, the amount of transplanted tissue applied is fixed (109 contiguous `transplant cells` in a roughly square configuration). Since all transplanted organs undergo some degree of damage, a “successful” transplant was viewed

as the simulation having $>20\%$ of the transplanted tissue remaining (as reflected by the sum of the `life` variable of all the) after 1 year of simulated time (arbitrary percentage). Plausible behavior would consist of loss of all transplant tissue by the end of 1 year simulated time in the absence of immunosuppression (73).

- Simulation of immunosuppressive therapies: as noted in Section “Methods,” the SOTABM has the capability to simulate several antirejection therapies.
 - T-cell eradication therapy is simulated by the deactivation of 90% of all T-cell agents on day 2 post-transplant extending to day 14 post-transplant, at which time T-cell populations were allowed to recover. This rule was adapted from Ref. (60, 68), with an exclusive focus on the effect of anti-T-cell antibody therapy with respect to decreasing T-cell populations at doses approximately corresponding to use in human organ transplant.
 - The effect of calcineurin inhibition is simulated by the reduction of the probability that `naïve-CD8-ts` are converted to `cyto-CD8-ts` to 10% per encounter, while the effective preserving activation of `T-reg`s by `tol-host-DCs` consists of having activation occur at a probability of 80% per encounter; this effect was persistent during the 1 year of simulated time, reflecting the continued use of the therapeutic agent. These effects and values were extrapolated from information extracted from Ref. (69–72).
 - Simulation of cell transfer therapy using MSCs was simulated by the addition of 100 MSCs to the simulation following application of the transplant (58). This number of MSCs, relative to the number of PMNs (=200 at initialization) in the SOTABM, is within the range (lower end) of *in vivo* studies investigating MSC transfer therapy (58). PMNs were chosen as the reference cell population number due to the greater availability of their circulating numbers.

Simulation experiments of immunosuppressive strategies consisted of each intervention alone (parsed interventions), T-cell eradication therapy plus calcineurin inhibition (approximation of current clinical practice), and T-cell eradication therapy plus calcineurin inhibition plus MSC transplant (hypothetical). Parsed immunomodulation simulations are considered component testing for the SOTABM’s simulation of immunosuppression. However, since clinical data do not exist for such interventions in isolation, the SOTABM’s output can only be viewed in the most qualitative fashion aimed at producing plausible results. The clinical reference outcome focuses on 1-year graft survival in the T-cell eradication + calcineurin inhibition group, which most closely approximates current standard clinical practice. Given the fact that the SOTABM utilizes a generic transplanted tissue, reference values were drawn from a range of SOTs: specifically kidney, liver, and heart. The reference range for renal transplant (cadaveric, due to the allogenic nature of the generic transplanted tissue in the SOTABM) was a 1-year graft survival range of 89–91% (74). The reference range for hepatic transplant was a 1-year graft survival of 71–80% (the range representing the difference between deceased cardiac donors and deceased brain donors, a distinction not within the SOTABM’s current representational capacity) (75). The

reference range for cardiac transplant was a 1-year graft survival of 83–89% (range reflecting stratification of high to low risk transplants in a study on the effect of case volume on outcome) (76). While there are several ongoing clinical trials for MSC transfer, explicit data for 1-year graft survival currently do not exist for this intervention (47, 54, 58, 59); therefore, the “hypothetical” condition of MSC transfer + T-cell eradication + calcineurin inhibition is considered a prediction pending the reporting from those trials.

RESULTS

Baseline Immune Response to Injury and Infection

In the absence of any perturbation, the cell levels and tissue integrity of the SOTABM were dynamically stable, as would be expected. The results of the parameter sweeps of initial perturbation demonstrated plausible behavior for both sterile tissue injury and infection. Simulated infection demonstrates an initial inflection point with respect to the transition from complete survival at initial infection = 50 (survival = 100%), with progressively worsening likelihood of survival at increments of 10 of initial infection until reaching a second point, beyond which there is always system death (initial infection = 110 with survival = 0%); see Figure 3. Similarly, with respect to sterile injury, the earlier

transition point from complete recovery (100% survival) was at initial injury = 90, with an upper transition into complete lethality (0% survival) at initial injury = 150 (see Figure 4).

Baseline Immune Response to Transplant

As expected, there were no simulation runs with transplant tissue survival at the end of 1 year simulated time; the average time to critical transplant tissue loss was 14.6 days of simulated time, with the longest transplant survival ~21 days. This is slightly greater than the recognized timeframe of 10–13 days for cell-mediated tissue graft rejection, but not vastly so (73).

Simulation of Immunosuppressive Therapies

These results are depicted in Figure 5. There were 100 replicates ($N = 100$) for all conditions, with the total simulated time represented by a simulation run = 1 year. The results of the simulated immunosuppressive therapies are as follows:

- Parsed modalities: T-cell eradication therapy alone = 37% graft survival (note no re-dosing for episodes of acute rejection); calcineurin inhibition alone = 60% graft survival; and MSC transfer alone = 40% graft survival (no re-dosing but immortal MSCs). As noted earlier, since corresponding clinical data does not exist for each of these therapeutic interventions in

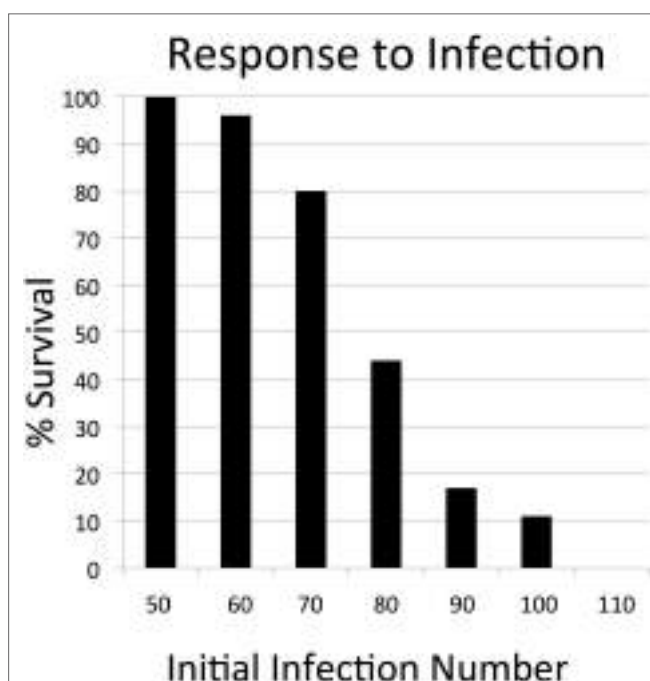


FIGURE 3 | Parameter sweep of the SOTABM for infection. This figure depicts the transition zone from 100% survival (below initial infection number = 50) toward 0% survival (above initial infection number = 110). These results demonstrate that the response of the SOTABM to infection is appropriately and plausibly bounded, meaning that there was an initial infection number below which the system always healed and an initial infection number above which the system always died. There were 100 replicates ($N = 100$) for each condition simulated, simulated time = 28 days.

These results demonstrate that the response of the SOTABM to infection is appropriately and plausibly bounded, meaning that there was an initial infection number below which the system always healed and an initial infection number above which the system always died. There were 100 replicates ($N = 100$) for each condition simulated, simulated time = 28 days.

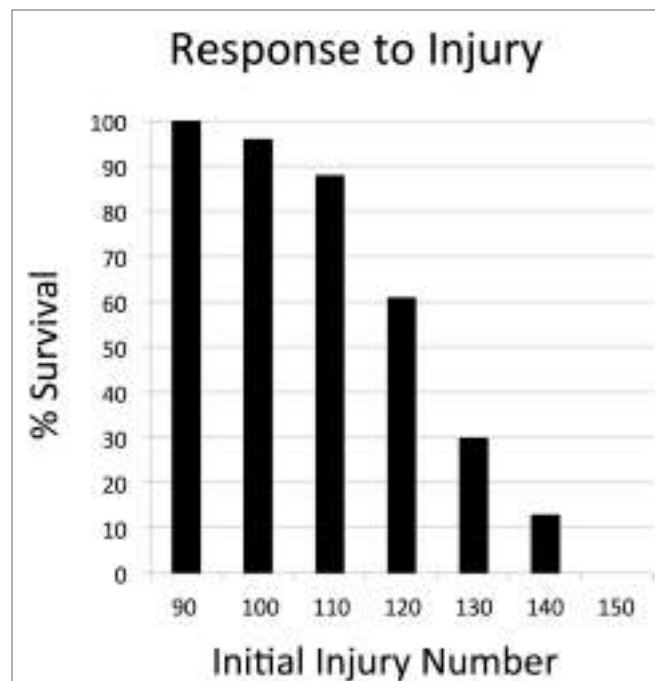


FIGURE 4 | Parameter sweep of the SOTABM for tissue injury. This figure depicts the transition zone from 100% survival (below initial injury number = 90) toward 0% survival (above initial injury number = 150). These results demonstrate that the response of the SOTABM to tissue trauma is appropriately and plausibly bounded. $N = 100$ for each condition simulated, simulated time = 28 days. The behaviors displayed in Figures 3 and 4 with respect to non-transplant conditions where inflammation and immune responses are recognized to occur serve as verification points for the SOTABM.

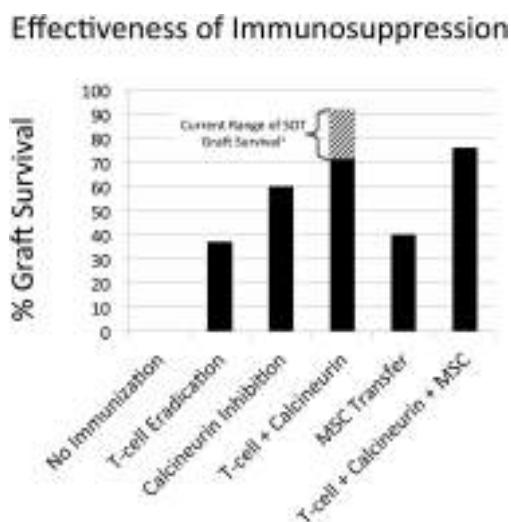


FIGURE 5 | Effectiveness of different immunosuppression simulations in the SOTABM. This figure depicts the results of first no immunosuppression, then the following simulated immunosuppressive therapies alone and in combination: T-cell eradication therapy alone = 37% graft survival (note no re-dosing for episodes of acute rejection); calcineurin inhibition = 60% graft survival; combination therapy of T-cell eradication with calcineurin inhibition = 72% graft survival; MSC transfer alone = 40% graft survival (no re-dosing but immortal MSCs); and T-cell eradication plus calcineurin inhibition plus MSC transfer = 76% graft survival. $N = 100$ for all conditions, total simulated time = 1 year. Note: ¹Aggregated solid organ transplant (SOT) 1-year graft survival range of 71–91% incorporating outcomes from renal, hepatic, and cardiac transplants (74–76).

isolation, the results of the SOTABM can only be evaluated in a highly qualitative fashion. Given this limitation, each modality plausibly has some beneficial effect on 1-year graft survival, but with a plausibly lower efficacy than combination therapy approximating current practice.

- Approximated current therapy: combination therapy of T-cell eradication with calcineurin inhibition = 72% graft survival; compare to a range of 1-year graft survival of 71–91% incorporating outcomes from renal, hepatic, and cardiac transplants (74–76). Simulation 1-year graft survival was lower than reported clinical rate. However, this can be explained by the fact that the current set of simulated immunosuppressive regimens did not allow for re-dosing of immunosuppression for episodes of acute rejection, as would be the case in the clinical situation.
- Hypothetical MSC transfer: T-cell eradication plus calcineurin inhibition plus MSC transfer = 76% graft survival. As noted earlier, there currently does not exist an appropriate data set for comparison. The slight increase in 1-year graft survival is plausible but must remain only a prediction from the SOTABM pending the reporting of the outcomes of the ongoing clinical trials.

DISCUSSION

The most fundamental goal of biomedical research is to develop the ability to effectively and beneficially control the trajectory

between health and disease; in short, the practice of medicine is a control problem. The ability to exercise control requires a putative mechanism by which the control can be exercised, and this in turn requires an understanding of the overall and aggregate structure in which the individual mechanisms reside. Furthermore, effective control does not necessarily require comprehensive knowledge of the system being controlled; what is required is a sufficiently detailed representation of the target system such that a control strategy can be developed and potentially tested. The use of selective abstraction is fundamental to the scientific process: it is universally utilized as a means of gaining insight, increasing the general applicability of acquired knowledge, and from a practical standpoint, identifying what constitutes actionable knowledge. Unfortunately, there is a general paucity of abstract thinking in biology; a situation with historical and cultural antecedents (41). Therefore, the current challenge that faces the biological (and biomedical) research communities is gaining the ability to facilitate abstract representations of mechanistic knowledge in order to best leverage the vast sets of data that are currently being generated. It has been proposed that dynamic computational models, and ABMs in particular, can aid in affecting this translational goal (22, 39).

The SOTABM is an initial step at developing an agent-based modeling framework to do this for transplant immunology, representing a highly abstracted model of the components and processes of the immune response, upon which various perturbations, including transplant, can be applied. The design philosophy of the SOTABM emphasizes its ability to represent a greater range of conditions (i.e., response to infection, tissue injury, and transplant challenge) rather than striving for “precision” with respect to replicating a specific disease process. This, in fact, is how biological systems function: they have an underlying set of functions that have been acted upon by evolution in a selection process that favors the ability to deal with heterogeneous, disparate, and potentially novel conditions. Without this ability to have conserved core functionality, evolution of biological systems could not occur. Therefore, this initial presentation of the SOTABM emphasizes the ability of the system to recover from a range of perturbations, rather than necessarily trying to create a highly detailed representation aimed specifically at simulating solid organ transplantation. As such, the SOTABM utilizes the minimally sufficient control structure that maps to the biological system while being able to produce the desired behavioral features. Once this iteration of the model is deemed sufficient, the next step is to identify features of the reference system that are not adequately represented; at this point, additional detail is added to the model. This is the iterative refinement process defined by Hunt et al. (6, 21) and represents a model design and development strategy that is consistent with the Popperian paradigm that science progresses via sequential falsification.

The current version of the SOTABM generally, plausibly, and qualitatively reproduces the inflammatory/immune system response to different types of perturbations while incorporating a set of minimally detailed components and primary features necessary in characterizing early adaptive immunity. The simulation experiments concerning the response of the SOTABM to infection and injury represent plausibility checks, particularly since the

cellular–molecular control structure represented in the SOTABM arose through evolution to meet these types of perturbations. Put a different way, a model that solely focuses on the response to transplant would have limited biological plausibility, since the evolutionary forces that led to the development of the control structure would not be accounted for. It is only in the context of a model that does produce plausible responses to evolutionarily relevant conditions that the behavior of the model in response to an “artificial” situation (i.e., SOT) can be reasonably assessed. The fact that even given its high degree of abstraction and biological incompleteness the SOTABM is able to generate qualitatively plausible responses to a range of perturbation points to a fundamental soundness of the knowledge representation incorporated into the model. However, there are clear limitations to the current version of the SOTABM, several of which are listed below:

- As a model created in Netlogo, the SOTABM inherits the limitations associated with that modeling environment, as would be the case with any computational model of virtually any form. The benefits of Netlogo are that it has a very low initial threshold for use, possessing an excellent tutorial and a robust library of example models; it allows a novice modeler to fairly rapidly engage in the model-creation process. However, this ease-of-use carries with it a set of hidden dangers, most prominently related to the fact one can readily fall into the trap that with increasing facility in the use of the tool one starts to think of their reference system in primarily terms of that tool, rather than as a subject in of itself. This is not an issue unique to NetLogo, rather it is a pervasive issue that not only affects computational modeling but also affects experimental research, where the tools for investigation begin taking precedence and coloring the interpretation of the reference system itself. The aphorism describing this phenomenon is: “To one with a hammer everything looks like a nail.” The solution this challenge is the use of cross platform validation, where the underlying conceptual model is implemented in a set of different, ideally unrelated modeling methods. Full discussion of this issue is beyond the scope of this paper, except to say that this is an issue that the modeling community struggles with, and where recognition of the challenge is currently the best, most prudent strategy.
- Moving on to specific limitations of the SOTABM within the context of its development environment, the lack of adjustment of therapeutic regimen to treat episodic acute rejection. In the clinical setting, there is considerable surveillance looking for signs of early rejection, and these episodes are addressed with temporary augmentation of the immunosuppressive regimen. The current cycle of simulation experiments do not reflect this practice.
- Lack of sufficient model detail with respect to the mechanisms of immunosuppression. While above we have made the argument concerning the benefits of abstraction, there is a definite point at which the failures of a particular abstraction level become evident. This may be most pronounced when dealing with putative mechanisms of control. In the case of simulated immunosuppression in the SOTABM, the abstractions made with respect to the life cycle of immune cells, and the various

stages of activation possibly resulted in a too-coarse graining of responses the system; in short the abstractions made enforced a more binary, and less nuanced, set of possible trajectories for the different cellular populations and their activation status.

- Solid organ transplant does not occur without tissue trauma from the initial surgery. In fact, there can be a huge variation in the amount of surgical trauma/resuscitation associated with a transplant, which in turn is due to a large amount of variance in the presurgical morbid state of the patient. These factors clearly influence the success of the overall transplant, but due to the inherent interactive complexity of this clinically relevant condition, it is essentially impossible to parse out how each of those factors might actually come into play for a particular individual. A suggestion for that process of parsing is the goal of this initial paper: by decomposing the different possible functional components of the overall transplant patient, the sets of conditions presented here should be thought of as semi-idealized, reductionist interpretations of the admittedly complex system dynamics. The process is analogous to the rationale for using simpler, reduced biological proxy experimental platforms to do research (cell cultures, tightly controlled animals, etc.), but with significant and critical differences. The first of these differences is the fact that computational models are transparent with respect to the mechanisms being evaluated: there are no “hidden variables” (i.e., biological components or functions). This means that ABMs will only do what is put into them, and therefore their failure to be made to generate a desired behavior is direct evidence of their insufficiency (thereby achieving the goal of falsification). The second difference is that their transparent, modular structure allows ABMs to be aggregated (perhaps “reverse parsed”) in a fashion that is not currently feasible in experimental biology. While there are several steps in this direction (i.e., linked “organs-on-a-chip”), the current translational step from *in vitro* to *in vivo* experimental platforms is opaque to a whole host of processes and interactions that cannot be identified or characterized.

Recognizing the costs of the abstractions and omissions made in the current version of the SOTABM provides a guide for the necessary refinements to be made in its next iterations. Importantly, the ability to modularly extend the SOTABM to more closely match the richness of the cellular subtypes and response capabilities in the early adaptive immune response is one of its key intended features. It is hoped that this initial implementation of the SOTABM will demonstrate its promise as a framework that can serve to integrate the continually evolving knowledge concerning transplant immunity and help fulfill the promise of dynamic knowledge representation as a means of addressing the Translational Dilemma.

ACKNOWLEDGMENTS

This work was supported in part by the NIH NIDDK P30DK42086 grant. This work was also supported by Grant NIH 1RO1-GM-115839-01.

REFERENCES

- Food and Drug Administration. *Innovation or Stagnation: Challenge and Opportunity on the Critical Path to New Medical Products*. Silver Spring, MD: Food and Drug Administration (2004). p. 1–38.
- An G. Closing the scientific loop: bridging correlation and causality in the petaflop age. *Sci Transl Med* (2010) **2**(41):41s34. doi:10.1126/scitranslmed.3000390
- An G, Mi Q, Dutta-Moscato J, Vodovotz Y. Agent-based models in translational systems biology. *Wiley Interdiscip Rev Syst Biol Med* (2009) **1**(2):159–71. doi:10.1002/wsbm.45
- Bankes SC. Agent-based modeling: a revolution? *Proc Natl Acad Sci U S A* (2002) **99**(Suppl 3):7199–200. doi:10.1073/pnas.072081299
- Bonabeau E. Agent-based modeling: methods and techniques for simulating human systems. *Proc Natl Acad Sci U S A* (2002) **99**(Suppl 3):7280–7. doi:10.1073/pnas.082080899
- Hunt CA, Ropella GE, Lam TN, Tang J, Kim SH, Engelberg JA, et al. At the biological modeling and simulation frontier. *Pharm Res* (2009) **26**(11):2369–400. doi:10.1007/s11095-009-9958-3
- Walker DC, Southgate J. The virtual cell – a candidate co-ordinator for ‘middle-out’ modeling of biological systems. *Brief Bioinform* (2009) **10**(4):450–61. doi:10.1093/bib/bbp010
- Zhang L, Athale CA, Deisboeck TS. Development of a three-dimensional multiscale agent-based tumor model: simulating gene-protein interaction profiles, cell phenotypes and multicellular patterns in brain cancer. *J Theor Biol* (2007) **244**(1):96–107. doi:10.1016/j.jtbi.2006.06.034
- Santoni D, Pedicini M, Castiglione F. Implementation of a regulatory gene network to simulate the TH1/2 differentiation in an agent-based model of hypersensitivity reactions. *Bioinformatics* (2008) **24**(11):1374–80. doi:10.1093/bioinformatics/btn135
- Fallahi-Sichani M, El-Kebir M, Marino S, Kirschner DE, Linderman JJ, et al. Multiscale computational modeling reveals a critical role for TNF-alpha receptor 1 dynamics in tuberculosis granuloma formation. *J Immunol* (2011) **186**(6):3472–83. doi:10.4049/jimmunol.1003299
- Hoehme S, Drasdo D. A cell-based simulation software for multi-cellular systems. *Bioinformatics* (2010) **26**(20):2641–2. doi:10.1093/bioinformatics/btq437
- Adra S, Sun T, MacNeil S, Holcombe M, Smallwood R. Development of a three dimensional multiscale computational model of the human epidermis. *PLoS One* (2010) **5**(1):e8511. doi:10.1371/journal.pone.0008511
- Christley S, Alber MS, Newman SA. Patterns of mesenchymal condensation in a multiscale, discrete stochastic model. *PLoS Comput Biol* (2007) **3**(4):e76. doi:10.1371/journal.pcbi.0030076
- Grimm V, Railsback SF. Pattern-oriented modelling: a ‘multi-scope’ for predictive systems ecology. *Philos Trans R Soc Lond B Biol Sci* (2012) **367**(1586):298–310. doi:10.1098/rstb.2011.0180
- Grimm V, Revilla E, Berger U, Jeltsch F, Mooij WM, Railsback SF, et al. Pattern-oriented modeling of agent-based complex systems: lessons from ecology. *Science* (2005) **310**(5750):987–91. doi:10.1126/science.1116681
- Macy M, Willer R. From factors to actors: computational sociology and agent-based modeling. *Annu Rev Sociol* (2002) **28**:143–66. doi:10.1146/annurev.soc.28.110601.141117
- Tesfatsion L. Agent-based computational economics: growing economies from the bottom up. *Artif Life* (2002) **8**(1):55–82. doi:10.1162/106454602753694765
- Parker J, Epstein J. A distributed platform for global-scale agent-based models of disease transmission. *ACM Trans Model Comput Simul* (2011) **22**(1):2. doi:10.1145/2043635.2043637
- An G. Agent-based computer simulation and sirs: building a bridge between basic science and clinical trials. *Shock* (2001) **16**(4):266–73. doi:10.1097/00024382-200116040-00006
- An G. In silico experiments of existing and hypothetical cytokine-directed clinical trials using agent-based modeling. *Crit Care Med* (2004) **32**(10):2050–60. doi:10.1097/01.CCM.0000139707.13729.7D
- Hunt CA, Ropella GE, Yan L, Hung DY, Roberts MS. Physiologically based synthetic models of hepatic disposition. *J Pharmacokinet Pharmacodyn* (2006) **33**(6):737–72. doi:10.1007/s10928-006-9031-3
- Deissenberg C, van der Hoog S, Dawid H. EURACE: a massively parallel agent-based model of the European economy. *Appl Math Comput* (2008) **204**(2):541–52. doi:10.1016/j.amc.2008.05.116
- Mansury Y, Diggory M, Deisboeck TS. Evolutionary game theory in an agent-based brain tumor model: exploring the ‘Genotype-Phenotype’ link. *J Theor Biol* (2006) **238**(1):146–56. doi:10.1016/j.jtbi.2005.05.027
- Engelberg JA, Ropella GE, Hunt CA. Essential operating principles for tumor spheroid growth. *BMC Syst Biol* (2008) **2**(1):110. doi:10.1186/1752-0509-2-110
- Deisboeck TS, Berens ME, Kansal AR, Torquato S, Stemmer-Rachamimov AO, Chiocca EA. Pattern of self-organization in tumour systems: complex growth dynamics in a novel brain tumour spheroid model. *Cell Prolif* (2001) **34**(2):115–34. doi:10.1046/j.1365-2184.2001.00202.x
- Chen S, Ganguli S, Hunt CA. An agent-based computational approach for representing aspects of in vitro multi-cellular tumor spheroid growth. *Conf Proc IEEE Eng Med Biol Soc* (2004) **1**:691–4. doi:10.1109/IEMBS.2004.1403252
- Thorne BC, Bailey A, Benedict K, Peirce-Cottler S. Modeling blood vessel growth and leukocyte extravasation in ischemic injury: an integrated agent-based and finite element analysis approach. *J Crit Care* (2006) **21**(4):346. doi:10.1016/j.jcrc.2006.10.007
- Tang J, Ley KE, Hunt CA. Dynamics of in silico leukocyte rolling, activation, and adhesion. *BMC Syst Biol* (2007) **1**:14. doi:10.1186/1752-0509-1-14
- Tang J, Hunt CA, Mellein J, Ley K. Simulating leukocyte-venule interactions – a novel agent-oriented approach. *Conf Proc IEEE Eng Med Biol Soc* (2004) **7**:4978–81. doi:10.1109/IEMBS.2004.1404376
- Bailey AM, Thorne BC, Peirce SM. Multi-cell agent-based simulation of the microvasculature to study the dynamics of circulating inflammatory cell trafficking. *Ann Biomed Eng* (2007) **35**(6):916–36. doi:10.1007/s10439-007-9266-1
- Bailey AM, Lawrence MB, Shang H, Katz AJ, Peirce SM. Agent-based model of therapeutic adipose-derived stromal cell trafficking during ischemia predicts ability to roll on P-selectin. *PLoS Comput Biol* (2009) **5**(2):e1000294. doi:10.1371/journal.pcbi.1000294
- Peer X, An G. Agent-based model of fecal microbial transplant effect on bile acid metabolism on suppressing *Clostridium difficile* infection: an example of agent-based modeling of intestinal bacterial infection. *J Pharmacokinet Pharmacodyn* (2014) **41**(5):493–507. doi:10.1007/s10928-014-9381-1
- Seal JB, Alverdy JC, Zaborina O, An G. Agent-based dynamic knowledge representation of *Pseudomonas aeruginosa* virulence activation in the stressed gut: towards characterizing host-pathogen interactions in gut-derived sepsis. *Theor Biol Med Model* (2011) **8**:33. doi:10.1186/1742-4682-8-33
- Wendelsdorf KV, Alam M, Bassaganya-Riera J, Bisset K, Eubank S, Hontecillas R, et al. ENteric Immunity SImlulator: a tool for in silico study of gastroenteric infections. *IEEE Trans Nanobioscience* (2012) **11**(3):273–88. doi:10.1109/TNB.2012.2211891
- Cockrell RC, Christley S, An G. Investigation of inflammation and tissue patterning in the gut using a spatially explicit general-purpose model of enteric tissue (SEGMEnT). *PLoS Comput Biol* (2014) **10**(3):e1003507. doi:10.1371/journal.pcbi.1003507
- Cockrell RC, Christley S, Chang E, An G. Towards anatomic scale agent-based modeling with a massively parallel spatially explicit general-purpose model of enteric tissue (SEGMEnT_HPC). *PLoS One* (2015) **10**(3):e0122192. doi:10.1371/journal.pone.0122192
- Mi Q, Rivière B, Clermont G, Steed DL, Vodovotz Y. Agent-based model of inflammation and wound healing: insights into diabetic foot ulcer pathology and the role of transforming growth factor-beta1. *Wound Repair Regen* (2007) **15**(5):671–82. doi:10.1111/j.1524-475X.2007.00271.x
- Walker DC, Hill G, Wood SM, Smallwood RH, Southgate J. Agent-based computational modeling of wounded epithelial cell monolayers. *IEEE Trans Nanobioscience* (2004) **3**(3):153–63. doi:10.1109/TNB.2004.833680
- An G. Dynamic knowledge representation using agent-based modeling: ontology instantiation and verification of conceptual models. *Methods Mol Biol* (2009) **500**:445–68. doi:10.1007/978-1-59745-525-1_15
- Kirschner DE, Chang ST, Riggs TW, Perry N, Linderman JJ. Toward a multiscale model of antigen presentation in immunity. *Immunol Rev* (2007) **216**:93–118. doi:10.1111/j.1600-065X.2007.00490.x

41. Vodovotz Y, An G. *Translational Systems Biology: Concepts and Practice for the Future of Biomedical Research*. Waltham, MA: Elsevier (2014). 178 p.
42. Balci O. Verification, validation and testing. In: Banks J, editor. *Handbook of Simulation: Principles, Methodology, Advances, Applications, and Practice*. New York, NY: John Wiley & Sons (1998). p. 335–96.
43. Balci O. A methodology for certification of modeling and simulation applications. *ACM Trans Model Comput Simul* (2001) **11**(4):352–77. doi:10.1145/508366.508369
44. Baldazzi V, Castiglione F, Bernaschi M. An enhanced agent based model of the immune system response. *Cell Immunol* (2006) **244**(2):77–9. doi:10.1016/j.cellimm.2006.12.006
45. Folcik VA, An GC, Orosz CG. The Basic Immune Simulator: an agent-based model to study the interactions between innate and adaptive immunity. *Theor Biol Med Model* (2007) **4**:39. doi:10.1186/1742-4682-4-39
46. Mata J, Cohn M. Cellular automata-based modeling program: synthetic immune system. *Immunol Rev* (2007) **216**:198–212. doi:10.1111/j.1600-065X.2007.00511.x
47. Wood KJ, Bushell A, Hester J. Regulatory immune cells in transplantation. *Nat Rev Immunol* (2012) **12**(6):417–30. doi:10.1038/nri3227
48. Wilensky U. NetLogo. *Center for Connected Learning and Computer-Based Modeling*. Evanston, IL: Northwestern University (1999).
49. Askar M. T helper subsets & regulatory T cells: rethinking the paradigm in the clinical context of solid organ transplantation. *Int J Immunogenet* (2014) **41**(3):185–94. doi:10.1111/iji.12106
50. Turner DL, Gordon CL, Farber DL. Tissue-resident T cells, in situ immunity and transplantation. *Immunol Rev* (2014) **258**(1):150–66. doi:10.1111/imr.12149
51. Rothstein DM, Camirand G. New insights into the mechanisms of Treg function. *Curr Opin Organ Transplant* (2015) **20**(4):376–84. doi:10.1097/MOT.0000000000000212
52. Spahn JH, Li W, Kreisel D. Innate immune cells in transplantation. *Curr Opin Organ Transplant* (2014) **19**(1):14–9. doi:10.1097/MOT.0000000000000041
53. Otterbein LE, Fan Z, Koulmanda M, Thronley T, Strom TB. Innate immunity for better or worse govern the allograft response. *Curr Opin Organ Transplant* (2015) **20**(1):8–12. doi:10.1097/MOT.0000000000000152
54. Cortinovis M, Casiraghi F, Remuzzi G, Perico N. Mesenchymal stromal cells to control donor-specific memory T cells in solid organ transplantation. *Curr Opin Organ Transplant* (2015) **20**(1):79–85. doi:10.1097/MOT.0000000000000145
55. Duffy MM, Ritter T, Ceredig R, Griffin MD. Mesenchymal stem cell effects on T-cell effector pathways. *Stem Cell Res Ther* (2011) **2**(4):34. doi:10.1186/scrt75
56. Cowan M, Chon WJ, Desai A, Andrews S, Bai Y, Veguilla V, et al. Impact of immunosuppression on recall immune responses to influenza vaccination in stable renal transplant recipients. *Transplantation* (2014) **97**(8):846–53. doi:10.1097/01.TP.0000438024.10375.2d
57. Chong AS, Alegre ML. The impact of infection and tissue damage in solid-organ transplantation. *Nat Rev Immunol* (2012) **12**(6):459–71. doi:10.1038/nri3215
58. Casiraghi F, Perico N, Remuzzi G. Mesenchymal stromal cells to promote solid organ transplantation tolerance. *Curr Opin Organ Transplant* (2013) **18**(1):51–8. doi:10.1097/MOT.0b013e32835c5016
59. Monguio-Tortajada M, Lauzurica-Valdemoros R, Borras FE. Tolerance in organ transplantation: from conventional immunosuppression to extracellular vesicles. *Front Immunol* (2014) **5**:416. doi:10.3389/fimmu.2014.00416
60. Mohty M. Mechanisms of action of antithymocyte globulin: T-cell depletion and beyond. *Leukemia* (2007) **21**(7):1387–94. doi:10.1038/sj.leu.2404683
61. Kwan T, Wu H, Chadban SJ. Macrophages in renal transplantation: roles and therapeutic implications. *Cell Immunol* (2014) **291**(1–2):58–64. doi:10.1016/j.cellimm.2014.05.009
62. Mannon RB. Macrophages: contributors to allograft dysfunction, repair, or innocent bystanders? *Curr Opin Organ Transplant* (2012) **17**(1):20–5. doi:10.1097/MOT.0b013e32834ee5b6
63. Morelli AE. Dendritic cells of myeloid lineage: the masterminds behind acute allograft rejection. *Curr Opin Organ Transplant* (2014) **19**(1):20–7. doi:10.1097/MOT.0000000000000039
64. Zhuang Q, Lakkis FG. Dendritic cells and innate immunity in kidney transplantation. *Kidney Int* (2015) **87**(4):712–8. doi:10.1038/ki.2014.430
65. Keating A. Mesenchymal stromal cells: new directions. *Cell Stem Cell* (2012) **10**(6):709–16. doi:10.1016/j.stem.2012.05.015
66. Xu G, Zhang L, Ren G, Yuan Z, Zhang Y, Zhao RC, et al. Immunosuppressive properties of cloned bone marrow mesenchymal stem cells. *Cell Res* (2007) **17**(3):240–8. doi:10.1038/cr.2007.4
67. da Silva Meirelles L, Chagastelles PC, Nardi NB. Mesenchymal stem cells reside in virtually all post-natal organs and tissues. *J Cell Sci* (2006) **119**(Pt 11):2204–13. doi:10.1242/jcs.02932
68. Prévile X, Flacher M, LeMauff B, Beauchard S, Davelu P, Tiollier J, et al. Mechanisms involved in antithymocyte globulin immunosuppressive activity in a nonhuman primate model. *Transplantation* (2001) **71**(3):460–8. doi:10.1097/00007890-200102150-00021
69. Herold KC, Lancki DW, Moldwin RL, Fitch FW. Immunosuppressive effects of cyclosporin A on cloned T cells. *J Immunol* (1986) **136**(4):1315–21.
70. Sadawa S, Suzuki G, Kawase Y, Takaku F. Novel Immunosuppressive agent, FK506: In vitro effects on the cloned T cell activation. *J Immunol* (1987) **139**(6):1797–803.
71. Tsuda K, Yamamoto K, Kitagawa H, Akeda T, Naka M, Niwa K, et al. Calcineurin inhibitors suppress cytokine production from memory T cells and differentiation of naive T cells into cytokine-producing mature T cells. *PLoS One* (2012) **7**(2):e31465. doi:10.1371/journal.pone.0031465
72. Koenen HJ, Michielsen EC, Verstappen J, Fasse E, Joosten I. Superior T-cell suppression by rapamycin and FK506 over rapamycin and cyclosporine A because of abrogated cytotoxic T-lymphocyte induction, impaired memory responses, and persistent apoptosis. *Transplantation* (2003) **75**(9):1581–90. doi:10.1097/01.TP.0000053752.87383.67
73. Janeway CA Jr, Travers P, Walport M, Schlomchik MJ, editors. Responses to alloantigens and transplant rejection. In: *Immunobiology: The Immune System in Health and Disease*. 5th edition. New York, NY: Garland Science (2001). Available from: <http://www.ncbi.nlm.nih.gov/books/NBK27163/>
74. Gondos A, Döhler B, Brenner H, Opelz G. Kidney graft survival in Europe and the United States: strikingly different long-term outcomes. *Transplantation* (2013) **95**(2):267–74. doi:10.1097/TP.0b013e3182708ea8
75. Mateo R, Cho Y, Singh G, Stapfer M, Donovan J, Kahn J, et al. Risk factors for graft survival after liver transplantation from donation after cardiac death donors: an analysis of OPTN/UNOS data. *Am J Transplant* (2006) **6**(4):791–6. doi:10.1111/j.1600-6143.2006.01243.x
76. Russo MJ, Iribarne A, Easterwood R, Ibrahimie AN, Davies R, Hong KN, et al. Post-heart transplant survival is inferior at low-volume centers across all risk strata. *Circulation* (2010) **122**(11 Suppl):S85–91. doi:10.1161/CIRCULATIONAHA.109.926659

Conflict of Interest Statement: The author declares that the research was conducted in the absence of any commercial or financial relationships that could be construed as a potential conflict of interest.

Copyright © 2015 An. This is an open-access article distributed under the terms of the Creative Commons Attribution License (CC BY). The use, distribution or reproduction in other forums is permitted, provided the original author(s) or licensor are credited and that the original publication in this journal is cited, in accordance with accepted academic practice. No use, distribution or reproduction is permitted which does not comply with these terms.



Combining Theoretical and Experimental Techniques to Study Murine Heart Transplant Rejection

Julia C. Arciero^{1*}, Andrew Maturo¹, Anirudh Arun², Byoung Chol Oh², Gerald Brandacher² and Giorgio Raimondi^{2*}

¹ Department of Mathematical Sciences, Indiana University-Purdue University Indianapolis, Indianapolis, IN, USA,

² Vascularized and Composite Allotransplantation Laboratory, Department of Plastic and Reconstructive Surgery, Johns Hopkins School of Medicine, Baltimore, MD, USA

OPEN ACCESS

Edited by:

Rene Duquesnoy,
University of Pittsburgh, USA

Reviewed by:

Eric Spierings,
Utrecht University, Netherlands
Judy Day,
University of Tennessee, USA

*Correspondence:

Julia C. Arciero
jarciero@iupui.edu;
Giorgio Raimondi
g.raimondi@jhmi.edu

Specialty section:

This article was submitted to
Alloimmunity and Transplantation,
a section of the
journal Frontiers in Immunology

Received: 02 May 2016

Accepted: 10 October 2016

Published: 07 November 2016

Citation:

Arciero JC, Maturo A, Arun A, Oh BC, Brandacher G and Raimondi G (2016)

Combining Theoretical and Experimental Techniques to Study Murine Heart Transplant Rejection.

Front. Immunol. 7:448.

doi: 10.3389/fimmu.2016.00448

The quality of life of organ transplant recipients is compromised by complications associated with life-long immunosuppression, such as hypertension, diabetes, opportunistic infections, and cancer. Moreover, the absence of established tolerance to the transplanted tissues causes limited long-term graft survival rates. Thus, there is a great medical need to understand the complex immune system interactions that lead to transplant rejection so that novel and effective strategies of intervention that redirect the system toward transplant acceptance (while preserving overall immune competence) can be identified. This study implements a systems biology approach in which an experimentally based mathematical model is used to predict how alterations in the immune response influence the rejection of mouse heart transplants. Five stages of conventional mouse heart transplantation are modeled using a system of 13 ordinary differential equations that tracks populations of both innate and adaptive immunity as well as proxies for pro- and anti-inflammatory factors within the graft and a representative draining lymph node. The model correctly reproduces known experimental outcomes, such as indefinite survival of the graft in the absence of CD4⁺ T cells and quick rejection in the absence of CD8⁺ T cells. The model predicts that decreasing the translocation rate of effector cells from the lymph node to the graft delays transplant rejection. Increasing the starting number of quiescent regulatory T cells in the model yields a significant but somewhat limited protective effect on graft survival. Surprisingly, the model shows that a delayed appearance of alloreactive T cells has an impact on graft survival that does not correlate linearly with the time delay. This computational model represents one of the first comprehensive approaches toward simulating the many interacting components of the immune system. Despite some limitations, the model provides important suggestions of experimental investigations that could improve the understanding of rejection. Overall, the systems biology approach used here is a first step in predicting treatments and interventions that can induce transplant tolerance while preserving the capacity of the immune system to protect against legitimate pathogens.

Keywords: mathematical model, transplant, rejection, immune response, antigen-presenting cells, T cells, cytokines

Abbreviations: APCs, antigen-presenting cells; POD, post-operative day; Treg, regulatory T cells.

INTRODUCTION

Organ transplantation is a life-saving surgical procedure through which the functionality of a failing organ can be restored via replacement with a functioning one. Transplants are performed for a wide variety of organs, including skin, heart, kidney, liver, pancreas, spleen, and lung (1). However, without the administration of immunosuppressive drugs, the recipient's immune system recognizes the transplanted tissue as a foreign and potentially dangerous material and responds with a massive immune attack that ultimately destroys the graft. This immune response represents a major roadblock in the development of effective therapeutic regimens for the care of patients requiring organ transplants. Current therapeutic regimens rely on chronic immunosuppression. However, the quality of life of transplant recipients is compromised by complications that derive from life-long immunosuppression (such as hypertension, diabetes, opportunistic infections, and cancer) and by the limited long-term graft survival rates due to the absence of established immune tolerance to the transplanted tissues. Ultimately, 20% or more of transplanted patients die by 5 years post-transplant. Thus, there is a pressing need for a new investigative approach to understand the systemic effects that arise from the dynamic interactions between components of the immune system and transplanted tissues.

Previous hypothesis-driven research has provided important insight into the complex interactions among the multiple components of the immune system, including T cells, antigen-presenting cells (APCs), and cytokines (2–10). Such studies have helped to determine the critical players and processes in transplant rejection. For example, the rationale for "costimulation blockade" therapies stems from such studies. These therapies, which target a key step of lymphocyte activation, aim to control T cell activation and promote transplant survival. They have been shown to be a potent strategy for promoting long-term acceptance of transplants in rodents (11–15) and primates (16–18). However, their clinical translation encountered serious difficulties, and ultimately costimulation blockade therapies were only approved as maintenance therapies (19) since they could not promote tolerance (20). To date, the only clinically successful avenue of transplant tolerance induction has been through protocols that induce hematopoietic chimerism (21, 22) (the coexistence of donor and recipient hematopoietic cells) via donor bone marrow co-transplantation with the organ to be transferred. This procedure requires heavy conditioning of patients and carries a significant risk of immunological complications (e.g., the development of graft versus host disease). Consequently, this approach is applicable only in a very restricted cohort of patients in need of a transplant. Thus, a valid and widely applicable strategy to alter the reactivity of the immune system of transplant recipients in a robust and reliable way is still needed.

Biological studies of rejection face various challenges. Experimental *in vivo* models of immune rejection can elucidate precise information regarding select immune cell dynamics and the production and distribution of cytokines. However, conclusions about the system as a whole and the generalizability of these conclusions to other species or types of allografts are further complicated by factors such as procedural variability between

models of rejection and variability in parameter measurements. These factors, in combination with the complexity of the immune response, motivate the use of an integrated theoretical and experimental approach to unravel the inter-connected components of the immune response that contribute to transplant rejection. A mathematical model of allograft rejection, refined by multiple clinical and experimental observations, can help to identify variables and parameters that play a significant role in immune system dynamics and yield a better understanding of the complex mechanisms of transplant rejection.

Several computational models have been implemented to predict the dynamics of the immune system in response to viral or bacterial infections (23–26), although only a few theoretical studies have addressed transplant rejection. A recent publication used agent-based modeling (ABM) to investigate solid organ transplant rejection (27). In their study, the model provides an abstract representation of the innate and adaptive immune components involved in the acute rejection process of a solid organ transplant. The study does not use experimentally based parameter values, but it gives a range of possible responses to a transplant challenge without replicating a specific disease process. Another recent study (28) used ordinary differential equations to model the impact of the initial inflammatory response to a surgical insult on overall graft damage. These studies have addressed general transplant immunology questions and have studied a very specific aspect of the initiation of the transplant rejection response, but they do not offer the capacity to capture the important intricacies of the rejection response in a combined experimental and theoretical system that could lead to useful predictions to design new experimentations. The mathematical model presented in the current study aims to provide useful theoretical predictions of transplant rejection based on biologically relevant parameter values, initial conditions, and cellular interactions.

The objectives of this study are (i) to develop a theoretical model to predict the effect of the immune response dynamics on the rejection of a murine heart transplant based on experimental measurements, and (ii) to identify new and effective strategies to promote transplant acceptance that could be investigated experimentally. The model is composed of a system of ordinary differential equations describing the cellular dynamics in the lymph node and graft in the context of a simulated acute rejection of murine heart allograft. The model equations and parameters are based on previous immune system models and are designed to incorporate key assumptions and experimental observations of the immune response to murine heart transplants. The model captures the known behavior of mouse heart rejection and recapitulates the effect of previously reported experimental manipulations. It also underscores the relative importance of the ratios of effector versus regulatory T cells (Tregs) on the speed of graft rejection. Importantly, the model predicts a previously unappreciated behavior when altering the timing of T cell exposure to the graft, providing details for the design of new experimentations that could confirm or refute these findings. Ultimately, we believe this model could become an innovative tool to improve our understanding of transplant rejection and significantly aid in the design of new and effective strategies of immune intervention.

MATERIALS AND METHODS

Model Development

In this study, a mathematical model of murine heart transplants is developed to investigate the interactions between the host immune system and transplanted graft. A compartmental model is used in which all interactions are assumed to occur in either the graft or the draining lymph node. A separate compartment for blood is not included, but the rates of exit and entry of the various cells into the graft or lymph node are assumed to account for transit time in the blood. **Table 1** provides the definition and description of all the variables tracked by this model. As with any model, some assumptions and simplifications are necessary to address a specific question using quantitative techniques.

The following list provides a summary of the assumptions made in this study:

- *Antigen-presenting cells*: a single population of APCs is defined in the model and includes the populations of dendritic cells, macrophages, and B cells; no distinction is made between the origin of the APCs (donor or recipient);
- *Antigen presentation*: direct, indirect, and semi-direct antigen presentation pathways are grouped into a single function;
- *Rejection mechanisms*: only cell-mediated mechanisms of graft cell destruction (by effector T cells and inflammatory APCs) are included since the absence of B cells and associated antibody production in mouse heart transplant models (obtained via genetic manipulation or depletion strategies) does not extend graft survival (29);
- *Lymphoid tissue*: the activation of the immune response is restricted to an ideal lymph node that drains the graft. The contribution of the response by multiple lymphoid tissues is accounted for by amplifying the translocation rate of activated T cells from a single lymph node to the graft;
- *Naïve T cells*: the population of graft-reactive T cells is considered to be homogeneously naïve. No contribution of memory T cells is considered at this stage. A continuous output of newly generated T cells (from the thymus) is assumed to maintain a constant number of naïve T cells in the lymph node. Of the total T cell population, 5% are considered to be alloreactive (30);

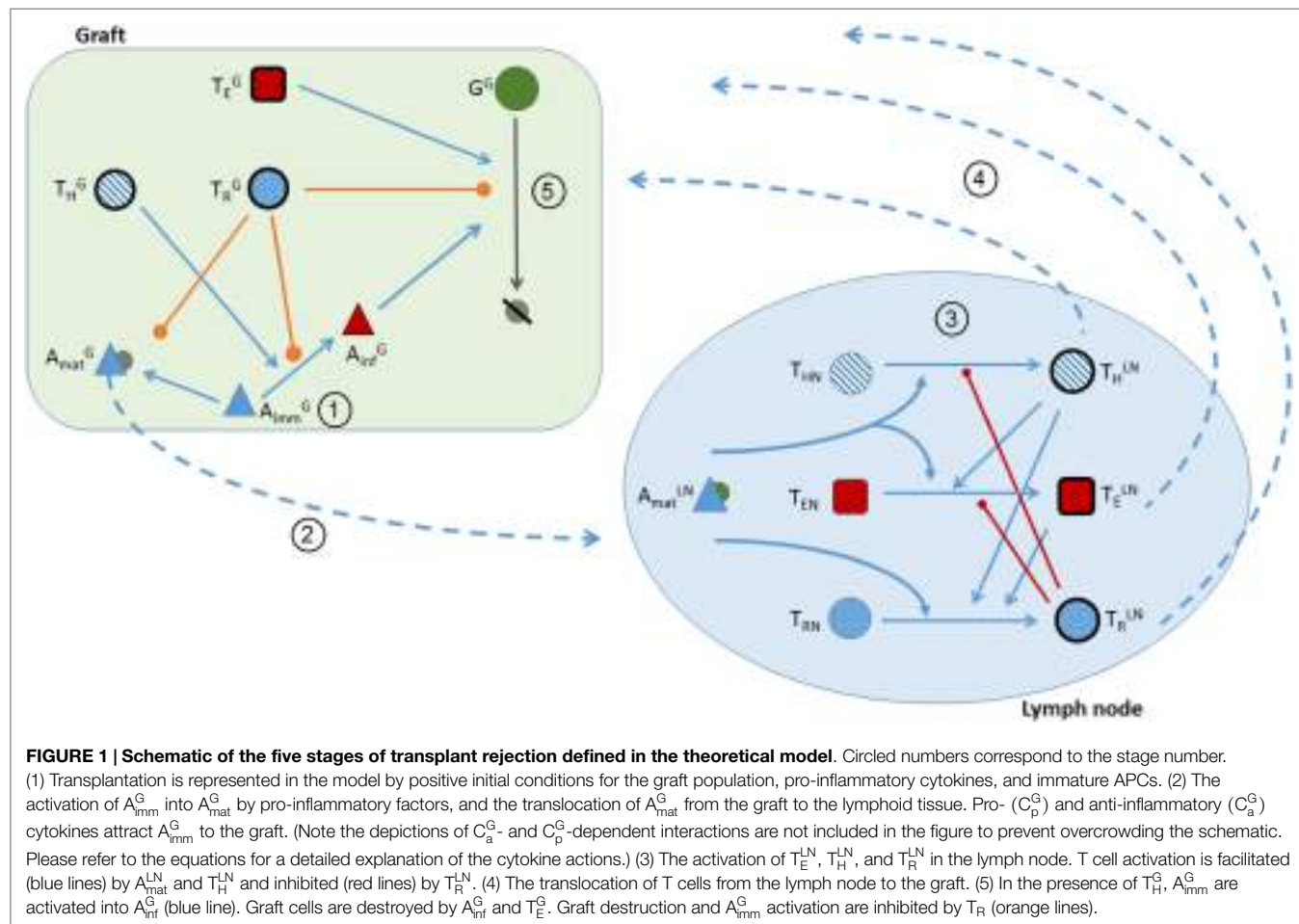
TABLE 1 | Description of model variables.

Variable	Description	Location
A_{mat}^{LN}	Mature antigen-presenting cells	Lymph node
T_E^{LN}	Activated effector T cells	
T_R^{LN}	Activated regulatory T cells	
T_H^{LN}	Activated helper T cells	
A_{mat}^G	Mature antigen-presenting cells	Graft
A_{imm}^G	Immature antigen-presenting cells	
A_{inf}^G	Inflammatory antigen-presenting cells	
T_E^G	Activated effector T cells	
T_R^G	Activated regulatory T cells	
T_H^G	Activated helper T cells	
G^G	Graft cells	
C_p^G	Pro-inflammatory cytokine	
C_a^G	Anti-inflammatory cytokine	

- *Inflammatory response*: the danger signals generated by the surgical procedure of transplantation (e.g., surgical trauma, ischemia/reperfusion injury, and potential exposure to bacterial and viral components) (31) and the ensuing release of inflammatory cytokines (i.e., IL-6, IL-18, TNF, IP-10, IL-1) by graft tissues and innate immune components are simplified and represented in a single population (C_p^G). No contribution to the rejection response by concomitant protective immune responses (anti-pathogens) is assumed. Moreover, as no specific quantification of each of inflammatory factors is currently available in the literature, their functions and behavior are represented with a single model variable. C_p^G has both inflammatory and chemotactic functions, and its behavior is initially modeled based on the production and accumulation of IL-6, the most representative inflammatory cytokine in transplantation as previously reported (32, 33);
- *Anti-inflammatory response*: the anti-inflammatory cytokines (i.e., IL-10, TGF-β, IL-35, pro-resolving mediators) normally produced by graft tissues and cells of the immune system as compensatory mechanisms to the inflammatory response initiated by the transplant and by the rejection response are all included in a single population (C_a^G). As per C_p^G , there is no transplant-specific quantification available for these factors and C_a^G is mainly modeled on the behavior reported for IL-10 in the regulation of immune responses (34–36).
- *Graft cells turnover*: the growth of heart cells is considered negligible in the model based on reported data (37).

With these assumptions, the dynamics between the immune system and the graft are described in the following five stages (and are depicted in **Figure 1**):

1. *Transplantation*: transplantation (introduction of the graft) occurs at day 0 and is captured by the model using the following initial conditions (listed in **Table 2**) for the graft population (G^G), pro-inflammatory cytokines (C_p^G), and immature APCs (A_{imm}^G): $G^G(0) = 5,600,000$ cells (38, 39), $C_p^G(0) = 50$ pg/ml (32, 33), and $A_{imm}^G = 2,000$ cells (40, 41). $G^G(0)$ was chosen by extrapolating the number of cells in a mouse heart based on the average mass of a mouse heart and the average cell density of a human heart. Pro-inflammatory cytokines are assumed to be present at time 0 since transplantation is associated with surgical trauma and exposure to bacterial and viral agents. Additionally, during the procedure, the reconnection to the recipient circulation initiates the process of ischemia/reperfusion injury, causing rapid accumulation of inflammatory mediators (31, 42, 43). Although there is a general agreement on the presence of inflammatory elements at time 0, the overall amount is not known and, thus, an arbitrary value is chosen here. This value reflects the kinetics of mRNA expression and plasma accumulation of IL-6 – a key “danger signal” in the activation of the immune system in transplantation – that have been described previously (32, 33). The presence of these inflammatory cytokines leads to a rapid influx of host immature APCs into the graft (representing the influx of circulating monocytes rapidly converting in the tissues into APCs).

**TABLE 2 | Initial values for model variables.**

Variable	Initial value	Unit
$A_{\text{mat}}^{\text{LN}}$	0	cells
T_E^{LN}	0	cells
T_R^{LN}	0	cells
T_H^{LN}	0	cells
A_{mat}^G	200	cells
A_{imm}^G	2,000	cells
A_{inf}^G	0	cells
T_E^G	0	cells
T_R^G	0	cells
T_H^G	0	cells
G^G	5.6e6	cells
C_p^G	50	pg/ml
C_a^G	0	pg/ml

2. APC maturation and presentation of donor antigens in the lymph node: once exposed to C_p^G , immature APCs are activated into mature APCs in the graft (A_{mat}^G). The maturation of APCs contributes to an increased accumulation of pro-inflammatory factors as well as, in a delayed fashion, to the production of anti-inflammatory factors (C_a^G) (34–36). Once mature, APCs exit the graft and travel to the draining lymphoid tissue.

3. Activation of T cells in the lymph node: in the theoretical model of the lymph node, naïve CD8⁺ effector T cells (T_E^{LN}), naïve Tregs (T_R^{LN}), and naïve CD4⁺ helper T cells (T_H^{LN}) that have the capacity to recognize donor antigens are assumed to be present initially at background levels of 55,000, 9,500, and 70,000 cells, respectively. Upon entering the lymph node, $A_{\text{mat}}^{\text{LN}}$ facilitate the activation of T cells (6, 10). As shown in Figure 1, $A_{\text{mat}}^{\text{LN}}$ are necessary to promote the activation of naïve CD8⁺ (T_E^{LN}), CD4⁺ (T_H^{LN}), and regulatory (T_R^{LN}) T cells in the lymph node. CD8⁺ T cell activation is dependent on the licensing of interacting APCs by activated CD4⁺ T cells. Once activated, Tregs inhibit the activation of CD8⁺ and CD4⁺ T cells. T cell proliferation in the lymph node depends on the autocrine and paracrine effects of growth factors (e.g., IL-2). Tregs are unable to produce and secrete these growth factors and, thus, their proliferation is delayed and dependent on the presence of activated CD4⁺ and CD8⁺ T cells (44).

4. T cell infiltration of the graft: following their activation, T_E^{LN} , T_H^{LN} , and T_R^{LN} exit the lymph node and search for the inflamed tissues of the graft. It is important to note that not all T cells exiting the lymph node will locate the graft. Also, though T cells originate from multiple lymph nodes, only one lymph node is explicitly depicted and described in the model for simplicity. The translocation rate parameters e_E , e_H , and e_R in Eqs 8–10 are multiplied by a factor k that accounts for the contribution

of these two phenomena to the number of cells entering the graft. Specifically, the parameter k is interpreted as the product of the percent of T cells that reach the graft and the number of lymph nodes (and spleen) from which T cells originate.

5. *Destruction of the graft:* in the graft, T_H^G promote the conversion of A_{imm}^G into inflammatory APCs (A_{inf}^G); this represents the activation of macrophages into inflammatory cells that release cytotoxic agents (e.g., reactive oxygen species) that induce death of surrounding graft cells. This process is inhibited by T_R^G (45, 46). The release of pro-inflammatory cytokines is promoted in the presence of A_{mat}^G , T_E^G , T_H^G , and A_{inf}^G . The release of C_a^G is assumed to depend on A_{mat}^G , T_R^G , C_p^G , G^G , and A_{inf}^G (47). The presence of C_a^G inhibits the conversion of A_{imm}^G into A_{mat}^G or A_{inf}^G . A_{inf}^G and T_E^G direct the destruction of the graft, while T_R^G inhibit graft destruction.

Model Equations

The interactions described in the five stages are modeled using a system of 13 ordinary differential equations that tracks cell populations and cytokine concentrations within the graft and lymph node. Many of the parameter values are taken directly from literature sources, some were obtained experimentally, and the remaining are estimated according to experimental assumptions and observations. The initial values of all model variables are given in Table 2. The model parameter values, units, and references are listed in Table 3.

The model equations describe the activation, proliferation, natural decay, destruction, and inhibition of the various populations when appropriate. The interactions in the lymph node are modeled using four equations, and the interactions in the graft are modeled using nine equations. The superscripts LN and G denote cell populations in the lymph node and graft, respectively.

In Eq. 1, the rate of change of mature APCs in the lymph node (A_{mat}^{LN}) is defined. This rate depends on the entrance of mature APCs from the graft at rate e_A (first term) and on the natural decay of A_{mat}^{LN} in the lymph node (second term).

$$\frac{dA_{mat}^{LN}}{dt} = e_A A_{mat}^G - \mu_A A_{mat}^{LN} \quad (1)$$

The naïve alloreactive T cell populations (T_{EN} , T_{RN} , and T_{HN}) in the lymph node are assumed to be constant since a background population of these cells is always present (due to thymopoiesis).

In Eq. 2, the rate of change in CD8⁺ T cells in the lymph node is shown to depend on T cell activation (term 1), decay (term 2), proliferation (term 3), and translocation (term 4). The activation of T_E^{LN} depends on the presence of both A_{mat}^{LN} and T_H^{LN} , while T_R^{LN} inhibit this process (10, 46, 51). Proliferation of the T_E^{LN} cells depends on A_{mat}^{LN} and T_E^{LN} and occurs at rate r_E (used as a proxy for the production, secretion, and autocrine effect of IL-2) (52). The translocation of T_E^{LN} from the lymph node is assumed to occur at rate e_E .

$$\begin{aligned} \frac{dT_E^{LN}}{dt} = & \frac{a_E T_{EN} A_{mat}^{LN} T_H^{LN}}{(\gamma_1 + A_{mat}^{LN})(\alpha_1 + T_R^{LN})} - \mu_E T_E^{LN} \\ & + \frac{r_E T_E^{LN} A_{mat}^{LN}}{\beta_1 + A_{mat}^{LN}} - e_E T_E^{LN} \end{aligned} \quad (2)$$

TABLE 3 | Names, values, units, and citations for all model parameters.

Equation	Parameter name	Value	Unit	Source
1	e_A	5.5	1/day	(24)
1	μ_A	1.2	1/day	(48)
2	T_{EN}	55,000	cells	Section "Experimental Data Collection"
2	a_E	3	1/day	(25)
2	γ_1	100	cells	(25)
2	α_1	2,500	cells	Estimated
2	μ_E	0.7	1/day	(25)
2	r_E	1.51	1/day	(25)
2	β_1	5,000	cells	Estimated
2	e_E	0.001	1/day	(24)
3	T_{RN}	9,500	cells	Section "Experimental Data Collection"
3	a_R	2.82e-4	1/day	Optimized
3	γ_2	1,000	cells	Estimated
3	μ_R	0.7	1/day	(24, 49)
3	r_R	0.02	1/day	Estimated
3	α_2	9,500	cells	Estimated
3	e_R	0.001	1/day	(24)
4	T_{HN}	70,000	cells	Section "Experimental Data Collection"
4	a_H	6,018.9	cells/day	Optimized
4	γ_3	100	cells	(25)
4	α_3	2,500	cells	Estimated
4	μ_H	0.4	1/day	(24, 25)
4	r_H	1.51	1/day	(25, 50)
4	γ_4	4,000	cells	(25)
4	e_H	0.001	1/day	(24)
5	a_{p1}	1,500	cells/day(pg/ml)	Optimized
5	η_1	10	pg/ml	Estimated
5	α_4	12,000	cells	Estimated
6	k_{C_P}	0.005	1/day/(pg/ml)	Optimized
6	μ_{Aimm}	60	1/day	Optimized
6	a_{p2}	3,844	1/day	Optimized
6	η_2	10	pg/ml	Estimated
6	α_5	12,000	cells	Estimated
7	μ_{Ainf}	1.2	1/day	(48)
8	k	15	–	Estimated
8	r_{EG}	0.3	1/day	Optimized
8	η_3	10	pg/ml	Estimated
8	β_2	4e6	cells	Estimated
9	r_{RG}	0.00375	1/day	Optimized
9	α_6	12,000	cells	Estimated
10	r_{HG}	0.755	1/day	Estimated
10	γ_5	4,000	cells	Estimated
10	η_4	10	pg/ml	Estimated
11	d_{inf}	0.055	1/day	Optimized
11	α_7	12,000	cells	Estimated
11	d_E	0.004	cells/day	Optimized
11	α_8	12,000	cells	Estimated
12	p_1	10.98	(pg/ml)/day	Optimized
12	α_9	12,000	cells	Estimated
12	p_2	0.024	(pg/ml)/day	Estimated
12	α_{10}	12,000	cells	Estimated
12	p_3	0.24	(pg/ml)/day	Estimated
12	α_{11}	12,000	cells	Estimated
12	p_4	10.95	(pg/ml)/day	Optimized
12	α_{12}	12,000	cells	Estimated
12	μ_{C_P}	0.15	1/day	Optimized
13	ξ_1	2.08e-4	(pg/ml)/cells/day	Estimated
13	ξ_2	6.3e-6	(pg/ml)/cells/day	Estimated
13	ξ_3	4.2e-9	1/cells/day	Estimated
13	ξ_4	2.5e-4	(pg/ml)/cells/day	Estimated
13	μ_{C_a}	0.05	1/day	Estimated

The rates of change of Tregs in the lymph node (Eq. 3) and CD4⁺ T cells in the lymph node (Eq. 4) contain the same four terms (activation, decay, proliferation, and exit) as the equation for CD8⁺ T cells, with a few important differences: the activation of T_R^{LN} and T_H^{LN} depends only on A_{mat}^{LN}, and the proliferation of T_R^{LN} occurs only in the presence of T_E^{LN} or T_H^{LN}. The activation of T_H^{LN} is inhibited by T_R^{LN} (10, 45).

$$\frac{dT_R^{LN}}{dt} = \frac{a_R T_{RN} A_{mat}^{LN}}{\gamma_2 + A_{mat}^{LN}} - \mu_R T_R^{LN} + \frac{r_R T_R^{LN} (T_E^{LN} + T_H^{LN})}{\alpha_2 + T_R^{LN}} - e_R T_R^{LN} \quad (3)$$

$$\begin{aligned} \frac{dT_H^{LN}}{dt} &= \frac{a_H T_{HN} A_{mat}^{LN}}{(\gamma_3 + A_{mat}^{LN})(\alpha_3 + T_R^{LN})} - \mu_H T_H^{LN} \\ &+ \frac{r_H T_H^{LN} A_{mat}^{LN}}{\gamma_4 + A_{mat}^{LN}} - e_H T_H^{LN} \end{aligned} \quad (4)$$

The rate of change of the A_{imm}^G population in the graft is defined in Eq. 5. The first term represents the influx of A_{imm}^G due to the presence of the graft and pro-inflammatory cytokines. The second term accounts for the natural decay of A_{imm}^G. The third term indicates the loss of immature APCs once they become activated into A_{mat}^G. The fourth term defines the T_H^G-mediated activation of A_{imm}^G into A_{inf}^G. In both of these last two terms, the conversion of A_{imm}^G into activated populations is inhibited by C_a^G and T_R^G (35, 47, 51, 53, 54). The functional form describing the inhibition by C_a^G is chosen to emphasize that the rate is a decreasing sigmoidal function of C_a^G.

$$\begin{aligned} \frac{dA_{imm}^G}{dt} &= k_{C_p} C_p^G G^G - \mu_{Aimm} A_{imm}^G - a_{p1} \left(1 - \frac{(C_a^G)^2}{\eta_1^2 + (C_a^G)^2} \right) \\ &\times \left(\frac{A_{imm}^G C_p^G}{\alpha_4 + T_R^G} \right) - a_{p2} \left(1 - \frac{(C_a^G)^2}{\eta_2^2 + (C_a^G)^2} \right) \left(\frac{A_{imm}^G T_H^G}{\alpha_5 + T_R^G} \right) \end{aligned} \quad (5)$$

Equation 6 describes the dynamics of mature APCs in the graft (A_{mat}^G). The first term defines the activation of A_{mat}^G by C_p^G, which is inhibited by C_a^G and T_R^G (35, 47, 51, 53, 54). The second term is the natural decay of A_{mat}^G, and the last term accounts for the exit of A_{mat}^G from the graft to the lymph node.

$$\frac{dA_{mat}^G}{dt} = a_{p1} \left(1 - \frac{(C_a^G)^2}{\eta_1^2 + (C_a^G)^2} \right) \left(\frac{A_{imm}^G C_p^G}{\alpha_4 + T_R^G} \right) - \mu_A A_{mat}^G - e_A A_{mat}^G \quad (6)$$

In Eq. 7, inflammatory APCs are differentiated from A_{imm}^G in the presence of T_H^G and inhibited by C_a^G and T_R^G (term 1) (35, 47, 51, 53, 54) and are assumed to exhibit natural decay (term 2).

$$\frac{dA_{inf}^G}{dt} = a_{p2} \left(1 - \frac{(C_a^G)^2}{\eta_2^2 + (C_a^G)^2} \right) \left(\frac{A_{imm}^G T_H^G}{\alpha_5 + T_R^G} \right) - \mu_{Ainf} A_{inf}^G \quad (7)$$

The rates of change for CD8⁺, regulatory, and CD4⁺ T cells in the graft (Eqs 8, 9, and 10, respectively) depend on the rate at

which they enter the graft (term 1), their natural decay (term 2), and their proliferation (term 3). The proliferation of T_E^G and T_H^G is inhibited by C_a^G (36). The parameter k that multiplies the exit rate of T cells from the lymph node accounts for the fact that not all T cells exiting the lymph node reach the graft and that T cells arrive from multiple lymph nodes. The value for k is obtained from the product of the percent of T cells that reach the graft and the number of lymph nodes from which T cells originate.

$$\frac{dT_E^G}{dt} = k e_E T_E^{LN} - \mu_E T_E^G + r_{EG} \left(1 - \frac{(C_a^G)^2}{\eta_3^2 + (C_a^G)^2} \right) \frac{T_E^G G^G}{\beta_2 + G^G} \quad (8)$$

$$\frac{dT_H^G}{dt} = k e_H T_H^{LN} - \mu_H T_H^G + \frac{r_{HG} T_R^G (T_E^G + T_H^G)}{\alpha_6 + T_R^G} \quad (9)$$

$$\frac{dT_R^G}{dt} = k e_R T_R^{LN} - \mu_R T_R^G + r_{RG} \left(1 - \frac{(C_a^G)^2}{\eta_4^2 + (C_a^G)^2} \right) \frac{T_R^G A_{mat}^G}{\gamma_5 + A_{mat}^G} \quad (10)$$

Equation 11 describes the dynamics of the mass of the graft. The first and second terms represent the destruction of the graft due to A_{inf}^G and T_E^G, respectively. T_R^G work to inhibit the destruction of the graft through mechanisms that differ from the ones used in the lymph node. It is recognized that in non-lymphoid tissues, T_R^G do not inhibit the accumulation, nor the proliferation, of A_{imm}^G, T_E^G, and T_H^G. Instead, they prevent damage via inhibition of the destructive activities of A_{inf}^G and T_E^G (in addition to preventing the conversion of A_{imm}^G into A_{inf}^G and A_{mat}^G, depicted in Eqs. 6 and 7) (54–56). No growth of graft cells is assumed in this model as stated in our model assumptions.

$$\frac{dG^G}{dt} = - \frac{d_{inf} A_{inf}^G G^G}{(\alpha_7 + T_R^G)} - \frac{d_E T_E^G G^G}{(\alpha_8 + T_R^G)} \quad (11)$$

As defined in Eq. 12, the release of pro-inflammatory cytokines is triggered by the conversion of A_{imm}^G into A_{mat}^G and A_{inf}^G (terms 1 and 4) as well as by the execution of effector functions by both T_E^G and T_H^G recognizing their target (10) (terms 2 and 3). The release of C_p^G by each of these cells is inhibited by T_R^G (46, 54). The natural decay of C_p^G is modeled in the last term.

$$\frac{dC_p^G}{dt} = \frac{\rho_1 A_{mat}^G}{\alpha_9 + T_R^G} + \frac{\rho_2 T_E^G}{\alpha_{10} + T_R^G} + \frac{\rho_3 T_H^G}{\alpha_{11} + T_R^G} + \frac{\rho_4 A_{inf}^G}{\alpha_{12} + T_R^G} - \mu_{C_p} C_p^G \quad (12)$$

Equation 13 describes the release of C_a^G due to the conversion of A_{imm}^G into A_{mat}^G and A_{inf}^G – a regulatory pathway embedded in the process of activation to prevent uncontrolled reactivity (35) – and due to activity of T_R^G (46) that infiltrate the graft (terms 1, 4, and 2, respectively). Upon encountering pro-inflammatory cytokines, the graft tissue also produces anti-inflammatory mediators (term 3). The last term gives the natural decay of C_a^G. Since the four populations leading to the production of C_a^G are already inhibited in the presence of C_a^G, additional inhibition is not included in any of the terms.

$$\frac{dC_a^G}{dt} = \xi_1 A_{mat}^G + \xi_2 T_R^G + \xi_3 C_p^G G^G + \xi_4 A_{inf}^G - \mu_{C_a} C_a^G \quad (13)$$

Experimental Data Collection

Male 8- to 10-week-old Balb/C (H-2^d), and C57BL/6 (B6; H-2^b) mice were purchased from the Jackson Laboratory (Bar Harbor, ME, USA) and housed in specific pathogen-free facilities at Johns Hopkins University, Baltimore, MD, USA. All experiments were conducted according to Institutional Animal Care and Use Committee-approved protocols.

Heterotopic (intra-abdominal) heart transplantation was performed from BALB/c to B6 mice, as previously described (57). On day 7 post-transplantation, cells from grafts were isolated using an adaptation of the technique described by Setoguchi et al. (58). Briefly, tissues were digested at 37°C via 3 consecutive 15-min incubations in PBS containing Collagenase IV (560 U/ml; Worthington) DNase I (275 U/ml; Amresco), and Dispase II (0.4 U/ml; Roche). Leukocytes were enriched using a 24% Histodenz (Sigma-Aldrich)-based gradient separation. These preparations were then used to quantify the content of CD4⁺, CD8⁺, and Tregs in the rejecting hearts via flow cytometry. Cells were stained using anti-CD4⁺ and anti-CD8⁺ mAb (from BD Bioscience) and anti-Foxp3 mAb (Affymetrix/eBioscience) according to the manufacturer protocols; samples were acquired using a BD LSR-II flow cytometer. Data were analyzed via FlowJo analysis software (FlowJo, LLC).

Table 4 summarizes the absolute counts and relative ratios of T cell subsets infiltrating a rejecting heart on post-operative day (POD) 7 deriving from such analysis. From these data, the biological variability observed between animals in the total number of each subset that infiltrate the heart is clearly evident. Strikingly, however, the ratios among T cell subsets were maintained within very narrow ranges. Consequently, we used the average number of T cells to set the scale for the number of T cells in the model, and we optimized various model parameters to the observed ratios of T cells.

A similar approach was used to determine the average number of each T cell subset in a typical lymph node. Our data agree with a previously published data set (3). Briefly, collection of 16 lymph nodes from multiple animals averaged the identification of 17e6 CD8⁺ T cells, 22e6 CD4⁺ T cells, and 3e6 Treg. This renders 1.1e6 CD8⁺ T cells, 1.4e6 CD4⁺ T cells, and 0.19e6 Treg in the average lymph node. Considering that ~5% of T cells are reactive against donor antigens, the average lymph nodes contains (at time 0) 55,000 CD8⁺ T cells, 70,000 CD4⁺ T cells, and 9,500 Treg.

Parameter Estimation

The model contains 61 parameters. Many of the values of these parameters have been obtained directly from experimental studies

TABLE 4 | Absolute counts and relative ratios of T cell subsets infiltrating a rejecting murine heart on POD 7.

	CD8	CD4	CD8/CD4 ratio	Treg	Treg (% of CD4)
Heart #1	2.7e6	5.4e5	5	7.4e4	13.6
Heart #2	4.3e5	8.3e4	5.3	1.2e4	14.9
Heart #3	6.5e5	1.8e5	3.7	2.5e4	14.1
Average	1.27e6	2.7e5	4.7	3.7e4	14.2
SE	6e5	1.2e5	0.4	1.5e4	0.3

(1–6, 8–10, 26, 32, 33, 46, 47, 50–52, 57, 59–68) or other mathematical models of the immune system (3, 23–26, 48, 69–74). **Table 3** provides a list of all the model parameter values and sources for their values when possible. A definition of “estimated” in **Table 3** indicates that the value was not found directly in the literature but was estimated according to known relationships and ratios among cell populations in the model. For example, due to the potency and cellular similarities of Tregs and helper T cells, the activation rate of T_R^{LN} is assumed to be smaller than the activation rate of T_H^{LN} (46). As another example, the death rate of A_{inf}^G is assumed to equal the death rate of A_{mat}^G . The constant values for T_{EN} and T_{HN} are obtained from experiments conducted in the present study (**Table 4**). According to reported ratios (26, 46, 57), the T_{RN} population should be chosen to be about one-tenth of the helper T cell initial populations.

Several remaining model parameters are optimized (and are defined as “optimized” in **Table 3**) to satisfy the following experimental observations:

- (1) *Presence of all T cells*
 - a. *APC conditions* (40, 41)
 - i. A_{mat}^G have a peak population of ~18,000 cells.
 - ii. A_{imm}^G have a peak population of ~12,000 cells.
 - iii. A_{mat}^G and A_{imm}^G peak between days 1 and 3.
 - b. *Graft destruction* (66)
 - i. A 75% reduction of the graft mass occurs by 12–14 days following transplantation.
 - c. *T cell ratios* (**Table 4** and see Experimental Data Collection)
 - i. The maximum T_E^G value is approximately five times greater than the maximum T_H^G value (ratio of average $T_E^G:T_H^G$ values is 4.7, **Table 4**).
 - ii. The maximum T_H^G value is approximately seven times greater than the maximum T_R^G value (ratio of average $T_H^G:T_R^G$ values is 7.29, **Table 4**).
 - iii. The maximum number of T_E^{LN} occurs at ~4 days post-transplantation.
 - iv. The maximum number of T_E^G occurs at ~6 days post-transplantation.
- (2) *Absence of helper T cells* (7, 64)
 - No graft rejection.
- (3) *Absence of effector T cells* (7, 64)
 - Rejection should be delayed slightly.
- (4) *Absence of all T cells* (40, 41)
 - a. No damage to the graft.
 - b. APC measures:
 - i. Immature APCs: 23000, 12000, 2100, and 2000 cells on days 1, 3, 5, and 10.
 - ii. Mature APCs: 17000, 12000, 2400, 3000 on days 1, 3, 5, and 10.

RESULTS

Model Verification

The following four model simulations were used to confirm that the model results indeed reflect the assumptions on which the model was built in terms of expected physiological behavior.

Timing of Graft Rejection

In the absence of any external manipulation (i.e., administration of immunosuppressive drugs or any immunomodulatory intervention), experimental murine cardiac transplants are rejected at ~12–14 days after transplantation. Tanaka et al. (66) performed *in vivo* visualization of murine cardiac allograft rejection and identified the cessation of the heartbeat to occur on day 12, which corresponded to a 75% reduction in the measured luminescence of donor tissue from transgenic luciferase-GFP (green fluorescent protein)-modified mice. The present model

uses this as an approximate metric, defining graft rejection once the number of graft cells has decreased by 75% of their initial number. **Figure 2A** shows the time dynamics of graft rejection predicted by the model. The behavior of other key populations including APCs in the graft, T cells in the lymph node, T cells in the graft, and cytokines in the graft are shown in **Figures 2B–F**. The number of T cells in the lymph node peaks around days 6–7 in the lymph node and days 7–9 in the graft, which agrees with experimental observations (70). The ratios of $T_E^G:T_H^G$ and $T_H^G:T_R^G$ at their peaks are calculated to be 4.7 and 7.29, respectively, in the

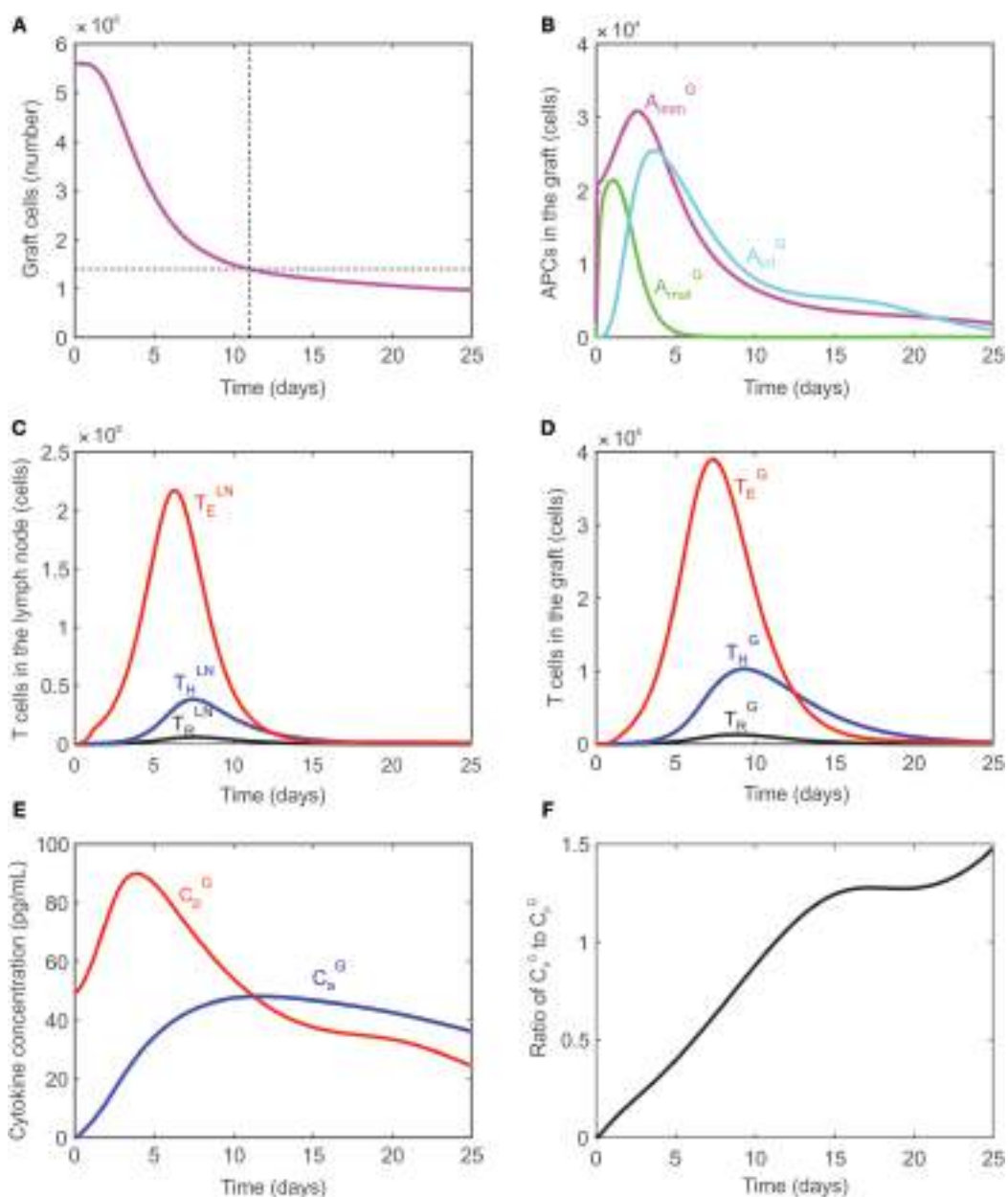


FIGURE 2 | (A) Graft rejection is predicted to occur ~11 days following transplantation. **(B)** Model predicted values of immature APCs (A_{imm}^G , magenta), mature APCs (A_{mat}^G , green), and inflammatory APCs (A_{inf}^G , cyan) in the graft. **(C)** Model predicted values of regulatory T cells (black), CD4⁺ T cells (blue), CD8⁺ T cells (red) in the lymph node. **(D)** Model predicted values of regulatory T cells (black), CD4⁺ T cells (blue), CD8⁺ T cells (red) in the graft. **(E)** Model predicted concentration of pro-inflammatory cytokines (C_p^G , red) and anti-inflammatory cytokines (C_a^G , blue) in the graft. **(F)** Ratio of $C_a^G:C_p^G$ in the graft.

graft, which are consistent with experimental values obtained in this study (**Table 4**).

Graft Rejection in the Absence of CD8⁺ T Cells (T_E)

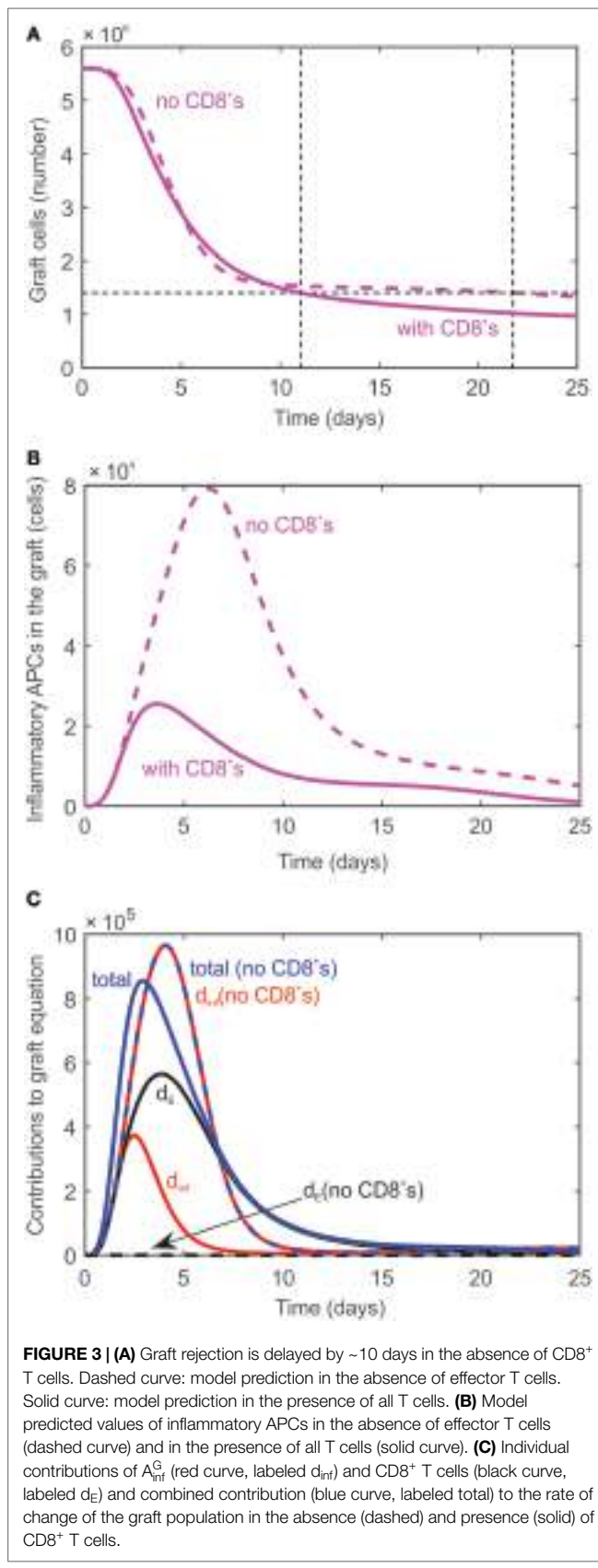
As demonstrated experimentally (7), transplant rejection can occur even if no CD8⁺ cells are present in the system; the time to rejection is just slightly delayed. The absence of CD8⁺ cells is simulated in the model by modifying the initial value of naïve effector T cells to be T_{EN} = 0. As a result, no effector T cells are generated in the lymph node, but graft rejection is predicted to occur at day 22 (dashed curve, **Figure 3A**) instead of day 11 when all T cells are present (solid curve, **Figure 3A**). Rejection is predicted to occur despite the absence of CD8⁺ T cells since activated CD4⁺ T cells in the graft promote the differentiation of inflammatory APCs (**Figure 3B**) which cause graft destruction. **Figure 3C** serves to explain why the graft is not destroyed sooner when no CD8⁺ T cells are present given that A_{inf}^G is much higher in their absence (**Figure 3B**). When all T cells are present, the graft is destroyed by both A_{inf}^G and CD8⁺ T cells (terms 1 and 2 in Eq. 11, respectively). The contribution of each of these terms to the rate of change of the graft population is plotted in **Figure 3C** (solid curves). Specifically, the contribution of the A_{inf}^G term (labeled d_{inf}) is shown in red, the contribution of the CD8⁺ T cells when they are present (labeled d_E) is shown in black, and the sum of these contributions (labeled total) is shown in blue. The dashed curves correspond to these same cases when CD8⁺ T cells are absent. Note that in this case the contribution of A_{inf}^G (dashed red curve) and the sum of the contributions (dashed blue curve) lie on top of each other since the contribution of the CD8⁺ T cells is zero (black dashed curve). As can be seen in **Figure 3C**, the contribution of A_{inf}^G when CD8⁺ T cells are absent exceeds the total solid blue curve until a time point between days 5 and 10 when the blue solid curve exceeds the dashed blue curve. This explains the steep decline in graft population initially in the absence of T cells followed by a slower decay than when all T cells are present.

Graft Acceptance in the Absence of All T Cells

As discussed in Ref. (10, 75), animals with no T cells (i.e., no CD4⁺ T cells, no CD8⁺ T cells, and no Tregs) are incapable of rejecting transplants. To simulate conditions of no T cells in the model, the naïve T cell populations are set to 0: T_{EN} = T_{RN} = T_{HN} = 0. As a result, no T cells are generated in the lymph node or graft. Although A_{mat}^G are activated, the absence of T cells or A_{inf}^G prevents any damage to the graft (**Figure 4A**), which survives indefinitely. The APC dynamics in the graft under these conditions are compared with data reported by Oberbarnscheidt et al. (40) in **Figure 4B**. It shows a fairly accurate description of the trend of A_{mat}^G with, however, an overestimation of the accumulation of A_{imm}^G, a result that we attribute to the model assumptions employed (see Model Limitations). The levels of the pro- and anti-inflammatory cytokines are shown in **Figure 4C**.

Graft Acceptance in the Absence of T_H

Several studies (7, 52, 64) have demonstrated that the presence of CD4⁺ T cells is a necessary and sufficient condition for rejection.



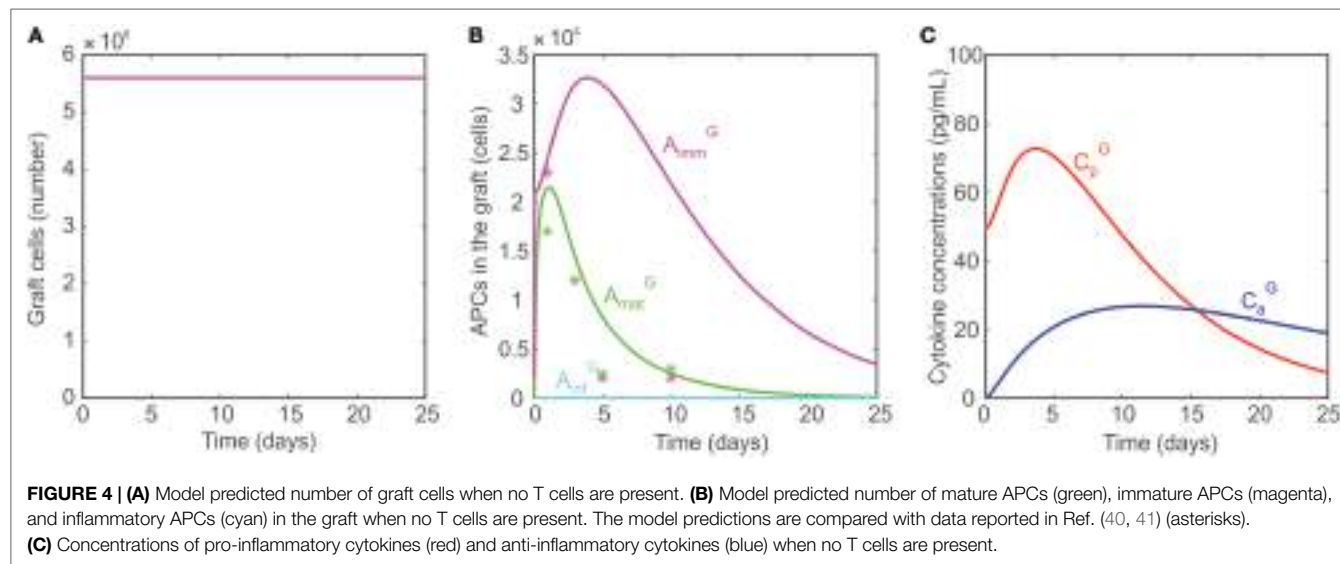


FIGURE 4 | (A) Model predicted number of graft cells when no T cells are present. **(B)** Model predicted number of mature APCs (green), immature APCs (magenta), and inflammatory APCs (cyan) in the graft when no T cells are present. The model predictions are compared with data reported in Ref. (40, 41) (asterisks). **(C)** Concentrations of pro-inflammatory cytokines (red) and anti-inflammatory cytokines (blue) when no T cells are present.

In accordance with this, the model reproduces the finding that in the absence of CD4⁺ T cells in the lymph node ($T_{HN} = 0$), the graft is accepted since no damage-inducing cells are activated without the contribution of CD4⁺ T cells.

Model Simulations

The model is used to assess the effect of altering the number of naïve Tregs (adoptive transfer), altering the translocation rate of T cells from the lymph node to the graft, and performing a transient peri-transplant depletion of T cells. Insight from simulation-generated hypotheses may have eventual implications for designing improved therapeutic strategies that promote tolerance of transplants.

Adoptive Transfer of Regulatory T Cells

Adoptive transfer is a technique by which T cells are obtained from an animal, stimulated in a polyclonal or antigen-specific fashion, and grown in culture. The cells are then transferred back into the original animal or into a separate animal with the overall goal of expanding the frequency of those T cells. Ultimately, this procedure can be exploited to increase or decrease the reactivity of the immune system. Adoptive transfer has been employed using Treg, aiming to counter graft destruction, and is currently under active investigation for its clinical translation (67, 76). The size, frequency, and type of these transfers can vary greatly depending on the system and overall treatment goal. Here, a single injection of naïve Tregs into the lymph node immediately prior to transplantation is simulated by varying T_{RN} from 9,500 cells to 3e8 cells. **Figure 5** shows that the graft survival time increases non-linearly with the injection dose. However, fairly rapid transplant rejection is still observed, as expected (67). The model reproduces previous observations that indicate the simple increase of T_{RN} would have a very limited impact on transplant survival unless combined with ideal complementary strategies, such as immunosuppression (in a form that does not affect Treg activity, but only effector T cells) and pre-activation of the injected Tregs (to effectively reduce the levels of the other T cells so that a large ratio of T_R to T cells is maintained).

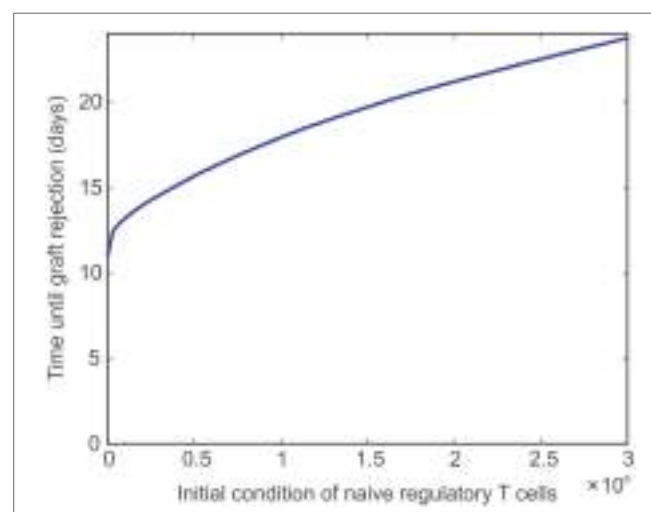


FIGURE 5 | Impact of naïve Treg adoptive transfer on graft survival.

Model predicted values of time until transplant rejection as the initial (and constant) level of naïve regulatory T cells is varied between 9,500 and 3e8 cells.

Translocation Rates

The ease with which T cells can travel between the lymph node and the graft is expected to influence the destruction of the graft. For example, decreasing the rate (e_E) at which T_E cells translocate from the lymph node to the graft should extend the survival of the graft, though not indefinitely. **Figure 6** depicts the effect of e_E alone on graft survival time (i.e., e_E is varied while the other translocation rates are held constant $e_H = e_R = 0.001 \text{ day}^{-1}$, magenta curve) or in combination with the translocation rate of CD4⁺ cells (i.e., e_E and e_H are varied and assumed equal to each other while $e_R = 0.001 \text{ day}^{-1}$, blue curve) or with the translocation rate of Tregs (i.e., e_E and e_H and e_R are all varied and assumed equal to each other, black curve). Under normal model conditions, $e_E = e_H = e_R = 0.001 \text{ day}^{-1}$. If e_E is increased, the graft survival time is decreased from baseline. If both e_E and e_H are increased, the graft survival time is even more decreased.

However, if e_E , e_H , and e_R are increased, the survival time is longer because more Tregs are present to inhibit the effects of the CD8⁺ and CD4⁺ T cells. The logic is reversed to the left of $e_E = 0.001 \text{ day}^{-1}$.

Delayed Injection of T Cells

In **Figure 7**, the model is used to simulate the effect of introducing T cells into a system that originally has no T cells for a fixed number of days [simulations for 10 (red), 20 (blue), 30 (black), 40 (magenta), and 50 (green) days are shown]. These simulations were used to assess the ability of the model to reproduce the outcome of published experiments in which T cells were introduced

into a lymphopenic animal 50 days after heart transplantation. The rationale for this test was that the healing process would make the graft incapable of initiating the rejection response. The reported results, however, refuted that hypothesis and showed a complete rejection initiated even when T cells were introduced 50 days after transplant (2). The model presented in the current study fails to predict this outcome, but provides valuable insight into the behavior of the system modeled. For example, the red curve in **Figure 7A** shows that the model predicts graft acceptance when no T cells are present and graft destruction once T cells are introduced starting at day 10. As indicated by the additional curves in **Figure 7A**, the steady state population of graft cells (e.g., the population of graft cells after 200 days) does not change monotonically with the number of days till lymphocyte injection. That is, the steady-state number of graft cells is higher if T cells are injected at 20 days instead of 10 days, but lower if T cells are injected at 40 days instead of 10 days. This unexpected behavior is summarized in **Figure 7B**, which shows the population of graft cells at 200 days as a function of the day at which T cells are injected. This graph clearly shows the non-monotonic relationship between these values.

DISCUSSION

In this study, a mathematical model of transplant rejection that encompasses both innate and adaptive elements of the immune response is presented. The model is based on combining experimentally observed ratios of different types of T cells in the lymph node and graft as well as the time at which their numbers are maximum together with defined characteristics of the immune response that have been reported in the literature (2–10, 26, 46, 47, 50, 51, 57, 60, 64, 66, 67, 75, 77). Our efforts in the development of this transplant rejection model were driven by its ultimate application as a tool to provide a better understanding of the complex dynamics that underlie the rejection response and to provide a novel and powerful perspective to predict new methods for preventing graft rejection. Three hypothetical immune interventions are explored in this study: modulation of the frequency of naïve Tregs, alteration of the migration of T cells to the graft, and

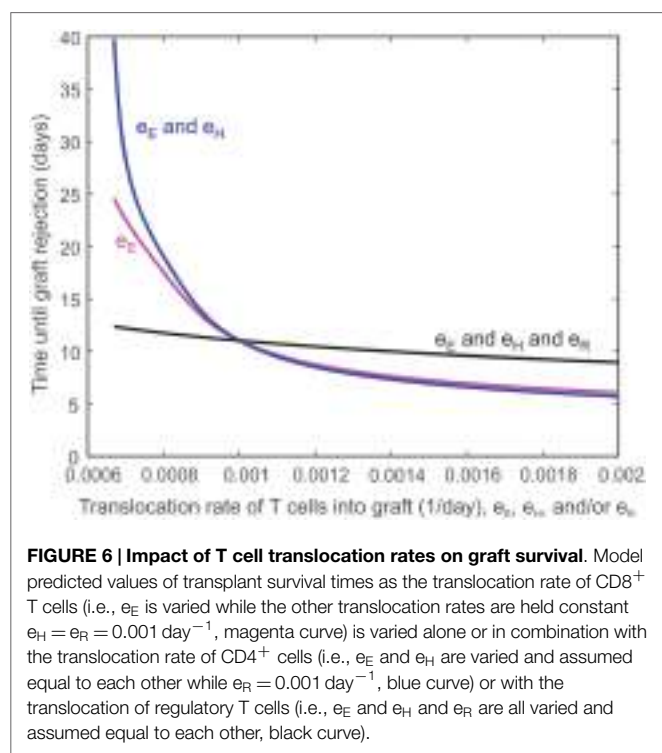
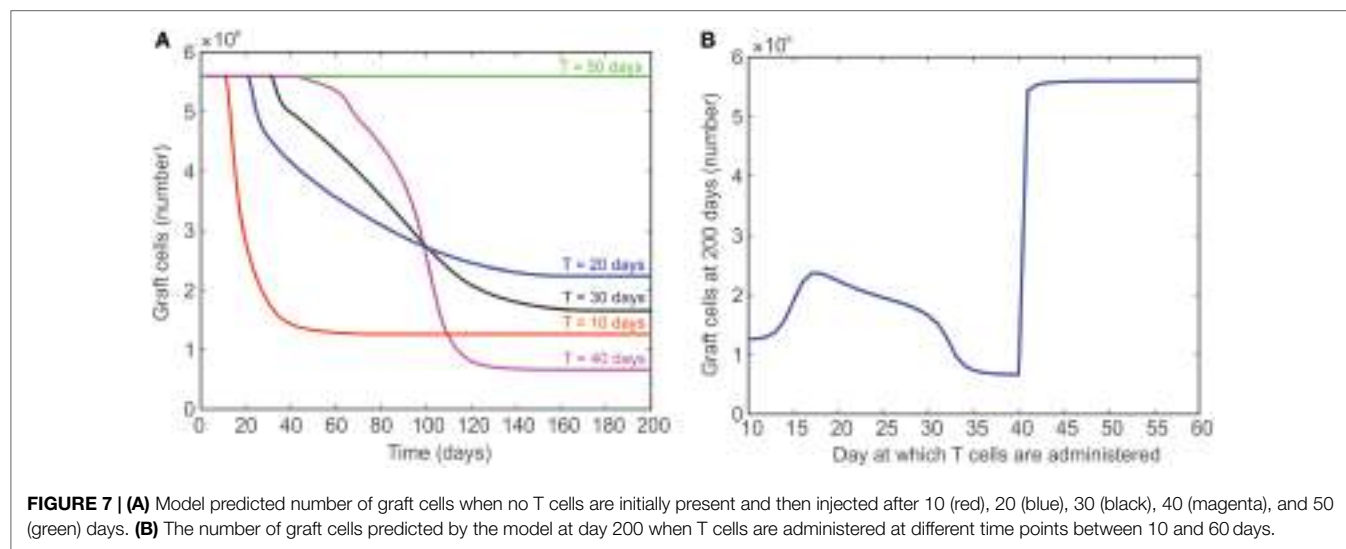


FIGURE 6 | Impact of T cell translocation rates on graft survival. Model predicted values of transplant survival times as the translocation rate of CD8⁺ T cells (i.e., e_E) is varied while the other translocation rates are held constant $e_H = e_R = 0.001 \text{ day}^{-1}$, magenta curve) is varied alone or in combination with the translocation rate of CD4⁺ cells (i.e., e_E and e_H are varied and assumed equal to each other while $e_R = 0.001 \text{ day}^{-1}$, blue curve) or with the translocation of regulatory T cells (i.e., e_E and e_H and e_R are all varied and assumed equal to each other, black curve).



transient depletion of the T cell pool. First, we considered a simple experiment of adoptive transfer of naïve Tregs simulating conditions where the starting number of resting Tregs in the lymph node was altered. Our model indicates that a higher number of Tregs causes an increase in the time to allograft rejection (**Figure 5**). As expected, however, the impact on graft protection is modest and requires what would be a non-physiological augmentation of Treg numbers to achieve a therapeutic effect. As indicated below, this model is well suited to investigate which combination of strategies could maximize the impact of Treg adoptive transfer (67). For example, although indirectly, the model simulations already suggest a powerful effect of activated Treg migrating to the graft (see comments on third simulation below). While this paper only considers a simple example, the ultimate goal of adoptive transfer is to maintain a high level of Tregs so that they accumulate in both the lymph node and the graft (46, 47, 57, 67). Achieving the greatest possible ratio of Treg to other T cells would yield the maximum inhibitory effect on the activation of T_E^G , T_H^G , C_p^G , A_{mat}^G , and A_{inf}^G , and, as a result, provide a significant protection to the graft.

Second, as shown in **Figure 6**, reducing the translocation rate of T_E^{LN} has a non-linear effect on graft destruction. For example, a 50% decrease in e_E yields an 82% increase in graft survival time, while a 50% increase in e_E decreases the graft survival time by 34%. Decreasing both the translocation rate of T_E^{LN} and the translocation rate of T_H^{LN} causes an even more pronounced increase in graft survival time. This protective effect is not only due to a more limited damage inflicted directly by a reduced number of translocating T cells but is also due to the powerful suppressive effect of Tregs that localize to the graft. In fact, the concomitant reduction of e_R with e_E and e_H shows a much more limited prolongation of graft survival. This behavior helps to explain why the inhibition of T_E^{LN} translocation to the graft has a more beneficial effect than their complete absence (**Figure 3**). This is probably due to the contribution of T_E^{LN} to the expansion of Tregs in the lymph node that would then more efficiently control the remaining immune response, a situation that would not occur in the absence of T_E^{LN} . Thus, the manipulation of activated T cell migration could have a more profound therapeutic effect than the prevention of their activation or their deletion, as long as the migration of activated Tregs is not concomitantly affected. Such complex dynamics could contribute to understanding the disparate therapeutic effects observed when targeting specific chemokine receptors (78, 79). Alternatively, this result highlights the importance of using activated Tregs rather than resting ones for adoptive transfer strategies.

Third, the theoretically predicted non-linear and non-monotonic relationship between graft survival and the delayed appearance of alloreactive T cells suggests that new experiments to confirm such a relationship are needed to determine if the results suggest a new method for promoting graft survival. The model prediction is in discordance with the experimental observation that the re-introduction of T cells 50 days post-transplant causes a prompt rejection response (2). This underscores the need to adapt the theoretical model to incorporate other important mechanisms that would contribute to such an outcome. At the same time, this discrepancy indicates that the basic principles implemented

in our model are not sufficient to explain the intricate behavior of the immune system and suggest that additional scenarios need to be investigated experimentally. We can speculate two plausible scenarios: (a) the accumulation of pro-inflammatory mediators follows a longer kinetic that supports delayed activation (though not observed experimentally), or (b) the phenomenon of lymphopenia-induced proliferation of T cells (observed when T cells are transferred into a lymphopenic mouse) causes the non-specific activation of T cells that can travel directly to the graft and initiate the rejection response (80). The experimental validation of these possible hypotheses would strengthen the understanding of the non-linear and non-monotonic behavior predicted in this scenario by our model. For example, the model prediction of graft rejection when T cells are administered at 40 days versus the model prediction of near graft acceptance when T cells are administered at 42 days warrants additional investigation. This improved understanding would be essential in determining the extent to which the transient elimination of T cells would be more effective and, possibly, what combinatorial intervention strategy would maximize this effect.

Model Limitations

Some of the choices and assumptions made in this study limit the capabilities of the model. First, the model focuses on the interactions of T cells, APCs, and inflammatory cytokines, but does not include small-scale details, such as cell signaling or the secretion of various factors. Additionally, cytokines are grouped into two categories (pro- and anti-inflammatory signals) and are tracked only in the graft, not in the lymph node. Considering the vast number of individual cytokine molecules involved in a full immune response as well as their independent dynamics, the relative strength of their effects on the overall immune system (as well as independent effects on individual cell types), and their unique production and decay rates, a model that accounts for each cytokine molecule individually will rapidly become complicated and cumbersome. But, studies show that the overall balance of these signals and their specific varieties can significantly impact graft outcome (4, 6, 33, 47). Effects of pro- and anti-inflammatory cytokines are assumed to be included in parameters such as r_E , r_R , and r_H . The tradeoff of specificity for simplicity allows the model to reproduce general behavior.

Some of the diversity and antigen-specificity of the various cell populations are generally neglected in the model. B cells and memory T cells are excluded, allowing the model to be compared with experimental preparations only involving a naïve T cell repertoire (6, 7, 9, 50, 64, 77, 81). One aspect of initiation of acute organ rejection includes cross-reactivity of non-naïve T cells cross-reacting against specific foreign MHC molecules (HLA in humans) presented by graft cells. The contributions of non-naïve T cells can vary widely, depending on the immunological history of the individual (including the formation of heterologous immunity toward the transplant), and serve as a point of customization that can be adjusted in subsequent iterations of this model. The model also does not accurately represent the accumulation of immature APC in the graft when no T cells are present in the system. This limitation likely derives from the

simplification of incorporating multiple APC types into one variable and having A_{inf}^G and A_{mat}^G originating from the same starting population. Moreover, the effects of mechanisms of tolerization, namely the induction of T cell anergy by immature APC or the conversion of T cells into Tregs, are not presently included but could be incorporated in the future. These processes contribute significantly to the underlying anti-inflammatory processes, as they allow A_{imm}^G and T_R^G to inhibit activated cells in ways currently not being modeled. Modeling these factors may require probabilistic considerations of co-stimulatory encounters of antigen with or without pro-inflammatory signals. Additionally, graft rejection experiments typically conclude upon rejection and no further measurements of the graft mass are taken. Thus, any model predictions post-rejection unfortunately cannot be compared to available experimental observations.

The model also assumes that the entire graft is attacked at day 0. In reality, due to the three-dimensional heterogeneity of the system, sites undergoing an inflammatory response are damaged more. There are also early and late inflammatory populations that could be included in the model using a time delay. This would require converting the system into delay differential equations, as in (25).

Model Extensions

Excitingly, despite the presented limitations, multiple avenues of experimentation to understand the rejection response and to assess the efficacy of therapeutic interventions are suggested by the results obtained with this model. For example, the current model predicts that altering the T_{RN} population has a significant impact on graft survival, as shown in **Figures 5 and 6**. The size, timing, and repetition of Treg transfers can vary widely; many experiments have started to identify appropriate combinations for maximizing graft life (10, 46, 47, 51, 57, 67, 77). This model can be used to simulate a multitude of adoptive transfer regimens that may or may not have been explored experimentally. In addition, pharmaceutical immunosuppression can be simulated by targeting terms in the equations that represent chemical pathways. In particular, there is much interest in directly manipulating pro- and anti-inflammatory signals as novel immunosuppressive strategies; model simulation could help to identify optimal regimens. The model can also be used to assess the compatibility between

the current strategy of immunosuppression and experimental immune interventions and guide the identification of optimal conversion strategies. Moreover, future iterations of the model could encompass the heterogeneity of reactivity of each individual repertoire of alloreactive T cells (combined with the extent of mismatch in HLA molecules between donor and recipient) to achieve a more “personalized” level of intervention – an ideal goal of current medical research. Overall, the model can be used to hypothesize that pathways are viable targets for pharmaceutical intervention based on parameter sensitivity analysis and model dynamics. Combined with a continuous cycle of suggested experimentation and model optimization, this approach has potential for valuable contributions in the quest of transplant tolerance induction.

AUTHOR CONTRIBUTIONS

JA, AM, AA, BO, GB, and GR contributed to the theoretical elaboration of the computational model described herein; JA and AM wrote the model script; JA, AM, and AA performed model simulations; BO, GB, and GR executed all wet-lab experiments; JA, AM, AA, BO, GB, and GR wrote the manuscript while providing critical feedback.

ACKNOWLEDGMENTS

We thank Dr. Yoram Vodovotz, Dr. James Faeder, and Ms. Joyeeta Dutta-Moscato for invaluable feedback in the initial elaboration of the theoretical model of transplant rejection. We also thank Xiaoling Zhang of the Ross Research Flow Cytometry Core (Johns Hopkins University) for invaluable assistance with all flow cytometry-based experiments.

FUNDING

This work was supported by a Burroughs Wellcome Fund BWF 1014050 Collaborative Research Travel Grant (to JA), the IUPUI School of Science Institute for Mathematical Modeling and Computational Science Grant to Enhance Interdisciplinary Research and Education (iM2CS-GEIRE) award (to JA), a National Institutes of Health grant number UL1TR000005 in the form of a CTSI-PEIR (to GR), and grant number R21HL127355 (to GR).

REFERENCES

- Caplan AL. Organ transplants: the costs of success. *Hastings Cent Rep* (1983) 13(6):23–32. doi:10.2307/3560741
- Bingaman AW, Ha J, Waitze SY, Durham MM, Cho HR, Tucker-Burden C, et al. Vigorous allograft rejection in the absence of danger. *J Immunol* (2000) 164(6):3065–71. doi:10.4049/jimmunol.164.6.3065
- Catron DM, Itano AA, Pape KA, Mueller DL, Jenkins MK. Visualizing the first 50 hr of the primary immune response to a soluble antigen. *Immunity* (2004) 21(3):341–7. doi:10.1016/j.jimmuni.2004.08.007
- Dai Z, Lakkis FG. The role of cytokines, CTLA-4 and costimulation in transplant tolerance and rejection. *Curr Opin Immunol* (1999) 11(5):504–8. doi:10.1016/S0952-7915(99)00008-4
- He G, Hart J, Kim OS, Szot GL, Siegel CT, Thistlethwaite JR, et al. The role of CD8 and CD4 T cells in intestinal allograft rejection: a comparison of monoclonal antibody-treated and knockout mice. *Transplantation* (1999) 67(1):131–7. doi:10.1097/00007890-199901150-00022
- Heeger PS. T-cell allorecognition and transplant rejection: a summary and update. *Am J Transplant* (2003) 3(5):525–33. doi:10.1034/j.1600-6143.2003.00123.x
- Krieger NR, Yin DP, Fathman CG. CD4+ but not CD8+ cells are essential for allorejection. *J Exp Med* (1996) 184(5):2013–8. doi:10.1084/jem.184.5.2013
- Linderman JJ, Riggs T, Pande M, Miller M, Marino S, Kirschner DE. Characterizing the dynamics of CD4+ T cell priming within a lymph node. *J Immunol* (2010) 184(6):2873–85. doi:10.4049/jimmunol.0903117
- van Maurik Av, Herber M, Wood KJ, Jones ND. Cutting edge: CD4+CD25+ alloantigen-specific immunoregulatory cells that can prevent CD8+ T cell-mediated graft rejection: implications for anti-CD154 immunotherapy. *J Immunol* (2002) 169(10):5401–4. doi:10.4049/jimmunol.169.10.5401

10. Wood KJ, Goto R. Mechanisms of rejection: current perspectives. *Transplantation* (2012) 93(1):1–10. doi:10.1097/TP.0b013e31823cab44
11. Turka LA, Linsley PS, Lin H, Brady W, Leiden JM, Wei RQ, et al. T-cell activation by the CD28 ligand B7 is required for cardiac allograft rejection in vivo. *Proc Natl Acad Sci U S A* (1992) 89:11102–5. doi:10.1073/pnas.89.22.11102
12. Pearson TC, Alexander DZ, Corbascio M, Hendrix R, Ritchie SC, Linsley PS, et al. Analysis of the B7 costimulatory pathway in allograft rejection. *Transplantation* (1997) 63(10):1463–9. doi:10.1097/00007890-199705270-00016
13. Pearson TC, Alexander DZ, Winn KJ, Linsley PS, Lowry RP, Larsen CP. Transplantation tolerance induced by CTLA4-Ig. *Transplantation* (1994) 57(12):1701–6. doi:10.1097/00007890-199457120-00002
14. Sayegh MH, Akalin E, Hancock WW, Russell ME, Carpenter CB, Linsley PS, et al. CD28-B7 blockade after alloantigenic challenge in vivo inhibits Th1 cytokines but spares Th2. *J Exp Med* (1995) 181(5):1869–74. doi:10.1084/jem.181.5.1869
15. Lenschow DJ, Zeng Y, Thistlethwaite JR, Montag A, Brady W, Gibson MG, et al. Long-term survival of xenogeneic pancreatic islet grafts induced by CTLA4Ig. *Science* (1992) 257:789–92. doi:10.1126/science.1323143
16. Kirk AD, Harlan DM, Armstrong NN, Davis TA, Dong Y, Gray GS, et al. CTLA4-Ig and anti-CD40L prevent renal allograft rejection in primates. *Proc Natl Acad Sci U S A* (1997) 94:8789–94. doi:10.1073/pnas.94.16.8789
17. Levisetti MG, Padrid PA, Szot GL, Mittal N, Meehan SM, Wardrip CL, et al. Immunosuppressive effects of human CTLA4Ig in a non-human primate model of allogeneic pancreatic islet transplantation. *J Immunol* (1997) 159(11):5187–91.
18. Adams AB, Shirasugi N, Jones TR, Durham MM, Strobert EA, Cowan S, et al. Development of a chimeric anti-CD40 monoclonal antibody that synergizes with LEA29Y to prolong islet allograft survival. *J Immunol* (2005) 174(1):542–50. doi:10.4049/jimmunol.174.1.542
19. Vincenti F, Dritsolis A, Kirkpatrick P, Belatacept. *Nat Rev Drug Discov* (2011) 10(9):655–6. doi:10.1038/nrd3536
20. Riella LV, Sayegh MH. T-cell co-stimulatory blockade in transplantation: two steps forward one step back! *Expert Opin Biol Ther* (2013) 13(11):1557–68. doi:10.1517/14712598.2013.845661
21. Sachs DH, Sykes M, Kawai T, Cosimi AB. Immuno-intervention for the induction of transplantation tolerance through mixed chimerism. *Semin Immunol* (2011) 23(3):165–73. doi:10.1016/j.smim.2011.07.001
22. Leventhal J, Abecassis M, Miller J, Gallon L, Tollerud D, Elliott MJ, et al. Tolerance induction in HLA disparate living donor kidney transplantation by donor stem cell infusion: durable chimerism predicts outcome. *Transplantation* (2013) 95(1):169–76. doi:10.1097/TP.0b013e3182782fc1
23. Kim PS, Levy D, Lee PP. Modeling and simulation of the immune system as a self-regulating network. *Methods Enzymol* (2009) 467:79–109. doi:10.1016/S0076-6879(09)67004-X
24. Kim PS, Lee PP, Levy D. Modeling regulation mechanisms in the immune system. *J Theor Biol* (2007) 246(1):33–69. doi:10.1016/j.jtbi.2006.12.012
25. Lee HY, Topham DJ, Park SY, Hollenbaugh J, Treanor J, Mosmann TR, et al. Simulation and prediction of the adaptive immune response to influenza A virus infection. *J Virol* (2009) 83(14):7151–65. doi:10.1128/JVI.00098-09
26. Caridade M, Graca L, Ribeiro RM. Mechanisms underlying CD4+ Treg immune regulation in the adult: from experiments to models. *Front Immunol* (2013) 4:378. doi:10.3389/fimmu.2013.00378
27. An G. Introduction of a framework for dynamic knowledge representation of the control structure of transplant immunology: employing the power of abstraction with solid organ transplant agent-based model. *Front Immunol* (2015) 6:561. doi:10.3389/fimmu.2015.00561
28. Day JD, Metes DM, Vodovotz Y. Mathematical modeling of early cellular innate and adaptive immune responses to ischemia/reperfusion injury and solid organ allotransplantation. *Front Immunol* (2015) 6:484. doi:10.3389/fimmu.2015.00484
29. Chong AS, Alegre ML, Miller ML, Fairchild RL. Lessons and limits of mouse models. *Cold Spring Harb Perspect Med* (2013) 3(12):a015495. doi:10.1101/cshperspect.a015495
30. Suchin EJ, Langmuir PB, Palmer E, Sayegh MH, Wells AD, Turka LA. Quantifying the frequency of alloreactive T cells in vivo: new answers to an old question. *J Immunol* (2001) 166(2):973–81. doi:10.4049/jimmunol.166.2.973
31. Chong AS, Alegre ML. The impact of infection and tissue damage in solid-organ transplantation. *Nat Rev Immunol* (2012) 12(6):459–71. doi:10.1038/nri3215
32. He H, Stone JR, Perkins DL. Analysis of robust innate immune response after transplantation in the absence of adaptive immunity. *Transplantation* (2002) 73(6):853–61. doi:10.1097/00007890-200203270-00005
33. Liang Y, Christopher K, Finn PW, Colson YL, Perkins DL. Graft produced interleukin-6 functions as a danger signal and promotes rejection after transplantation. *Transplantation* (2007) 84(6):771–7. doi:10.1097/01.tp.0000281384.24333.0b
34. Moore KW, de Waal Malefyt R, Coffman RL, O'Garra A. Interleukin-10 and the interleukin-10 receptor. *Annu Rev Immunol* (2001) 19:683–765. doi:10.1146/annurev.immunol.19.1.683
35. Murray PJ, Smale ST. Restraint of inflammatory signaling by interdependent strata of negative regulatory pathways. *Nat Immunol* (2012) 13(10):916–24. doi:10.1038/ni.2391
36. Sabat R, Grütz G, Warszawska K, Kirsch S, Witte E, Wolk K, et al. Biology of interleukin-10. *Cytokine Growth Factor Rev* (2010) 21(5):331–44. doi:10.1016/j.cytofr.2010.09.002
37. Malliaras K, Zhang Y, Seinfeld J, Galang G, Tseliou E, Cheng K, et al. Cardiomyocyte proliferation and progenitor cell recruitment underlie therapeutic regeneration after myocardial infarction in the adult mouse heart. *EMBO Mol Med* (2013) 5(2):191–209. doi:10.1002/emmm.201201737
38. Doevedans PA, Daemen MJ, de Muinck ED, Smits JF. Cardiovascular phenotyping in mice. *Cardiovasc Res* (1998) 39(1):34–49. doi:10.1016/S0008-6363(98)00073-X
39. Tirziu D, Giordano FJ, Simons M. Cell communications in the heart. *Circulation* (2010) 122(9):928–37. doi:10.1161/CIRCULATIONHA.108.847731
40. Oberbarnscheidt MH, Zeng Q, Li Q, Dai H, Williams AL, Shlomchik WD, et al. Non-self recognition by monocytes initiates allograft rejection. *J Clin Invest* (2014) 124(8):3579–89. doi:10.1172/JCI74370
41. Su CA, Iida S, Abe T, Fairchild RL. Endogenous memory CD8 T cells directly mediate cardiac allograft rejection. *Am J Transplant* (2014) 14(3):568–79. doi:10.1111/ajt.12605
42. Mori DN, Kreisel D, Fullerton JN, Gilroy DW, Goldstein DR. Inflammatory triggers of acute rejection of organ allografts. *Immunol Rev* (2014) 258(1):132–44. doi:10.1111/imr.12146
43. Walsh PT, Strom TB, Turka LA. Routes to transplant tolerance versus rejection: the role of cytokines. *Immunity* (2004) 20(2):121–31. doi:10.1016/S1074-7613(04)00024-X
44. O'Gorman WE, Dooms H, Thorne SH, Kuswanto WF, Simonds EF, Krutzik PO, et al. The initial phase of an immune response functions to activate regulatory T cells. *J Immunol* (2009) 183(1):332–9. doi:10.4049/jimmunol.0900691
45. Wood KJ, Bushell A, Hester J. Regulatory immune cells in transplantation. *Nat Rev Immunol* (2012) 12(6):417–30. doi:10.1038/nri3227
46. Wood KJ, Sakaguchi S. Regulatory T cells in transplantation tolerance. *Nat Rev Immunol* (2003) 3(3):199–210. doi:10.1038/nri1027
47. Zhang N, Schröppel B, Lal G, Jakubzick C, Mao X, Chen D, et al. Regulatory T cells sequentially migrate from inflamed tissues to draining lymph nodes to suppress the alloimmune response. *Immunity* (2009) 30(3):458–69. doi:10.1016/j.immuni.2008.12.022
48. Day J, Rubin J, Vodovotz Y, Chow CC, Reynolds A, Clermont G. A reduced mathematical model of the acute inflammatory response II. Capturing scenarios of repeated endotoxin administration. *J Theor Biol* (2006) 242(1):237–56. doi:10.1016/j.jtbi.2006.02.015
49. Kronik N, Kogan Y, Elishmereni M, Halevi-Tobias K, Vuk-Pavlović S, Agur Z. Predicting outcomes of prostate cancer immunotherapy by personalized mathematical models. *PLoS One* (2010) 5(12):e15482. doi:10.1371/journal.pone.0015482
50. De Boer RJ, Homann D, Perelson AS. Different dynamics of CD4+ and CD8+ T cell responses during and after acute lymphocytic choriomeningitis virus infection. *J Immunol* (2003) 171(8):3928–35. doi:10.4049/jimmunol.171.8.3928
51. Joffre O, Santolaria T, Calise D, Al Saati T, Hudrisier D, Romagnoli P, et al. Prevention of acute and chronic allograft rejection with CD4+CD25+Foxp3+ regulatory T lymphocytes. *Nat Med* (2008) 14(1):88–92. doi:10.1038/nm1688
52. Filatenkov AA, Jacovetty EL, Fischer UB, Curtsinger JM, Mescher MF, Ingulli E. CD4 T cell-dependent conditioning of dendritic cells to produce IL-12 results in CD8-mediated graft rejection and avoidance of tolerance. *J Immunol* (2005) 174(11):6909–17. doi:10.4049/jimmunol.174.11.6909
53. Sakaguchi S, Yamaguchi T, Nomura T, Ono M. Regulatory T cells and immune tolerance. *Cell* (2008) 133(5):775–87. doi:10.1016/j.cell.2008.05.009

54. Vignali DA, Collison LW, Workman CJ. How regulatory T cells work. *Nat Rev Immunol* (2008) 8(7):523–32. doi:10.1038/nri2343
55. Gratz IK, Campbell DJ. Organ-specific and memory Treg cells: specificity, development, function, and maintenance. *Front Immunol* (2014) 5:333. doi:10.3389/fimmu.2014.00333
56. Shevach EM. Mechanisms of foxp3+ T regulatory cell-mediated suppression. *Immunity* (2009) 30(5):636–45. doi:10.1016/j.immuni.2009.04.010
57. Raimondi G, Sumpter TL, Matta BM, Pillai M, Corbitt N, Vodovotz Y, et al. Mammalian target of rapamycin inhibition and alloantigen-specific regulatory T cells synergize to promote long-term graft survival in immunocompetent recipients. *J Immunol* (2010) 184(2):624–36. doi:10.4049/jimmunol.0900936
58. Setoguchi K, Schenck AD, Ishii D, Hattori Y, Baldwin WM III, Tanabe K, et al. LFA-1 antagonism inhibits early infiltration of endogenous memory CD8 T cells into cardiac allografts and donor-reactive T cell priming. *Am J Transplant* (2011) 11(5):923–35. doi:10.1111/j.1600-6143.2011.03492.x
59. Brandwood A, Noble KR, Schindhelm K. Phagocytosis of carbon particles by macrophages in vitro. *Biomaterials* (1992) 13(9):646–8. doi:10.1016/0142-9612(92)90035-M
60. Chalasani G, Li Q, Konieczny BT, Smith-Diggs L, Wrobel B, Dai Z, et al. The allograft defines the type of rejection (acute versus chronic) in the face of an established effector immune response. *J Immunol* (2004) 172(12):7813–20. doi:10.4049/jimmunol.172.12.7813
61. Fu H, Kishore M, Gittens B, Wang G, Coe D, Komarowska I, et al. Self-recognition of the endothelium enables regulatory T-cell trafficking and defines the kinetics of immune regulation. *Nat Commun* (2014) 5:3436. doi:10.1038/ncomms4436
62. Giannoudis PV, Harwood PJ, Loughenbury P, Van Griensven M, Krettek C, Pape HC. Correlation between IL-6 levels and the systemic inflammatory response score: can an IL-6 cutoff predict a SIRS state? *J Trauma* (2008) 65(3):646–52. doi:10.1097/TA.0b013e3181820d48
63. Krieger NR, Fathman CG. The use of CD4 and CD8 knockout mice to study the role of T-cell subsets in allotransplant rejection. *J Heart Lung Transplant* (1997) 16(3):263–7.
64. Pietra BA, Wiseman A, Bolwerk A, Rizeq M, Gill RG. CD4 T cell-mediated cardiac allograft rejection requires donor but not host MHC class II. *J Clin Invest* (2000) 106(8):1003–10. doi:10.1172/JCI10467
65. Regoes RR, Barber DL, Ahmed R, Antia R. Estimation of the rate of killing by cytotoxic T lymphocytes in vivo. *Proc Natl Acad Sci U S A* (2007) 104(5):1599–603. doi:10.1073/pnas.0508830104
66. Tanaka M, Swijnenburg RJ, Gunawan F, Cao YA, Yang Y, Caffarelli AD, et al. In vivo visualization of cardiac allograft rejection and trafficking passenger leukocytes using bioluminescence imaging. *Circulation* (2005) 112(9 Suppl):I105–10. doi:10.1161/CIRCULATIONAHA.104.524777
67. Tang Q, Lee K. Regulatory T-cell therapy for transplantation: how many cells do we need? *Curr Opin Organ Transplant* (2012) 17(4):349–54. doi:10.1097/MOT.0b013e328355a992
68. Turnquist HR, Raimondi G, Zahorchak AF, Fischer RT, Wang Z, Thomson AW. Rapamycin-conditioned dendritic cells are poor stimulators of allogeneic CD4+ T cells, but enrich for antigen-specific Foxp3+ T regulatory cells and promote organ transplant tolerance. *J Immunol* (2007) 178(11):7018–31. doi:10.4049/jimmunol.178.11.7018
69. Arciero JC, Ermentrout GB, Upperman JS, Vodovotz Y, Rubin JE. Using a mathematical model to analyze the role of probiotics and inflammation in necrotizing enterocolitis. *PLoS One* (2010) 5(4):e10066. doi:10.1371/journal.pone.0010066
70. Kirschner DE, Chang ST, Riggs TW, Perry N, Linderman JJ. Toward a multiscale model of antigen presentation in immunity. *Immunol Rev* (2007) 216:93–118. doi:10.1111/j.1600-065X.2007.00490.x
71. León K, Carneiro J, Pérez R, Montero E, Lage A. Natural and induced tolerance in an immune network model. *J Theor Biol* (1998) 193(3):519–34. doi:10.1006/jtbi.1998.0720
72. León K, Pérez R, Lage A, Carneiro J. Modelling T-cell-mediated suppression dependent on interactions in multicellular conjugates. *J Theor Biol* (2000) 207(2):231–54. doi:10.1006/jtbi.2000.2169
73. Regoes RR, Yates A, Antia R. Mathematical models of cytotoxic T-lymphocyte killing. *Immunol Cell Biol* (2007) 85(4):274–9. doi:10.1038/sj.icb.7100053
74. Reynolds A, Rubin J, Clermont G, Day J, Vodovotz Y, Ermentrout GB. A reduced mathematical model of the acute inflammatory response: I. Derivation of model and analysis of anti-inflammation. *J Theor Biol* (2006) 242(1):220–36. doi:10.1016/j.jtbi.2006.02.016
75. Zecher D, Li Q, Williams AL, Walters JT, Baddoura FK, Chalasani G, et al. Innate immunity alone is not sufficient for chronic rejection but predisposes healed allografts to T cell-mediated pathology. *Transpl Immunol* (2012) 26(2–3):113–8. doi:10.1016/j.trim.2011.12.006
76. van der Net JB, Bushell A, Wood KJ, Harden PN. Regulatory T cells: first steps of clinical application in solid organ transplantation. *Transpl Int* (2016) 29(1):3–11. doi:10.1111/tri.12608
77. Wang J, Zhang L, Tang J, Jiang S, Wang X. Adoptive transfer of transplantation tolerance mediated by CD4+CD25+ and CD8+CD28- regulatory T cells induced by anti-donor-specific T-cell vaccination. *Transplant Proc* (2008) 40(5):1612–7. doi:10.1016/j.transproceed.2008.02.079
78. Hancock WW. Chemokine receptor-dependent alloresponses. *Immunol Rev* (2003) 196:37–50. doi:10.1046/j.1600-065X.2003.00084.x
79. Hancock WW, Wang L, Ye Q, Han R, Lee I. Chemokines and their receptors as markers of allograft rejection and targets for immunosuppression. *Curr Opin Immunol* (2003) 15(5):479–86. doi:10.1016/S0952-7915(03)00103-1
80. Tchao NK, Turka LA. Lymphodepletion and homeostatic proliferation: implications for transplantation. *Am J Transplant* (2012) 12(5):1079–90. doi:10.1111/j.1600-6143.2012.04008.x
81. Vu MD, Amanullah F, Li Y, Demirci G, Sayegh MH, Li XC. Different costimulatory and growth factor requirements for CD4+ and CD8+ T cell-mediated rejection. *J Immunol* (2004) 173(1):214–21. doi:10.4049/jimmunol.173.1.214

Conflict of Interest Statement: The authors declare that the research was conducted in the absence of any commercial or financial relationships that could be construed as a potential conflict of interest.

Copyright © 2016 Arciero, Maturo, Arun, Oh, Brandacher and Raimondi. This is an open-access article distributed under the terms of the Creative Commons Attribution License (CC BY). The use, distribution or reproduction in other forums is permitted, provided the original author(s) or licensor are credited and that the original publication in this journal is cited, in accordance with accepted academic practice. No use, distribution or reproduction is permitted which does not comply with these terms.



Mathematical modeling of early cellular innate and adaptive immune responses to ischemia/reperfusion injury and solid organ allotransplantation

Judy D. Day^{1,2*}, Diana M. Metes³ and Yoram Vodovotz^{4,5}

OPEN ACCESS

Edited by:

Julia Arciero,
Indiana University-Purdue University
Indianapolis, USA

Reviewed by:

Reem Al-Daccak,
Institut National de la Santé et de la
Recherche Médicale, France
Jonathan Forde,
Hobart and William Smith Colleges,
USA

*Correspondence:

Judy D. Day,
Department of Mathematics,
University of Tennessee, 227 Ayres
Hall, 1403 Circle Drive, Knoxville,
TN 37996-1320, USA
judyday@utk.edu

Specialty section:

This article was submitted to
Alloimmunity and Transplantation, a
section of the journal
Frontiers in Immunology

Received: 19 May 2015

Accepted: 07 September 2015

Published: 25 September 2015

Citation:

Day JD, Metes DM and Vodovotz Y
(2015) Mathematical modeling of
early cellular innate and adaptive
immune responses to ischemia/
reperfusion injury and solid organ
allotransplantation.

Front. Immunol. 6:484.

doi: 10.3389/fimmu.2015.00484

A mathematical model of the early inflammatory response in transplantation is formulated with ordinary differential equations. We first consider the inflammatory events associated only with the initial surgical procedure and the subsequent ischemia/reperfusion (I/R) events that cause tissue damage to the host as well as the donor graft. These events release damage-associated molecular pattern molecules (DAMPs), thereby initiating an acute inflammatory response. In simulations of this model, resolution of inflammation depends on the severity of the tissue damage caused by these events and the patient's (co)-mortalities. We augment a portion of a previously published mathematical model of acute inflammation with the inflammatory effects of T cells in the absence of antigenic allograft mismatch (but with DAMP release proportional to the degree of graft damage prior to transplant). Finally, we include the antigenic mismatch of the graft, which leads to the stimulation of potent memory T cell responses, leading to further DAMP release from the graft and concomitant increase in allograft damage. Regulatory mechanisms are also included at the final stage. Our simulations suggest that surgical injury and I/R-induced graft damage can be well-tolerated by the recipient when each is present alone, but that their combination (along with antigenic mismatch) may lead to acute rejection, as seen clinically in a subset of patients. An emergent phenomenon from our simulations is that low-level DAMP release can tolerize the recipient to a mismatched allograft, whereas different restimulation regimens resulted in an exaggerated rejection response, in agreement with published studies. We suggest that mechanistic mathematical models might serve as an adjunct for patient- or sub-group-specific predictions, simulated clinical studies, and rational design of immunosuppression.

Keywords: DAMPs, allo-recognition, ischemia/reperfusion injury, transplant, equation-based model, ordinary differential equations

Introduction

Solid organ transplantation represents the treatment of choice for end-stage organ failure-associated diseases, and has proved effective at extending and improving the quality of life of patients. Approximately 22,000 patients receive solid organ transplants every year in the United States, according to United Network for Organ Sharing¹. While 1-year outcomes after solid organ transplantation are excellent, the long-term outcomes are still mediocre, and range from 70% survival rate for kidney transplantation to 40–50% survival for heart/lung and intestine transplantation at 5 years (1–3). These poor long-term outcomes depend on multiple factors related to both donor and recipient, but are in their vast majority dictated by initial polyclonal, multimodal, and redundant innate and adaptive immune responses of the recipient directed against the allograft (4). These early immune responses occur both locally and systemically, in response to non-specific inflammatory damage-associated molecular pattern molecules (DAMPs) or to allo-antigen (allo-Ag)-specific major histocompatibility complex (MHC)-mismatch. These responses may be triggered by (i) the transplant surgery procedure (5); (ii) the type and the quality of the graft, including the level of ischemia/reperfusion (I/R) injury (IRI) post-revascularization; and (iii) the level of pre-formed cellular (T cells) allogeneic and heterologous immunologic memory responses (4, 6).

Inflammation and Immunity in Solid Organ Transplantation

While most work in the transplant field has focused on the antigen-driven immune processes that drive graft rejection, recent work has begun to focus on the interplay between early innate immune mechanisms and subsequent antigen-driven responses (7–10). In this respect, the transplant community has begun to acknowledge the tightly woven interplay between innate and adaptive immunity that has been recognized in other fields (11–20). These studies have pointed to multiple intersecting pathways by which early stress or injury leads to activation of innate and adaptive lymphoid pathways. Key among these pathways are those driven by DAMPs, which play intracellular housekeeping roles normally but which are released both locally and systemically upon stress, injury, or infection (21, 22). DAMPs activate classical innate immune cells such as macrophages and polymorphonuclear cells (PMN; i.e., neutrophils), but also stimulate dendritic cells (DC) to drive cytotoxic (Tc) and helper (TH) T cell activation/polarization (23–26). In addition, non-conventional $\gamma\delta$ -T cells, natural killer (NK)-T cells, as well as TH1 and TH17 cells (along with innate cells) provide other points of intersection between innate and antigen-specific (adaptive) immune responses (6, 27).

The transplantation procedure involves oxygen deprivation (ischemia) in the recipient host tissues as well as in the donor graft due to the time interval from donor organ removal to its placement in the recipient host. Once the transplant is complete, blood flow resumes, a process known as reperfusion. The I/R

event is well-known to cause injury (IRI) to tissues, in addition to any direct tissue damage from the surgical procedure. These injurious events further initiate release of DAMPs, and this abates as IRI resolves (28–31). However, DAMPs initiate an acute inflammatory cascade involving the early expression of adhesion and co-stimulation molecules, chemokine release, and the inflammatory cytokine production by innate immune cells as well as memory T cells. Briefly, neutrophils respond to DAMPs by extruding highly inflammatory DNA material [neutrophil extracellular traps (NETs)] that trigger monocytes and tissue macrophages to secrete interleukins (IL-) IL-1 β , IL-6, and tumor necrosis factor- α (TNF- α). In turn, these pro-inflammatory cytokines stimulate monocyte-derived DC to produce IL-12, a pivotal cytokine for generation of type-1 immunity (6, 27, 32, 33). In addition, activated monocytes can release IL-23, a cytokine critical for recruitment of IL-17-producing $\gamma\delta$ -T cells, responsible in turn for neutrophil chemotaxis and activation (34, 35). As a result of the innate immune cell cytokine storm, the direct response to DAMPs, $\gamma\delta$ -T cells, and memory T cells further contribute to IRI by IL-17 and interferon- γ (IFN- γ) release and costimulatory molecule up-regulation in an allo-Ag-independent manner (27, 36, 37).

A second layer of effector and inflammatory molecules is released by pre-formed alloreactive memory Type-1 and Type-17 T cells in response to graft mismatched allo-Ag recognition. The levels of T cell pre-sensitization of the recipient to the donor correlate directly with early acute rejection episodes (38). The ensuing inflammation acts as a feedback loop, and may further cause tissue damage that drives additional release of DAMPs and allo-Ags. Resolution of cellular and tissue inflammation triggered by surgery, IRI, and subsequent DAMP release is mediated by innate regulatory macrophages (M2 and Mreg), intrinsic regulatory cytokines [IL-10, IL-4, and transforming growth factor- β 1 (TGF- β 1)] along with T regulatory cells (Tregs) in animal models of heart, kidney, and liver transplantation (27, 39–42), while pre-formed alloreactive memory T cells seem less sensitive to regulation by Tregs (43).

These immunologic events may play a significant role in driving the diverse outcomes that accompany organ transplantation in various cases of apparent antigenic mismatch. We use the term “apparent antigenic mismatch” since the response to allo-Ag includes multiple factors, such as (1) actual allo-Ag differences; (2) individual, genetically predetermined thresholds of immune activation in response to a given degree of antigenic mismatch; (3) pre-existing levels of memory T cells; and (4) individual-specific response to immunosuppressive therapy.

Modern organ transplantation has utilized potent strategies to control these unwanted, early immune responses. Specifically, thorough pre-transplant screening of recipient's pre-formed donor-specific allo-antibody reactivity against the donor (cross-match screening for humoral sensitization) is combined with depleting or non-depleting induction therapy at organ implantation and with versatile maintenance immunosuppression (44–46). All of these methods seek to mitigate the deleterious effects of immunity while allowing regulatory molecules and cells to develop. Notably, these strategies target mostly adaptive immune cells such as T cells, leaving the innate

¹<http://optn.transplant.hrsa.gov/>

immune players mostly unchecked. Thus, patients with elevated DAMP release and inflammation – due to significant IRI after reperfusion that carry undetected memory T cells to the donor MHC – may experience early rejection episodes despite proper pre-transplant screening, induction therapy, and maintenance immunosuppression. This contrasts with non-sensitized or minimally sensitized patients who experience minimal IRI due to live donation and/or optimal MHC matching, resulting in either indolent subclinical inflammation or in uneventful clinical course with desirable quiescent outcomes. For example, acute cellular rejection (ACR) events in the first 3 months after kidney transplantation occur in 10–12% of patients, while biopsy-proven subclinical rejection occurs in an additional 15–18% of kidney recipients (47).

Deciphering the Complexity of Inflammation and Immunity with Mathematical Models

The foregoing discussion suggests an emerging paradigm in which context and timing matter more than semantic distinctions among immune/inflammatory responses: in essence, inflammation/innate immunity triggers early memory lymphoid pathways that can subsequently become more focused after exposure to specific antigens, while chronic inflammation might be thought of as the chronic restarting of acute inflammation (48). In this context, attempting to define and predict responses under particular circumstances, especially in individuals, becomes almost overwhelmingly complex.

Mathematical modeling provides a key tool by which to study the integrated innate/adaptive response or acute/chronic inflammatory response and thereby untangle some of this complexity (48–50). Therefore, such models provide a means to drive novel hypotheses with regard to complex immune processes like those involved in the transplantation procedure and can assist in identifying viable – and possibly novel – points of control or diagnostic biomarkers. Multiple mathematical models that integrate innate and adaptive immune responses have been developed over the past decade to address diverse questions and disease states (51–54). However, a comprehensive mathematical model of organ transplantation is as yet lacking, and the complexity of the immune events involved in the procedure reiterates the need for such an approach. Complex systems, especially biological ones, are notoriously sensitive to initial conditions (55, 56). Thus, to address the solid organ transplant process comprehensively, we hypothesize the need to model not only the transplant and its antigenic properties, but also the initial conditions relating to the transplant surgery and subsequent IRI as drivers of innate immunity. Indeed, prior mathematical modeling studies have suggested the need to model the underlying process, for example, in the case of the role of underlying trauma in the setting of hemorrhagic shock (57).

The modeling simulations in this present study suggest that surgical injury and graft damage can be well-tolerated by the recipient when each is present alone, but that their combination (along with antigenic mismatch) may lead to acute rejection. An

emergent phenomenon from our simulations is that low-level DAMP release can tolerize the recipient to a mismatched graft under specific restimulation settings, while other restimulation regimens lead to an exaggerated rejection response.

Results

To examine the early stages of inflammatory/immune responses to an organ transplant, including investigating the role of IRI in transplantation, we developed a mathematical model that includes the inflammatory hallmarks of IRI as well as the immune responses elicited by the apparent antigenic mismatch of the graft. As described above, we use the term “apparent antigenic mismatch” to comprise (1) actual antigenic differences; (2) individual, genetically predetermined thresholds of immune activation in response to a given degree of antigenic mismatch; (3) pre-existing levels of memory T cells; and (4) individual-specific response to immunosuppressive therapy.

The degree of this apparent antigenic mismatch is governed by a parameter, α , wherein a value of zero implies that the graft has 0% apparent mismatch with the host and a value of 1 implies complete (i.e., 100%) apparent mismatch. The model is initiated with a specified level of initial damage to the host and to the graft from the surgery and I/R, and thus the model simulations begin at approximately the time that transplant surgery is concluded (~8 h after the surgery begins), at which time reperfusion would occur.

In order to increase our ability to analyze qualitatively the driving forces behind diverse transplant outcomes, we simplify the number of components considered in the model and aim to create an abstract representation of the processes mentioned above. We focus on the following core scenarios and outcomes:

1. Clinical quiescence: the graft, following transplantation, shows no signs of inflammatory infiltrates. This is represented by model simulations showing little or no graft damage and corresponding to fully or almost fully recovered graft functionality.
2. Acute clinical rejection: the graft, following transplantation, sustains levels of damage from the host response that cause it to lose functionality, occurring in the first 3 months after transplant. This is represented by model simulations showing high graft damage and corresponding poor graft functionality very early after the simulation is initiated (i.e., after the transplant is completed).
3. Subclinical inflammation: the allograft, following transplantation, shows no apparent clinical signs of organ damage, but subclinical levels of inflammation and cellular infiltrates are detected in the protocol biopsies in the first 3 months after surgery. This is represented by model simulations showing either stabilized but diminished graft functionality due to lingering inflammation, or non-stabilized, poor graft functionality due to oscillating inflammatory responses driven by T cells.

The Mathematical Model

Figure 1 provides a schematic of all the components and interactions included in the model equations. **Table 1** provides a

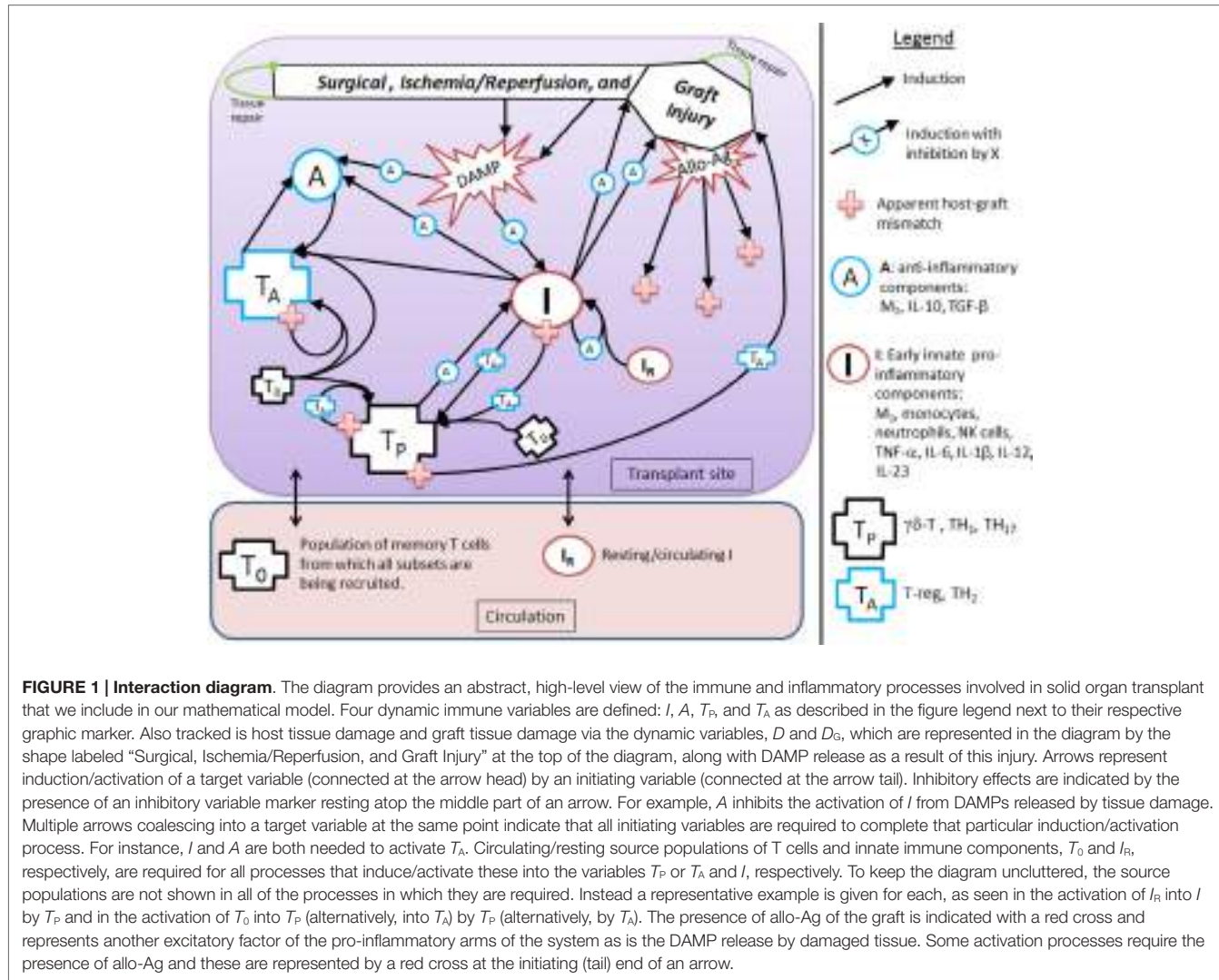


FIGURE 1 | Interaction diagram. The diagram provides an abstract, high-level view of the immune and inflammatory processes involved in solid organ transplant that we include in our mathematical model. Four dynamic immune variables are defined: I , A , T_P , and T_A as described in the figure legend next to their respective graphic marker. Also tracked is host tissue damage and graft tissue damage via the dynamic variables, D and D_G , which are represented in the diagram by the shape labeled "Surgical, Ischemia/Reperfusion, and Graft Injury" at the top of the diagram, along with DAMP release as a result of this injury. Arrows represent induction/activation of a target variable (connected at the arrow head) by an initiating variable (connected at the arrow tail). Inhibitory effects are indicated by the presence of an inhibitory variable resting atop the middle part of an arrow. For example, A inhibits the activation of I from DAMPs released by tissue damage. Multiple arrows coalescing into a target variable at the same point indicate that all initiating variables are required to complete that particular induction/activation process. For instance, I and A are both needed to activate T_A . Circulating/resting source populations of T cells and innate immune components, T_0 and I_R , respectively, are required for all processes that induce/activate these into the variables T_P or T_A and I , respectively. To keep the diagram uncluttered, the source populations are not shown in all of the processes in which they are required. Instead a representative example is given for each, as seen in the activation of I_R into I by T_P and in the activation of T_0 into T_P (alternatively, into T_A) by T_P (alternatively, by T_A). The presence of allo-Ag of the graft is indicated with a red cross and represents another excitatory factor of the pro-inflammatory arms of the system as is the DAMP release by damaged tissue. Some activation processes require the presence of allo-Ag and these are represented by a red cross at the initiating (tail) end of an arrow.

TABLE 1 | Dynamic model variables.

Dynamic model variable name	Description	Initial condition(s)
D	Tissue damage to recipient host; measured in arbitrary units: D -units	$D(0) = D_0 \geq 0$ due to surgery and ischemia reperfusion injury of host
D_G	Graft tissue damage; measured in arbitrary units: D_G -units	$D_G(0) = D_{G0} \geq 0$ due to ischemia reperfusion injury of graft
I	Early innate pro-inflammatory components, such as tissue M1 macrophages, monocytes, neutrophils, TNF- α , and natural killer (NK) cells; measured in arbitrary units: I -units	$I(0) = I_0 = 0$ in all of the scenarios considered
A	Anti-inflammatory mediators such as IL-10 and TGF- β ; measured in arbitrary units: A -units	$A(0) = A_0 = 0.125$ maintains a background level at homeostasis (69)
T_P	Pro-inflammatory T cells such as $\gamma\delta$ -T cells, TH1 cells, and TH17 cells; measured in arbitrary units: T_P -units	$T_P(0) = T_{P0} = 0$
T_A	Anti-inflammatory T cells such as TH2 and regulatory T cells; measured in arbitrary units: T_A -units	$T_A(0) = T_{A0} = 0$

description of the dynamic model variables and **Table 3** in the Section "Materials and Methods" explains the auxiliary model variables. The dynamic model variables are those whose rates

change over time and are modeled with an ordinary differential equation (ODE); whereas auxiliary variables are functions of dynamic variables. We first discuss the interactions that are

pro-inflammatory and then discuss how these processes initiate and/or are inhibited by the anti-inflammatory components, all based on the immunology discussed in Section “Inflammation and Immunity in Solid Organ Transplantation.” The model does not currently take into consideration explicitly the immunosuppressive therapies given before/during the transplantation procedure, though the effect of immunosuppression is in a sense contained in the concept of apparent antigenic mismatch. We envision testing specific immunosuppression mechanisms (e.g., killing of all inflammatory cells vs. specific killing of T cells) in future iterations of this model.

The goal of this modeling exercise is to understand the dynamics of the transplant procedure from a more abstract perspective, in which we group multiple components into a single variable. While this level of abstraction will in no way allow a quantitative prediction of specific mediators and cells, this approach does allow for an examination of the overall qualitative dynamics of this system in which excitatory and inhibitory mechanisms interact. The early innate components of the model, denoted by the variable I , incorporate the general pro-inflammatory effects of cells such as tissue-resident M1 macrophages, circulating monocytes, neutrophils, and NK cells as well as cytokines such as TNF- α , IL-6, IL-1 β , IL-12, and IL-23. Pro-inflammatory T cells are represented by the variable T_B , and incorporate the general properties of $\gamma\delta$ -T cells, TH1, and TH17 T cell subsets. Also included are anti-inflammatory components, denoted by A , which include M2 macrophages, IL-10, and TGF- β 1. In addition, anti-inflammatory T cells are denoted by the variable T_A and are comprised of T regulatory and TH2 T cells. There are also two dynamic variables that track the rate of change of tissue damage: one for host tissue, denoted by the variable D , and another for graft tissue, denoted by the variable D_G . These six dynamic variables are modeled with ODEs that describe how the rates of these entities change over time as they interact with one another under different simulation scenarios. The variables have arbitrary units, as we are not aiming to match them with quantitative data but instead examine their dynamic behavior. The time scale is in hours. Whereas some parameters governing the various rates of the interactions are estimated from the literature when possible (e.g., from half-lives of cells and inflammatory mediators), the parameters are largely estimated to constrain the model to display basic biologically feasible behavior; see Section “Materials and Methods” for more information.

Figure 1 shows that D and I interact in a positive feedback loop that is inhibited by A . This models the effect of DAMPs released by tissue damaged due to IRI. This process is driven by early innate immune components, resulting in the activation of pro-inflammatory components from a resting/circulating population, I_R (5). These activated pro-inflammatory components cause further tissue damage; but the activation is inhibited by anti-inflammatory influences in a “checks-and-balances” manner. However, severe damage can cause an unabated positive feedback loop among these components, resulting in an unresolved response (31, 57). In the absence of graft placement (i.e., considering the surgical procedure alone), the innate pro-inflammatory components can also induce pro-inflammatory memory T cell recruitment from a circulating T cell population, T_0 (9, 58). In the presence of the

anti-inflammatory components, A , the innate components, I , can induce Tregs and TH2 cells, represented by T_A . Many of these activation/induction processes are inhibited by either A or T_A (27, 41, 59–61). This describes the interactions surrounding the surgical procedure and IRI of the host.

When a solid organ is transplanted, we considered that it would have some initial IRI due to the removal and transport procedures. In addition, the organ could subsequently be damaged by the pro-inflammatory components (both innate and T cell-mediated) present at the transplant site, even in the absence of allo-Ag (58). We model graft functionality (percent), G , as a function of this damage, D_G (see **Table 3** in “Materials and Methods”). Subsequently, we include a parameter (α) governing the mismatch factor to scale the response from innate and T cell pro-inflammatory components in response to an allograft. **Figure 1** also shows that graft injury can release DAMPs, which in turn can activate innate immune components as discussed above. Furthermore, the presence of a graft with a positive antigenic mismatch factor, governed by the parameter α , will cause antigen-specific memory T cells to infiltrate and cause further injury to the graft. This process is modeled by a gain to D_G . This damage will reduce graft function, G , as illustrated in the inset figure of **Table 3**, and consequently will reduce the percentage of graft tissue available to harm further.

With a positive graft mismatch factor, the early innate pro-inflammatory components, such as monocytes and M1 macrophages, through allo-recognition, will provide additional and specific activation via DC of the pro-inflammatory memory T cells, T_P (10, 58). This process is indicated in **Figure 1** by the arrow coming from I into T_P , with the apparent host-graft mismatch marker (red plus sign) present at the tail end of the arrow. In keeping with the abstract model representation of these processes, we do not include the DC component directly, yet the process is implicit in the interactions. Additionally, a positive graft mismatch factor will enhance further recruitment/activation of both pro- and anti-inflammatory T cells, from the source T cell population, T_0 , by already activated components of these types. Again, various processes are inhibited by A and/or T_A , as indicated in the legend of **Figure 1** by an induction arrow that has a particular variable marker sitting atop it in the middle.

In the Section “Materials and Methods,” the construction of the model is discussed and the full model is given by Eqs 1–6, with the model parameter descriptions and values used in the simulations given in **Table 4**. The equations are solved numerically to produce time courses of each of the system variables or states (see Materials and Methods). These resulting time courses are translated to clinical outcomes in the following manner. In general, we define a pre-surgery initial condition for the model variables as $(I_0, D_0, A_0, D_{G0}, T_{P0}, T_{A0}) = (0, 0, 0.125, 0, 0, 0)$, which indicate that all system components are at their background values. This state is referred to as the baseline equilibrium. This setting assumes that there are no underlying immune conditions prior to transplant surgery, which is typically not realistic in the case of transplant recipients. Future iterations of the model could incorporate prior host health conditions. The system can be perturbed from this baseline state, for instance, by setting a

non-zero initial condition for D and/or D_G , which indicates the presence of damaged tissue to host and/or graft, respectively, due to IRI. The rates at which system variables change as a function of time are governed by the Eqs 1–6. A simulation in which the variables' time courses return to the background levels, after a brief transient increase away from this state due to perturbation, is translated as a healthy outcome. **Figures 2A–D** display a basic healthy outcome scenario in terms of host health.

On the other hand, an unhealthy outcome is presumed if the departure away from the healthy equilibrium is not transient but instead causes the variables to approach a different equilibrium that has elevated levels of the variable states. The unhealthy equilibrium implies host health failure and, when a graft is considered, graft failure as well. Alternatively, one could define a level of cumulative damage that could be considered as irreparable, rather than defining non-recovery only by the system's long-term behavior; we did not explore this possibility in the present study.

Figures 2E–H display a basic unhealthy outcome scenario in terms of host health. When a graft placement is considered (with and without apparent mismatch), outcomes also include the percent graft functionality, where a steady-state graft functionality value of 12% represents outright graft failure. See **Figures 3A–D**, for instance.

Simulation: Ischemia/Reperfusion Injury Without Graft Placement (i.e., $G = 0$)

As a first scenario, we consider only the aspects of the inflammatory response of the host involved during the surgical transplant procedure in the absence of a graft placement. This scenario could also be viewed as a look at the trauma of transplant surgery or an instance of accidental blunt trauma, in general. To simulate this situation, we set the initial condition for the host damage variable, D , to a non-zero value, and remove the presence of the graft, G , from the model. All other variable initial conditions

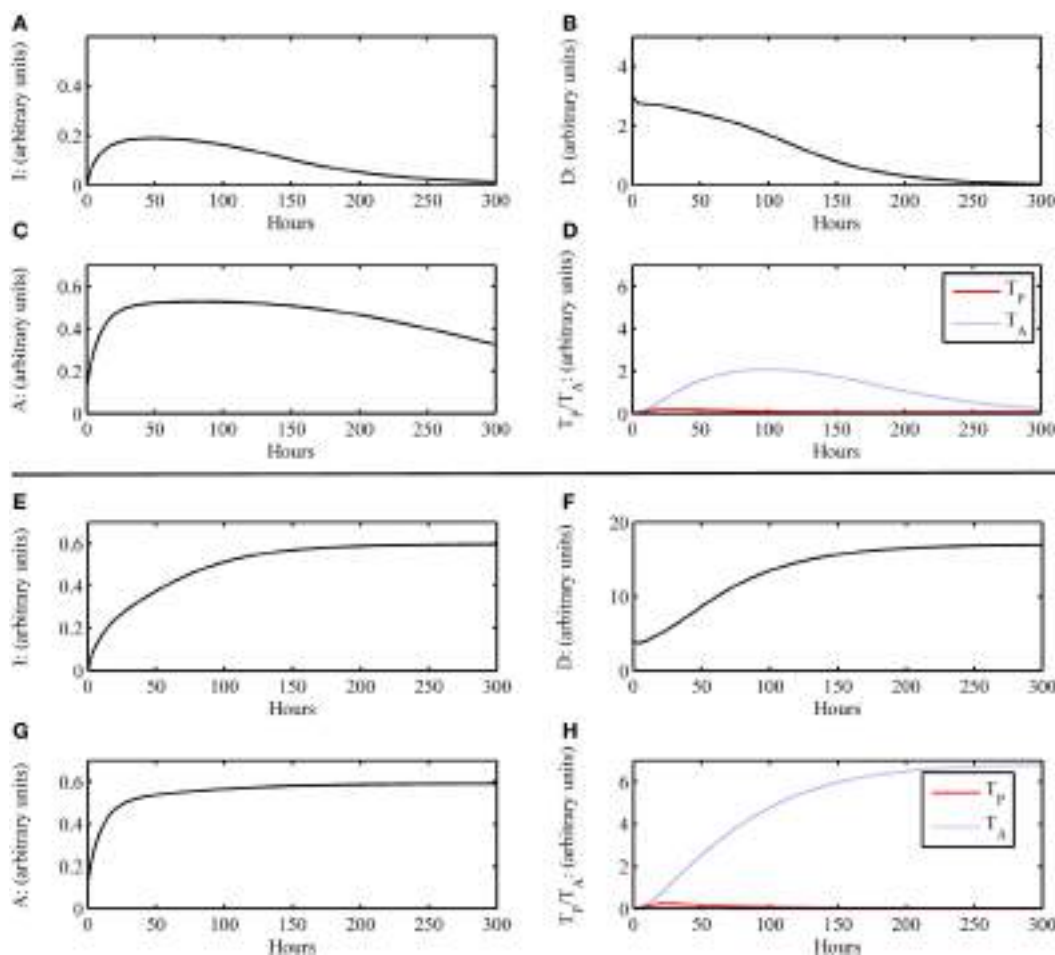


FIGURE 2 | Simulation results of the inflammatory cascade following transplant surgery only without graft placement (i.e., $G = 0$). (A–D) Below a certain threshold, initial host tissue damage caused by IRI incites an inflammatory response that resolves to baseline levels. Initial condition for this simulation was ($I_0, D_0, A_0, D_{G0}, T_{P0}, T_{A0}$) = (0, 3, 0, 0.125, 0, 0) with parameters as given in **Table 4**. For $D < 4$, this outcome is possible. **(E–H)** Above a certain threshold, initial host tissue damage caused by IRI incites an inflammatory response that does not resolve and results in host health failure. Note that this scenario is not the one we would consider for transplant conditions, but demonstrate the scope of the model dynamics to produce theoretically possible outcomes of traumatic injury. Initial condition for this simulation was ($I_0, D_0, A_0, D_{G0}, T_{P0}, T_{A0}$) = (0, 4, 0, 0.125, 0, 0) with parameters as given in **Table 4**. For $D \geq 4$, this outcome is possible.

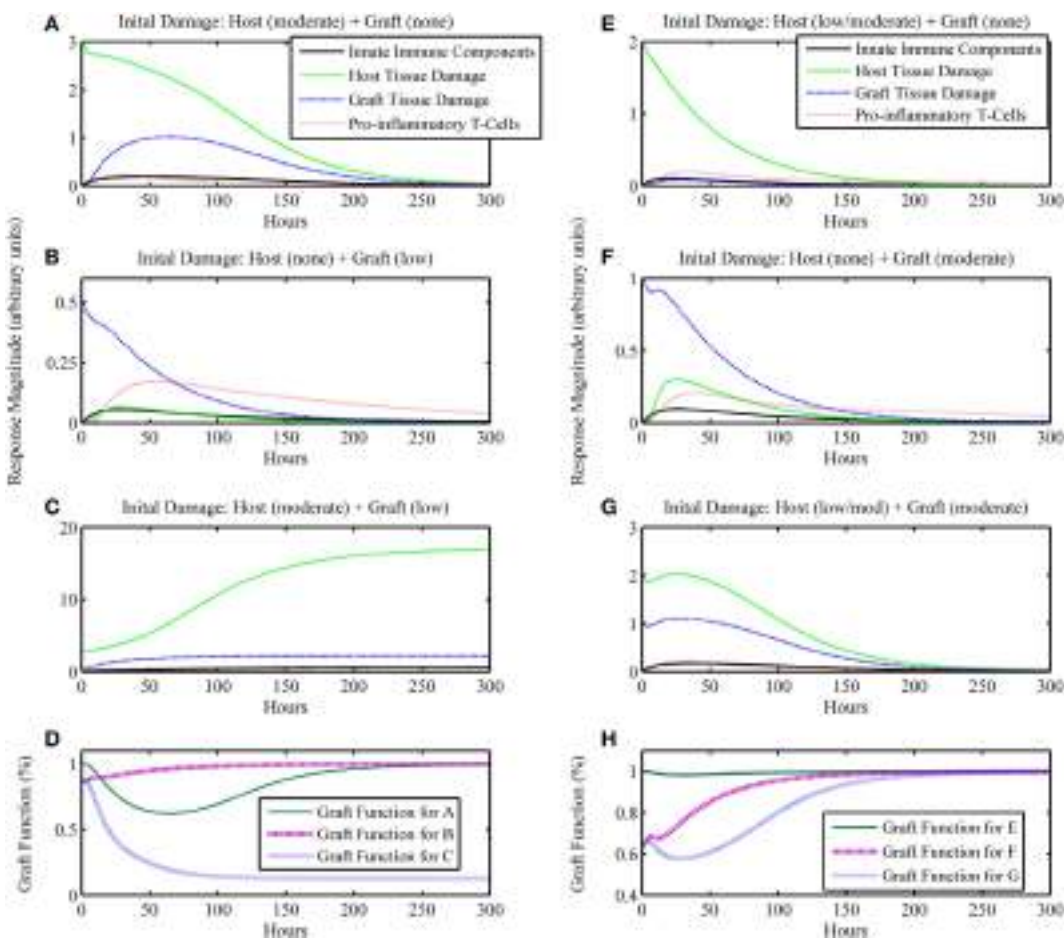


FIGURE 3 | Simulation results of the inflammatory cascade following transplant surgery and non-allo-Ag graft placement (i.e., $\alpha = 0$). Combined initial host and graft IRI can synergize to incite an inflammatory response that (**A–D**) cannot resolve, causing graft failure or (**E–H**) transiently decrease graft function significantly. (**A–C**) present a series of simulations in which (**A**) a moderate level of initial surgical IRI in the host is considered with no corresponding graft IRI associated with the placement, (**B**) no initial surgical IRI in the host is considered with a low level of initial graft IRI, or (**C**) the moderate level of initial surgical IRI in the host of simulation (**A**) is coupled with the low level of initial graft IRI of simulation (**B**). In (**D**), the graft functionality curves corresponding to simulations (**A–C**) are shown. The “Graft function for C” time course in (**D**) displays the synergy to severely affect graft function such that the graft fails, shown as functionality decreasing to and remaining at 12%. Similarly, panels (**E–G**) display outcomes for (**E**) a low/moderate level of initial surgical IRI in the host with no corresponding graft IRI associated with the placement, (**F**) no initial surgical IRI in the host with a corresponding moderate level of initial graft IRI, or (**G**) the combination of the low/moderate initial level of surgical IRI in the host from simulation (**E**) with the moderate level of initial graft IRI from simulation (**F**). In (**H**), the graft functionality curves corresponding with (**E–G**) are shown. The “Graft function for G” time course in (**H**) displays the synergy to significantly affect graft function, but only transiently after which the graft functionality fully recovers. Initial conditions for (**C**): $(I_0, D_0, A_0, D_{G0}, T_{P0}, T_{A0}) = (0, 3, 0.5, 0.125, 0, 0)$; initial conditions for (**G**): $(I_0, D_0, A_0, D_{G0}, T_{P0}, T_{A0}) = (0, 2, 1, 0.125, 0, 0)$.

are set to their healthy state baseline values. **Figures 2A–D** show that an inflammatory response is incited (e.g., levels of I , etc. increase from baseline values) for some initial level of host tissue injury corresponding to DAMP release. We note that this response resolves completely in a reasonable time frame. In other words, the inherent inhibitory mechanisms provided by the anti-inflammatory variables, A and T_A , are sufficient to regulate the response correctly. However, in **Figures 2E–H**, the initial level of IRI was high enough to cause irreparable damage, an unlikely situation in today's modern operating theater, yet a theoretically possible outcome. Thus, our model displays feasible qualitative behavior related to surgical trauma.

Simulation: Ischemia/Reperfusion Injury with Graft Placement But with No Apparent Antigenic Mismatch (i.e., $\alpha = 0$)

The next iteration of simulations considers not only the IRI to the host from surgery but also the IRI associated with the graft due to the processes of harvest from donor and transportation to the recipient host. We assume that initial graft functionality starting at a percentage lower than 100% is a result of IRI due to the harvest and transport procedures, and not an indicator of the functionality that it had when still intact in the host from whom the graft was harvested. Thus, 100% in our model would mean 100% of the total functionality exhibited by a

given organ pre-transplant. Presumably, organs harvested for transplant were functioning “normally,” such that they did not have existing damage affecting this *normal* function. However, this value could be lower if an organ were harvested from an older or less healthy donor (a scenario we did not explore explicitly). For this simulation set, we assume that the graft and host are identical, and therefore do not consider any interactions that involve allo-recognition due to mismatch (i.e., the parameter governing mismatch intensity is set to zero: $\alpha = 0$). The model also displays feasible qualitative behavior for possible outcomes when considering ranges of injury severity. In **Figures 3A–D**, we show that initial host damage combined with initial graft damage can synergize to result in graft failure, whereas each of these challenges separately did not. **Figures 3E–H** show synergy as well, but in a less extreme manner, wherein the graft does not fail and recovers fully. However, as seen in **Figure 3H**, the time course for “Graft Function for G” shows that the negative effects on graft function from IRI reduce graft function by 60% at one point in the simulation. This result suggests that the non-specific, detrimental effects of inflammatory processes initiated by IRI may make the graft much more vulnerable in cases where host-graft mismatch is considered. We explore mismatch scenarios in the next two sections.

Simulation: Ischemia Reperfusion Injury with Graft Placement and Varying Apparent Antigenic Mismatch Levels (i.e., $\alpha > 0$)

In this next simulation set, we consider varying levels of host-graft mismatch, and thus the interactions shown in **Figure 1** involving allo-recognition come into play. We use the initial condition $(I_0, D_0, A_0, D_{G0}, T_{P0}, T_{A0}) = (0, 2, 1, 0.125, 0, 0)$ as in **Figure 3G**, and set α to different values within the interval $[0,1]$ in the multiple simulation runs. **Figures 4A–D** display four qualitatively different outcome scenarios corresponding to ranges of the mismatch parameter, α . Each figure panel displays the graft functionality results of multiple simulation runs for values of α within the specified ranges. In these various scenarios, we observe outcomes corresponding to the clinical scenarios mentioned earlier at the beginning of Section “Results.” Clinical quiescence is represented in **Figure 4A**, where there is little or no graft damage and full or nearly full graft functionality is achieved and retained. Acute clinical rejection is represented in **Figure 4D**, where poor graft functionality is seen very early after the simulation is initiated (i.e., after the transplant is completed), and failure is predicted to occur within less than a month’s time. The subclinical inflammation outcome is represented in **Figures 4B,C**. In **Figure 4B**, we interpret the smaller oscillations as *subclinical chronic inflammation* predicted to resolve on the order of 1–3 months (shown for

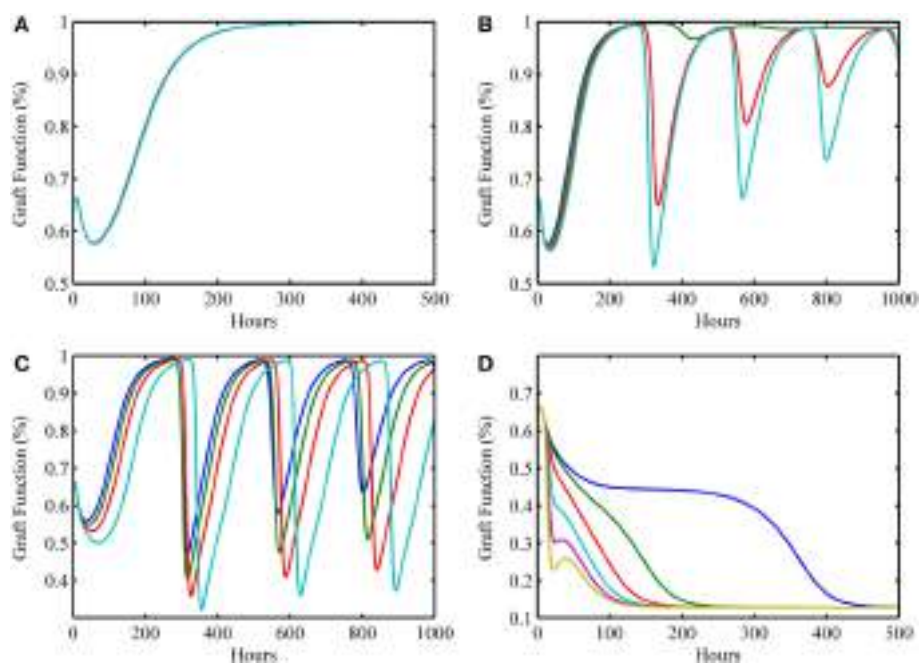


FIGURE 4 | Simulation results showing outcomes of transplant surgery with placement of allo-Ag graft for various degrees of apparent mismatch (i.e., $\alpha > 0$). The initial condition used in **Figure 3G** [i.e., $(I_0, D_0, A_0, D_{G0}, T_{P0}, T_{A0}) = (0, 2, 1, 0.125, 0, 0)$] was also used here but now various values of the apparent mismatch factor parameter, α , were explored to observe the effects of initial host and graft tissue damage from IRI in conjunction with allo-recognition. **(A)** With low mismatch factor ($\alpha = 0–0.03$), graft tolerance is seen. **(B)** Within a higher range ($\alpha = 0.04–0.25$), damped oscillations in graft functionality appear but resolve to greater than 95% functionality in the long term with values of α on the higher end of the range taking months to resolve and stabilize. **(C)** Within the next highest interval ($\alpha = 0.29–0.5$), undamped oscillations are apparent. This indicates a regime where graft function is affected by chronic inflammation driven by T cells that flares up and subsides periodically. **(D)** The last interval ($\alpha = 0.55–1.0$) displays acute graft failure within 400 h for α values near the minimum of this range and within 125 h near the maximum of this range.

TABLE 2 | Minimal initial graft function required for graft survival given a particular mismatch intensity factor.

Value of α	Minimal graft functionality percent [or $D_G(0)$ value]	Ending graft functionality percentage (steady state value of G)
0	20% (or 1.9)	100%
0.1	20% (or 1.9)	99%
0.2	20% (or 1.9)	97%
0.3	20% (or 1.9)	75–97% oscillation range
0.4	20% (or 1.9)	48–99% oscillation range
0.5–0.6	20% (or 1.9)	38–99% oscillation range
0.7	24% (or 1.8)	27–99% oscillation range
0.8–1.0	No cutoff exists	Graft failure (13%)

Ending graft functionality percentages are with respect to an initial assumed 100% functionality that a given organ had pre-transplant, as explained in Section "Simulation: Ischemia/Reperfusion Injury with Graft Placement But with No Apparent Antigenic Mismatch (i.e., $\alpha = 0$)."

up to 1000 h (~42 days), since the recovery behavior is different from, and takes longer than, the graft tolerance recovery scenario of **Figure 4A**. Furthermore, since in **Figure 4B** the damped oscillations are such that (1) graft health does not decrease too often nor too greatly below the original graft health level; and (2) an acceptable recovery is seen eventually (i.e., graft health is greater than 95%), we interpret this behavior as *subclinical*. In other words, the graft is in comparable or better condition than when it was first transplanted, but it is not maintaining optimal function until much later. Note that **Figure 4A** could also be classified as *subclinical*, but the length of time in which graft health is not ideal is much shorter relative to the scenarios in **Figure 4B**. Thus, we do not classify **Figure 4A** as a *chronic* scenario. In **Figure 4C**, the oscillations are larger and do not resolve as in **Figure 4B**. We equate this outcome with long-term rejection since a high and steady level of graft function is never observed as T cells cause inflammation and subsequent damage to flare up and subside repeatedly. This prediction points to a scenario leading to graft failure, even though there are times when there is only *subclinical* inflammation, and a good level of graft function is observed.

Table 2 displays a summary of minimal initial graft functionality percentages (corresponding to an initial value of D_G) from which outright graft failure (i.e., ending graft functionality of 12%) is avoidable, given a particular value of α . For $\sim 0.032 < \alpha < \sim 0.3$, the healthy stable equilibrium is replaced by a suboptimal healthy stable equilibrium. Higher α values outside this range give rise to oscillations that indicate worsening graft function, with the minimal graft functionality of the oscillatory range reaching 27% as α approaches 0.7. For $\alpha > \sim 0.75$, outright graft failure is the only outcome and the ending graft functionality equilibrium value is 12%.

Simulations of Preconditioning Scenarios

In some simulations, an initial level of host tissue damage can act as a preconditioning factor in promoting graft survival. While the release of DAMPs from injured tissue incites pro-inflammatory components, the cascade also involves induction of anti-inflammatory mediators. If the pro-inflammatory levels from this initial surgical DAMP release are below some threshold, and the corresponding anti-inflammatory cell/mediator levels are above

some threshold at the time the additional DAMP release happens from an IR-injured graft, then an attenuated damage response may be possible. We depict one such simulation experiment of this preconditioning phenomenon, shown in **Figure 5**. This type of preconditioning, in which the response to a second insult is lower than that for the first, is called "tolerance" and has been reported widely in multiple settings of acute inflammation (62, 63). Indeed, a similar tolerance phenomenon was reproduced in a mathematical model of the host immune response to repeated endotoxin challenge (64). That study also demonstrated that repeated endotoxin challenges that were not timed carefully displayed potentiation of the inflammatory response, another manifestation of preconditioning typically known as priming (65). The analogous potentiation feature was seen in the present model in **Figure 3D** even with no mismatch factor present. We interpret this outcome to be similar to the scenario in which a graft is rejected, and the patient undergoes repeat transplantation. The outcomes in this setting are known to be poor (44, 66). Thus, the timing of the excitatory and inhibitory mechanisms involved in the entire transplant process is important to understand in order for therapeutic strategies to positively synergize with these events.

Discussion

The integrated nature of inflammatory and antigen-specific immunity that underlie the response to organ transplantation has largely defied a synthetic understanding. This complexity can often be observed in the form of emergent phenomena that cannot be predicted based on an understanding of the component parts of the immune system, and may be at the root of the need for life-long immunosuppression post-transplantation. We suggest that the development of novel treatment strategies for organ transplantation can be aided greatly by mechanistic mathematical models such as the one presented here, because inevitably, independent mechanisms must be integrated in order to predict higher-order system properties in a clinically relevant manner. We regard a mechanistic model as one that describes "rules" for how the individual model components interact and evolve with time. We use the term "mechanistic" to distinguish this type of model from statistical or data-driven models, in which quantitative associations are defined, rather than abstracted mechanisms.

The past decade has witnessed such a synthesis in the form of simplified (reduced-order) computational models of acute inflammation, which have yielded useful insights into the mechanisms and pathophysiology of critical illness (64, 67–69). However, such models are at best only capable of general, high-level predictions, which are not sufficiently specific so as to be testable in individual patients or in *in vitro/in vivo* experiments. Alternatively, modeling biological systems in a realistic fashion often necessitates complex, large-scale models describing the underlying system dynamics (54, 70, 71). An important advantage of such mechanistic models is that they can allow for quantitative predictions (48, 49, 56, 72–76) and clinically translational connections of molecular mechanisms to pathophysiology (77), with the ultimate goal of improving the drug development process (78).

Mechanistic models have helped suggest the central role of DAMPs in acute inflammation (49, 75–76, 79–84). Mechanistic

modeling has also helped elucidate the forces driving inflammatory preconditioning, namely the different inflammatory responses that ensue when multiple stimuli are given in succession (64, 85–90). Other applications of mechanistic modeling involve the understanding of multifactorial therapies for acute inflammatory diseases (91, 92). Key translational applications such as *in silico* clinical trials based on mechanistic models of inflammation and damage/dysfunction were pioneered in the arena of acute inflammation (71, 93, 94). These models have grown in sophistication, and are beginning to show the potential for predicting the inflammatory responses of large, outbred animals (78, 95, 96) and individual human subjects (71, 97, 98).

The unmet need for new treatments and diagnostic modalities allowing ultimately for long-term graft survival with low or no immunosuppression in organ transplantation is acute. While decades of work have led to many novel insights from the molecular to the physiological level, the net result has remained centered around life-long immunosuppression. We suggest that this is not because the effort has not been worthwhile or because promising candidate approaches were not pursued. Rather, it is our contention that what has not taken place is the process of synthesis of these insights into a larger whole. Computational modeling is a promising avenue for such synthesis; however, the current approach is based purely on statistical tools by which to associate multiple variables to outcomes.

In the present study, we created a mechanistic mathematical model based on ODEs that describe key mechanisms of innate and adaptive immunity and that span the full process of transplantation. This model focuses on the very early inflammatory events linked to the surgery, IRI, and memory T cell attack, events cross-modulated by each other and which translate into significant subclinical and clinical manifestations in only a subset of organ transplant recipients. However, these complex, early inflammatory events, as they do occur, may set the tone for either excellent or poor long-term allograft and patient outcomes. Thus, key outputs of our model include the prediction of that surgical injury and I/R-induced graft damage can be well-tolerated by the recipient when each is present alone, but that their combination (along with antigenic mismatch) may lead to acute rejection, as seen clinically in a subset of patients (38, 47). An emergent phenomenon from our simulations is that low-level DAMP release can tolerize the recipient to a mismatched allograft, whereas different restimulation regimens can drive an exaggerated rejection response. This former prediction is in agreement with published studies showing that preconditioning with the DAMP high-mobility group box 1 (HMGB1) can reduce the severity of inflammation and damage in the setting of graft IRI (99).

Limitations of this mechanistic mathematical model reside in the fact that the induction therapy and the maintenance immunosuppression are not considered in the model, and this is an area for expansion and augmentation of our modeling work. Moreover, this mechanistic mathematical model that predicts early innate and adaptive immune events is a generic one: each organ may have its own distinctive signature of early immune events. Thus, further augmentation of our model would involve making organ-specific variants. Additional limitations include the fact that this is a relatively abstract model, in which multiple

mechanisms are lumped into single variables. As such, this model cannot be directly verified in a quantitative manner, other than as concerns the relative timing of various events. One key area where this limitation is apparent concerns the aforementioned emergent tolerization behavior as a function of prior exposure to damaged graft tissue, which we hypothesize as being due to DAMPs such as HMGB1 (99). Given tolerization is a manifestation of similar mechanisms to those that drive injury, and that HMGB1 can drive hepatic injury through activation of DCs (100), it is tempting to speculate that DCs are a key cell type in this process. Thus, future modeling work focused on examining this tolerization mechanism (or alternative mechanisms) in the context on organ-specific environments is warranted. In addition, a greater in-depth mathematical analysis can be done to gain deeper insights into the dynamics, which becomes especially helpful when the models are more closely tied to experimental and clinical data.

Despite these limitations, this model was capable of reproducing a rich set of biological and clinical behaviors. Simulations of this model under various initial conditions of IRI, graft injury, and degree of antigenic mismatch yielded a broad spectrum of outcomes from nearly complete graft function to outright (acute or chronic) rejection. Importantly, this model also yielded behaviors such as tolerization (durable unresponsiveness to donor-antigens) through preconditioning, as well as the harmful alternative outcome of more severe graft failure upon retransplantation. Future iterations of this model could address these limitations and additionally explore the effects of variability that would naturally exist from patient to patient with respect to host health and immune function (94). Consequently, mathematical/engineering control methodologies could be employed on the models to suggest early therapeutic intervention strategies for this complex immune system (101).

In conclusion, we suggest that this model is a stepping stone toward further insights, not only into the response to allotransplantation but also for other disease states. Several diseases with or without an immunologic trigger have been recently determined to have inflammation as a common fingerprint. Therefore, understanding diseases according to their common biological mechanism and using systems biology, mathematical modeling, and bioinformatics/data-driven modeling methods to interrogate the immune response before, during, and after perturbation will help not only to predict clinical outcomes but also guide prompt and precise targeting of new therapies (46, 102).

Materials and Methods

We formulate the model by building upon the approach and principles of prior modeling work to provide the foundation for the current model (64, 69). In this prior work, an abstract, four-equation model of the acute inflammatory response to bacterial pathogen and to Gram-negative bacterial endotoxin was developed. The approach considered various subsystems as a way to tractably analyze and calibrate the qualitative behavior of parts of the larger system to gain a greater understanding of which entities governed certain dynamic properties in the larger system. We refer to this modeling process as a “subsystem modeling approach.” The Reynolds et al.’s model displayed rich qualitative

behavior that corresponded to multiple clinical outcomes seen in cases of severe systemic inflammation due to bacterial pathogen and experimental studies of endotoxemia and tolerance. The general dynamical components of this prior model, when considered without a pathogenic or endotoxin insult, also correspond well to an abstract representation of the immune response to traumatic insult. Thus, the current model adopts a similar strategy and mindset for the development of the current model of immune responses in transplantation.

All model simulations and analysis were performed with XPPAUT (103). To create **Figures 2–5**, the numerical data produced from the XPPAUT simulations were exported to MATLAB® (R2013b, The Mathworks Inc., Natick, MA, USA). Additional calculations were performed with MAPLE (2015, Maplesoft™, Waterloo, ON, Canada). The complete mathematical model given by the ODE system (1)–(6) was analyzed using the subsystems approach mentioned above wherein the dynamics of a few interacting variables are examined prior to combining the equations altogether. Parameter values used in this section can be found in **Table 4**. In the subsystems we discuss throughout this section, of most interest is the number and stability properties of equilibria and how these change with parameter value changes. Equilibria of a system of differential

equations occur at the intersections of nullclines which are the equations resulting from setting each differential equation to zero and solving the resulting system of algebraic equations. The points that satisfy this are naturally the system states at which there is zero rate of change (e.g., $\frac{dx}{dt} = 0$), indicating an equilibrium state or fixed point. The dynamics of the ODE system are organized around these special points. For a system of two variables, the nullclines are especially useful for a geometric analysis of the system states and to observe how the shapes and positions of the nullclines change with changes to parameters or functional forms of the equation terms. Small perturbations of the system away from an equilibrium that cause the system solutions to return to the equilibrium as $t \rightarrow \infty$ define a locally asymptotically stable (or simply *stable*) equilibrium. If, on the other hand, the perturbation causes solutions to move away from said equilibrium, then we call the equilibrium *unstable*. We only concern ourselves with biologically feasible equilibria which are those in the positive orthant. The variables of the system are necessarily formulated to remain positive for all time and all parameters are positive as well. For more details regarding the terminology and mathematical analysis used, consult for instance (104).

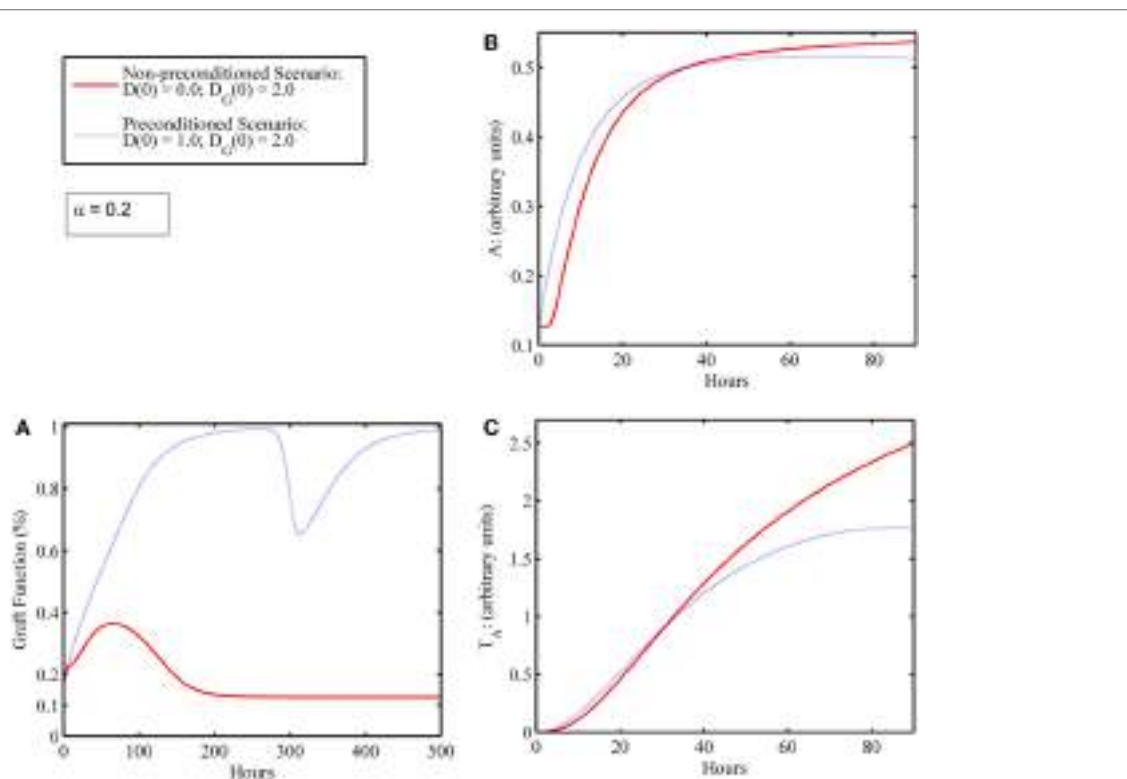


FIGURE 5 | Preconditioning phenomena: initial surgical IRI allows damaged graft to recover compared to scenario wherein graft failure occurs in the absence of initial surgical damage. **(A)** Graft functionality with (blue) and without (red) an initial level of host I/R damage, $D(0)$. Initial graft damage [$D_G(0) = 2$] along with a low initial level of host tissue damage [$D(0) = 1$] results in graft recovery to full functionality (blue); whereas initial graft damage [$D_G(0) = 2$] without the low initial level of host damage [$D(0) = 0$] leads to graft failure (red). **(B)** The anti-inflammatory components, A , and **(C)** anti-inflammatory T cells, T_A , with (blue) and without (red) an initial level of host IRI, $D(0)$. Comparing the red and blue time courses for both anti-inflammatory variables (A and T_A) in **(B,C)**, one observes a slight increase in levels (blue above red) in the first 24 h or so. This increase in the anti-inflammatory variables (especially of A) induced by the very inflammatory cascade that was due to DAMP release actually allows for graft survival.

$$\frac{dI}{dt} = \frac{s_{ir}R}{\mu_{ir} + R} - \underbrace{\mu_i I}_{\text{Loss due to natural decay}}, \quad (1)$$

See equation for R below; gain from activation of resting/circulating innate components by host and graft damage-induced DAMPs release and activated pro-inflammatory innate and T cell components; inhibited by anti-inflammatory components, A

where $R = \frac{k_{id}(D + D_G) + k_{ii}I + k_{itp}T_p}{1 + (A/a_\infty)^2}$ (see Table 3);

$$\frac{dD}{dt} = k_{di} \cdot f \left(\frac{I}{1 + (A/a_\infty)^2} \right) - \underbrace{\mu_d D}_{\text{Loss due to tissue repair/regeneration}}, \quad (2)$$

$f(x) = \frac{x^6}{x^6 + x_{di}^6}$; Gain from injurious effects of pro-inflammatory innate components on host tissue
Inhibition by I-associated anti-inflammatory components, A

$$\frac{dD_G}{dt} = -\underbrace{\mu_d D_G}_{\text{Loss due to tissue repair/regeneration}} + k_{dig}G \cdot f \left(\frac{I}{1 + (A/a_\infty)^2} \right) \quad (3)$$

Gain from injurious effects of pro-inflammatory innate components on graft tissue
Inhibition by I-associated anti-inflammatory components, A

$$+ \alpha k_{dgt} G f \left(\frac{T_p}{1 + (T_A/b_\infty)^2} \right), \quad (3)$$

Gain from injurious effects on graft tissue by alloreactive memory T-cells
Inhibition by anti-inflammatory T-cells

$$\frac{dA}{dt} = -\underbrace{\mu_a A}_{\text{Loss due to natural decay}} + \underbrace{s_a}_{\text{Source term}} + \frac{(I + k_{aid}D) / \left(1 + (A/a_\infty)^2 \right)}{1 + \left((I + k_{aid}D) / \left(1 + (A/a_\infty)^2 \right) \right)}, \quad (4)$$

Gain from production by innate pro-inflammatory components and host tissue damage with saturation and with self-regulating inhibition

$$+ \underbrace{k_{ata} T_A}_{\text{Gain from production by regulatory/anti-inflammatory T-cells, T_A}},$$

$$\frac{dT_p}{dt} = k_{tpi} T_0 \frac{I}{1 + \left(T_A/b_\infty \right)^2} + \underbrace{\alpha k_{tpig} T_0 \frac{I \cdot G}{1 + \left(T_A/b_\infty \right)^2}}_{\text{Gain from activation of T cells by alloreactive innate components, I; G; inhibited by regulatory/anti-inflammatory T cells, T_A}} + \underbrace{\alpha \cdot k_{tpog} T_0 \frac{T_p \cdot G}{1 + \left(T_A/b_\infty \right)^2}}_{\text{Gain from activation of T cells by alloreactive activated T cells, Tp-G; inhibited by regulatory/anti-inflammatory T cells, T_A}} - \underbrace{\mu_{tp} T_p}_{\text{Loss due to natural decay}}, \quad (5)$$

$$\frac{dT_A}{dt} = \underbrace{k_{taia} T_0 \cdot I \cdot A}_{\text{Gain from activation of T cells by innate components, I, in the presence of anti-inflammatory components, A}} + \underbrace{\alpha \cdot k_{tagt} T_0 \cdot G \cdot \frac{T_A}{1 + T_A}}_{\text{Gain from activation of T cells by alloreactive activated T regulatory/anti-inflammatory T cells, TA-G, with saturation}} - \underbrace{\mu_{ta} T_A}_{\text{Loss due to natural decay}}, \quad (6)$$

D_{Total/I} Subsystem: Total Damage and Early Innate Components

We will first consider a subsystem that examines the dynamics of tissue damage and associated DAMP release with the early innate components of interest herein, as described in **Table 1**. In (69), it was shown that a similar subsystem involving damage and early pro-inflammatory phagocytes contained a stable healthy equilibrium as well as another stable equilibrium corresponding to elevated damage and elevated immune components. We build upon the structure developed there to construct our subsystem here and discuss the resulting analysis afterward. We note that the terms contained within the ODEs that we formulate are based on the principle of mass action kinetics. For instance, **Table 5** provides the system of reactions involving the resting/circulating innate components, I_R , and the activated innate components, I . **Table 3** then provides the details on how we use a quasi-steady-state assumption to reduce the I_R/I system to a single equation, based on the rapid nature of the activation process.

For the analysis of the D_{Total}/I subsystem, we model the activation of resting/circulating pro-inflammatory innate components as described in Section “Deciphering the Complexity of Inflammation and Immunity with Mathematical Models” but ignore for now any inhibitory effects from anti-inflammatory components or additional activation by pro-inflammatory T cells and thus arrive at Eq. 7.

$$\frac{dI}{dt} = \frac{s_{ir}(k_{id}D_{Total} + k_{ii}I)}{\mu_{ir} + (k_{id}D_{Total} + k_{ii}I)} - \mu_i I \quad (7)$$

$$\frac{dD_{\text{Total}}}{dt} = \underbrace{k_{\text{di}} \cdot f(I)}_{\text{Gain from effects of early innate components on host tissue}} - \underbrace{\mu_d(D_{\text{Total}})}_{\text{Loss from tissue repair/regeneration}} + \underbrace{k_{\text{dig}} \cdot f(I \cdot G)}_{\text{Gain from effects of early innate components on graft tissue}}, \quad (8)$$

$$\text{where } f(x) = \frac{x^6}{x^6 + x_{\text{di}}^6}.$$

The total tissue damage can be modeled by combining tissue injury caused (a) to host tissues from the early innate components responding to DAMP release and (b) to the graft, G , by either early innate components, I , or by pro-inflammatory T cells, T_B , the latter of which is ignored for the analysis of the D_{Total} /I subsystem. Thus, we formulate Eq. 8, where a decay term of the total damage is also incorporated to account for a combination of tissue repair and regeneration. Graft health, G , is a function of graft damage, D_G as discussed in **Table 3**. Note that since Eq. 8 is for total damage and not just graft damage, the parameters k_{gdg} and x_{gdg} have a slightly different meaning in this subsystem than they will in the full system, where the D_{Total} equation is separated into two equations: one to represent the damage to the host, D , and another to represent the damage to the graft, D_G . This

separation is done later in order to distinguish between damage done in general and graft-specific damage. Additionally, the inhibitory effects of anti-inflammatory components, A and T_A , are later incorporated as is the additional damage to graft tissue by activated pro-inflammatory T cell subsets, T_P .

As in (69), we assume that the ability of the innate immune components to create damage saturates when these components are very large relative to their baseline levels. We also incorporate the Hill-type function given as $f(x)$ under Eq. 8 with a hill-coefficient of 6. We note that the choice of a hill coefficient in Reynolds et al. was made to ensure that the healthy equilibrium of the subsystem has a reasonable basin of attraction. Using the parameter values given in **Table 4**, this modified system behaves as in the prior work, with the I and D_{Total} nullclines intersecting at $(0,0)$ and at two additional points in the positive quadrant. The “healthy equilibrium” $(D_{\text{Total}}, I) = (0,0)$ is locally asymptotically stable when $\mu_i > \frac{s_{ir} k_{ii}}{\mu_{ir}}$, which is the same criteria reached in (69) for the analogous parameters, even with the modifications made for this current focus. Furthermore, an unstable saddle equilibrium separates the basins of attraction of the healthy equilibrium and the other stable equilibrium $(D_{\text{Total}}, I) \approx (1.2, 17.5)$, as observed in the prior work. Thus, the underlying structure of bi-stability is

TABLE 3 | Auxiliary model variables.

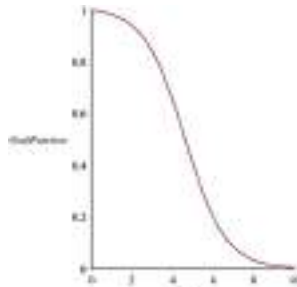
Auxiliary variables	Variable description, equation, and modeling explanation
I_R	<p>Resting/Circulating population of I components, such as neutrophils and monocytes, from which the I population is activated. When the I_R population is activated into I, via DAMPs for example, we assume that the activation is rapid and employs a quasi-steady state assumption. (See Table 5 for reactions governing I_R and I.) The result is incorporated into the equations in which I_R appears. (arbitrary units: I_R-units)</p> $I_R = \frac{s_{ir}}{\mu_{ir} + k_{id}(D + D_G) + k_{ii}I + k_{ip}T_P},$ <p>derived from assuming that the following equation is in quasi-steady state:</p> $\frac{dI_R}{dt} = s_{ir} - \mu_{ir}I_R - (k_{id}(D + D_G) + k_{ii}I + k_{ip}T_P)I_R.$ <p>In the equation for I, we let $R = \frac{k_{id}(D + D_G) + k_{ii}I + k_{ip}T_P}{1 + (A/A_{\infty})^2}$ which incorporates the inhibitory effects of the anti-inflammatory mediators, represented in the variable, A, on the activation of I.</p>
T_0	<p>Population of inactivated memory T cells from which the T cell subsets, T_P and T_A, are produced. The T_0 population is also assumed to be in quasi-steady state and the result is incorporated into the equations in which T_0 appears. (arbitrary units: T_0-units)</p> $T_0 = \frac{s_{t0}(1 + T_A)}{\alpha k_{t0t0}T_A \cdot G + (\mu_{t0} + k_{tp}I + \alpha k_{tpig}I \cdot G + k_{ta}A \cdot I + \alpha k_{tpig}T_P \cdot G)(1 + T_A)},$ <p>derived from assuming that the following equation is in quasi-steady state:</p> $\frac{dT_0}{dt} = s_{t0} - \mu_{t0}T_0 - k_{tp}I \cdot T_0 - \alpha k_{tpig}T_0 \cdot I \cdot G - \alpha k_{tpig}T_0 \cdot T_P \cdot G - k_{ta}A \cdot I \cdot T_0 - \alpha k_{t0t0}T_0 \cdot G \frac{T_A}{1 + T_A}.$
G	<p>Graft health/functionality; measured as a percentage with 0 indicating 0% functionality and 1 indicating 100% functionality. Graft health is defined as a function of associated graft damage, D_G:</p> $G = 1 - \frac{1 - e^{\frac{-D_G}{k_{gdg}}}}{1 + k_{gdg}e^{\frac{-D_G}{k_{gdg}}}}$ <p>[Frame1] The parameters k_{gdg} and x_{gdg} scale the level of the variable D_G to relate it to the loss of graft functionality, denoted by the term $\frac{1 - e^{\frac{-D_G}{k_{gdg}}}}{1 + k_{gdg}e^{\frac{-D_G}{k_{gdg}}}}$ in the equation for G.</p> <p>See inset figure for an example response curve of G.</p> 

TABLE 4 | Model parameters.

Name	Description/source	Value/units	Name	Description/source	Value/units
K_{ii}^*	Activation of innate components by previously activated innate pro-inflammatory components	0.01/ I -units/h	S_a^*	Source term for anti-inflammatory components (A)	0.0125 A -units/h
S_{ir}^*	Source of resting/circulating inactivated innate pro-inflammatory components	0.08 I_R -units/h	k_{ai}^*	Maximum induction rate of anti-inflammatory components by activated pro-inflammatory innate components	0.04 A -units/h
μ_{ir}^*	Natural decay/turnover rate of resting/circulating inactivated pro-inflammatory innate components	0.12/h	k_{aid}^*	Relative effectiveness of activated pro-inflammatory innate components and damaged tissue/DAMPs to induce anti-inflammatory components (A)	48.0 I -units/ D -units
μ_i^*	Natural decay/turnover rate of activated pro-inflammatory innate components	0.05/h	μ_a^*	Decay rate of anti-inflammatory components (A)	0.1/h
k_{id}^*	Activation of resting/circulating pro-inflammatory innate components by DAMP release from damaged host and graft tissue	0.02/ $(D-D_G)$ -units/h	k_{ata}	Maximum induction rate of anti-inflammatory components (A) by anti-inflammatory T cells (T_A)	0.001/ A -units/ T_A -units/h
k_{tp}	Activation of resting/circulating pro-inflammatory innate components by activated/memory pro-inflammatory T cells	0.008/ T_P -units/h	S_{i0}	Source of inactivated memory T cells	1.0 T_0 -units/h
k_{di}^*	Maximum rate of host tissue damage by activated pro-inflammatory innate components	0.35 D -units/h	μ_{i0}	Decay rate of inactivated memory T cells, T_0 .	0.05/h
x_{di}^*	Determines level of activated pro-inflammatory innate components that increases damage production to half its max	0.06 I -units	k_{tpi}	Maximum activation rate of memory T cells by pro-inflammatory innate components	0.008/ I -units/h
k_{dgig}	Maximum rate of graft tissue damage by activated pro-inflammatory innate components	0.35 D_G -units/h	k_{tpig}	Maximum activation rate of memory T cells by pro-inflammatory innate components in the presence of allo-Ag	0.02/ I -units/h
μ_d^*	Decay rate of host and of graft tissue damage representing repair/regeneration of injured tissue	0.02/h	k_{tpi0g}	Maximum activation rate of memory T cells by alloreactive activated memory T cells	0.02/h
α	Scaling parameter that governs the level of apparent mismatch between host and graft $\alpha = 0$ indicates 0% mismatch; $\alpha = 1$ indicates 100% mismatch	$\alpha \in [0,1]$ dimension-less	μ_{ip}	Decay rate of activated pro-inflammatory memory T cells	0.03/h
k_{dgtP}	Maximum rate of damage by pro-inflammatory T cells to graft tissue scaled by the parameter α ; set to be greater than k_{id} and k_{dgig} to indicate greater potency of alloreactive T cells	0.7 D_G -units/h	k_{taia}	Maximum induction of anti-inflammatory T cells by pro- and anti-inflammatory innate components	0.04/ I -units/ A -units/h
x_{dgtP}	Determines the level of pro-inflammatory T cells that increases graft tissue damage to half its max	1 D_G -units	k_{taioG}	Maximum activation rate of anti-inflammatory T cells by already activated alloreactive anti-inflammatory T cells	0.001/h
k_{gdg}	Tuning parameter that governs the response curve of the graft function, G (See Table 3)	10 dimension-less	μ_{ta}	Decay rate of activated anti-inflammatory T cells	0.03/h
x_{gdg}	Tuning parameter that governs the response curve of the graft function, G (See Table 3)	0.5 D_G -units	b_{∞}	Controls the strength at which the anti-inflammatory T cells (T_A) inhibit various processes	0.5 T_A -units
a^*	Controls the strength at which the anti-inflammatory components (A) inhibit various processes	0.28 A -units			

Parameters marked with an asterisk retain the baseline value as set in (69).

TABLE 5 | Reactions involved in the I_R/I subsystem.

$I_R \xrightarrow{k_{ir}(D+D_G)+k_{ip}I+k_{tp}T_p} I$	Activation of resting/circulating innate components, I_R , by damaged host tissue, D , damaged graft tissue, D_G , activated innate cells or mediators, I , and pro-inflammatory T cells, T_p
$* \xrightarrow{s_{ir}} I_R$	Source of resting/circulating innate components, I_R
$I_R \xrightarrow{\mu_r} *$	Natural decay of resting/circulating innate components, I_R
$I \xrightarrow{\mu_i} *$	Natural decay of activated innate components, I

present in the D_{Total}/I subsystem we developed here. This means that the system has the ability to display different outcomes, depending on the initial conditions of the variables that we test. These outcomes are then translated qualitatively into clinical scenarios as discussed in Section “Results.”

Additionally, we know from the prior results that the incorporation of the anti-inflammatory component when treated as a constant will yield a loss of this bi-stability when the level of the anti-inflammatory component exceeds a value of 0.6264 and only the healthy equilibrium remains stable. Therefore, when we incorporate the analogous dynamic anti-inflammatory component, A , into the full model, we wish to make sure to calibrate any additions to A such that the maximum level of A does not exceed the 0.6264 threshold, since this would produce unreasonable (i.e., non-biological) behavior. For instance, if this threshold were exceeded, the D_{Total}/I subsystem would be incapable of reaching an unhealthy equilibrium while other components of the model, such as activated pro-inflammatory T cells or graft damage (when separated from total damage), would remain elevated. The conditions for bi-stability noted above will not be changed when we combine subsystems at the end.

The I/T_p Subsystem

$$\frac{dI}{dt} = \frac{s_{ir}k_{ii}I}{\mu_{ir} + k_{ii}I} - \mu_i I \quad (9)$$

$$\frac{dT_p}{dt} = k_{tp}T_0 \cdot I - \mu_{tp}T_p, \quad (10)$$

The I/T_p system has one or two non-negative equilibria depending on the parameter values. If we fix the values for the parameters that appeared in the D_{Total}/I system, the following parameters govern the number and stability of the equilibria: k_{tp} , s_{ir} , μ_{ir} , k_{ii} . The point $(I, T_p) = (0,0)$ is always an equilibrium and is stable for $k_{tp} = 0.01$, $s_{ir} = 1$, $\mu_{ir} = 0.05$, and $k_{ii} = 0.01$. Since we have an estimate for the half-life of activated T cells (unpublished work) which translates to a rate of 0.03/h, we estimate the half-life of inactivated memory T cells to be slightly longer than this at 0.05/h. Also we fix the source term, s_{ir} , to a value of 1 and then determine the values of k_{tp} and k_{ii} such that the $(0,0)$ equilibrium is stable and that the rate at which trajectories approach this equilibrium is not unduly slow, which is related to the position of the nullclines. For simplicity, we let $k_{tp}=k_{ii}$ since there is a lack of

information regarding the relative strength at which one incites the other. Setting the value of $k_{tp} = 0.008 = k_{ii}$ allows for each variable to contribute to recruiting the other by a non-negligible amount in this subsystem and are, as a pair of values, not too close to a bifurcation value where the nullclines would cross a second time. In other words, if their values are set to 0.01, for example, then $(0,0)$ will be unstable; however, we wish for this subsystem to have $(0,0)$ stable under these parameters so that neither I nor T_p will drive sustained T_p or I levels, respectively. Therefore, when connected to the damage equations, when each is sustained at an elevated equilibrium, this will depend on feedback from the damage they incite, rather than just each other.

The D_G/T_p (and G) Subsystem

$$\frac{dD_G}{dt} = -\mu_d D_G + \alpha k_{dgp} G \cdot f(T_p), \quad (11)$$

$$\text{where } f(x) = \frac{x^6}{x^6 + x_{di}^6};$$

$$\frac{dT_p}{dt} = \alpha \cdot k_{tp0} T_0 \cdot T_p \cdot G - \mu_{tp} T_p. \quad (12)$$

For the D_G/T_p subsystem that includes the auxiliary variable G , the same type of functional form used in modeling damage to host (D) via innate cells (I) is employed to model the graft damage, D_G , created by pro-inflammatory T cells, T_p . The parameter values are set according to **Table 4**. Bi-stability is not a feature of this system, but when there are no T_p T cells, then $(0,0)$ is always stable; and for low mismatch factor (i.e., $\alpha \leq 0.074$), $(0,0)$ is stable. As α increases through this, $(0,0)$ becomes unstable and a new equilibrium of interest is born and is stable (spiral). For values close to 0.075, the approach to the equilibrium is quite slow away from the stable manifolds of the equilibrium. When $\alpha = 0.08$, the positive equilibrium is a stable spiral which establishes the presence of damped oscillations in this subsystem. Naturally, as T cells destroy graft tissue, there is less tissue to destroy, but as the tissue regenerates, the T cells can then destroy this regenerated tissue. Also, as T cell numbers increase the source for new ones is depleted until the turnover/death of existing activated T cell subsets allow for the activation of more (literally the way the source/recruitment term is modeled) – this could be interpreted as a wait time for replenishment of the T cell source from the bone marrow. Understanding the tissue repair process and time scale relative to T cell behavior could help calibrate this aspect better. For instance, tissue repair/regeneration may be hindered significantly in disease states and therefore may depend on the existing level of damaged tissue.

The $D_G/T_p/I$ (and G) Subsystem

The $D_G/T_p/I$ subsystem which includes the auxiliary variable G is given by Eqs 13 and 14 and displays bi-stability for the parameters listed in **Table 4** (with $\alpha = 0$). Note that the D_{Total}/I subsystem is partially contained in this 3-variable subsystem. Initial graft damage values in which $D_G(0) > 0.095$ lead to graft/host failure. Recall that this behavior is in the absence of any anti-inflammatory

inhibition; so very little graft damage can lead to failure in this subsystem even without a positive mismatch factor. For very low initial graft damage [e.g., $D_G(0) = 0.08$ or ~2% graft damage] and for low graft mismatch (e.g., $\alpha = 0.01$), survival is possible. Though the ranges of pairs of values of initial graft damage and α that produce survival outcomes is limited, the presence of bistability exists and the presence of inhibitory components added later allow this range to increase. For some $D_G(0)$ and α value pairs [e.g., $D_G(0) = 0.08$ and $\alpha = 0.02$], graft functionality remains very high (~99%) for ~230 h (~1 week) after which it decreases rapidly to its ending steady-state functionality value of 13% by ~300 h.

If considering the presence of activated memory T cells at time zero [i.e., $T_p(0) > 0$], the time to graft failure greatly decreases. For example with $D_G(0) = 0.08$ and $\alpha = 0.02$, when $T_p(0) = 1$ functionality decreases to 13% by 50 vs. 300 h without an initial population of activated memory T cells. A similar result occurs when there is an initial population of activated innate inflammatory components, I . For example, with $D_G(0) = 0.08$, $\alpha = 0.02$, and $T_p(0) = 0$, when $I(0) = 0.01$, graft functionality decreases to 13% by 165 vs. 300 h without an initial population of activated innate inflammatory components.

$$\frac{dI}{dt} = \frac{s_{ir} R_i}{\mu_{ir} + R_i} - \mu_i I, \quad (13)$$

where $R_i = k_{id} D_G + k_{ii} I + k_{ip} T_p$;

$$\frac{dD_G}{dt} = -\mu_d D_G + k_{dgig} G \cdot f(I) + \alpha k_{dgtp} G f(T_p), \quad (14)$$

$$\text{where } f(x) = \frac{x^6}{x^6 + x_{di}^6};$$

$$\frac{dT_p}{dt} = k_{tpi} T_0 \cdot I + \alpha k_{tpig} T_0 \cdot I \cdot G + \alpha k_{tpog} T_0 \cdot T_p \cdot G - \mu_{tp} T_p. \quad (15)$$

References

- Shyu S, Dew MA, Pilewski JM, DeVito Dabbs AJ, Zaldonis DB, Studer SM, et al. Five-year outcomes with alemtuzumab induction after lung transplantation. *J Heart Lung Transplant* (2011) **30**(7):743–54. doi:10.1016/j.healun.2011.01.714
- Grant D, Abu-Elmagd K, Mazariegos G, Vianna R, Langnas A, Mangus R, et al. Intestinal transplant registry report: global activity and trends. *Am J Transplant* (2015) **15**(1):210–9. doi:10.1111/ajt.12979
- Hellemans R, Hazzan M, Durand D, Mourad G, Lang P, Kessler M, et al. Daclizumab versus rabbit antithymocyte globulin in high-risk renal transplants: five-year follow-up of a randomized study. *Am J Transplant* (2015) **15**(7):1923–32. doi:10.1111/ajt.13191
- Rosenblum JM, Kirk AD. Recollective homeostasis and the immune consequences of peritransplant depletional induction therapy. *Immunol Rev* (2014) **258**(1):167–82. doi:10.1111/imr.12155
- Arii S, Teramoto K, Kawamura T. Current progress in the understanding of and therapeutic strategies for ischemia and reperfusion injury of the liver. *J Hepatobiliary Pancreat Surg* (2003) **10**:189–94. doi:10.1007/s00534-002-0720-z
- Spahn JH, Li W, Kreisel D. Innate immune cells in transplantation. *Curr Opin Organ Transplant* (2014) **19**(1):14–9. doi:10.1097/MOT.0000000000000041

Anti-Inflammatory Effects

The parameter values for the anti-inflammatory components, A , were set as in Reynolds et al. where applicable and the additional parameters in this category were estimated to calibrate the baseline responses. For instance, the contribution of T_A to A was calibrated such that maximum T_A levels would not allow A to exceed its threshold value of 0.6264 as discussed previously. Additionally, in the case of severe initial tissue damage, it is possible that this positive feedback between DAMP release caused by tissue injury and inflammation causing further tissue injury may not resolve, and thus lead the way to multi organ failure and death. In the current state-of-the-art, the transplantation procedure and donor graft condition are such that the surgical procedure and associated I/R are typically not the cause of organ failure. However, theoretically, this scenario is possible and helps to calibrate the extreme cases of the model such that complete resolution is not the only outcome possible regardless of initial conditions and parameter values. Thus, the inhibitory effects of A and T_A combined do not overly and unrealistically dampen the inflammatory arm of the responses. We retain the positive background level of the anti-inflammatory component at the non-perturbed healthy equilibrium, A , as set in Reynolds et al.: $A(0) = A_0 = 0.125$ (69).

Acknowledgments

This work was partially supported by the National Science Foundation under Contract NSF-DMS 1122462 (JD) as well as by National Institute of General Medical Sciences grant P50-GM-53789 (YV). This work was inspired through participation in the *Lymphoid cells in acute inflammation* Investigative Workshop at the National Institute for Mathematical and Biological Synthesis, sponsored by the National Science Foundation through NSF Award #DBI-1300426, with additional support from The University of Tennessee, Knoxville.

- He H, Stone JR, Perkins DL. Analysis of differential immune responses induced by innate and adaptive immunity following transplantation. *Immunology* (2003) **109**(2):185–96. doi:10.1046/j.1365-2567.2003.01641.x
- Andrade CF, Waddell TK, Keshavjee S, Liu M. Innate immunity and organ transplantation: the potential role of toll-like receptors. *Am J Transplant* (2005) **5**(5):969–75. doi:10.1111/j.1600-6143.2005.00829.x
- Oberbarnscheidt MH, Lakkis FG. Innate allorecognition. *Immunol Rev* (2014) **258**:145–9. doi:10.1111/imr.12153
- Zhuang Q, Lakkis FG. Dendritic cells and innate immunity in kidney transplantation. *Kidney Int* (2015) **87**(4):712–8. doi:10.1038/ki.2014.430
- Lo D, Feng L, Li L, Carson MJ, Crowley M, Pauza M, et al. Integrating innate and adaptive immunity in the whole animal. *Immunol Rev* (1999) **169**:225–39. doi:10.1111/j.1600-065X.1999.tb01318.x
- Luster AD. The role of chemokines in linking innate and adaptive immunity. *Curr Opin Immunol* (2002) **14**(1):129–35. doi:10.1016/S0952-7915(01)00308-9
- Dempsey PW, Vaidya SA, Cheng G. The art of war: innate and adaptive immune responses. *Cell Mol Life Sci* (2003) **60**(12):2604–21. doi:10.1007/s00018-003-3180-y
- Eisenbarth SC, Cassel S, Bottomly K. Understanding asthma pathogenesis: linking innate and adaptive immunity. *Curr Opin Pediatr* (2004) **16**(6):659–66. doi:10.1097/01.mop.0000145920.00101.e4

15. Marshall JC, Charbonney E, Gonzalez PD. The immune system in critical illness. *Clin Chest Med* (2008) **29**(4):605–616, vii. doi:10.1016/j.ccm.2008.08.001
16. Venet F, Chung CS, Monneret G, Huang X, Horner B, Garber M, et al. Regulatory T cell populations in sepsis and trauma. *J Leukoc Biol* (2008) **83**(3):523–35. doi:10.1189/jlb.0607371
17. Palm NW, Medzhitov R. Pattern recognition receptors and control of adaptive immunity. *Immunol Rev* (2009) **227**(1):221–33. doi:10.1111/j.1600-065X.2008.00731.x
18. Oberg HH, Juricke M, Kabelitz D, Wesch D. Regulation of T cell activation by TLR ligands. *Eur J Cell Biol* (2011) **90**(6–7):582–92. doi:10.1016/j.ejcb.2010.11.012
19. Xiao W, Mindrinos MN, Seok J, Cuschieri J, Cuenca AG, Gao H, et al. A genomic storm in critically injured humans. *J Exp Med* (2011) **208**(13):2581–90. doi:10.1084/jem.20111354
20. Ferreira LM. Gammadelta T cells: innately adaptive immune cells? *Int Rev Immunol* (2013) **32**(3):223–48. doi:10.3109/08830185.2013.783831
21. Tang D, Kang R, Coyne CB, Zeh HJ, Lotze MT. PAMPs and DAMPs: signal 0s that spur autophagy and immunity. *Immunol Rev* (2012) **249**(1):158–75. doi:10.1111/j.1600-065X.2012.01146.x
22. Yang H, Antoine DJ, Andersson U, Tracey KJ. The many faces of HMGB1: molecular structure-functional activity in inflammation, apoptosis, and chemotaxis. *J Leukoc Biol* (2013) **93**(6):865–73. doi:10.1189/jlb.1212662
23. Jaeschke H. Reactive oxygen and mechanisms of inflammatory liver injury: present concepts. *J Gastroenterol Hepatol* (2011) **26**(Suppl 1):173–9. doi:10.1111/j.1440-1746.2010.06592.x
24. Rosin DL, Okusa MD. Dangers within: DAMP responses to damage and cell death in kidney disease. *J Am Soc Nephrol* (2011) **22**(3):416–25. doi:10.1681/ASN.2010040430
25. Zelenay S, Reis e Sousa C. Adaptive immunity after cell death. *Trends Immunol* (2013) **34**(7):329–35. doi:10.1016/j.it.2013.03.005
26. Pouwels SD, Heijink IH, ten Hacken NH, Vandenabeele P, Krysko DV, Nawijn MC, et al. DAMPs activating innate and adaptive immune responses in COPD. *Mucosal Immunol* (2014) **7**(2):215–26. doi:10.1038/mi.2013.77
27. Rao J, Lu L, Zhai Y. T cells in organ ischemia reperfusion injury. *Curr Opin Organ Transplant* (2014) **19**(2):115–20. doi:10.1097/MOT.0000000000000064
28. Wilhelm MJ, Pratschke J, Laskowski I, Tilney NL. Ischemia and reperfusion injury. *Transplant Rev* (2003) **17**:140–57. doi:10.1016/S0955-470X(03)00040-5
29. Foley DP, Chari RS. Ischemia-reperfusion injury in transplantation: novel mechanisms and protective strategies. *Transplant Rev* (2007) **21**:43–53. doi:10.1016/j.trre.2007.01.004
30. Kosiradzki M, Rowiński W. Ischemia/reperfusion injury in kidney transplantation: mechanisms and prevention. *Transplant Proc* (2008) **40**:3279–88. doi:10.1016/j.transproceed.2008.10.004
31. Kaczorowski DJ, Tsung A, Billiar TR. Innate immune mechanisms in ischemia/reperfusion. *Front Biosci (Elite Ed)* (2009) **1**:91–8. doi:10.2741/e10
32. Mannon RB. Macrophages: contributors to allograft dysfunction, repair, or innocent bystanders? *Curr Opin Organ Transplant* (2012) **17**(1):20–5. doi:10.1097/MOT.0b013e32834ee5b6
33. Huang H, Tohme S, Al-Khafaji AB, Tai S, Loughran P, Chen L, et al. DAMPs-activated neutrophil extracellular trap exacerbates sterile inflammatory liver injury. *Hepatology* (2015) **62**(2):600–14. doi:10.1002/hep.27841
34. Hochegger K, Schatz T, Eller P, Tagwerker A, Heininger D, Mayer G, et al. Role of alpha/beta and gamma/delta T cells in renal ischemia-reperfusion injury. *Am J Physiol Renal Physiol* (2007) **293**(3):F741–7. doi:10.1152/ajprenal.00486.2006
35. Shichita T, Sugiyama Y, Ooboshi H, Sugimori H, Nakagawa R, Takada I, et al. Pivotal role of cerebral interleukin-17-producing gammadeltaT cells in the delayed phase of ischemic brain injury. *Nat Med* (2009) **15**(8):946–50. doi:10.1038/nm.1999
36. Satpute SR, Park JM, Jang HR, Agreda P, Liu MC, Gandolfo MT, et al. The role for T cell repertoire/antigen-specific interactions in experimental kidney ischemia reperfusion injury. *J Immunol* (2009) **183**(2):984–92. doi:10.4049/jimmunol.0801928
37. Shen X, Wang Y, Gao F, Ren F, Busuttil RW, Kupiec-Weglinski JW, et al. CD4 T cells promote tissue inflammation via CD40 signaling without de novo activation in a murine model of liver ischemia/reperfusion injury. *Hepatology* (2009) **50**(5):1537–46. doi:10.1002/hep.23153
38. Li XC, Kloc M, Ghobrial RM. Memory T cells in transplantation – progress and challenges. *Curr Opin Organ Transplant* (2013) **18**(4):387–92. doi:10.1097/MOT.0b013e3283626130
39. Gandolfo MT, Jang HR, Bagnasco SM, Ko GJ, Agreda P, Satpute SR, et al. Foxp3+ regulatory T cells participate in repair of ischemic acute kidney injury. *Kidney Int* (2009) **76**(7):717–29. doi:10.1038/ki.2009.259
40. Liesz A, Suri-Payer E, Veltkamp C, Doerr H, Sommer C, Rivest S, et al. Regulatory T cells are key cerebroprotective immunomodulators in acute experimental stroke. *Nat Med* (2009) **15**(2):192–9. doi:10.1038/nm.1927
41. Feng M, Wang Q, Zhang F, Lu L. Ex vivo induced regulatory T cells regulate inflammatory response of Kupffer cells by TGF-beta and attenuate liver ischemia reperfusion injury. *Int Immunopharmacol* (2012) **12**(1):189–96. doi:10.1016/j.intimp.2011.11.010
42. Riquelme P, Tomiuk S, Kammler A, Fandrich F, Schlitt HJ, Geissler EK, et al. IFN-gamma-induced iNOS expression in mouse regulatory macrophages prolongs allograft survival in fully immunocompetent recipients. *Mol Ther* (2013) **21**(2):409–22. doi:10.1038/mt.2012.168
43. Page AJ, Ford ML, Kirk AD. Memory T-cell-specific therapeutics in organ transplantation. *Curr Opin Organ Transplant* (2009) **14**(6):643–9. doi:10.1097/MOT.0b013e328332bd4a
44. Salvadori M, Bertoni E. Renal transplant allocation criteria, desensitization strategies and immunosuppressive therapy in retransplant renal patients. *J Nephrol* (2012) **25**(6):890–9. doi:10.5301/jn.5000207
45. Zwang NA, Turka LA. Homeostatic expansion as a barrier to lymphocyte depletion strategies. *Curr Opin Organ Transplant* (2014) **19**(4):357–62. doi:10.1097/MOT.0000000000000096
46. McDonald-Hyman C, Turka LA, Blazar BR. Advances and challenges in immunotherapy for solid organ and hematopoietic stem cell transplantation. *Sci Transl Med* (2015) **7**(280):280rv282. doi:10.1126/scitranslmed.aaa6853
47. Mehta R, Sood P, Cherukuri A, Chen S, Mour G, Wu C, et al. Impact of subclinical rejection (SCR) and acute clinical (ACR) in renal transplant recipients [abstract]. *Am J Transplant* (2015) **15**(Suppl 3). Available from: <http://www.atcmeetingabstracts.com/abstract/impact-of-subclinical-rejection-scr-and-acute-clinical-acr-in-renal-transplant-recipients/>
48. Vodovotz Y, Billiar TR. *In silico* modeling: methods and applications to trauma and sepsis. *Crit Care Med* (2013) **41**(8):2008–14. doi:10.1097/CCM.0b013e31829a6eb4
49. Vodovotz Y, An G. *Complex Systems and Computational Biology Approaches to Acute Inflammation*. New York, NY: Springer (2013).
50. An G, Vodovotz V. *Translational Systems Biology: Concepts and Practice for the Future of Biomedical Research*. New York, NY: Elsevier (2014).
51. Folcik VA, An GC, Orosz CG. The basic immune simulator: an agent-based model to study the interactions between innate and adaptive immunity. *Theor Biol Med Model* (2007) **4**:39. doi:10.1186/1742-4682-4-39
52. Klinke DJ II. A multi-scale model of dendritic cell education and trafficking in the lung: implications for T cell polarization. *Ann Biomed Eng* (2007) **35**(6):937–55. doi:10.1007/s10439-007-9318-6
53. Gurarie D, Karl S, Zimmerman PA, King CH, St Pierre TG, Davis TM. Mathematical modeling of malaria infection with innate and adaptive immunity in individuals and agent-based communities. *PLoS One* (2012) **7**(3):e34040. doi:10.1371/journal.pone.0034040
54. Carbo A, Hontecillas R, Kronsteiner B, Viladomiu M, Pedragosa M, Lu P, et al. Systems modeling of molecular mechanisms controlling cytokine-driven CD4+ T cell differentiation and phenotype plasticity. *PLoS Comput Biol* (2013) **9**(4):e1003027. doi:10.1371/journal.pcbi.1003027
55. Edelstein-Keshet L. *Mathematical Models in Biology*. New York, NY: Random House (1988).
56. Vodovotz Y, Constantine G, Rubin J, Csete M, Voit EO, An G. Mechanistic simulations of inflammation: current state and future prospects. *Math Biosci* (2009) **217**:1–10. doi:10.1016/j.mbs.2008.07.013
57. Lagoa CE, Bartels J, Baratt A, Tseng G, Clermont G, Fink MP, et al. The role of initial trauma in the host's response to injury and hemorrhage: insights from a correlation of mathematical simulations and hepatic transcriptomic analysis. *Shock* (2006) **26**:592–600. doi:10.1097/01.shk.0000232272.03602.0a

58. Oberbarnscheidt MH, Zeng Q, Li Q, Dai H, Williams AL, Shlomchik WD, et al. Non-self recognition by monocytes initiates allograft rejection. *J Clin Invest* (2014) **124**:3579–89. doi:10.1172/JCI74370
59. Bogdan C, Vodovotz Y, Nathan C. Macrophage deactivation by interleukin 10. *J Exp Med* (1991) **174**(6):1549–55. doi:10.1084/jem.174.6.1549
60. de Waal Malefyt R, Abrams J, Bennett B, Figdor CG, de Vries JE. Interleukin 10(IL-10) inhibits cytokine synthesis by human monocytes: an autoregulatory role of IL-10 produced by monocytes. *J Exp Med* (1991) **174**(5):1209–20. doi:10.1084/jem.174.5.1209
61. Svetritina V, Jakubovsky J, Hulin I. *Inflammation and Fever. Pathophysiology: Principles of Diseases*. Academic Electronic Press (1995).
62. Cavaillon JM, Pitton C, Fitting C. Endotoxin tolerance is not a LPS-specific phenomenon: partial mimicry with IL-1, IL-10, and TGF- β . *J Endotoxin Res* (1994) **1**:21–9.
63. Cavaillon JM. The nonspecific nature of endotoxin tolerance. *Trends Microbiol* (1995) **3**(8):320–4. doi:10.1016/S0966-842X(00)88963-5
64. Day J, Rubin J, Vodovotz Y, Chow CC, Reynolds A, Clermont G. A reduced mathematical model of the acute inflammatory response: II. Capturing scenarios of repeated endotoxin administration. *J Theor Biol* (2006) **242**(1):237–56. doi:10.1016/j.jtbi.2006.02.015
65. Johnston RB Jr, Kitagawa S. Molecular basis for the enhanced respiratory burst of activated macrophages. *Fed Proc* (1985) **44**(14):2927–32.
66. Zahr Eldeen F, Mabrouk Mourad M, Liossis C, Bramhall SR. Liver retransplant for primary disease recurrence. *Exp Clin Transplant* (2014) **12**(3):175–83.
67. Alt W, Lauffenburger DA. Transient behavior of a chemotaxis system modeling certain types of tissue inflammation. *J Math Biol* (1987) **24**(6):691–722. doi:10.1007/BF00275511
68. Kumar R, Clermont G, Vodovotz Y, Chow CC. The dynamics of acute inflammation. *J Theor Biol* (2004) **230**(2):145–55. doi:10.1016/j.jtbi.2004.04.044
69. Reynolds A, Rubin J, Clermont G, Day J, Vodovotz Y, Bard Ermentrout G. A reduced mathematical model of the acute inflammatory response: I. Derivation of model and analysis of anti-inflammation. *J Theor Biol* (2006) **242**:220–36. doi:10.1016/j.jtbi.2006.02.016
70. Fiala D, Lomas KJ, Stohrer M. A computer model of human thermoregulation for a wide range of environmental conditions: the passive system. *J Appl Physiol* (1985) **87**(5):1957–72.
71. Brown D, Namas RA, Almahmoud K, Zaaqqa A, Sarkar J, Barclay DA, et al. Trauma *in silico*: individual-specific mathematical models and virtual clinical populations. *Sci Transl Med* (2015) **7**:285ra261. doi:10.1126/scitranslmed.aaa3636
72. Bruce JM, Clark JJ. Models of heat production and critical temperature for growing pigs. *Anim Prod* (1979) **28**:353–69. doi:10.1017/S0003356100023266
73. Black JL, Campbell RG, Williams IH, James KJ, Davies GT. Simulation of energy and amino acid utilisation in the pig. *Res Dev Agric* (1986) **3**:121–45.
74. Kendall BE, Briggs CJ, Murdoch WW, Turchin P, Ellner SP, McCauley E, et al. Why do populations cycle? A synthesis of statistical and mechanistic modeling approaches. *Ecology* (1999) **80**:1789–805. doi:10.2307/177237
75. An G, Nieman G, Vodovotz Y. Computational and systems biology in trauma and sepsis: current state and future perspectives. *Int J Burns Trauma* (2012) **2**(1):1–10.
76. An G. *Translational Systems Biology: Concepts and Practice for the Future of Biomedical Research*. New York, NY: Elsevier (2014).
77. An G. Closing the scientific loop: bridging correlation and causality in the petalopage. *Sci Transl Med* (2010) **2**:41s34. doi:10.1126/scitranslmed.3000390
78. An G, Bartels J, Vodovotz Y. *In silico* augmentation of the drug development pipeline: examples from the study of acute inflammation. *Drug Dev Res* (2011) **72**:1–14. doi:10.1002/ddr.20396
79. An G, Nieman G, Vodovotz Y. Toward computational identification of multiscale tipping points in multiple organ failure. *Ann Biomed Eng* (2012) **40**:2412–24. doi:10.1007/s10439-012-0565-9
80. Vodovotz Y, Csete M, Bartels J, Chang S, An G. Translational systems biology of inflammation. *PLoS Comput Biol* (2008) **4**:e1000014. doi:10.1371/journal.pcbi.0040001
81. Vodovotz Y, An G. Systems biology and inflammation. In: Yan Q, editor. *Systems Biology in Drug Discovery and Development: Methods and Protocols*. Totowa, NJ: Springer Science & Business Media (2009). p. 181–201.
82. Vodovotz Y. Translational systems biology of inflammation and healing. *Wound Repair Regen* (2010) **18**(1):3–7. doi:10.1111/j.1524-475X.2009.00566.x
83. Vodovotz Y, Constantine G, Faeder J, Mi Q, Rubin J, Sarkar J, et al. Translational systems approaches to the biology of inflammation and healing. *Immunopharmacol Immunotoxicol* (2010) **32**:181–95. doi:10.3109/08923970903369867
84. Namas R, Zamora R, Namas R, An G, Doyle J, Dick TE, et al. Sepsis: something old, something new, and a systems view. *J Crit Care* (2012) **27**:e311–4. doi:10.1016/j.jcrc.2011.05.025
85. An G. A model of TLR4 signaling and tolerance using a qualitative, particle event-based method: introduction of spatially configured stochastic reaction chambers (SCSRC). *Math Biosci* (2009) **217**:43–52. doi:10.1016/j.mbs.2008.10.001
86. An G, Faeder JR. Detailed qualitative dynamic knowledge representation using a BioNetGen model of TLR-4 signaling and preconditioning. *Math Biosci* (2009) **217**:53–63. doi:10.1016/j.mbs.2008.08.013
87. Foteinou PT, Calvano SE, Lowry SF, Androulakis IP. Modeling endotoxin-induced systemic inflammation using an indirect response approach. *Math Biosci* (2009) **217**:27–42. doi:10.1016/j.mbs.2008.09.003
88. Rivière B, Epshteyn Y, Swigon D, Vodovotz Y. A simple mathematical model of signaling resulting from the binding of lipopolysaccharide with toll-like receptor 4 demonstrates inherent preconditioning behavior. *Math Biosci* (2009) **217**:19–26. doi:10.1016/j.mbs.2008.10.002
89. Yang Q, Calvano SE, Lowry SF, Androulakis IP. A dual negative regulation model of toll-like receptor 4 signaling for endotoxin preconditioning in human endotoxemia. *Math Biosci* (2011) **232**(2):151–63. doi:10.1016/j.mbs.2011.05.005
90. Fu Y, Glaros T, Zhu M, Wang P, Wu Z, Tyson JJ, et al. Network topologies and dynamics leading to endotoxin tolerance and priming in innate immune cells. *PLoS Comput Biol* (2012) **8**(5):e1002526. doi:10.1371/journal.pcbi.1002526
91. Namas R, Namas R, Lagoa C, Barclay D, Mi Q, Zamora R, et al. Hemoadsorption reprograms inflammation in experimental Gram-negative septic fibrin peritonitis: insights from *in vivo* and *in silico* studies. *Mol Med* (2012) **18**:1366–74. doi:10.2119/molmed.2012.00106
92. Song SO, Hogg J, Peng ZY, Parker R, Kellum JA, Clermont G. Ensemble models of neutrophil trafficking in severe sepsis. *PLoS Comput Biol* (2012) **8**(3):e1002422. doi:10.1371/journal.pcbi.1002422
93. An G. In-silico experiments of existing and hypothetical cytokine-directed clinical trials using agent based modeling. *Crit Care Med* (2004) **32**:2050–60. doi:10.1097/01.CCM.0000139707.13729.7D
94. Clermont G, Bartels J, Kumar R, Constantine G, Vodovotz Y, Chow C. In silico design of clinical trials: a method coming of age. *Crit Care Med* (2004) **32**(10):2061–70. doi:10.1097/01.CCM.0000142394.28791.C3
95. Mi Q, Li NYK, Ziraldo C, Ghuma A, Mikheev M, Squires R, et al. Translational systems biology of inflammation: potential applications to personalized medicine. *Per Med* (2010) **7**:549–59. doi:10.2217/pme.10.45
96. Nieman K, Brown D, Sarkar J, Kubala B, Ziraldo C, Vieau C, et al. A two-compartment mathematical model of endotoxin-induced inflammatory and physiologic alterations in swine. *Crit Care Med* (2012) **40**:1052–63. doi:10.1097/CCM.0b013e31823e986a
97. Li NYK, Verdolini K, Clermont G, Mi Q, Hebda PA, Vodovotz Y. A patient-specific *in silico* model of inflammation and healing tested in acute vocal fold injury. *PLoS One* (2008) **3**:e2789. doi:10.1371/journal.pone.0002789
98. Solovyev A, Mi Q, Tzen Y-T, Brienza D, Vodovotz Y. Hybrid equation-/agent-based model of ischemia-induced hyperemia and pressure ulcer formation predicts greater propensity to ulcerate in subjects with spinal cord injury. *PLoS Comput Biol* (2013) **9**:e1003070. doi:10.1371/journal.pcbi.1003070
99. Izuishi K, Tsung A, Jeyabalan G, Critchlow ND, Li J, Tracey KJ, et al. Cutting edge: high-mobility group box 1 preconditioning protects against liver ischemia-reperfusion injury. *J Immunol* (2006) **176**(12):7154–8. doi:10.4049/jimmunol.176.12.7154
100. Tsung A, Zheng N, Jeyabalan G, Izuishi K, Klune JR, Geller DA, et al. Increasing numbers of hepatic dendritic cells promote HMGB1-mediated ischemia-reperfusion injury. *J Leukoc Biol* (2007) **81**(1):119–28. doi:10.1189/jlb.0706468

101. Day J, Rubin J, Clermont G. Using nonlinear model predictive control to find optimal therapeutic strategies to modulate inflammation. *Math Biosci Eng* (2010) 7(4):739–63. doi:10.3934/mbe.2010.7.739
102. Bluestone JA, Tang Q. Immunotherapy: making the case for precision medicine. *Sci Transl Med* (2015) 7(280):280ed283. doi:10.1126/scitranslmed.aaa9846
103. Bard Ermentrout G. *Simulating, Analyzing, and Animating Dynamical Systems: A Guide to XPPAUT for Researchers and Students*. Philadelphia, PA: Society for Industrial and Applied Mathematics (2002).
104. Strogatz SH. *Nonlinear Dynamics and Chaos: With Applications to Physics, Biology, Chemistry, and Engineering*. Cambridge, MA: Perseus Books Publishing, LLC (1994).

Conflict of Interest Statement: Yoram Vodovotz is a co-founder and stakeholder in Immunetrics, Inc. This conflict is being managed by the University of Pittsburgh under all pertinent institutional and federal regulations. The remaining co-authors declare that the research was conducted in the absence of any commercial or financial relationships that could be construed as a potential conflict of interest.

Copyright © 2015 Day, Metes and Vodovotz. This is an open-access article distributed under the terms of the Creative Commons Attribution License (CC BY). The use, distribution or reproduction in other forums is permitted, provided the original author(s) or licensor are credited and that the original publication in this journal is cited, in accordance with accepted academic practice. No use, distribution or reproduction is permitted which does not comply with these terms.

Immune tolerance maintained by cooperative interactions between T cells and antigen presenting cells shapes a diverse TCR repertoire

Katharine Best^{1,2}, Benny Chain^{1*} and Chris Watkins³

¹ Division of Infection and Immunity, University College London, London, UK, ² Centre for Mathematics, Physics and Engineering in the Life Sciences and Experimental Biology (CoMPLEX), University College London, London, UK, ³ Department of Computer Science, Royal Holloway, University of London, London, UK

OPEN ACCESS

Edited by:

Giorgio Raimondi,
Johns Hopkins School of Medicine,
USA

Reviewed by:

James Richard Moore,
Georgia Institute of Technology, USA
Yvula Elhanati,
Centre National de la Recherche
Scientifique, France

*Correspondence:

Benny Chain,
Division of Infection and Immunity,
Cruciform Building, Gower Street,
London WC1E 6BT, UK
b.chain@ucl.ac.uk

Specialty section:

This article was submitted to
Alloimmunity and Transplantation,
a section of the journal
Frontiers in Immunology

Received: 01 May 2015

Accepted: 02 July 2015

Published: 07 August 2015

Citation:

Best K, Chain B and Watkins C (2015) Immune tolerance maintained by cooperative interactions between T cells and antigen presenting cells shapes a diverse TCR repertoire. *Front. Immunol.* 6:360.

doi: 10.3389/fimmu.2015.00360

The T cell population in an individual needs to avoid harmful activation by self peptides while maintaining the ability to respond to an unknown set of foreign peptides. This property is acquired by a combination of thymic and extra-thymic mechanisms. We extend current models for the development of self/non-self discrimination to consider the acquisition of self-tolerance as an emergent system level property of the overall T cell receptor repertoire. We propose that tolerance is established at the level of the antigen presenting cell/T cell cluster, which facilitates and integrates cooperative interactions between T cells of different specificities. The threshold for self-reactivity is therefore imposed at a population level, and not at the level of the individual T cell/antigen encounter. Mathematically, the model can be formulated as a linear programming optimization problem that can be implemented as a multiplicative update algorithm, which shows a rapid convergence to a stable state. The model constrains self-reactivity within a predefined threshold, but maintains repertoire diversity and cross reactivity which are key characteristics of human T cell immunity. We show further that the size of individual clones in the model repertoire becomes heterogeneous, and that new clones can establish themselves even when the repertoire has stabilized. Our study combines the salient features of the “danger” model of self/non-self discrimination with the concepts of quorum sensing, and extends repertoire generation models to encompass the establishment of tolerance. Furthermore, the dynamic and continuous repertoire reshaping, which underlies tolerance in this model, suggests opportunities for therapeutic intervention to achieve long-term tolerance following transplantation.

Keywords: immune tolerance, T cell population, dendritic cells, TCR repertoire, linear programming

1. Introduction

Vertebrate immune system recognition uses antigen receptors produced by stochastic and hence unpredictable molecular recombination events. In this study, we propose a new explanation for how the T cell compartment of the immune system may use a stochastic set of receptors whose specificities are not predetermined to develop a useful repertoire. The requirements we impose are that the repertoire of antigen receptors should cover the set of non-self antigens as comprehensively as possible, in order to provide robust protection against any potential exposure to infectious

pathogens. At the same time, the system must remain tolerant to the set of self-antigens and generally avoid autoimmunity. The fundamental aspect of our hypothesis is that self/non-self discrimination is an emergent property of the combined population of T cells, and cannot be linked by a one-to-one mapping to the individual binding strength spectrum of individual T cells and their receptors. The model we propose has important implications in the context of transplantation, since it suggests that the repertoire can be re-learnt throughout life, thus allowing an opportunity for long-term acquisition of graft-tolerance.

The clonal theory of immune responses, and its corollary, clonal deletion as a mechanism leading to self-tolerance, were developed primarily in the context of antibody and B cells (1). The theory was subsequently extended to T cells, and self-tolerance was proposed to result from clonal deletion in the thymus (2). Indeed thymic-tolerance induction remains a major feature of current models of T cell function. Nevertheless, a number of features of T cell recognition distinguish it from antibody recognition, and have suggested that repertoire selection may obey a modified form of rules.

A first important difference lies in the average affinity of T cell receptor (TCR) for its antigen. At least for the subset of alpha/beta receptor carrying T cells (which is the main focus of this study), which recognize major histocompatibility complex/peptide complexes (pMHC), this affinity is in the order of 10^{-5} – 10^{-6} M, which is some three orders of magnitude less than that for antibody/antigen recognition (3). In addition, only a small proportion of the TCR-binding surface recognizes the antigenic target peptide itself, while the rest binds to the host MHC. A consequence of these characteristics is that the individual TCRs exhibit a great deal of promiscuity: many TCRs bind to the same peptide, while many peptides can be bound by the same TCR (4, 5). The combination of low individual affinities, and a large degree of cross-reactivity have led to the development of an elegant cooperative model of T cell recognition, the “quorum-sensing model” (6), which proposes that functional T cell responses are the product of cooperative interactions between T cells with different receptors. The decision of whether to respond or not is made at the population level, rather being determined solely at the level of an individual T cell/antigen presenting cell encounter.

Another fundamental distinction between T and B cells is that naive T cells require activation by antigen presented on the surface of an antigen presenting cell (APC), usually a dendritic cell. The APC provides the T cells with a high density array of MHC molecules carrying a diverse set of self and non-self peptides, but also a set of additional membrane bound and secreted signals which are necessary for productive T cell activation (7). Dendritic cells can interact simultaneously and consecutively with many different T cells (10–20 cells at any one time, and in the order of 200–400/h) forming an APC/T cell cluster (8–10). Such a cluster is an obvious candidate for the site of “quorum-sensing”, with the cluster, rather than the individual cell, acting as the unit of response. Cooperative behavior between cells within a cluster has been documented by us and others (11, 12). However, the antigen presenting activity of dendritic cells is not a static property. Dendritic cells switch from a “resting” state to an “active” state,

and this transition is determined to a great extent by signals from innate immunity (13). Since resting dendritic cells do not provide the signals necessary for naive T cell activation, they become the “gate keepers” of adaptive immunity, and dendritic cell activation becomes a key decision point in determining whether an antigenic stimulus leads to immune activation. Resting dendritic cells may not only fail to induce productive T cell activation, but may actively induce tolerance (14). Indeed, subsets of immature dendritic cells have been shown to kill T cells in particular circumstances (15). The concept of tolerogenic dendritic cells underlies the influential “danger” model (16, 17), which postulates that self-tolerance results from the fact that self antigens are generally presented to T cells in the absence of innate immune responses. Thus self/non-self discrimination, at least outside the thymus, is determined as much by the dendritic cell and its interaction with innate immunity as by the T cell compartment itself.

Models for self-tolerance are still dominated by the concept of positive and negative selection operating on each individual T cell independently. The question of the mechanism for setting precise thresholds for positive or negative selection, so as to maximize response to non-self but minimize response to self, continue to be much debated (18, 19) and models have been developed that demonstrate the impact of these thresholds on the T cell response to self peptides (20, 21). The mechanisms for establishing self-tolerance outside the thymus are also debated, although “natural” T regulatory cells seem to play an important role (22, 23).

The very extensive literature on the induction of self-tolerance has generally been distinct from the smaller corpus of papers which deal specifically with repertoire generation. A number of models for repertoire generation have been proposed. The key experimental observations which all models must encompass are the persistently high diversity of the naive T cell pool (24), the ability for new clones to emerge and establish themselves in the repertoire (25), and the variable clone size which was an unexpected feature of the naive repertoire (26). The majority of previous models, which often have an “ecological” flavor, focus on clonal competition for a limited pool of presented self-antigens to drive clonal diversity and clonal size heterogeneity. Competition between T cells for access to pMHC results in stabilization of clone sizes when all available binding sites are occupied (27) and increased diversity as those T cells that are more different from others and therefore occupy a niche are favored (28, 29). In order to explain the emergence of new clones, and to prevent the development of a repertoire dominated by the clones with optimum affinities, a natural death rate of all clones is often assumed.

In the new model outlined below, we combine repertoire generation and self/non-self discrimination into a single process. We integrate cooperative behavior (quorum sensing) into the process of naive T cell repertoire generation, and explicitly model a system in which T cell receptors bind many different antigens with a range of different affinities. The model can be formalized as a linear programming (LP) optimization problem. It shows a rapid convergence to a stable state, in which self-reactivity is maintained below a fixed threshold. The model focuses on the shaping of the T cell repertoire in the absence of immune challenge, and in this work we do not consider the changes to the repertoire following

activation in detail. Instead, we investigate the potential of the system to mount an immune response and introduce measures of the T cell population's coverage of potential non-self antigens. We show that despite the restrictions imposed by the linear constraints that ensure self-tolerance, the repertoire remains diverse, coverage is preserved and the size of individual clones is heterogeneous. The diversity of the constrained repertoire becomes an important factor when challenge with foreign antigens does occur, and we find that this model is able to reshape the population to retain both TCR diversity and the potential to respond to non-self more strongly than self.

2. Materials and Methods

2.1. A Simple Computational Model

We introduce a simple computational model, and then we consider possible variations of the model and possible underlying mechanisms.

We suppose that the T cell system "learns" in the following way to recognize self, and to react to self up to but not beyond response thresholds, which are determined by the APCs (in this study we prefer the more generic term APC, although the most important cell type in maintenance of the naive T cell repertoire is probably the dendritic cell). Each inactive APC carries a set of self-antigens bound to MHC and is continually "scanned" by T cells. Some of the TCRs of these T cells recognize one of the presented pMHC complexes on the surface of the APC; T cells scan the surface of the APC, stop for a period related to the strength of interaction with pMHC and then release themselves, allowing other cells an opportunity to assay their affinity to the presented antigens (8). In this model, we ignore any potential effects of ecological competition between T cells for pMHC binding sites in order to study the effects of the quorum sensing behavior.

We suppose that the APC can detect the strength of the antigen specific binding between each T cell and the APC, and we further hypothesize that the APC maintains a record of the total APC/T cell binding, using some (possibly leaky) integration mechanism over a sliding time window. The APC does not need to "know" which antigen has caused the T cell to bind, and still less which TCR clonotype the T cell expresses. The strength of signal in this model could arise from a combination of a strong affinity between pMHC and a specific TCR, or the presence of high concentrations of a particular pMHC. The model does not distinguish between these parameters but allocates an overall signal strength to each T cell/APC encounter.

We suppose that the APCs regulate the numbers of T cells in the following simple way. If the combined binding signal strength registered within a fixed time period by an APC exceeds some threshold value, then the APC sends a "kill signal" (either actively or passively) to each T cell that is bound currently or binds subsequently (15). These T cells, or some fraction of them, then die. Since the APC is recording the integrated signal over a sliding time window, this value will subsequently fall to below the signal threshold and the APC will then switch off the kill signal. The molecular mechanisms which could mediate such models are discussed below, but at this stage, we focus on the mathematical properties of such a model.

We implement a simplified version of the model described above. The biological validity of these assumptions and the extension of the model to more realistic but more complex scenarios are discussed later. We suppose that there are N different T cell clonotypes, with abundances at time $t = 0$ of $\mathbf{x}^0 = (x_1^0, x_2^0, \dots, x_N^0)$. In reality, the abundances would be integer counts, but in this model, we treat them as positive real numbers.

We denote the binding strength between a T cell clonotype i and self-peptide MHC complex ("spMHC") k as q_{ik} . We consider a model in which each (non-activated) APC presents a particular combination (or "profile") of spMHCs. The spMHC profile j contains an amount a_{kj} of spMHC k , and we suppose there are M such profiles that T cells may encounter. The overall binding strength of T cell i for APC profile j is then $b_{ij} = \sum_k q_{ik} a_{kj}$. Note that when we refer to binding strength, we are describing a quantity that represents the amount of signal that the APC integrates due to the T cell-APC encounter.

Each T cell may have non-zero binding strength to many spMHC complexes, and each spMHC complex may bind to many T cells: the matrix of spMHC to T cell binding strengths $Q = (q_{ik})$ is assumed to be sparse, non-negative, and with multiple positive entries in each row and column. The matrix of binding strengths of T cells to antigen profiles, $B = (b_{ij})$, therefore, is non-negative, and less sparse than Q , because each antigenic profile contains multiple spMHC complexes. B is non-negative because an APC cannot present a negative amount of antigen; that is, the a_{kj} are non-negative. Note that we do not consider the T cell to pMHC binding strengths q_{ik} – instead we generate the T cell to APC profile binding strengths b_{ij} by sampling from an assumed distribution, described later.

On these assumptions, the total strength with which all T cells bind to an APC with spMHC profile j is:

$$r_j(\mathbf{x}) = \sum_i x_i b_{ij} \quad (1)$$

where \mathbf{x} is the vector of clonotype abundances at time t . Writing $\mathbf{b}_j = (b_{1j}, \dots, b_{Nj})$, we obtain:

$$r_j(\mathbf{x}) = \mathbf{b}_j \cdot \mathbf{x} \quad (2)$$

We set a threshold binding rate τ above which each APC will issue a kill signal to any T cell that is bound; that is, the APC presenting spMHC profile j issues kill signals to any T cells bound to it if $r_j(\mathbf{x}) > \tau$. In principle, τ is a threshold that can be locally defined by the antigen presenting system: it can depend on the APC microenvironment or intrinsic antigen presenting parameters such as the MHC haplotypes. In this initial implementation, we have assumed τ is constant over all APCs. The rate at which T cell i is eliminated by "kill" signals from APCs of type j is proportional to the strength of the binding interaction of each T cell with that spMHC profile j , such that:

$$\begin{aligned} &\text{Kill signals for clonotype } i \text{ from APC type } j \\ &= \eta \phi(\mathbf{b}_j \cdot \mathbf{x} - \tau_j) b_{ij} x_i \end{aligned} \quad (3)$$

where η is a rate parameter, $\phi(\mathbf{b}_j \cdot \mathbf{x} - \tau_j)$ is the fraction of all T cells binding to APC j that receive a kill signal, and x_i is the

abundance of T cells of type i . Our hypothesis is that kill signals are only issued when the rate of binding to APCs is greater than τ ; this hypothesis is expressed in terms of the function $\phi(z)$, which is some non-decreasing function such that $0 \leq \phi(z) \leq 1$ for all real z . $\phi(z)$ should be small or zero for $z < 0$, and we suppose that $\phi(z)$ rises toward 1 rapidly for $z \geq 0$. The simplest choice for ϕ would be the Heaviside function $H(z) = 1$ if $z \geq 0$ and $H(z) = 0$ if $z < 0$; a more biologically realistic function would be continuous and differentiable, such as the logistic function $\phi(z) = \frac{1}{1 + \exp(-\alpha z)}$, for some suitable scale parameter α . The implementation captured in equation (3) further assumes each APC, and hence each spMHC profile j , occurs once, but the model is easily extended to incorporate variable APC numbers for each antigen profile.

So far, the model only has a mechanism for killing T cells: there must also be a method for T cells to multiply. Although it is clear that naive cells must see self-antigens in order to survive, the quantitative relationship between antigen-binding strength and proliferation in the context of T cell homeostatic proliferation remains unclear. Here, we adopt the simplest assumption, namely that all T cells spontaneously divide at some rate ν , although a model relating ν to binding strength could also be implemented.

Using these assumptions, we obtain that for each clonotype i :

$$\dot{x}_i = \nu x_i - \eta \sum_j \phi(\mathbf{b}_j \cdot \mathbf{x} - \tau_j) b_{ij} x_i \quad (4)$$

so that

$$\frac{\dot{x}_i}{x_i} = \nu - \eta \sum_j \phi(\mathbf{b}_j \cdot \mathbf{x} - \tau_j) b_{ij} \quad (5)$$

We can demonstrate rather simply that the optimization will indeed always converge. For a suitable choice of ϕ the right hand side can be written as the gradient of a convex function of \mathbf{x} . Observe that:

$$\Phi(u) = \int_{-\infty}^u \phi(z) dz \quad (6)$$

exists for plausible choices of ϕ , and is convex and differentiable provided that $\phi(z)$ is non-decreasing and continuous. Then define:

$$f_j(\mathbf{x}) = \Phi(\mathbf{b}_j \cdot \mathbf{x} - \tau_j) \quad (7)$$

Each f_j is convex in \mathbf{x} , and note that:

$$\frac{\partial f_j(\mathbf{x})}{\partial x_i} = \phi(\mathbf{b}_j \cdot \mathbf{x} - \tau_j) b_{ij} \quad (8)$$

Now define:

$$F(\mathbf{x}) = -\nu \sum_i x_i + \eta \sum_j f_j(\mathbf{x}) \quad (9)$$

which is a sum of convex differentiable functions. The scalar function $F(\mathbf{x})$ is constructed so that

$$\frac{\partial F(\mathbf{x})}{\partial x_i} = -\nu + \eta \sum_j \phi(\mathbf{b}_j \cdot \mathbf{x} - \tau_j) b_{ij} = -\frac{\dot{x}_i}{x_i}$$

so that the rate of change of \mathbf{x} is expressed as:

$$\dot{x}_i = x_i \frac{\partial F(\mathbf{x})}{\partial x_i}$$

We can now write the rate of change of $F(\mathbf{x})$ as:

$$\frac{dF(\mathbf{x})}{dt} = \dot{\mathbf{x}} \cdot \nabla F(\mathbf{x}) \quad (10)$$

$$= - \sum_i x_i \left(\frac{\partial F(\mathbf{x})}{\partial x_i} \right)^2 \quad (11)$$

$$\leq 0 \text{ since all } x_i \text{ are positive} \quad (12)$$

F is convex and differentiable, because it is the sum of convex, differentiable functions, and F therefore has a unique minimum in the region of interest, which is the non-negative quadrant. At this minimum, all constraints $\mathbf{b}_j \cdot \mathbf{x} \leq \tau_j$ will be approximately satisfied, provided that the growth rate ν is small compared to the “kill rates” from the APCs.

From equation (11), we know that the value of F , which includes a sum of measures of constraint violation, must decrease over time. However, it says little about the rate of convergence toward the minimum of F . In the Supplementary Material, we present a stronger analysis of the convergence of the process of equation (4), by identifying it with a version of the multiplicative weight updating algorithms surveyed by (30). This analysis establishes regret bounds for such updates on a possibly time-varying set of constraints. We note that equation (4) could be solved by standard differential equation methods, provided the rate of killing (and the rate of proliferation) remains constant. Under these conditions, the iterations become equivalent to a fixed time step, which can be allowed to decrease to the continuous case. However, we prefer to use the iterative algorithm we describe below because the discrete time steps are readily interpretable in terms of cellular events (e.g., T cell/APC interactions) and because the regret bounds it establishes are robust to variations in rate. The model therefore leaves open the possibility of introducing time-dependent and tissue-dependent variations in rates in future extensions of the basic model.

The implementation outlined above gives rise to a series of constraints on T cell abundances, which are captured by a series of linear inequalities as outlined above. An iterative method to solve this linear programming problem is set out below, and can be given a feasible biological interpretation. The proliferation rate ν is set so that in the absence of any “kill signals”, the T cell population would double in one unit of time, and the rate η of T cell killing is set relative to this.

1. Calculate the immune response to each profile, $r(j) \leftarrow \sum_i x_i b_{ij}$ for all j .
2. Determine for which self-profiles the response threshold has been violated, $v(j) \leftarrow [r(j) > \tau]$ for all i .
3. Adjust the T cell clonotype abundances,
 $x(i) \leftarrow x(i) \left(1 + \nu \delta t - \eta \delta t \sum_j b_{ij} v_j \right)$.

The multiplicative update analysis discussed in the Supplementary Material provides strong guarantees for time-varying constraints, corresponding to the case where APCs present varying combinations of antigens over time.

2.2. Assessing the Potential for an Immune Response

In order to investigate the potential of the reshaped T cell population to mount an immune response to previously unencountered antigens, we create a set of new independently generated antigenic profiles, which were not part of the set on which the T cell population has been trained. We refer to these as “non-self profiles”. The binding strength of each existing TCR for each new profile is selected independently of its given affinities for all the self profiles, although the value is selected from the same probability distribution. We use these non-self profiles to test whether under our assumptions the T cell repertoire will achieve the dual objectives of maintaining self-tolerance, while at the same time maintaining as broad and strong a repertoire for non-self as possible.

Note that we do not model an immune response to these new profiles in this work. If the APC remains in a tolerogenic state, the introduction of new non-self profiles will typically violate the constraints, but this will result in additional T cell killing and the system will gradually readjust to remain within the immune activation threshold. We envisage that if the APC were switched to an immunogenic state (for example by exposure to innate immune danger signals) then crossing the threshold would result in activation of all APC bound T cells, resulting in an effector immune response.

We measure the ability of the T cell population to respond to a non-self profile as the total potential T cell response, calculated as $r_j(\mathbf{x}) = \sum_i x_i c_{ij}$ for non-self profile j , where $C = (c_{ij})$ is the matrix

of binding strengths between T cell clonotypes and non-self profiles. It is important to note that we are not simulating the behavior of the T cell population on immune challenge here, but assessing the potential of the reshaped repertoire to respond to previously unencountered profiles. In order to measure the “success” of the reshaped repertoire, we can consider its coverage of the potential non-self antigen space. The first coverage measure we use in this study is the ratio of the mean total response against non-self profiles to the mean total response against self profiles: coverage = $\frac{\bar{r}_{ns}}{\bar{r}_s}$ for self profiles s and non-self profiles ns . Alternatively, we also measure the coverage as the proportion of non-self profiles that give a potential T cell response greater than the average response to self profiles, i.e., $|\{ns : r_{ns} > \bar{r}_s\}|$ expressed as a fraction of the total number of non-self profiles modeled.

3. Results

3.1. Clone Size Adjustment Algorithm Reaches a Solution of the Repertoire Constraints: Violations are Resolved Rapidly and Repertoire is Optimized Slowly

We first simulate a very simplified repertoire to allow us to visualize the action of the update algorithm. We start with two T cell clonotypes and three spMHC profiles. The clonotypes have binding strengths for each of the profiles as detailed in **Figure 1G**. In this simulation, each profile is given the same total response threshold (=1), above which there will be harmful autoimmunity.

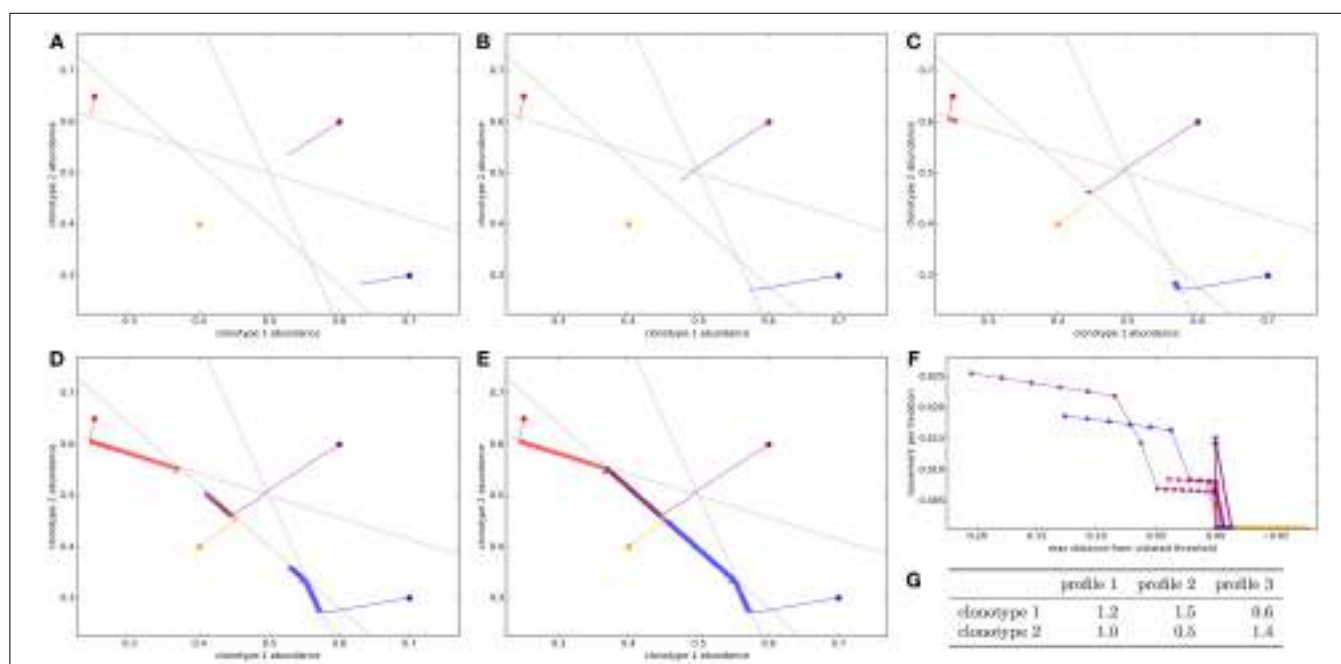


FIGURE 1 | Optimization of the T cell population to avoid autoimmunity while maximizing T cell numbers in a simplified system with two clonotypes and three spMHC profiles. The update algorithm is initiated with different initial clonotype abundances each represented by a different color. The colored lines track the changes in clonotype abundance over iterations of the update algorithm (**A–E**). The clone abundances after (**A**) 5, (**B**) 10, (**C**) 100, (**D**) 1,000, or (**E**) 10,000 iterations of the update algorithm. The gray lines indicate the constraint that total T cell response should be less than the

threshold for each of the spMHC profiles (**F**). For each of the starting repertoire configurations, the relationship between the Euclidean distance moved by the repertoire configuration in an iteration of the update algorithm and the distance from the furthest violated threshold, or if there are no violations the distance to the nearest threshold (**G**). The affinities between clonotypes and spMHC profiles. Other model parameters for all panels are: $\tau = 1$, the self-response threshold for each spMHC profile, $\nu = \ln 2 \delta t^{-1}$, the growth rate and $\eta = 0.01001 \delta t^{-1}$, the learning rate.

The other parameters of the update algorithm are set out in the legend of **Figure 1**.

The self-response thresholds for each profile and the binding strengths between clonotypes and spMHC profiles (**Figure 1G**) give constraints on allowable repertoires. If x_i is the abundance of clonotype i , to avoid autoimmunity we require that:

$$\begin{aligned} 1.2x_1 + 1.0x_2 &\leq 1 \\ 1.5x_1 + 0.5x_2 &\leq 1 \\ 0.6x_1 + 1.4x_2 &\leq 1 \end{aligned}$$

We repeatedly simulate the update algorithm with different starting repertoire configurations. Each starting configuration is represented as a color in **Figure 1**. The panels in this figure show a time course of the update algorithm working on each initial repertoire configuration.

We see that if the initial repertoire configuration violates one or more of the response constraints, the update algorithm very quickly shapes the repertoire (by adjusting clonotype abundances) to a point where there is no autoimmunity (**Figure 1B**, 10 iterations). By contrast, when no threshold is violated by the starting configuration of the repertoire (yellow path in **Figure 1**), the repertoire does not move very far from the initial configuration in the first cycles.

Once the repertoire has been moved to a configuration where all constraints are satisfied, the update algorithm continues to allow each clonotype to grow as abundant as possible while remaining inside the “feasible region” (**Figures 1C–E**). For this arrangement of affinities, the “optimum” repertoire in terms of having the highest total abundance while avoiding autoimmunity is at a single vertex of the feasible region, and we can see that the update algorithm moves each of the initial repertoires slowly toward this point.

The speed which the clonotype abundances are adjusted is dependent on the severity of the violation of the thresholds, as the update rule is designed to do through the negative learning rate, η . This can be quantified by considering the Euclidean distance moved by the repertoire configuration in a timestep as a function of the Euclidean distance by which the current configuration violates a threshold (**Figure 1F**). There is a strong positive relationship between the severity of the violation and the speed with which the update algorithm adjusts the clonotype abundances.

3.2. Positive Selection of Clonotypes Based on Self-Profile Binding Strength is Required for Successful Immune-Tolerance

We next simulated the update algorithm with a larger number of T cell clonotypes and spMHC profiles (**Figure 2**). For each clonotype-profile pair, the binding strength (b_{ij} for clonotype i and profile j) is set to zero with probability $1 - \gamma$. If the binding strength is not set to zero it is selected at random from a left-censored normal distribution. For simplicity, we set the response threshold to be equal to 1 for all self profiles.

We run the update algorithm and record the abundance of each clonotype at each iteration. Note that under our constant growth rate assumption, iterations can be thought of as directly equivalent to T cell generations. We set the growth rate ν such that one

unit time is equal to one T cell generation, giving one T cell generation in approximately 1387 iterations. The total T cell response to a spMHC profile can be calculated as the sum of abundance \times binding strength for each T cell clonotype ($r_j = \sum_i x_i b_{ij}$ for spMHC profile j). We can then define successful immune tolerance as the reshaping of the T cell population into one where the total T cell response to any spMHC profile (r_j for self-profile j) is below the threshold τ . The mean total response to spMHC profiles over time (**Figure 2A**, solid line) is initially well controlled at the allowed threshold. However, after approximately 10 generation times algorithm, the control of the response breaks down and there is an increased average response to self, above the allowable threshold.

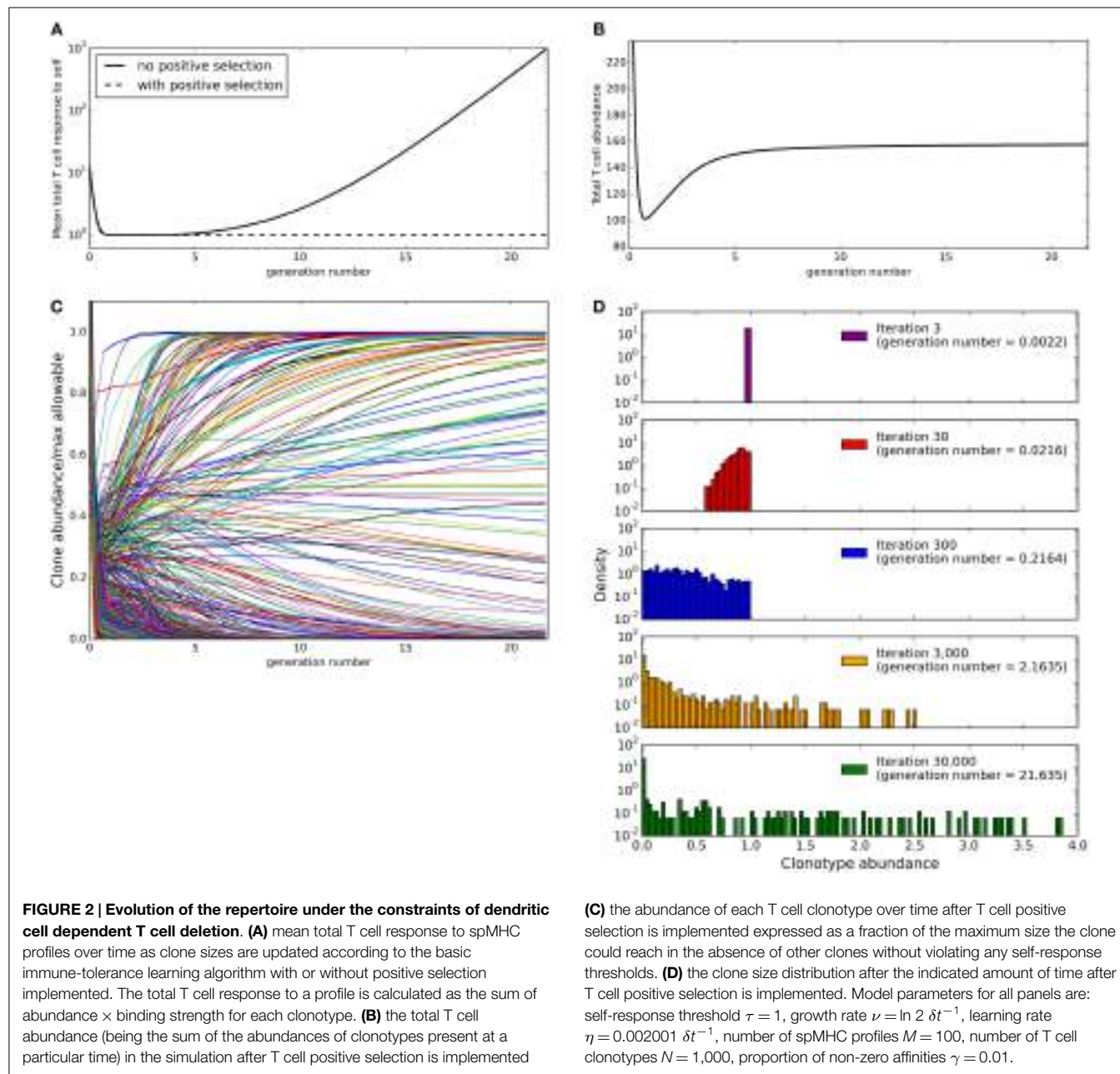
We noted that those clonotypes that are highly abundant after running our simulation for 30,000 cycles of the update algorithm have low maximum binding strength to spMHC profiles. We can see the reason for breakdown of control of self response if we consider a clonotype of abundance 1 that has zero binding strength for all self profiles except one, for which it has binding strength b . Then after one iteration of the update algorithm, the clonotype will have abundance $(1 + \nu)$ or $(1 + \nu \delta t - \eta \delta t b)$ depending on whether the total T cell response to the profile for which it has non-zero binding strength is below the allowable self-response threshold τ or not. In order to avoid uncontrolled growth of the clonotype, we would require that $(1 + \nu \delta t - \eta \delta t b) < 1$, which is equivalent to requiring that $b > \nu/\eta$. Therefore, we suggest that the inability of the update algorithm to control average self response is due to the presence of clonotypes for which the maximum binding strength to any of the self profiles is below ν/η . This indicates the requirement for some form of positive selection.

In its simplest form, positive selection would take the form of a function which deletes all clones whose maximum binding strength for any self profile is below ν/η . A more realistic function could make the growth rate in any one cycle depend on the average binding strength to self profiles or to the maximum binding strength to a randomly selected sample of “encountered” self profiles. In the following work, we implement the simplest form of the affinity-dependent selection, by eliminating all clonotypes with maximum binding strength to self profiles below ν/η before the update algorithm begins.

We implement this positive selection of clonotypes and re-run the simulation with the same parameters (detailed in **Figure 2** legend). The total T cell response to self profiles is now tightly controlled at the allowable threshold (**Figure 2A**, dashed line). It is, however, possible under this model that if a clonotype escapes positive selection it slowly increases in size indefinitely.

3.3. Total Population Size Homeostasis but Increased Clonotype Abundance Heterogeneity as a Function of Time

Naive TCR repertoires are made up of clonotypes with a broad range of abundances. We therefore examined the abundance distribution produced by the model presented in this paper. Since our implementation of the model uses continuous rather than discrete abundances, abundances never reach zero but become arbitrarily small. In order to consider the abundance distribution, we therefore set a lower threshold below which a clone is considered to be



deleted. In this work, we consider a clonotype to be completely absent when its abundance falls below a threshold defined by $N/10^8$ where N is the number of clonotypes in the simulation. This threshold was chosen based on consideration of a mouse immune system, which has in the order of 10^8 T cells in total. If N different clonotypes of equal abundance are present in this repertoire, each clonotype could be considered to have a starting abundance of $10^8/N$. Hence, if a clone contracts by a factor of $>10^8/N$, its abundance would fall below 1 and hence the clonotype can be considered as eliminated. Since the abundance of each clonotype at the start of the model is arbitrarily initiated at a value of one, this is equivalent to defining a clone with an abundance of lower than $N/10^8$ as deleted.

We first considered the total size of the T cell compartment as a function of time. At every timepoint during the simulation, we can calculate the total size of the repertoire as the sum of the clonotype abundances that are above the “presence” threshold of $N/10^8$ (**Figure 2B**). We see that this initially contracts as self-response constraint violations are resolved, but then expands (driven by the positive learning rate increasing the abundance of each clonotype when constraints are not violated) until a stable level is reached where growth and negative selection are balanced. If all other parameters of the model are fixed, the eventual total size of the T cell compartment at homeostasis is strongly correlated to the number of clonotypes present in the repertoire at the beginning of the simulation.

We then consider the abundances of individual clonotypes. The maximum allowable size for a clonotype in the model can be defined as the self-response threshold divided by the maximum binding strength that the clonotype has for any self profile, i.e.,

$$m_i = \frac{\tau}{\max_j b_{ij}}$$

is the maximum allowable size for clonotype i . For each of the clonotypes in the simulation, we consider its abundance (expressed as a proportion of the maximum allowable abundance m_i for that clonotype) across time (**Figure 2C**). Some clonotypes are present close to their maximum allowable size m_i , presumably due to lack of cross-reactivity with other profiles or other clonotypes, while some clonotypes are quickly removed from the repertoire. It is interesting to note that while the total T cell abundance stabilizes rapidly (**Figure 2B**), the individual clonotype sizes remain dynamic even in later stages of the simulation. The clone size distribution (**Figure 2D**) spreads to include smaller clonotypes during the initial part of the simulation, then starts to include larger clonotypes as well in later iterations. At the end of our simulation, there is a large spread of clone sizes in which large and small clones co-exist, as observed experimentally, rather than a repertoire completely dominated by a few large clonotypes.

3.4. Increased Number of T Cell Clonotypes Provides Greater Repertoire Coverage

A successful T cell population needs to be able to control immune response to self but at the same time must provide broad coverage against a range of unknown non-self antigens that the individual might encounter. The mean total potential T cell response to self and non-self profiles (\pm standard deviation) across iterations is shown for one set of simulation parameters in **Figure 3A**. This shows that the response to self is well controlled at the allowed threshold τ . By contrast, the average response to non-self pMHC profiles becomes higher as the model shapes the repertoire. However, the non-self responses become very heterogeneous. After 30,000 iterations, the response to all self profiles is at or near the allowed threshold while the majority of non-self profiles result in more T cell binding, and therefore a larger potential T cell response (**Figure 3B**). However, there are also a number of non-self profiles that create a lower response than that of self profiles. These presumably represent “holes” in the repertoire coverage.

We assess the ability of the reshaped repertoire to cover the potential non-self antigen pool via the two coverage measures described earlier. We ran the update algorithm a number of times with the number of T cell clonotypes (N) ranging between 400 and 25,600 and number of spMHC profiles (M) ranging between 100 and 1,600 (only running combinations where $M < N$). Other parameters of the simulation are detailed in **Figure 3** legend. We considered the evolution of the ratio of mean self potential response to mean non-self potential response across cycles of the algorithm (**Figure 3C**) and see that this increases until it is above 1 (indicating higher potential response to non-self than self profiles) for all parameter sets. The repertoire coverage, using this measure, depends on the total number of T cell clonotypes in the repertoire at the start of the algorithm (**Figure 3D**).

The proportion of non-self profiles that the T cell population has the potential to respond to more strongly than it does to self

profiles is initially low but is increased as the update algorithm shapes the repertoire (**Figure 3E**). The success of the repertoire under this measure is again strongly correlated to the number of clonotypes (**Figure 3F**).

3.5. Clonotype Diversity and spMHC Profile Cross-Reactivity are Preserved by the Update Algorithm

We have demonstrated that the model described in this study produces a TCR repertoire that respects self-response thresholds, but violates the thresholds when exposed to non-self antigen profiles. It has been observed that the TCR repertoire in an individual remains diverse (many different clonotypes are present, with cross-reactivity between clonotypes and profiles) until old-age, when a few dominant clonotypes appear (31). We explored whether our selection model can retain diversity in the repertoire or whether the multiple linear constraints favor a sparse solution with few surviving clonotypes.

We first consider the proportion of starting clonotypes surviving (i.e., with an abundance greater than the lower limit defined above) as a function of time. The proportion of clonotypes present in the repertoire falls rapidly in the initial stages of repertoire reshaping and then stabilizes (**Figure 4A**, blue). The proportion of the initial clonotypes that remain after 30,000 cycles of the update algorithm is inversely correlated to the number of clonotypes in the simulation (**Figure 4B**, blue).

A key parameter of the adaptive immune system is the amount of information it can encode. The information content encoded in the repertoire (which depends on a combination of the number of different T cell clones, and also their relative size) can be captured by the Shannon Information (SI) Entropy, which is the log of the true diversity of order 1 (32). The SI coefficient of the repertoire initially decreases rapidly before stabilizing (**Figure 4A**, red). However, there is only a weak (and not statistically significant) correlation between the Shannon Information Entropy coefficient and the number of clonotypes in the simulation (**Figure 4B**, red).

Cross-reactivity, such that multiple TCRs can recognize the same pMHC profile and multiple pMHC profiles can be recognized by the same TCR, is a well-recognized feature of the T cell repertoire (4, 5). To investigate the evolution of cross-reactivity in our model, we measure the number (or proportion) of clonotypes which have non-zero binding strength for a single pMHC profile (i.e., $|\{i : b_{ij} > 0\}|$ for each profile j). The mean proportional cross-reactivity against self profiles decreases initially then begins to stabilize, while the mean cross-reactivity against non-self profiles is maintained (**Figure 4C**).

After running the simulation for 30,000 iterations of the update algorithm, the distributions of cross-reactivity against self and non-self profiles are clearly different (**Figure 4D**). The majority of non-self profiles are recognized by more TCR clonotypes than self profiles are, and the ratio of self:non-self cross-reactivity is not significantly correlated to the size of the simulation (**Figures 4E,F**).

3.6. New Clonotypes can Establish Themselves in a Stable Repertoire

The TCR repertoire is constantly being updated by the introduction of new T cells from the thymus, and new clonotypes can

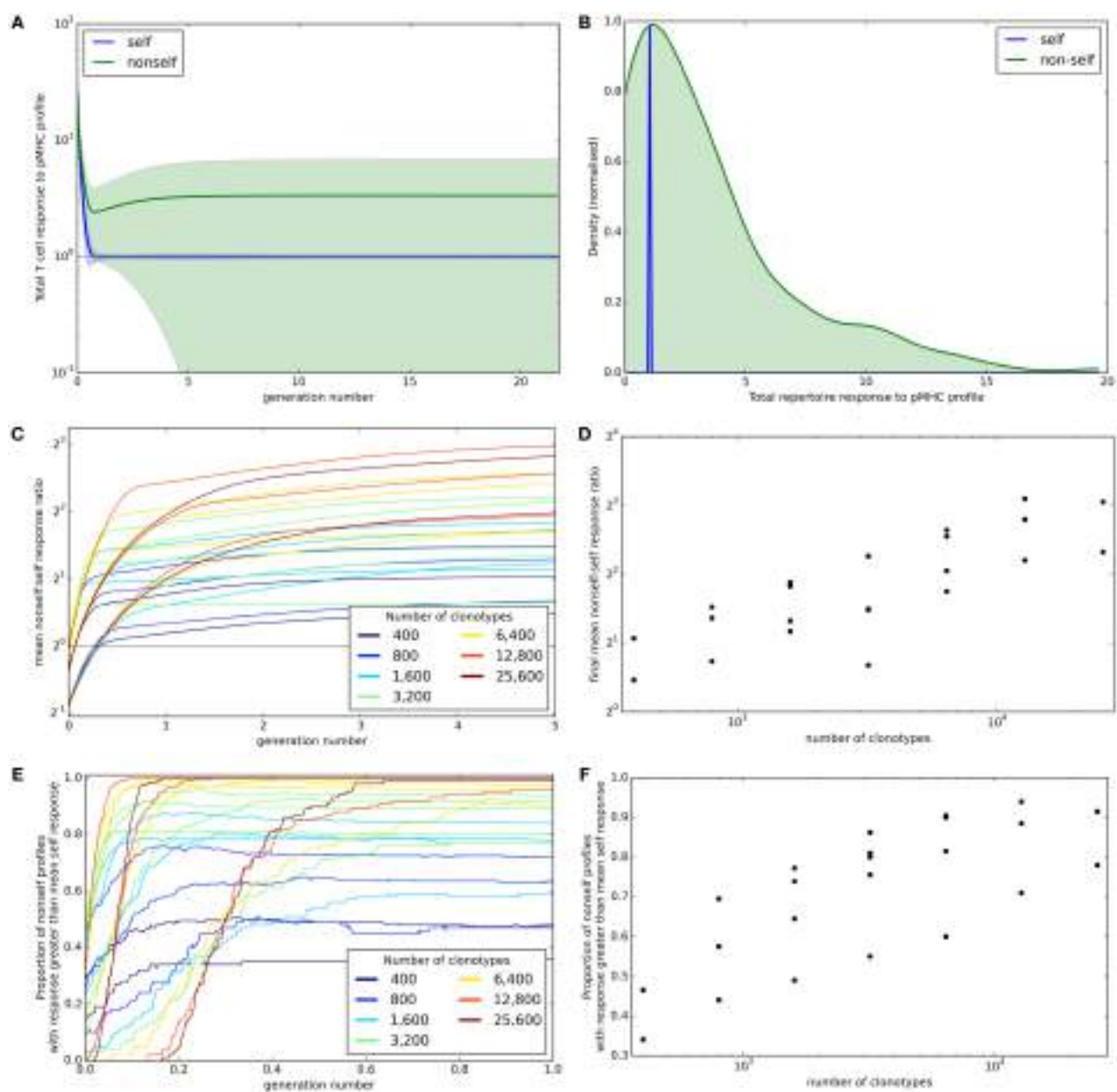


FIGURE 3 | Broad coverage to non-self is maintained during the development of a self-tolerance repertoire. (A) The mean (\pm standard deviation) total T cell response to self (blue) or non-self (green) pMHC profiles over time with $N = 2,000$ and $M = 200$. **(B)** After 30,000 iterations of the update algorithm with parameters as in **(A)**, the distribution of total T cell response to self (blue) and non-self (green) pMHC profiles. **(C)** The ability of the repertoire to successfully mount an immune response to non-self pMHC profiles, measured as the average total response to a non-self profile divided by the average total response to a self profile, over time. The number of T cell clonotypes in a simulation is indicated by color, with the number of self profiles simulated ranging between 100 and 800. **(D)** The relationship

between number of T cell clonotypes and the average total response to a non-self profile divided by the average total response to a self profile after 30,000 iterations of the update algorithm. **(E)** The proportion of non-self profiles that have a total T cell response greater than the mean response toward self profiles over time. The number of T cell clonotypes is indicated by color. **(F)** The relationship between the number of T cell clonotypes and the proportion of non-self profiles having a stronger total T cell response than the mean response to self profiles after 30,000 cycles of the update algorithm. Other model parameters for all panels are: self-response threshold $\tau = 1$, growth rate $\nu = \ln 2 \delta t^{-1}$, learning rate $\eta = 0.002001 \delta t^{-1}$ and proportion of non-zero affinities $\gamma = 0.01$.

establish themselves despite competition from the existing clonotypes. We explored whether the update algorithm of our model would allow introduction of new clonotypes. We ran the update algorithm for 30,000 iterations to produce a self tolerant and

stable repertoire and then selected 10 of the clonotypes present at random. We created 10 new duplicate clonotypes, with identical spMHC profile binding strength values as the selected clonotypes, and introduced them into the repertoire at an abundance equal

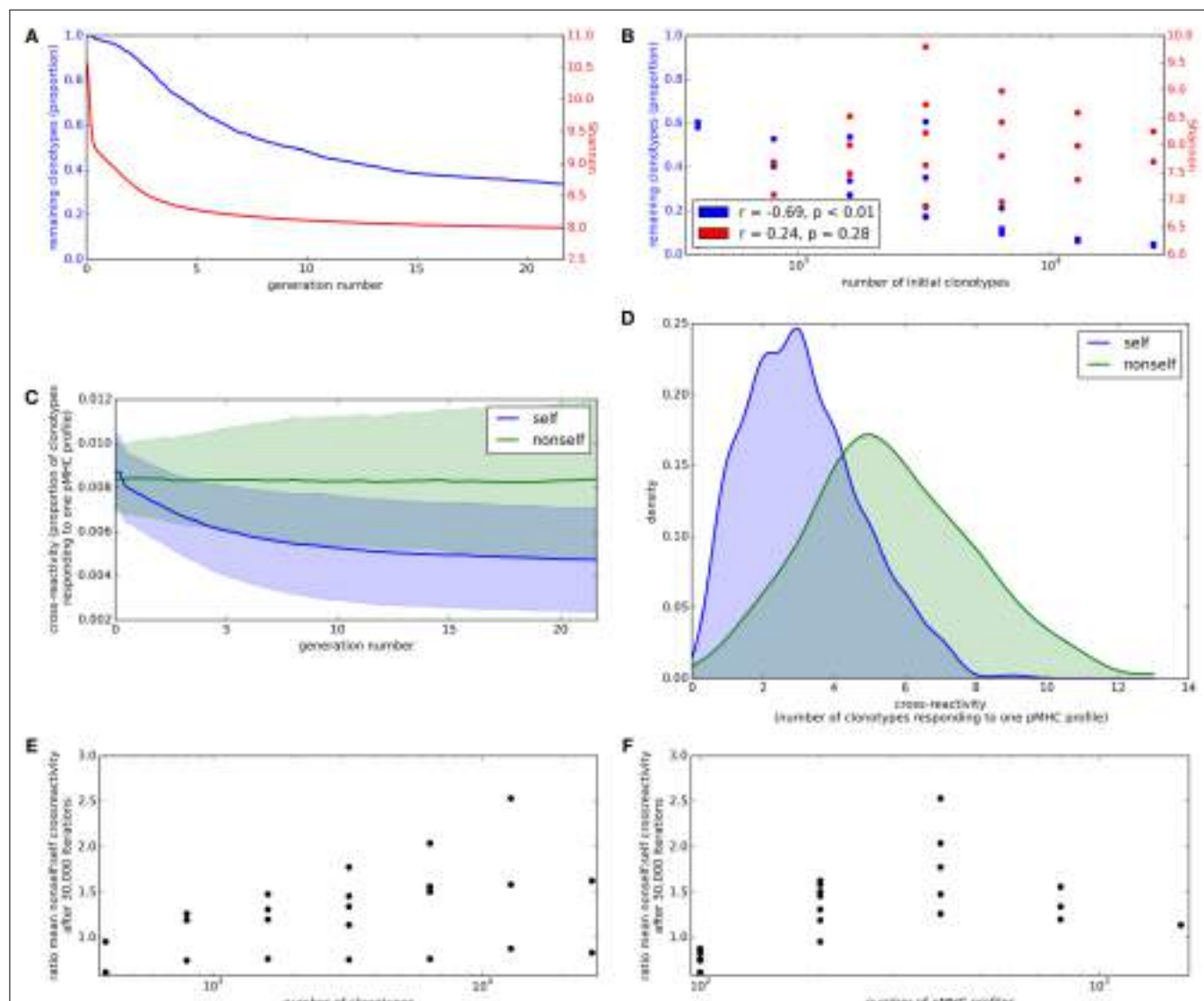


FIGURE 4 | Clonotype diversity and pMHC profile cross-reactivity are preserved by the update algorithm. **(A)** Blue: The proportion of clonotypes (after positive selection) that are present over time during simulation of the update algorithm. Red: The Shannon entropy of the repertoire over time. Simulation implemented with $N = 1,600$ and $M = 400$. **(B)** Relationship between number of clonotypes in the simulation and proportion of clonotypes remaining (blue) or Shannon entropy of the repertoire (red) after 30,000 iterations of the update algorithm. Simulation implemented with values of N between 400 and 25,600 and M between 100 and 800, with $M < N$. **(C)** Cross-reactivity of T cell clonotypes against self (blue) and non-self (green) pMHC profiles over time, run with $N = 3,200$ and $M = 400$. Cross-reactivity is measured as the proportion of present clonotypes that have non-zero binding strength for a given profile. Data shown is mean cross-reactivity across all profiles \pm standard deviation.

(D) Distribution of cross-reactivity across all self (blue) and non-self (green) pMHC profiles after 30,000 iterations of the update algorithm with $N = 3,200$ and $M = 400$. Cross-reactivity is measured as the absolute number of present clonotypes that have non-zero binding strength to a profile. **(E)** Relationship between the number of clonotypes present at the start of the update algorithm and the ratio of the mean cross-reactivity against non-self profiles to the mean cross-reactivity against self profiles after 30,000 cycles of the update algorithm. **(F)** Relationship between the number of self profiles in the update algorithm and the ratio of the mean cross-reactivity against non-self profiles to the mean cross-reactivity against self profiles after 30,000 cycles of the update algorithm. Other model parameters for all panels are: self-response threshold $\tau = 1$, growth rate $\nu = \ln 2 \delta t^{-1}$, learning rate $\eta = 0.002001 \delta t^{-1}$ and proportion of non-zero affinities $\gamma = 0.01$.

to the average abundance of the existing clonotypes. We then tracked both the original 10 clones and their duplicates for further iterations of the simulation.

The total T cell abundance increases transiently as new clonotypes are introduced but quickly returns to a stable level (**Figure 5A**). On introduction of the new duplicate clonotypes, the abundances of the original 10 clonotypes fall in order to

satisfy the self-response constraints (**Figure 5B**). Clonotypes with matched self-binding strength profiles are seen to tend toward the same abundance over the additional iterations of the model (**Figures 5C,D**). Although the abundances of the new clonotypes do not reach equality with the original clonotypes, the introduced clonotypes only disappear in cases where the original clonotypes are also deleted. The introduced clonotypes are able to remain in

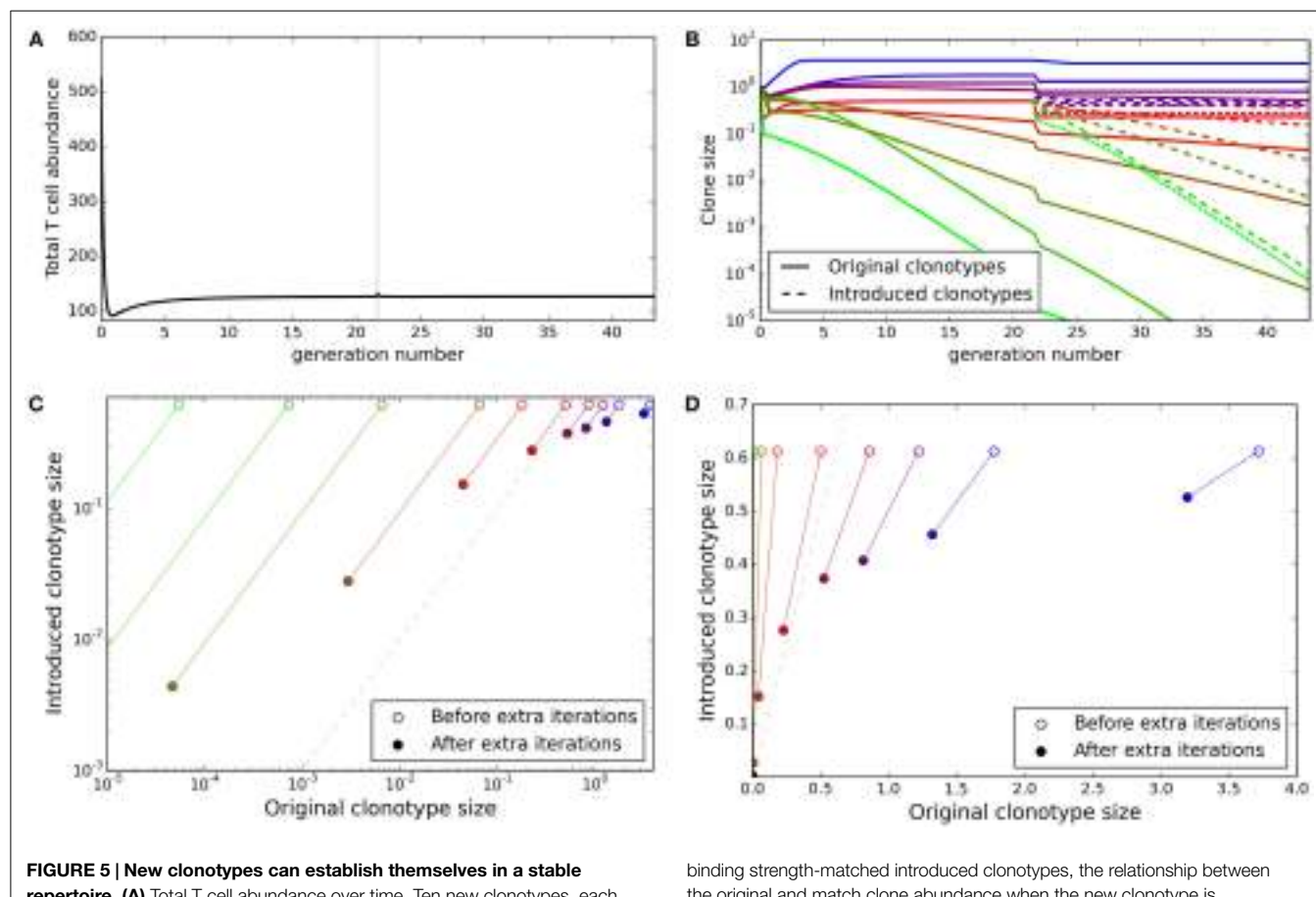


FIGURE 5 | New clonotypes can establish themselves in a stable repertoire. (A) Total T cell abundance over time. Ten new clonotypes, each with self profile binding strength vector matching an existing clonotype, are introduced (at the average clonotype abundance) after 30,000 iterations of the update algorithm. **(B)** The clonal abundance of 10 selected clonotypes over time. After 30,000 iterations of the update algorithm, 10 additional clonotypes are introduced (dashed lines), each with a self profile binding strengths equal to one of the original 10 clonotypes (colors represent binding strength profiles). **(C,D)** For each of the selected original clonotypes and the

binding strength-matched introduced clonotypes, the relationship between the original and match clone abundance when the new clonotype is introduced (open circles) and after running the simulation for an additional 30,000 iterations of the update algorithm (solid circles). The dashed gray line represents identical abundance of original and introduced clonotypes. Model parameters used for all panels are: self-response threshold $\tau = 1$, growth rate $\nu = \ln 2 \delta t^{-1}$, learning rate $\eta = 0.002001 \delta t^{-1}$, proportion of non-zero affinities $\gamma = 0.01$, number initial clonotypes $N = 1,000$, number self profiles $M = 100$.

the repertoire even when they are introduced at a lower abundance than an already established clonotype with the same self-response profile.

4. Discussion

We have outlined a simple computational model by which the T cell repertoire in an individual can be continually adjusted in order to optimize the chance of a successful response to unknown pathogens while minimizing the amount of dangerous T cell response to self. From a computational perspective, the update method can be thought of as a multiplicative weight update algorithm, and is shown to rapidly converge to a solution of the constraints. From a biological perspective, the model falls within the well-established framework of APC-based self-tolerance models (see below), but introduces the key features of cross-reactivity and T cell cooperativity. The model produces the desirable features of maintaining self-reactivity within a predefined threshold, while driving the development of a diverse repertoire, which can respond effectively to a broad selection of non-self antigens. The

model repertoire also reproduces the heterogeneous distribution of naive T cell clonotype abundance, which has been described by recent high throughput sequencing studies (33), and the extensive cross-reactivity which is another recently recognized feature of the T cell repertoire (5). We do not model an immune response in this work. If the APC remains in tolerogenic state, the introduction of new non-self pMHC profiles will violate the constraints, but this will result in additional T cell killing and the system will gradually readjust to remain within the immune activation threshold. If, however, the APC are switched to an immunogenic state (for example by exposure to innate immune danger signals) then crossing the threshold will result in activation of all APC bound T cells, resulting in an effector immune response.

The mechanisms whereby the vertebrate adaptive immune system avoids harmful reaction with self antigens but retains the ability to react with a large and unknown set of potential pathogens have been extensively discussed. The current molecular understanding of the stochastic recombination events, which generate adaptive immune receptors (antibody and the TCR), requires self-tolerance to be learnt rather inherited. The clonal deletion model

of (1) has remained the dominant paradigm for many decades. In the context of the T cell, this paradigm posits that T cells developing in the thymus die if they react with antigens (which in the context of the thymus are assumed to be predominantly self) with an affinity above a given threshold, whose value has been estimated to correspond to a disassociation constant of approximately $6 \mu\text{M}$ (34). Indeed special molecular mechanisms exist to ensure atopic expression of a whole range of non-thymic proteins in the thymus (35), presumably to ensure robust self-tolerance. The molecular mechanism of clonal deletion has also been studied intensively (36).

More recently, a number of immunologists have proposed the need for some form of extrathymic (peripheral) tolerance, since self-reactive mature T cells have been described in many cases. Such models include those in which self/non-self discrimination was assigned to the antigen presenting cell (typically a dendritic cell) rather than the T cell (16, 17). The essence of these models was to propose that APCs exist in two different functional states. Under resting conditions (e.g., in the absence of infection), the interaction between antigen on the APC and cognate T cell induces tolerance (either deletion, or anergy). When the APC is activated (typically via the innate immune system), the same interaction leads to activation, differentiation, and T cell effector function. A fundamental feature of these models is that the APC continues to present self-antigens in both states. However, since the immune system has been “educated” to tolerate self-reactive T cells during a resting period, and the majority of antigen presenting cells at any time continue to remain in a resting state, the T cell response to self-antigens presented together with non-self by the activated antigen presenting cells is small and transitory, and does not lead to significant pathology. The model presented in this paper lies squarely within the conceptual framework of these antigen presenting cell focused models of self/non-self discrimination. However, our model simplifies the system by assuming only a single type of APC. In reality, the immune system contains a heterogeneous mixture of antigen presenting cells, with a spectrum of tolerizing or activating activity (37). The extension of our model to incorporate antigen presenting cell heterogeneity will be an important goal of future work.

The molecular mechanisms by which antigen presenting cells induce tolerance remain an open question. Tolerogenic dendritic cells, which express granzyme and perforin, and induce T cell death in an antigen specific way, have been described (15). Dendritic cells also express several members of the Tumor Necrosis Factor (TNF) family, and its cognate receptors, the TNF receptor family. Some members of this family, for example CD40 and CD40L, are known to play a critical part in T cell activation. Impairment of this interaction leads to profound immunodeficiency (38). Furthermore, CD40 expression on antigen presenting cells is modulated by T cells, and the antigen presenting cell integrates signals from multiple T cells, providing a molecular mechanism for T cell cooperativity (39). Other members of the family, which can be expressed by dendritic cells, in contrast, deliver negative signals. The most well-studied example is the Fas/FasL interaction, and impairment of this interaction leads to a breakdown of self-tolerance (40–42). TNF itself can also induce

cell death via TNF receptor signals, although paradoxically it can also induce cell activation (43). The precise function of many of the more than 40 members of these families remains unknown, and their potential role in tolerance induction remains to be explored.

An interesting feature of our model is that it imposes a homeostatic limit on the total number of T cells, which depends on the self-tolerance threshold. There is extensive experimental evidence linking T cell homeostasis to inter-clonal competition for the survival/proliferation cytokine IL7 (44). An important challenge will be to integrate the phenomenon of clonal competition for a limited resource into our model. Indeed, it is possible to retain the computational infrastructure of our model but recast it emphasizing survival factors, rather than death signals. It may be the case that integration occurs in both APC and T cells, with the APC sending survival signals to bound T cells until a threshold level of binding is violated, at which point the survival signals cease. T cells would integrate the amount of survival signal received over a number of TCR-APC interactions and if this does not reach a sufficient level would die. This mechanism would increase the specificity of clonotype size adjustment, only reducing those clonotypes that repeatedly encounter APC for which the binding threshold is violated.

Of necessity, both our basic model and its implementation make a number of simplifying assumptions. The impact of some of these could be explored further by *in silico* experimentation. For example, it would be relatively straightforward to implement a model in which the proliferation of the T cells is likely to be dependent on the strength of the receptor/pMHC interaction. A more complex, but important, question to explore is the extent to which the averaging of the response over all antigen presenting cells adequately captures the real scenario, where self-tolerance must be distributed anatomically over the whole body, and where each antigen presenting cell only presents a subset of all possible self antigens.

Our model does not incorporate regulatory T cells, which are clearly an important part of the mechanisms of self-tolerance, and has been the basis for several previous theoretical models of self-tolerance (22, 23). These cells may be of particular importance for regulating those T cells with the highest affinity for self, which will still exist albeit at reduced numbers in our model, and which could be inadvertently triggered in the context of responses to non-self with potential pathogenic consequences.

The model we propose has interesting implications for inducing organ specific-tolerance in the context of allo-transplantation, which remains an unsolved problem in the context of clinical transplantation. The natural mechanisms, which maintain tolerance to self, are clearly insufficient in most cases to re-establish complete and lasting tolerance to an allograft in the absence of immune-suppression. This is perhaps not surprising since extrathymic-tolerance is only one component of tolerance, and in isolation may be insufficient. However, with better understanding of the molecular cell biology of tolerogenic dendritic cells, it may be possible to experimentally increase the activity or number of these cells and thus re-educate the peripheral repertoire versus tolerance.

In conclusion, we propose a model of self-tolerance, which incorporates T cell cooperativity (quorum-sensing) into the mechanism for balancing self-tolerance with immunocompetence. Once a stable repertoire has been produced, we imagine that on immune challenge individual groups of antigen presenting cells are switched into an activated state, where they present antigens and drive the establishment of effector and memory cells. However, the repertoire will have learnt tolerance and hence the response to self will be small and not pathogenic. A useful feature of the model is that the threshold for self reaction can be set locally, and hence may vary in different tissues. The balance between response and tolerance may therefore be dependent on the local micro-environment. The key prediction of our model is that perturbation of either the

existing T cell repertoire, or the presented pMHC landscape will cause widespread distributed changes to the overall repertoire, which will involve clones of many different specificities. The nature of these changes can be predicted by our model, and can be measured using the power of high throughput sequencing of TCR repertoires. Thus, our model will stimulate further hypothesis building and falsification, and lead to a better understanding of adaptive immunity and self-tolerance.

Supplementary Material

The Supplementary Material for this article can be found online at <http://journal.frontiersin.org/article/10.3389/fimmu.2015.00360>

References

- Burnet FM. A modification of Jerne's theory of antibody production using the concept of clonal selection. *CA Cancer J Clin* (1976) **26**(2):119–21.
- Kappler JW, Roehm N, Marrack P. T cell tolerance by clonal elimination in the thymus. *Cell* (1987) **49**(2):273–80. doi:10.1016/0092-8674(87)90568-X
- Krogsgaard M, Davis MM. How T cells 'see' antigen. *Nat Immunol* (2005) **6**(3):239–45. doi:10.1038/ni1173
- Birnbaum ME, Mendoza JL, Sethi DK, Dong S, Glanville J, Dobbins J, et al. Deconstructing the peptide-MHC specificity of T cell recognition. *Cell* (2014) **157**(5):1073–87. doi:10.1016/j.cell.2014.03.047
- Wooldridge L, Ekeruche-Makinde J, Van Den Berg HA, Skowera A, Miles JJ, Tan MP, et al. A single autoimmune T cell receptor recognizes more than a million different peptides. *J Biol Chem* (2012) **287**(2):1168–77. doi:10.1074/jbc.M111.289488
- Butler TC, Kardar M, Chakraborty AK. Quorum sensing allows T cells to discriminate between self and nonself. *Proc Natl Acad Sci USA* (2013) **110**(29):11833–8. doi:10.1073/pnas.1222467110
- Steinman RM. The dendritic cell system and its role in immunogenicity. *Annu Rev Immunol* (1991) **9**:271–96. doi:10.1146/annurev.iy.09.040191.001415
- Beltman JB, Marée AFM, Lynch JN, Miller MJ, de Boer RJ. Lymph node topology dictates T cell migration behavior. *J Exp Med* (2007) **204**(4):771–80. doi:10.1084/jem.20061278
- Miller MJ, Hejazi AS, Wei SH, Cahalan MD, Parker I. T cell repertoire scanning is promoted by dynamic dendritic cell behavior and random T cell motility in the lymph node. *Proc Natl Acad Sci USA* (2004) **101**(4):998–1003. doi:10.1073/pnas.0306407101
- Thomas N, Matejovicova L, Sriksulanukul W, Shawe-Taylor J, Chain B. Directional migration of recirculating lymphocytes through lymph nodes via random walks. *PLoS One* (2012) **7**:9. doi:10.1371/journal.pone.0045262
- Creusot RJ, Thomsen LL, Tite JP, Chain BM. Local cooperation dominates over competition between CD4+ T cells of different antigen/MHC specificity. *J Immunol* (2003) **171**:240–6. doi:10.4049/jimmunol.171.1.240
- Ridge JP, Di Rosa F, Matzinger P. A conditioned dendritic cell can be a temporal bridge between a CD4+ T-helper and a T-killer cell. *Nature* (1998) **393**(6684):474–8. doi:10.1038/30989
- Janeway CA, Medzhitov R. Innate immune recognition. *Annu Rev Immunol* (2002) **20**(2):197–216. doi:10.1146/annurev.immunol.20.083001.084359
- Matzinger P. The danger model: a renewed sense of self. *Science* (2002) **296**:301–5. doi:10.1126/science.1071059
- Zangi L, Klionsky YZ, Yarimi L, Bachar-Lustig E, Eidelstein Y, Shezen E, et al. Deletion of cognate CD8 T cells by immature dendritic cells: a novel role for perforin, granzyme A, TREM-1, and TLR7. *Blood* (2012) **120**(8):1647–57. doi:10.1182/blood-2012-02-410803
- Ibrahim MA, Chain BM, Katz DR. The injured cell: the role of the dendritic cell system as a sentinel receptor pathway. *Immunol Today* (1995) **16**:181–6. doi:10.1016/0167-5699(95)80118-9
- Matzinger P. Tolerance, danger, and the extended family. *Annu Rev Immunol* (1994) **12**:991–1045. doi:10.1146/annurev.iy.12.040194.005015
- Gascoigne NR, Acuto O. THEMIS: a critical TCR signal regulator for ligand discrimination. *Curr Opin Immunol* (2015) **33**:86–92. doi:10.1016/j.co.2015.01.020
- Stepanek O, Prabhakar AS, Osswald C, King CG, Bulek A, Naehor D, et al. Coreceptor scanning by the T cell receptor provides a mechanism for T cell tolerance. *Cell* (2014) **159**(2):333–45. doi:10.1016/j.cell.2014.08.042
- Bains I, van Santen HM, Seddon B, Yates AJ. Models of self-peptide sampling by developing T cells identify candidate mechanisms of thymic selection. *PLoS Comput Biol* (2013) **9**(7):e1003102. doi:10.1371/journal.pcbi.1003102
- Khailaie S, Robert PA, Toker A, Huehn J, Meyer-Hermann M. A signal integration model of thymic selection and natural regulatory T cell commitment. *J Immunol* (2014) **193**:5983–96. doi:10.4049/jimmunol.1400889
- Alexander HK, Wahl LM. Self-tolerance and autoimmunity in a regulatory T cell model. *Bull Math Biol* (2011) **73**(1):33–71. doi:10.1007/s11538-010-9519-2
- Carneiro J, Leon K, Caramalho I, Van Den Dool C, Gardner R, Oliveira V, et al. When three is not a crowd: a crossregulation model of the dynamics and repertoire selection of regulatory CD4+ T cells. *Immunol Rev* (2007) **216**(1):48–68. doi:10.1111/j.1600-065X.2007.00487.x
- Arstila TP. A direct estimate of the human T cell receptor diversity. *Science* (1999) **286**(5441):958–61. doi:10.1126/science.286.5441.958
- Berkley AM, Fink PJ. Cutting edge: CD8+ recent thymic emigrants exhibit increased responses to low-affinity ligands and improved access to peripheral sites of inflammation. *J Immunol* (2014) **193**(7):3262–6. doi:10.4049/jimmunol.1401870
- Robins HS, Campregher PV, Srivastava SK, Wacher A, Turtle CJ, Kahsai O, et al. Comprehensive assessment of T-cell receptor β-chain diversity in αβ T cells. *Immunobiology* (2009) **114**(19):4099–107. doi:10.1182/blood-2009-04-217604
- Boer RD, Perelson A. T cell repertoires and competitive exclusion. *J Theor Biol* (1994) **169**:375–90. doi:10.1006/jtbi.1994.1160
- Stirk ER, Lythe G, van den Berg HA, Molina-París C. Stochastic competitive exclusion in the maintenance of the naïve T cell repertoire. *J Theor Biol* (2010) **265**(3):396–410. doi:10.1016/j.jtbi.2010.05.004
- Stirk ER, Molina-París C, van den Berg HA. Stochastic niche structure and diversity maintenance in the T cell repertoire. *J Theor Biol* (2008) **255**(2):237–49. doi:10.1016/j.jtbi.2008.07.017
- Arora S, Hazan E, Kale S. The multiplicative weights update method: a meta-algorithm and applications. *Theory Comput* (2012) **8**:121–64. doi:10.4086/toc.2012.v008a006
- Britanova OV, Putintseva EV, Shugay M, Merzlyak EM, Turchaninova MA, Staroverov DB, et al. Age-related decrease in TCR repertoire diversity measured with deep and normalized sequence profiling. *J Immunol* (2014) **192**(6):2689–98. doi:10.4049/jimmunol.1302064
- Shannon CE. A mathematical theory of communication. *Bell Syst Tech J* (1948) **27**(3):379–423. doi:10.1002/j.1538-7305.1948.tb00917.x
- Qi Q, Liu Y, Cheng Y, Glanville J, Zhang D, Lee J-Y, et al. Diversity and clonal selection in the human T-cell repertoire. *Proc Natl Acad Sci USA* (2014) **111**(36):13139–44. doi:10.1073/pnas.1409155111
- Palmer E, Naehor D. Affinity threshold for thymic selection through a T-cell receptor-co-receptor zipper. *Nat Rev Immunol* (2009) **9**(3):207–13. doi:10.1038/nri2469

35. Anderson MS, Venanzio ES, Klein L, Chen Z, Berzins SP, Turley SJ, et al. Projection of an immunological self shadow within the thymus by the aire protein. *Science* (2002) **298**(5597):1395–401. doi:10.1126/science.1075958
36. Hogquist KA, Baldwin TA, Jameson SC. Central tolerance: learning self-control in the thymus. *Nat Rev Immunol* (2005) **5**(10):772–82. doi:10.1038/nri1707
37. Moore JR. The benefits of diversity: heterogenous DC populations allow for both immunity and tolerance. *J Theor Biol* (2014) **357**:86–102. doi:10.1016/j.jtbi.2014.04.034
38. Callard RE, Armitage RJ, Fanslow WC, Spriggs MK. CD40 ligand and its role in X-linked hyper-IgM syndrome. *Immunol Today* (1993) **14**(11):559–64. doi:10.1016/0167-5699(93)90188-Q
39. Abdi K, Singh NJ, Matzinger P. Lipopolysaccharide-activated dendritic cells: “exhausted” or alert and waiting? *J Immunol* (2012) **188**(12):5981–9. doi:10.4049/jimmunol.1102868
40. Izawa T, Kondo T, Kurosawa M, Oura R, Matsumoto K, Tanaka E, et al. Fas-independent T-cell apoptosis by dendritic cells controls autoimmune arthritis in MRL/lpr mice. *PLoS One* (2012) **7**:12. doi:10.1371/journal.pone.0048798
41. Naderi N, Moazzeni SM, Pourfathollah AA, Alimoghaddam K. High expression of fas ligand on cord blood dendritic cells: a possible immunoregulatory mechanism after cord blood transplantation. *Transplant Proc* (2011) **43**(10):3913–9. doi:10.1016/j.transproceed.2011.10.040
42. Xu X, Yi H, Guo Z, Qian C, Xia S, Yao Y, et al. Splenic stroma-educated regulatory dendritic cells induce apoptosis of activated CD4 T cells via FasL-enhanced IFN- γ and nitric oxide. *J Immunol* (2012) **188**(3):1168–77. doi:10.4049/jimmunol.1101696
43. Hsu H, Xiong J, Goeddel DV. The TNF receptor 1-associated protein TRADD signals cell death and NF-kappa B activation. *Cell* (1995) **81**:495–504. doi:10.1016/0092-8674(95)90070-5
44. Tan JT, Dudi E, LeRoy E, Murray R, Sprent J, Weinberg KI, et al. IL-7 is critical for homeostatic proliferation and survival of naive T cells. *Proc Natl Acad Sci USA* (2001) **98**(15):8732–7. doi:10.1073/pnas.161126098

Conflict of Interest Statement: The authors declare that the research was conducted in the absence of any commercial or financial relationships that could be construed as a potential conflict of interest.

Copyright © 2015 Best, Chain and Watkins. This is an open-access article distributed under the terms of the Creative Commons Attribution License (CC BY). The use, distribution or reproduction in other forums is permitted, provided the original author(s) or licensor are credited and that the original publication in this journal is cited, in accordance with accepted academic practice. No use, distribution or reproduction is permitted which does not comply with these terms.



The Limits of Linked Suppression for Regulatory T Cells

Toshiro Ito¹, Akira Yamada¹, Ibrahim Batal², Melissa Y. Yeung², Martina M. McGrath², Mohamed H. Sayegh², Anil Chandraker² and Takuya Ueno^{1,2*}

¹ Transplantation Unit, Surgical Services, Massachusetts General Hospital, Harvard Medical School, Boston, MA, USA

² Transplantation Research Center, Brigham and Women's Hospital and Children's Hospital, Harvard Medical School, Boston, MA, USA

Background: We have previously found that CD4⁺CD25⁺ regulatory T cells (Tregs) can adoptively transfer tolerance after its induction with costimulatory blockade in a mouse model of murine cardiac allograft transplantation. In these experiments, we tested an hypothesis with three components: (1) the Tregs that transfer tolerance have the capacity for linked suppression, (2) the determinants that stimulate the Tregs are expressed by the indirect pathway, and (3) the donor peptides contributing to these indirect determinants are derived from donor major histocompatibility complex (MHC) antigens (Ags).

OPEN ACCESS

Edited by:

Kathryn Wood,
University of Oxford, UK

Reviewed by:

Stanislaw Stepkowski,
University of Toledo College of
Medicine, USA
Dennis O. Adeegbe,
Dana Farber Cancer Institute and
Harvard Medical School, USA

*Correspondence:

Takuya Ueno
ueno.takuya@mgh.harvard.edu

Specialty section:

This article was submitted to
Alloimmunity and Transplantation,
a section of the journal
Frontiers in Immunology

Received: 04 December 2015

Accepted: 22 February 2016

Published: 09 March 2016

Citation:

Ito T, Yamada A, Batal I, Yeung MY,
McGrath MM, Sayegh MH,
Chandraker A and Ueno T (2016) The
Limits of Linked Suppression for
Regulatory T Cells.
Front. Immunol. 7:82.
doi: 10.3389/fimmu.2016.00082

Methods: First heart transplants were performed from the indicated donor strain to B10.D2 recipients along with costimulatory blockade treatment (250 µg i.p. injection of MR1 on day 0 and 250 µg i.p. injection of CTLA-4 Ig on day 2). At least 8 weeks later, a second heart transplant was performed to a new B10.D2 recipient who had been irradiated with 450 cGy. This recipient was given 40 × 10⁶ naive B10.D2 spleen cells + 40 × 10⁶ B10.D2 spleen cells from the first (tolerant) recipient. We performed three different types of heart transplants using various donors.

Results: (1) Tregs suppress the graft rejection in an Ag-specific manner. (2) Tregs generated in the face of MHC disparities suppress the rejection of grafts expressing third party MHC along with tolerant MHC.

Conclusion: The limits of linkage appear to be quantitative and not universally determined by either the indirect pathway or by peptides of donor MHC Ags.

Keywords: costimulation, indirect pathway, MHC class II, tolerance, regulatory T cells

INTRODUCTION

The physiologically unusual stimulation of T cells by donor antigen-presenting cells (APCs) has been called “direct” recognition, whereas stimulation by self-APCs, presenting peptides of donor origin, has been called “indirect” recognition. Direct recognition has been believed to be the major pathway involved in allograft rejection due to three basic observations, namely, (1) direct stimulation is very strong in a primary allogenic mixed lymphocyte reaction, (2) depletion of donor APCs can

Abbreviations: Ags, antigens; APCs, antigen-presenting cells; MHC, major histocompatibility complex; MST, median survival time; Tregs, regulatory T cells.

sometimes prolong allograft survival, and (3) donor major histocompatibility complex (MHC) antigens (Ags) are more important than minor Ags in causing graft rejection (1). Matching for MHC Ags achieves better allograft survival. Lechner and Batchelor showed the importance of MHC class II matching compared to MHC class I matching at least in the long-term survival (2). However, there are several remarkable reports of consequences of T cells responding via the indirect pathway. These reports showed the indirect pathway (a) helps for priming alloreactive CD8 T cells (3, 4), (b) is essential for tolerance induction in some models (5, 6), and (c) is involved in chronic transplant rejection (7, 8). In addition, several papers have shown the importance of an indirect response in allograft rejection (1, 3, 9, 10). Indirect

allorecognition contributes not only to acute graft rejection (2, 9) but also possibly to the continuing response to the allograft in the long term after transplantation (11). Previously, we tested the role of costimulatory blockade for prolonging allograft survival with using class II-deficient mice when only one or the other pathway of graft rejection was available. We found that to achieve long-term survival after costimulatory blockade requires that the recipient expresses MHC class II molecules (12). This result indicated that indefinite cardiac transplant survival could not be achieved in the absence of an intact indirect pathway. These results are consistent with the fact that at least a component of the regulatory T cell (Treg) response must involve recognition of peptides of donor Ags presented by recipient MHC molecules

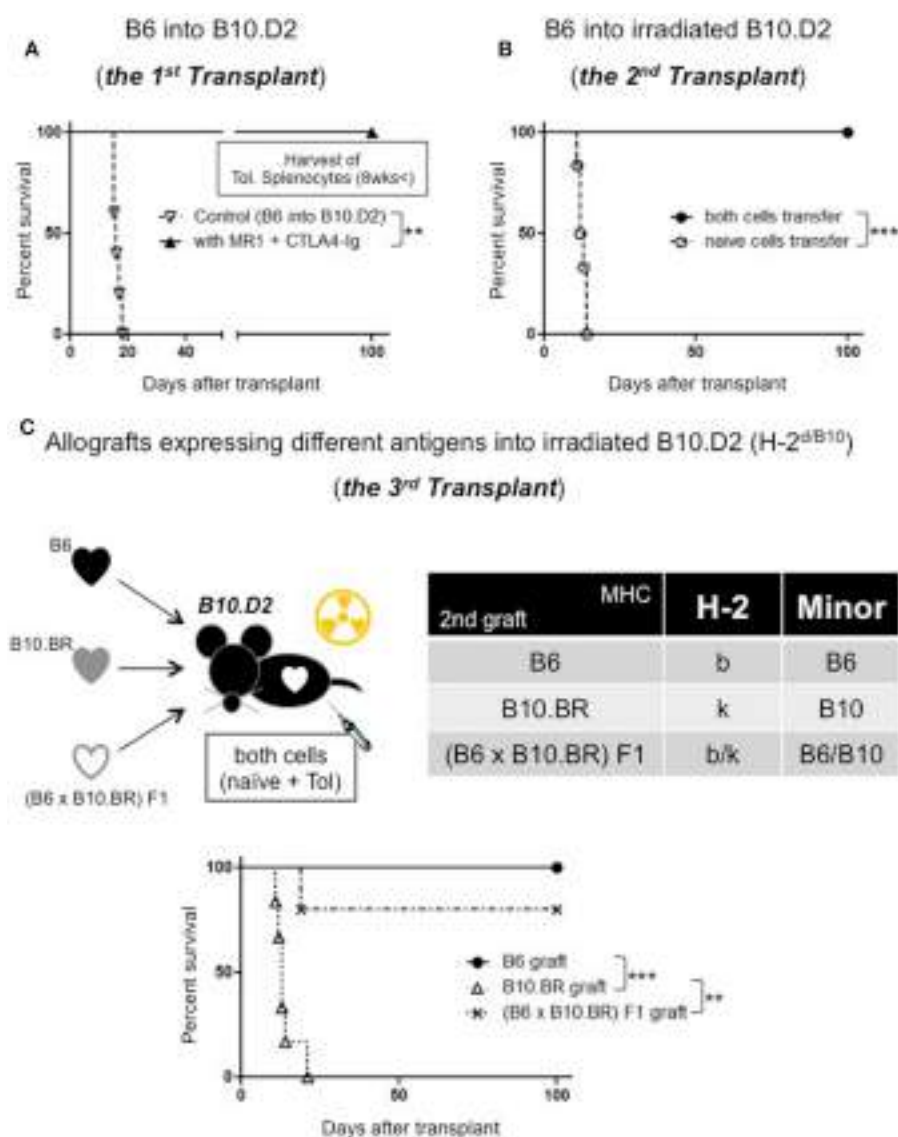


FIGURE 1 | (A) Allograft survival in B10.D2 recipients: (>100 days, $n = 5$, $p = 0.0017$ compared to control: 16.2 days, $n = 5$). **(B) Adoptive transfer model:** naive splenocytes transfer ($n = 6$), both naive and Tol. splenocytes transfer (100 days, $n = 6$, $p = 0.0007$). **(C) Linkage model:** B6 hearts (>100 days), B10.BR hearts (~23 days, $n = 6$, $p = 0.0006$) (B6 x B10.BR) F1 (>100 days, $n = 4/5$, $p = 0.0044$).

(13). Authors also mentioned that linked suppression can also be induced through the indirect pathway. However, little work seems to have addressed their direct role in transplantation. Therefore, in the current study, we tested whether the Tregs that transfer tolerance have the capacity for linked suppression.

METHODS AND RESULTS

First, we made B10.D2 (H-2^d) mice tolerant to B6 (H-2^b) with costimulatory blockade [250 µg intraperitoneal (i.p.) injection of MR1 on day 0 and 250 µg i.p. injection of CTLA-4 Ig on day 2] (**Figure 1A**). At least 8 weeks later, a second heart transplant was performed to a new B10.D2 recipient who had been irradiated with 450 cGy. All recipient received intravenous (i.v.) injection of naive 40×10^6 splenocytes + 40×10^6 splenocytes that are taken from the tolerant mice (tolerized splenocytes: Tol.) significantly prolonged graft survival compared to recipient received only naive splenocyte (12 ± 1 days compared to >100 , $p < 0.001$) (**Figure 1B**). After these results, we considered linkage of Tregs. Next, we performed a second transplant from B6 mice to irradiated B10.D2 mice. The second donors express the same MHC and minor Ags as the first graft or B10.BR heart grafts differ from the first graft in their MHC Ags or (B6 × B10.BR) F1 mice, which express both H-2^b and H-2^k Ags. After transplant, the mice received i.v. injection of naive and tolerized splenocytes. All B6 hearts survived over 100 days. But B10.BR hearts expressing third party MHC were rejected by 23 days (**Figure 1C**). (B10.BR × B6) F1 hearts expressing third party MHC with tolerant MHC showed 80% survival of over 100 days; however, CAV was observed in some specimen. The institutional subcommittee on research animal care at Massachusetts General Hospital approved all animal experiments.

DISCUSSION

Linked suppression has often been associated with Tregs, and its mechanisms must be important ones, as tolerance can be extended to whole MHC disparities when applied to cardiac transplantation. Tolerance was extended to third party transplant

Ags, even to MHC-encoded Ags, provided they are expressed on the same graft as the tolerated Ags in some models (14–17). Thus, its mechanism of immunoregulation in transplantation is very important. In addition, understanding interactions between linked suppression and Tregs can potentially be great advantage in the setting of transplantation to propagate the development of specific unresponsiveness once the process has been initiated.

Our preliminary data showed that Tregs suppress the graft rejection in an Ag-specific manner and Tregs generated in the face of MHC disparities suppress the rejection of grafts expressing third party MHC along with tolerant MHC.

CONCLUSION

The very limited comparison in this experiment will determine whether the patterns of gene expression can reliably distinguish a regulatory population from one that promotes rejection.

AUTHOR CONTRIBUTIONS

TU, TI, and AY participated in the performance of the research, performed the data collection, performed the statistical analysis, and contributed to the writing of the manuscript; IB, MY, and MM participated in the writing of the manuscript and performed review; and MS and TU designed the study and participated in review. AC participated in review.

ACKNOWLEDGMENTS

We thank Susan P. Shea and Karla S. Stenger for their invaluable technical assistance and Hugh Auchincloss Jr. for his advice and insight.

FUNDING

This work was supported by American Heart Association and JSPS KAKENHI. TU is a recipient of the American Heart Association Scientist Development Grant (11SDG5150000) and Grant-in-Aid for Challenging Exploratory Research (15K15479).

REFERENCES

- Gould DS, Auchincloss H Jr. Direct and indirect recognition: the role of MHC antigens in graft rejection. *Immunol Today* (1999) **20**:77–82. doi:10.1016/S0167-5699(98)01394-2
- Lechner RI, Batchelor JR. Restoration of immunogenicity to passenger cell-depleted kidney allografts by the addition of donor strain dendritic cells. *J Exp Med* (1982) **155**:31–41. doi:10.1084/jem.155.1.31
- Auchincloss H Jr, Sultan H. Antigen processing and presentation in transplantation. *Curr Opin Immunol* (1996) **8**:681–7. doi:10.1016/S0952-7915(96)80086-0
- Valujskikh A, Lantz O, Celli S, Matzinger P, Heeger PS. Cross-primed CD8(+) T cells mediate graft rejection via a distinct effector pathway. *Nat Immunol* (2002) **3**:844–51. doi:10.1038/ni831
- Kishimoto K, Yuan X, Auchincloss H Jr, Sharpe AH, Mandelbrot DA, Sayegh MH. Mechanism of action of donor-specific transfusion in inducing tolerance: role of donor MHC molecules, donor co-stimulatory molecules, and indirect antigen presentation. *J Am Soc Nephrol* (2004) **15**:2423–8. doi:10.1097/01 ASN.0000137883.20961.2D
- Lehmann PV, Matesic D, Benichou G, Heeger PS. Induction of T helper 2 immunity to an immunodominant allopeptide. *Transplantation* (1997) **64**:292–6. doi:10.1097/00007890-199707270-00020
- Hornick PI, Mason PD, Baker RJ, Hernandez-Fuentes M, Frasca L, Lombardi G, et al. Significant frequencies of T cells with indirect anti-donor specificity in heart graft recipients with chronic rejection. *Circulation* (2000) **101**:2405–10. doi:10.1161/01.CIR.101.20.2405
- Yamada A, Laufer TM, Gerth AJ, Chase CM, Colvin RB, Russell PS, et al. Further analysis of the T-cell subsets and pathways of murine cardiac allograft rejection. *Am J Transplant* (2003) **3**:23–7. doi:10.1034/j.1600-6143.2003.30105.x
- Auchincloss H Jr, Lee R, Shea S, Markowitz JS, Grusby MJ, Glimcher LH. The role of “indirect” recognition in initiating rejection of skin grafts from major histocompatibility complex class II-deficient mice. *Proc Natl Acad Sci U S A* (1993) **90**:3373–7. doi:10.1073/pnas.90.8.3373
- Sayegh MH, Carpenter CB. Role of indirect allorecognition in allograft rejection. *Int Rev Immunol* (1996) **13**:221–9. doi:10.3109/08830189609061749
- Wood KJ, Sakaguchi S. Regulatory T cells in transplantation tolerance. *Nat Rev Immunol* (2003) **3**:199–210. doi:10.1038/nri1027

12. Yamada A, Chandraker A, Laufer TM, Gerth AJ, Sayegh MH, Auchincloss H Jr. Recipient MHC class II expression is required to achieve long-term survival of murine cardiac allografts after costimulatory blockade. *J Immunol* (2001) **167**:5522–6. doi:10.4049/jimmunol.167.10.5522
13. Wise MP, Bemelman F, Cobbold SP, Waldmann H. Linked suppression of skin graft rejection can operate through indirect recognition. *J Immunol* (1998) **161**:5813–6.
14. Adeegbe D, Levy RB, Malek TR. Allogeneic T regulatory cell-mediated transplantation tolerance in adoptive therapy depends on dominant peripheral suppression and central tolerance. *Blood* (2010) **115**:1932–40. doi:10.1182/blood-2009-08-238584
15. Chen Z, Morgan R, Berger CS, Sandberg AA. Application of fluorescence in situ hybridization in hematological disorders. *Cancer Genet Cytogenet* (1992) **63**:62–9. doi:10.1016/0165-4608(92)90066-H
16. Davies JD, Leong LY, Mellor A, Cobbold SP, Waldmann H. T cell suppression in transplantation tolerance through linked recognition. *J Immunol* (1996) **156**:3602–7.
17. Wong W, Morris PJ, Wood KJ. Pretransplant administration of a single donor class I major histocompatibility complex molecule is sufficient for the indefinite survival of fully allogeneic cardiac allografts: evidence for linked epitope suppression. *Transplantation* (1997) **63**:1490–4. doi:10.1097/00007890-199705270-00020

Conflict of Interest Statement: The authors declare that the research was conducted in the absence of any commercial or financial relationships that could be construed as a potential conflict of interest.

Copyright © 2016 Ito, Yamada, Batal, Yeung, McGrath, Sayegh, Chandraker and Ueno. This is an open-access article distributed under the terms of the Creative Commons Attribution License (CC BY). The use, distribution or reproduction in other forums is permitted, provided the original author(s) or licensor are credited and that the original publication in this journal is cited, in accordance with accepted academic practice. No use, distribution or reproduction is permitted which does not comply with these terms.

Advantages of publishing in Frontiers



OPEN ACCESS

Articles are free to read,
for greatest visibility



COLLABORATIVE PEER-REVIEW

Designed to be rigorous
– yet also collaborative,
fair and constructive



FAST PUBLICATION

Average 85 days from
submission to publication
(across all journals)



COPYRIGHT TO AUTHORS

No limit to article
distribution and re-use



TRANSPARENT

Editors and reviewers
acknowledged by name
on published articles



SUPPORT

By our Swiss-based
editorial team



IMPACT METRICS

Advanced metrics
track your article's impact



GLOBAL SPREAD

5'100'000+ monthly
article views
and downloads



LOOP RESEARCH NETWORK

Our network
increases readership
for your article

Frontiers

EPFL Innovation Park, Building I • 1015 Lausanne • Switzerland
Tel +41 21 510 17 00 • Fax +41 21 510 17 01 • info@frontiersin.org
www.frontiersin.org

Find us on

